BETTER SHIPS, BLUE OCEANS

Determination of limiting wave heights for feeder ships due to green water

Summary, discussion and conclusions

Report No.	:	33327-1-SHIPS
Date	:	March 2022
Version	:	1.2
		Final Report

Determination of limiting wave heights for feeder ships due to green water

Summary, discussion and conclusions

MARIN order No.	:	33327
MARIN Project Manager	:	B. Abeil, MSc.
Ship model No.	:	10246
Model scale ratio	:	33
Number of pages	:	185
Ordered by	:	Ministry of Infrastucture and Water Management (MI&W) Directie Maritieme Zaken IBI/F&I/086 Postbox 20906 2500 EX The Hague
Order document	:	Opdrachtbrief 'Onderzoek Groen Water Feeders' (kenmerk: 31167741) dated 1 April, 2021
Reference	:	Onderzoek Groen Water Feeders
Reported by	:	B. Abeil, MSc.
Reviewed by	:	Dr. ir. R. van 't Veer and Dr. ir. B. Buchner

Version	Date	Version description
1.0	December 2021	Draft version of the report
1.1	March 2022	Updated draft version
1.2	March 2022	Final version

CONTENTS PAGE

CONTENTS (CONTINUED) PAGE

REVIEW OF TABLES, FIGURES AND PHOTO PAGES

Tables on the table pages

Figures on the figure pages

Photos on the photo pages

REVIEW OF DELIVERABLES

Table i-1: Deliverables of the current project phase[1]

Deliverable	Contains
MARIN report No. 33327-1-SHIPS Set of hard drives	- the present report, delivered in triplicate - copy of all videos taken during the model tests, delivered in triplicate

[1] At the time of writing.

NEDERLANDSTALIGE SAMENVATTING MET ADVIEZEN

Achtergrond

In de avond en nacht van 1 op 2 januari 2019 verloor het Ultra Large Container Ship (ULCS) MSC ZOE 342 containers ten noorden van de Waddeneilanden terwijl het in het verkeersscheidingsstelsel Terschelling-German Bight voer naar Bremerhaven in noordwester stormcondities. Dit resulteerde in grote vervuiling van de zee en Waddeneilanden. De combinatie van hoge (brekende) golven en ondiep water dwars op de vaarroutes resulteert boven de Waddeneilanden in complex gedrag van containerschepen en hun lading, waarbij verschillende fenomenen tegelijkertijd een rol spelen. Als onderdeel van het onderzoek met de Onderzoeksraad Voor Veiligheid (OVV), concludeerde MARIN[2] dat de volgende fenomenen de meest waarschijnlijke verklaringen voor het verliezen van containers zijn:

1. Extreme (golffrequente) scheepsbewegingen en versnellingen
2. Contact van het schip met de zeebodem
3. Impulsieve krachten van groenwater op de containers
4. Golfklappen tegen de romp van het schip.

Om het verliezen van containers dicht bij dit beschermde natuurgebied (Particularly Sensitive Sea Area, PSSA) in de toekomst te voorkomen, heeft het Ministerie van Infrastructuur en Waterstaat (I&W) MARIN in 2020 gevraagd te onderzoeken hoe containerschepen met andere afmetingen reageren op de condities boven de Waddeneilanden[3]: naast zeer grote containerschepen zoals de MSC ZOE (ULCS, typische lengte 379 m, breedte 59 m), een kortere en smallere ‘Panamax’ (typische lengte 278 m, breedte 32m) en een kleinere container ‘Feeder’ (typische lengte 163 meter, breedte 27 m).

Voor de kleinere ‘Feeders’ resulteerde dit in de volgende **voorlopige beperkende golfhoogtes** voor de situatie in dwarsgolven (de bepalende fenomenen per scheepstype en route staan steeds vetgedrukt):

Voorlopige beperkende golfhoogtes voor Feeder in dwarsgolven in vorige MARIN studie

Route	**FEEDER** Aannames: GM=0.8 tot 1.5m 0 tot 8 knopen 9.20 m diepgang Vrijboord 3.0 m
Noordelijke route (37.5m water diepte)	Hs > 7.5 m (versnellingen) Hs > 7.5 m (bodemcontact) **Hs ≈ 3.3 m (groenwater)**
Zuidelijke route (21.3m water diepte)	Hs > 6.5 m (versnellingen) Hs ≈ 5.5 m (bodemcontact) **Hs ≈ 3.4 m (groenwater)**

[2] Rapporten zijn te vinden op: https://www.onderzoeksraad.nl/en/page/13223/safe-container-transport-north-of-the-wadden-islands.-lessons-learned

[3] ‘Further Investigations into the Behaviour of Container Ships in Storms above the Wadden Islands’, Summary report, Report No. 32558-1-DIR, September 2020

Op basis van deze relatief lage waarden voor ‘Feeders’ heeft MARIN vervolgonderzoek aanbevolen voor deze kleinere schepen, met name gericht op het probleem van groenwater. Groenwater is het massieve zeewater dat tegen de containers kan aanslaan wanneer de golven boven de dekhoogte, het vrijboord, uitkomen.

Het belang van onderzoek naar kleinere schepen werd bevestigd toen de Feeder ‘Rauma’ op 11 februari 2020 boven de Wadden 7 containers verloor in golven met een significante golfhoogte (Hs) tussen 4.5 en 5.0 m. In vergelijkbare condities verloor de Feeder ‘Baltic Tern’ 5 containers op 7 april 2021.

Op basis van het vorige onderzoek deed MARIN de volgende aanbevelingen:

“We bevelen ook aan om het complexe probleem van groenwater belasting op de containers verder te onderzoeken, speciaal voor de kleinere schepen zoals Feeders met hun relatief lage vrijboord. Groenwater belasting is een beperkende factor voor deze schepen in beide routes. De (statistiek van) complexe niet-lineaire relatieve golfbewegingen, groenwater impacts en reacties van de (stapels) containers vragen verder onderzoek om het risiconiveau en de beperkende golfhoogtes nauwkeuriger te bepalen. Hierbij speelt ook de hoogte van het vrijboord een belangrijke rol. We bevelen aan om, naast dwarsgolven, ook naar situaties met golven (schuin) van voren te kijken. Met lage snelheid ‘met de kop op de golven gaan liggen’ is een logische keuze wanneer grote slingerbewegingen en groenwater optreden in dwarsgolven. Het is echter belangrijk te onderzoeken of er in golven (schuin op) de kop ook groen water tegen de containers aanslaat vanaf de zij of over de boeg.”
(…)
“We raden aan om tijdens dit onderzoek in kopgolven ook verder te kijken naar ‘parametrisch slingeren’. Parametrisch slingeren in kopgolven kan optreden bij bepaalde combinaties van golflengte, golfperiode en eigen slingerperiode van het schip. Het moet worden voorkomen dat de keuze om met de kop op de golven te gaan varen, alsnog resulteert in grote slingerbewegingen en containerverlies. Hoewel een eerste extra set van proeven geen parametrisch slingeren liet zien van het huidige kleine Feeder testmodel, raden we dit extra onderzoek aan om te er zeker van te zijn dat dit probleem zich niet voordoet (of kan worden voorkomen door goede instructies aan bemanningen).”

Het huidige rapport geeft een overzicht van het onderzoek dat gebaseerd is op deze aanbevelingen.

Samenvatting van het huidige onderzoek

In deze Nederlandstalige samenvatting wordt een kort overzicht gegeven van het uitgevoerde onderzoek. De details zijn te vinden in het Engelstalige rapport.

Op basis van de geldende regelgeving (Load Line 1966 Convention) en overzichten van huidige schepen (zoals RINA ‘Significant Ships’) is gekozen voor een basismodel van een Feeder met een lengte van 163.0 m en een breedte van 27.0 m. Een typische Feeder van deze lengte en het MARIN testmodel zijn weergegeven in de onderstaande figuur:


Links: Typische Feeder van deze lengte met veel voorkomende container configuratie
Rechts: MARIN model van een Feeder voor huidige modelproeven

Er is daarnaast een keuze gemaakt voor een aantal realistische vrijboordhoogtes (2.3 m, 3.8 m en 5.3 m) en verschillende configuraties van containers op het dek, zoals die voorkomen op Feeders. Deze zijn hieronder schematisch weergegeven:

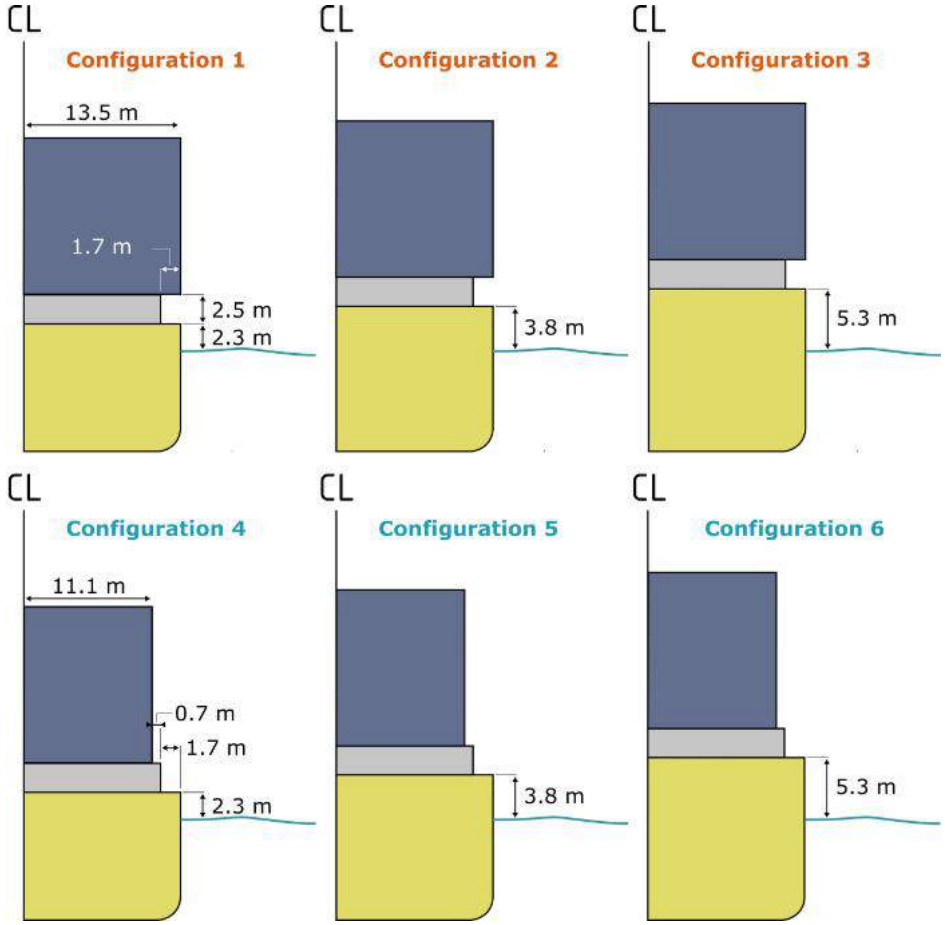

Onderzochte vrijboordhoogtes en containerfiguraties op dek

Wat omgevingscondities betreft, richtte het onderzoek zich op:

- Significante golfhoogtes zoals die voorkomen boven de Wadden: 1.2 m tot 7.5 m (met bijhorende golfperiodes)
- Golfrichtingen: kopgolven (180 graden), dwarsgolven (270 graden), schuin-voorinkomende golven (225 graden) en schuin-achterinkomende golven (315 graden)
- Waterdieptes: 21.3 m (zuidelijke route), 37.5 (noordelijke route) en 100.0 meter (diepwater Noordzee).

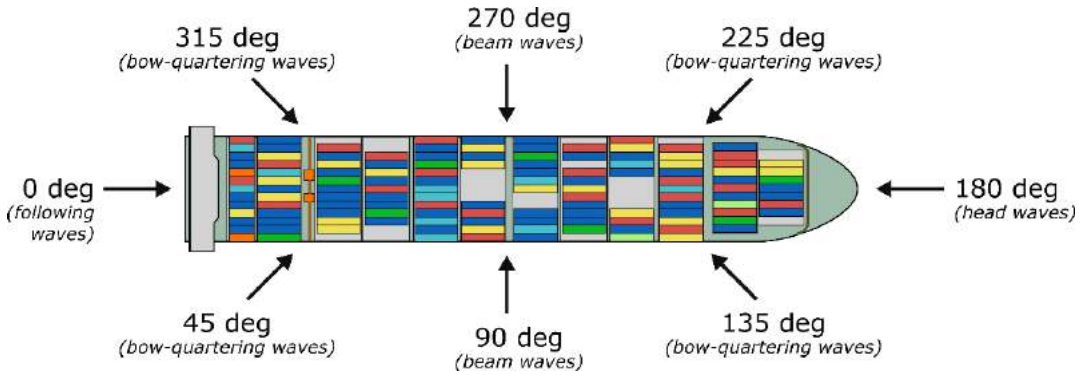

Definitie van golfrichtingen

Uitgebreide modelproeven in deze omgevingscondities gaven een goed beeld van de groenwaterbelasting die optreedt tegen de containers. Hieronder staan twee voorbeelden in dwarsgolven (270 graden) en schuin-achterinkomende golven (315 graden):

Voorbeelden van groenwater impacts in dwarsgolven (links) en schuin-achterinkomende golven (rechts)

Om een meer gedetailleerd inzicht te krijgen in de groenwaterbelasting op de containers, zijn daarna simulaties uitgevoerd met behulp van Computational Fluid Dynamics (CFD) met het COMFLOW-programma. De focus was hierbij op een aantal kritieke situaties die voorkwamen in de proeven. De figuren hieronder geven daar een aantal voorbeelden van.

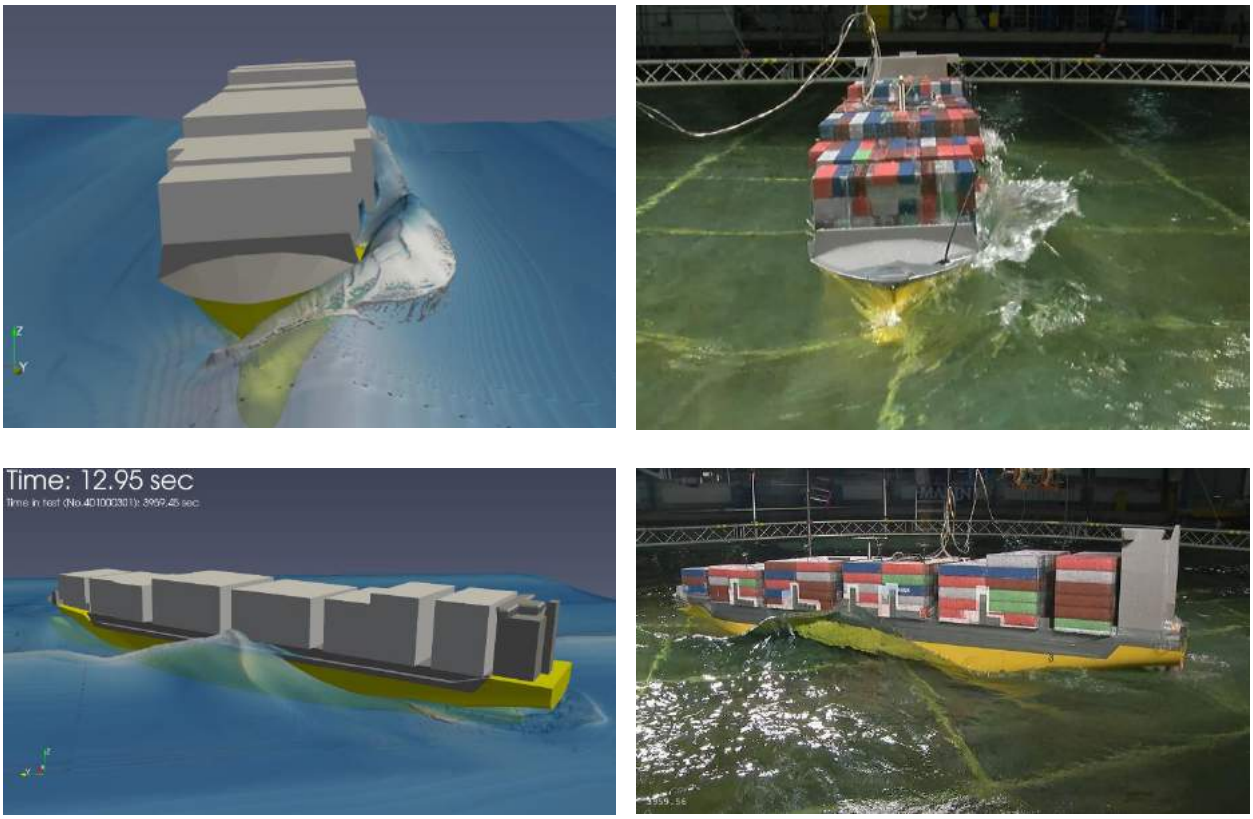

Vergelijk tussen COMFLOW CFD berekeningen en modelproeven in dwarsgolven (boven) en schuin-achterinkomende golven (onder)

De berekende dynamische drukken uit COMFLOW zijn daarna gebruikt om het gedrag van een stapel containers als gevolg van groenwaterbelasting te simuleren. Dit gebeurde met het Finite Element (FE) programma Abacus. Deze koppeling tussen de dynamische resultaten van CFD en FE berekeningen is uniek. De CFD berekeningen kosten zeer veel rekentijd op de zware supercomputer van MARIN: vele dagen rekentijd voor het uitvoeren van één simulatie.

In de figuur hieronder is het resultaat van een FE berekening te zien in één van de meest zware onderzochte situaties: de vervorming van de container nadat deze was geraakt door een klap groenwater. In dit geval werd de container als verloren beschouwd en waren de twistlocks met de containers erboven bezweken. Hierdoor kan de hele stapel containers over boord vallen.

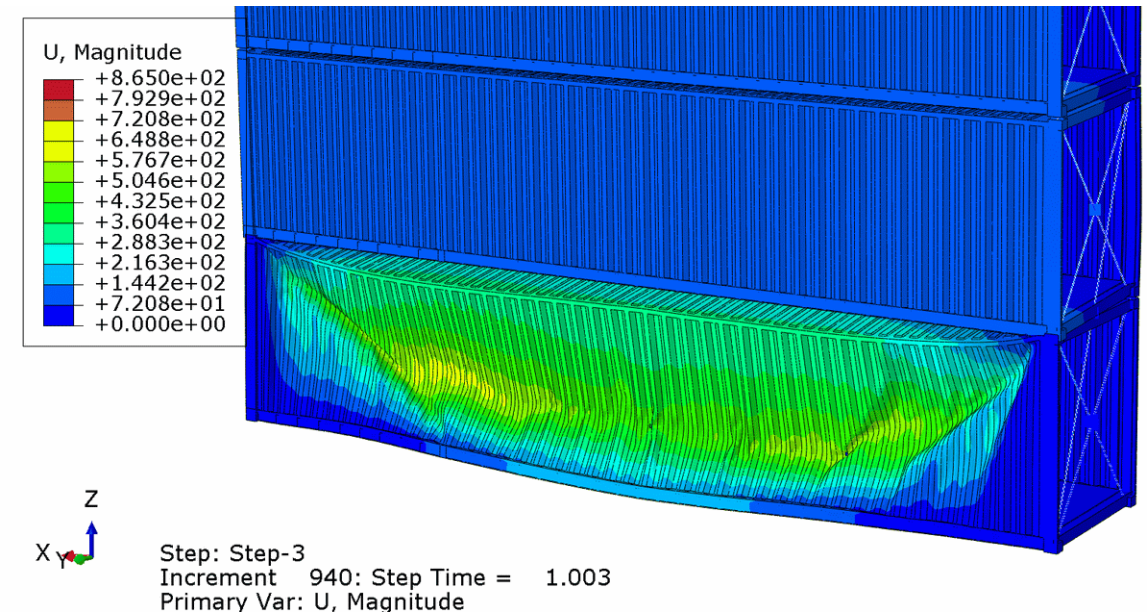

Beschadiging en vervorming van de container na FE simulatie van een kritieke case (simulatie 2-4)

De resultaten van deze berekeningen werden gebruikt om de bepalen welke relatieve golfhoogte tegen de containers toelaatbaar is zonder blijvende schade aan de containers.

Ook uit deze berekeningen komt een duidelijk verschil tussen de situatie in dwarsgolven (270 graden) en schuin achter inkomende golven (315 graden) zoals de onderstaande figuren laten zien. In dwarsgolven komt de groenwater klap direct over de volledige lengte van de container in korte tijd. In schuin achter inkomende golven verplaatst de druk en verplaatsing zich met de golftop die langs het schip loopt zodat de vervorming meer lokaal blijft.

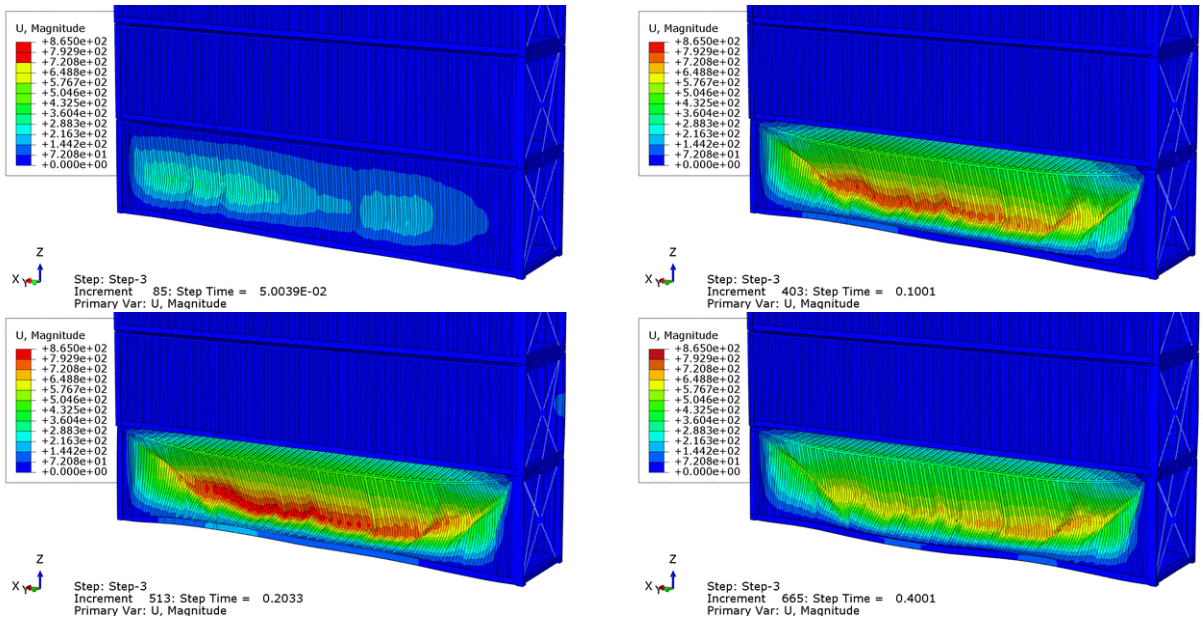

Vervorming container in tijd (0.05, 0.1, 0.2, 0.4 s) in dwarsgolven (270 graden): gehele container vervormt door gelijktijdige druk over volledige breedte (simulatie 2-4)

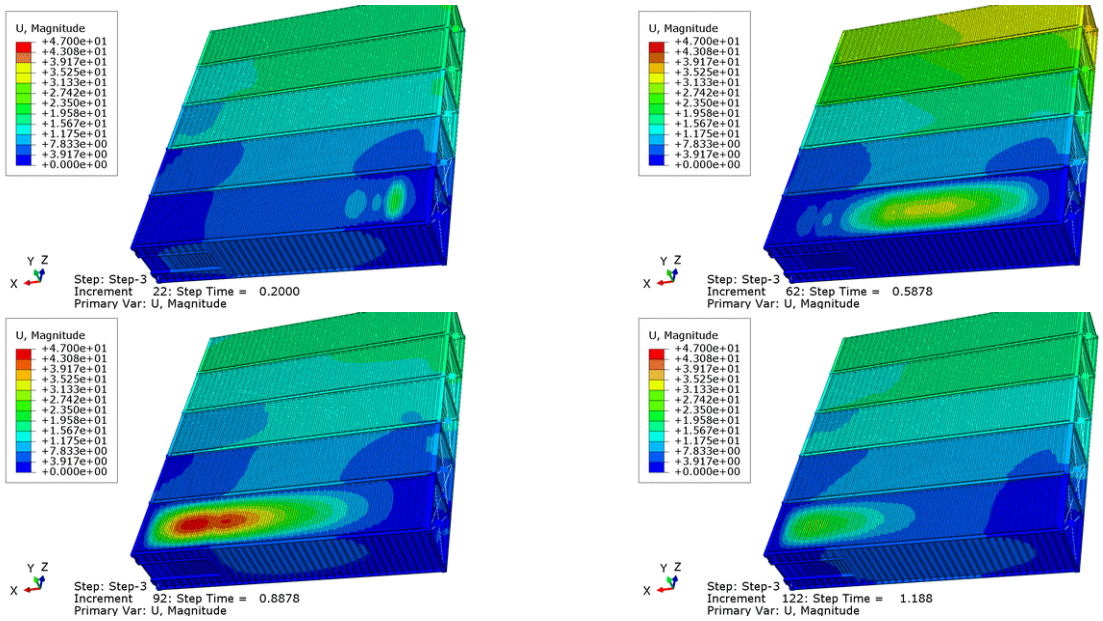

Vervorming container in tijd (0.4, 0.6, 0.8, 1.0s) in schuin-achterinkomende golven (315 graden): container vervormt lokaal en beperkt door golfpiek die van achter naar voren loopt (simulatie 2-6)

Resultaten

Uiteindelijk werden de resultaten van de uitgebreide modelproeven, groenwater simulaties met CFD en structurele (FE) berekeningen gecombineerd om tot beperkende golfhoogtes te komen voor groenwater belasting op Feeders. Dit is schematisch weergegeven in onderstaande figuur:

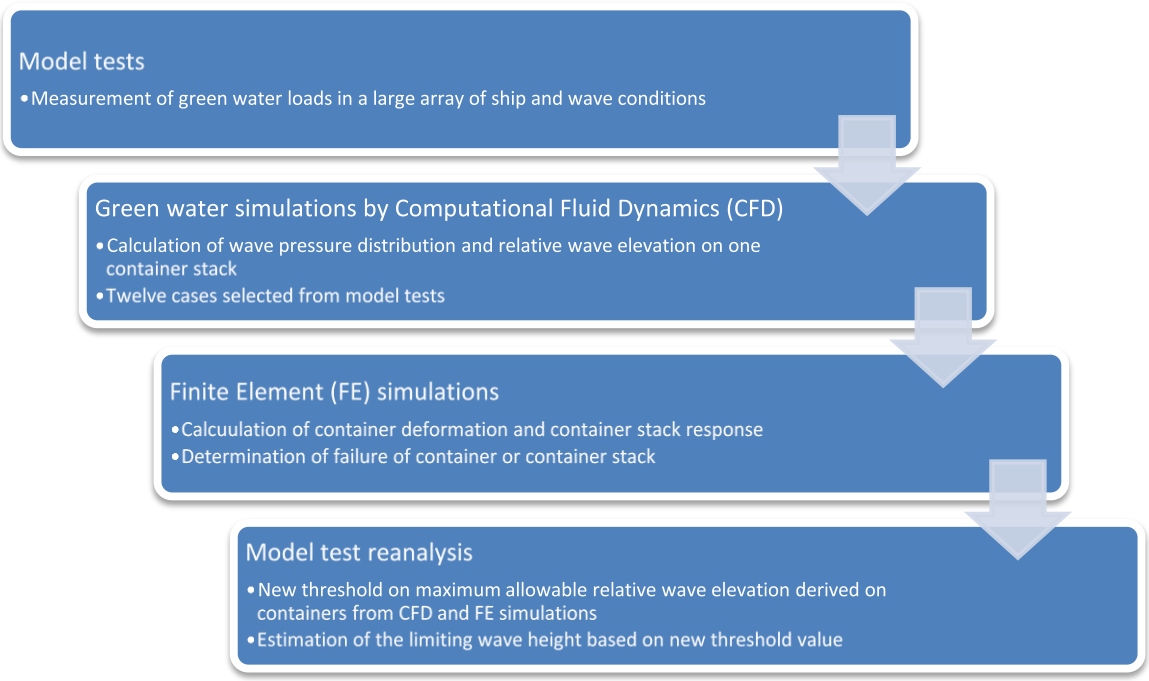

Methodiek voor het bepalen van de beperkende golfhoogtes

De resultaten van deze analyses zijn samengevat in de onderstaande tabel voor de onderzochte vrijboordhoogtes, containerconfiguraties en golfrichtingen:

Beperkende golfhoogtes voor 3 vrijboordhoogtes, 6 containerconfiguraties, 3 golfrichtingen en een waterdiepte van 21.3 meter

	Config 1	**Config 2**	**Config 3**	**Config 4**	**Config 5**	**Config 6**
Freeboard	**2.3 m**	**3.8 m**	**5.3 m**	**2.3 m**	**3.8 m**	**5.3 m**
135/225 graden	3.4 m	4.5 m	5.6 m	N/A[4]	4.6 m	N/A
90/270 graden	2.4 m	3.0 m	3.4 m	2.4 m	3.2 m	3.8 m
45/315 graden	3.5 m	4.9 m	6.0 m	N/A	N/A	N/A

Ook werd de gevoeligheid voor de waterdiepte bepaald voor configuratie 2:

Beperkende golfhoogtes voor 3 waterdieptes en 3 golfrichtingen (configuratie 2, vrijboord 3.8m)

Depth	**21.3 m**	**37.5 m**	**100 m**
135/225 graden	4.5 m	6.4 m	6.4 m
90/270 graden	3.0 m	3.1 m	3.1 m
45/315 graden	4.9 m	5.8 m	6.4 m

Ook werd gekeken naar de situatie in kopgolven: is deze kritiek wat betreft groenwater tegen de containers op de boeg en eventueel parametrische slingeren: slingeren in kopgolven?

De onderstaande figuur laat de groenwater belastingen zien in kopgolven in een range van golfcondities. Alleen bij golven van Hs = 7.5 m treden significante belastingen op de containers voorop het schip op.

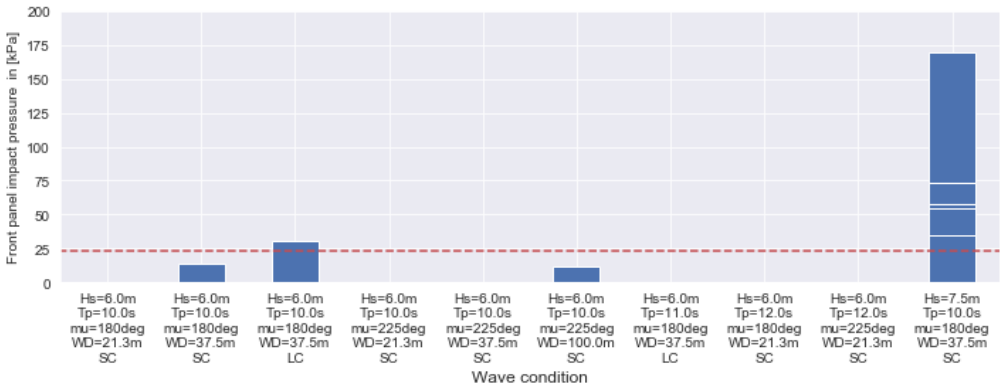

Groenwater belastingen op de voorkant van containers op de boeg in verschillende omgevingscondities

Tot slot werd onderzoek gedaan naar het mogelijk optreden van parametrisch slingeren in kopgolven. De onderstaande tabel geeft een overzicht van de resultaten. Alleen bij golven hoger de Hs = 6.0 meter treedt beperkt parametrisch slingeren op, maar de extreme slingerhoeken zijn beperkt. Slechts bij golven van Hs = 7.5 m observeren we dwarsscheeps versnellingen die in de buurt komen van de limieten zoals die door de classificatiemaatschappijen zijn bepaald in MARIN's vorige studie.

[4] Informatie niet beschikbaar ("Not Available")

Resultaten van de proeven gericht op het bepalen van parametrisch slingeren

Hs	Tp	Vs	Max roll amplitude	Max AY container amplitude
[m]	[s]	[kn]	[deg]	[m/s^2]
4.5	11.8	4	3.7	0.24
6.0	11.0	2	8.1	0.33
6.0	11.8	4	12.0	0.38
7.5	11.0	2	11.6	0.41

Conclusies en adviezen

De Nederlandse Kustwacht geeft om dit moment bij golven hoger dan Hs=3.3 meter het routeadvies[5] “om noodzakelijke maatregelen te nemen en/of een alternatieve koers”. Dit is gebaseerd op de resultaten van MARIN’s vorige studie in dwarsgolven (met een vrijboord van 3.0m).

De doelstelling van de huidige studie was om dit advies aan te scherpen wat betreft golfrichting en vrijboord. Wanneer we ons richten op de meest voorkomende configuratie van containers op het dek (in configuratie 1-3), dan komen we tot de volgende beperkende golfhoogtes:

Beperkende golfhoogtes als functie van vrijboord en golfrichting voor de meest voorkomende configuratie van containers op het dek

Vrijboord	**2.3 m**	**3.8 m**	**5.3 m**
135/225 graden (schuin-voorinkomend)	3.4 m	4.5 m	5.6 m
90/270 graden (dwarsgolven)	*2.4 m*	*3.0 m*	*3.4 m*
315 graden (schuin-achterinkomend)	3.5 m	4.9 m	6.0 m

De dwarsinkomende golven zijn nog steeds bepalend. Voor de range van onderzochte vrijboordhoogtes geldt een **beperkende golfhoogte** van 2.4-3.4m.

De resultaten voor de verschillende golfhoogtes laten zien dat dit advies onafhankelijk is van de waterdiepte:

Beperkende golfhoogtes als functie van waterdiepte (configuratie 2 met vrijboord 3.8m)

Waterdiepte	**21.3 m (zuidelijke route)**	**37.5 m (noordelijke route)**	**100 m (diepwater Noordzee)**
90/270 graden (dwarsgolven)	3.0 m	3.1 m	3.1 m

Als de golven nog hoger worden dan 3.0 meter, verslechterd de situatie in ondiep water wel sneller dan in dieper water.

De situatie in schuin voor- of achter inkomende golven (225 en 315 graden) wordt beter. De (relatieve) golven rond het schip worden minder hoog dan in pure dwarsgolven en de belasting op de container is meer lokaal en verplaatst zich met de golftop die langs het schip loopt. In dwarsgolven komt de groenwater klap direct over de volledige lengte van de container in korte tijd.

Maar het veiligste blijft om met de kop in de golven te gaan varen met lage snelheid (‘steken’). Tot golven van Hs=6.0 m zijn de belastingen op containers op de boeg in kopgolven beperkt en wordt er geen kritiek parametrisch slingeren geobserveerd.

[5] https://www.kustwacht.nl/nl/dossiers/routeadvies-waddeneilanden#routeadvies

1 INTRODUCTION

1.1 Background

In 2019 the Ministry of Infrastructure and Water Management requested MARIN to investigate the behaviour of three classes of container ships – a feeder, a Panamax and an ultra large container ship (ULCS) – in wave conditions encountered in the southern area of the North Sea[6]. The tests were meant to provide a better understanding of the relation between observed behaviour and risk for the ship to lose containers at sea, this in the aftermath of the MSC Zoe incident. One of the main conclusions from these investigations was that feeder ships are vulnerable to green water loading due to their particularly low freeboard: metocean data obtained from the ERA5 database show that the limiting wave height of 3.3 m, above which there is a present risk of green water impacts on containers, is exceeded during 350 hours cumulated over a year. Therefore, it was recommended to extend the scope of the investigations to obtain better insight in the complex problem of water loading on the containers, and establish the final limiting wave heights for this vessel. In its previous report, MARIN provided the following recommendations:

"Green water loading is the limiting factor for this type of ship on both routes. The (statistics of the) complex non-linear relative wave motions and impacts loads and response of (stacks of) containers need further study to determine the risk level and limiting wave heights more accurately. Also the freeboard height plays an important role in this. MARIN recommended to consider, beside beam waves, also head and bow-quartering waves in this investigation. Changing heading with the bow into the waves at slow speed seems a logical decision with large roll motions and green water in beam waves. However, it is important to investigate whether in head or bow-quartering waves, green water can also hit the containers from the side or over the bow.

Figure 1-1: Green water loading on the lowest tiers of deck containers on a feeder ship, MARIN report 32558-2-OB

As a response to occurrences of green water loads or excessive ship motions in oblique and beam waves the captain may decide to change the ship course so that she encounters the waves by the bow (head waves) at low speed or even zero speed, awaiting for the storm to die down. Nevertheless, preliminary calculations have shown that under such circumstances the ship might experience parametric rolling, because her limited size (up to approximately 200 m) becomes close to the shallow

[6] 'Further Investigations into the Behaviour of Container Ships in Storms above the Wadden Islands', Summary report, Report No. 32558-1-DIR, September 2020

water wave length. Therefore, the MARIN recommendations extend to include an investigation of parametric rolling for feeders:

"As part of this investigation we also recommended to further consider parametric rolling in head waves. Parametric rolling in head waves might occur for unfavorable combinations of wave length, wave period and natural roll period. It should be prevented that the decision to head into the waves, results in large motions due to parametric rolling. Although an extra set of tests on this topic did not show parametric rolling with the present small Feeder model, further tests are recommend to make sure this problem does not occur (or can be prevented by clear instructions to the crews."

1.2 Objectives

The objectives of the proposed investigations are:

- To better understand the process of green water loading on Feeders and the possible failure mechanisms for (stacks of) containers on the deck, including their statistics.
- To determine **final limiting wave heights** for green water on Feeders above the Wadden Islands, taking into account their freeboard and the wave heading relative to the ship.
- To better understand the possibility (and sensitivity) of parametric rolling of Feeders in head waves, to check whether a decision (or recommendation) to head into the waves in bad weather can result in parametric rolling and possible loss of containers.

1.3 Scope of work

The scope of work consisted of the following activities:

- Basin tests with a scale model of a typical feeder ship, which provide in the first place insight in the influence of parameters such as freeboard height, wave direction, etc… on the frequency of occurrence and intensity of green water on a feeder ship and their statistics. The tests serve also as a preliminary screening of the green water loads that will be further scrutinised by means of dedicated numerical simulations. Finally, the tests also allow to check the occurrence of parametric rolling in specific wave and speed conditions.
- Numerical simulations using Computational Fluid Dynamics aiming at reproducing a limited number of impacts witnessed during the basin tests, so that the underlying dynamics can be better understood.
- Finite Element Modelling computations of the cases considered in the aforementioned numerical simulations to determine the dynamics of stacks of deck containers.

2 FEEDER SHIP

In the following sections the selection of the feeder ship hull lines, freeboard heights and loading conditions for the model tests is discussed.

2.1 General considerations

The length and breadth of the feeder considered in the present study were kept identical to those of the case investigated in January 2020[7]. The draught were 8.0 and 8.7 m, which are representative of operational draughts of similar ships (AIS data). All particulars are provided on pages T1 and T2.

Table 2-1: Feeder ship main particulars

Description	Unit	Value
L_{PP}	[m]	163.0
B	[m]	27.0
D	[m]	11.0 - 14.0
T	[m]	8.0 - 8.7
Displ. (T=8.7 m)	[tons]	28,511

The hull lines were kept the same, except those at the bow where a more pronounced flare was adopted. The final lines are considered to be representative of an average feeder ship. The hull lines are shown on page F1.

2.2 Determination of freeboard height and freeboard type

Freeboard height

Because the occurrence of green water is sensitive to the freeboard height, it was important to obtain an overview of the freeboard of feeder ships. To do so two studies were conducted: the determination of the minimum freeboard based on the definitions of the 1966 Load Line Convention and a survey of freeboard heights of feeder ships with particulars similar to those listed in Table 2-1 from the Significant Ships database of the RINA in the period 1992-2021. For reference the freeboard height is understood as the vertical distance between the still waterline and the main deck at the side. From these studies three freeboard heights were considered in the tests: 2.3 m, 3.8 m and 5.3 m.

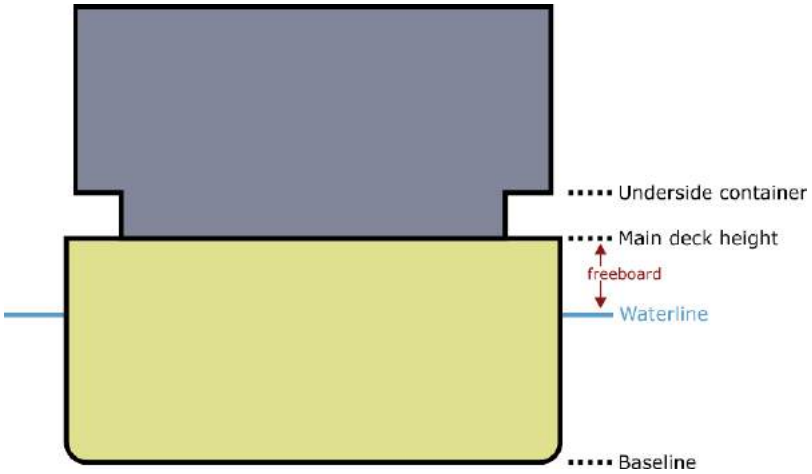

Figure 2-1: Freeboard definition

[7] Further Investigations into the Behaviour of Container Ships in Storms above the Wadden Islands', Summary report, Report No. 32558-1-DIR, September 2020

Because the minimum freeboard requirement as defined by the Load Line Convention depends on a large number of parameters (e.g. superstructure arrangement, block coefficient, etc…) a parameter variation study was carried out, considering 50,000 different combinations of all input parameters. The resulting minimum freeboard is shown by the green dots on Figure 2-2 (left figure). In this figure are also shown the freeboard heights from the RINA Significant Ships of length between 120 and 170 m (blue dots), the minimum freeboard requirement when Table 28 from the LL1966 Convention is applied without corrections (red line) and the lowest freeboard height considered during the model tests (2.3 m). It can be seen that the adopted lower freeboard height during the model tests is among the lowest possible according to the LL1966 Convention and the selection of Significant Ships. On the right figure of Figure 2-2 are shown the freeboard heights from the same selection of Significant Ships together with the three selected freeboard heights for the model tests. It can be seen that the adopted heights cover well the entire range of freeboard heights from the Significant Ships.

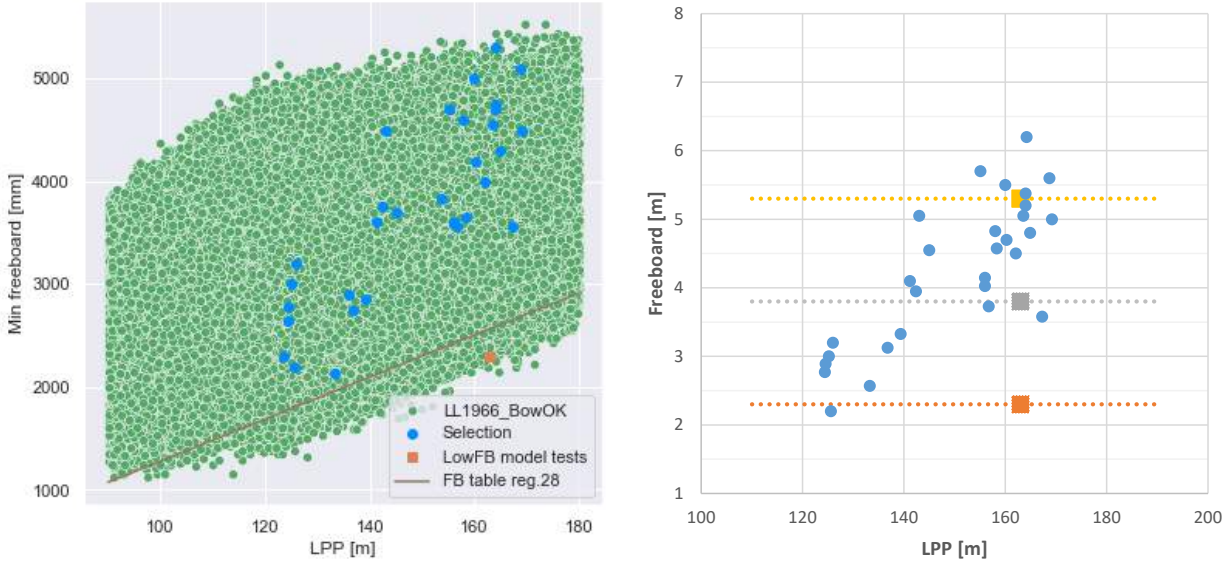

Figure 2-2: Freeboard height determination

Freeboard type

Next to the freeboard height the freeboard layout was considered to be of importance in the determination of green water loads on deck containers. Therefore research was undertaken to determine the possible freeboard layouts applied on feeder ships, based on available photographs. A selection of the ships looked at is presented in Figure 2-3: the 152 m “Wes Janine” (top left), the 169 m “Eilbek” (top right), the 168 m “Elysee” (bottom left) and the 151 m “Bernhard Schepers” (bottom right).

The research work showed that a dominant proportion of the ships has a freeboard layout comparable to that of the “Wes Janine” or “Bernhard Schepers”, with deck containers covering the entire ship breadth. In this layout the outermost containers lie only partly on the hatch cover, while the other part “hangs” above the side gangways. Because the underside of these containers is not sheltered by a plate cover, it is exposed to the outside environment. It is estimated that about two third of the container underside panel (meaning 1.7 m in width) is exposed. A very limited number of ships show a different layout. In the first place the Eilbek, on which the deck container rows do not extend over the complete breadth, leaving a gap to the ship side of approximately 1 m. All containers lie on the hatch cover. Differently, open-top containership Elysee features a very high side coaming (in red on the picture), behind which the containers are stowed. It should nevertheless be noted that the aftmost and foremost bays show a more classic layout, comparable to that of the “Wes Janine”.

Figure 2-3: Freeboard layout on four different feeder ships

In the light of the above it was decided to adopt two different freeboard layouts on the scale model. The first one derives from the more common layout, as encountered on the “Wes Janine” or the “Bernhard Schepers”. In this layout the depth of the gangway (in transverse direction) is estimated to be 1.7 m, the height 2.5 m. The second layout is similar to that as found on the Eilbek, hence with all containers are stowed on deck or hatch cover. For practical reasons during the tests a hatch head of 2.5 m as in the first layout remained. Photographs of the model with both layouts are shown in Figure 3-3.

3 BASIN MODEL TESTS

3.1 Scale model

A wooden model of the feeder was manufactured at a geometric scale of 1 to 33, designated model No. 10246. An overview of the model is shown in Figure 3-1. The model was equipped with an active propulsion system with MARIN stock propeller, one rudder and one pair of bilge keels. It should be noted that the bilge keel height was different between the green water tests at zero speed (0.5 m) and the parametric roll tests in transit (0.4 m). Propeller and other appendages particulars and drawings are found in pages T3, F10 and F11.

Variations in freeboard height were achieved by inserting wooden elements underneath the model's main deck. This means that the distance from keel to main deck was raised, the gangway height remaining the same in all configurations. Variations in freeboard type were realised by adding or removing superstructure elements located at the ship centreline. For reference a number was assigned to each combination of freeboard height and type, see Figure 3-2 and pages F3 to F8. Pictures of the model under configurations 1 and 5 is shown in Figure 3-3.

Figure 3-1: Overview of model No. 10246

The weight distribution of the model was adjusted prior to the tests based on preliminary estimations of ship displacement, inertia and CoG location. After each modification brought to the superstructure (change in freeboard height or type, see above) the metacentric height was checked by means of a heeling test. All configurations considered, the metacentric height was found to lie between 0.8 and 1.4 m (target: 1.2 m). The natural roll period was measured twice by means of a roll decay test: for configuration 1, prior to the start of the green water tests (19.6 s) and prior to the parametric roll tests in transit (20.9 s).

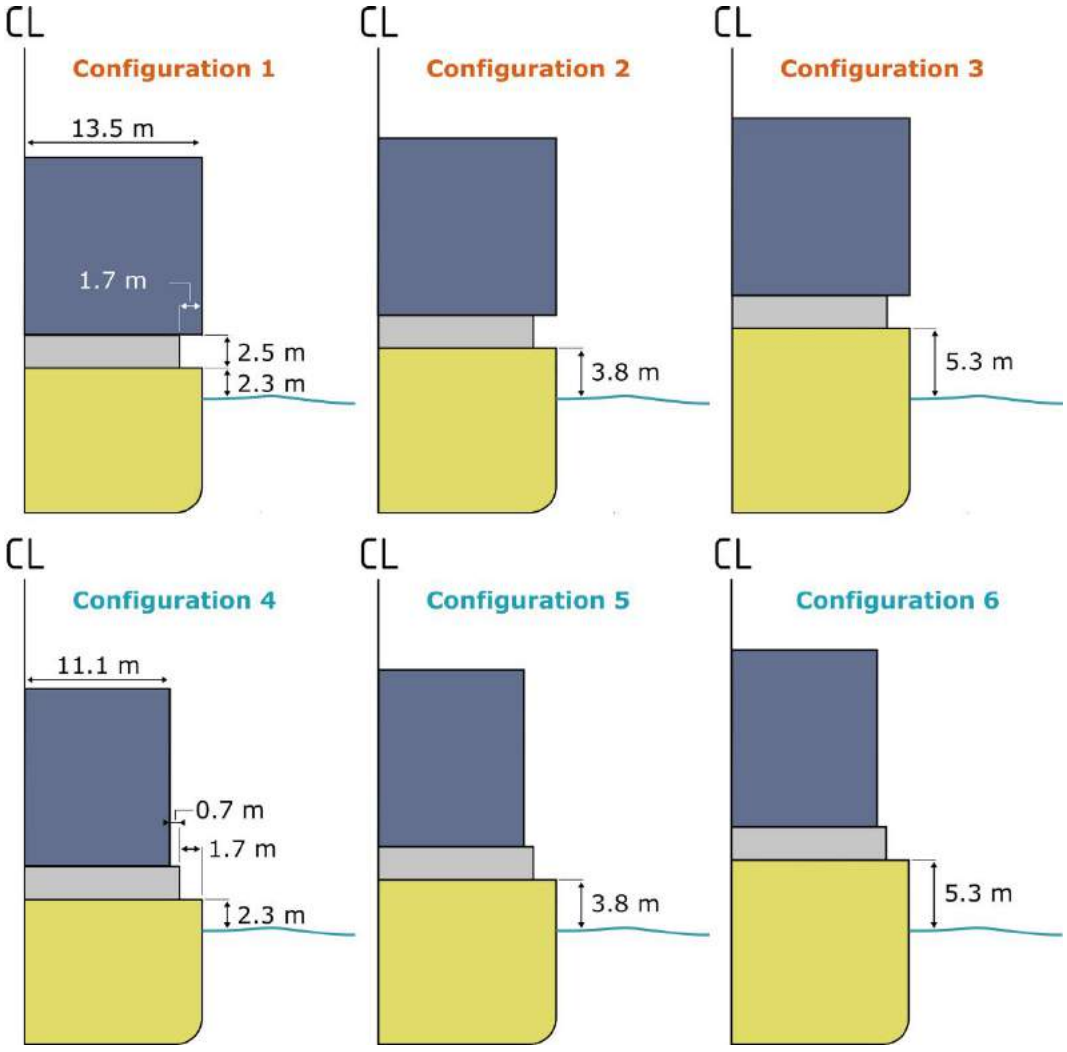

Figure 3-2: Freeboard configurations 1 to 6

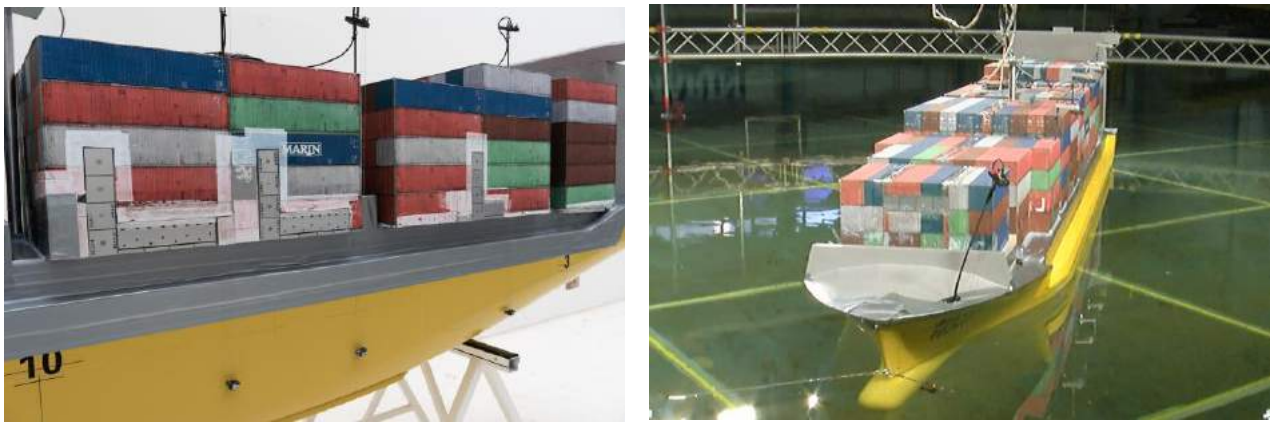

Figure 3-3: Adopted freeboard layouts on the scale model (left: Config. 1, right: Config. 5)

3.2 Test facility and arrangement

3.2.1 Green water loads model tests

The green water loads model tests were conducted in the Offshore Basin (OB) of MARIN which measures 45 x 36 x 10 m in length, width and depth. It is equipped with wave makers along two sides, consisting of flaps individually driven by an electric motor. This facilitates the generation of regular and long- and short-crested irregular waves from any direction. A carriage provides the required power and absorbs the measured data to the model via free-hanging umbilicals.

During the tests the free-floating model was kept in position by means of four mooring lines with soft springs fixed to the basin carriage ring, see page F13. The mooring arrangement, including spring stiffness and line pretension were chosen to minimise its effect on the ship motions. Dedicated motion decay tests in moored condition show that the period of the horizontal motions (surge, sway and yaw) is at least twice the natural roll period, which is deemed acceptable. The mooring stiffness and pretension are reported in page T7, the analysis of the decay tests in moored condition in Section B of the data report.

It should be noted that changes in wave heading relative to the ship was achieved by changing the heading of the model in the basin. This allowed to apply the same wave realisation for various wave headings, leading to a better comparability among wave headings and a reduction in wave calibration time.

3.2.2 Parametric roll model tests

The parametric roll model tests were conducted in the Shallow Water Basin (SWB) of MARIN which measures 220 x 15.75 x 1.15 m in length, width and (maximum) depth respectively. The basin depth can be adjusted by pumping water in and out the basin. It is equipped with one large piston-type wave maker at the short side driven by an electric motor. Because of the unique wave maker only long-crested waves can be generated.

During the tests the model was free-sailing, and self-propelled. The connections between model and carriage consisted only of free-hanging thin electric wires for the relay of measurement signals and power supply. These cables did not noticeably influence the motions of the model. The model steering was managed by an autopilot reacting on sway, yaw and yaw velocity. Autopilot settings are given in page T3.

Figure 3-4: Testing facilities (left: Offshore Basin, right: Shallow Water Basin)

3.3 Instrumentation, definitions and notations

3.3.1 Heading and coordinates

The coordinate system and related sign conventions follow ITTC standards. The heading (μ) of the vessel is given in a ship co-ordinate system; it is defined as the angle between the direction of wave propagation and the direction of the vessel's bow. The following sign convention for the heading and reference system for positions applies:

Table 3-1: Reference system

X=0	at aft perpendicular and positive forward
Y=0	at centreline and positive to portside
Z=0	at base line and positive upward

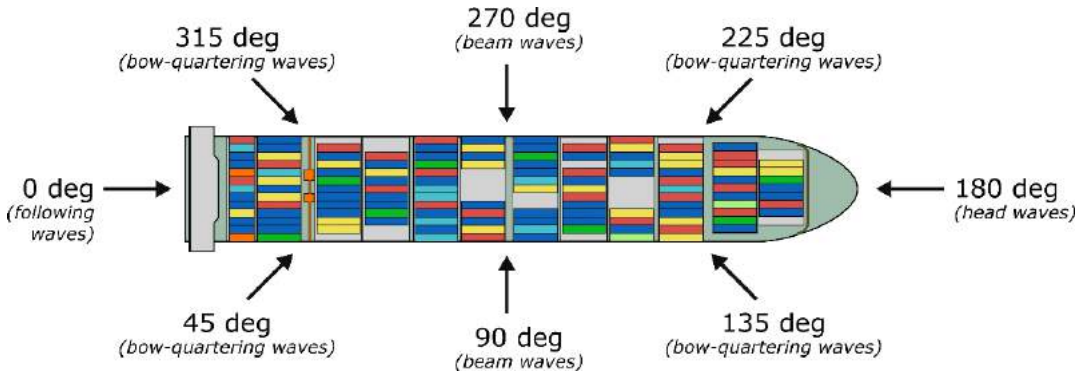

Figure 3-5: Heading convention

3.3.2 Notation and sign conventions

Table pages T4 through T6 summarise the notation and sign conventions adopted for the directly measured and derived signals. The most important of these are that translations are positive in the forward direction with respect to the vessel, to port side and upwards. Rotations are positive starboard down, bow down and bow to port.

3.3.3 Instrumentation

A complete description of the measured quantities and location of the measuring equipment is provided on pages T4 to T6, and F2 to F9. These include:

- **6 degrees of freedom** ship motions by means of optical tracking system;
- **Ship speed** by means of optical tracking system combined with the carriage position;
- **Ship-fixed longitudinal, transverse and vertical accelerations** by means of accelerometers at four locations in the model;
- **Wave loads at several container locations** by means of force panels of size 5 cm x 5 cm;
- **Relative wave elevation along the ship windward side** by means of resistive wave probes;
- **Rudder angle** by means of a potentiometer**;**
- **Propeller revolutions** by means of a digital encoder;
- **Incident wave elevation** at two locations, by means of resistive wave probes fixed to the carriage.

The ship 6DOF, speed, propeller revolutions and incident wave elevation were measured at a sampling rate of 100 Hz model scale (17.4 Hz full scale), accelerations, rudder angle and relative wave elevation at 200 Hz (34.8 Hz f.s.) and wave loads at container locations at 9,600 Hz (1671.1 Hz f.s.).

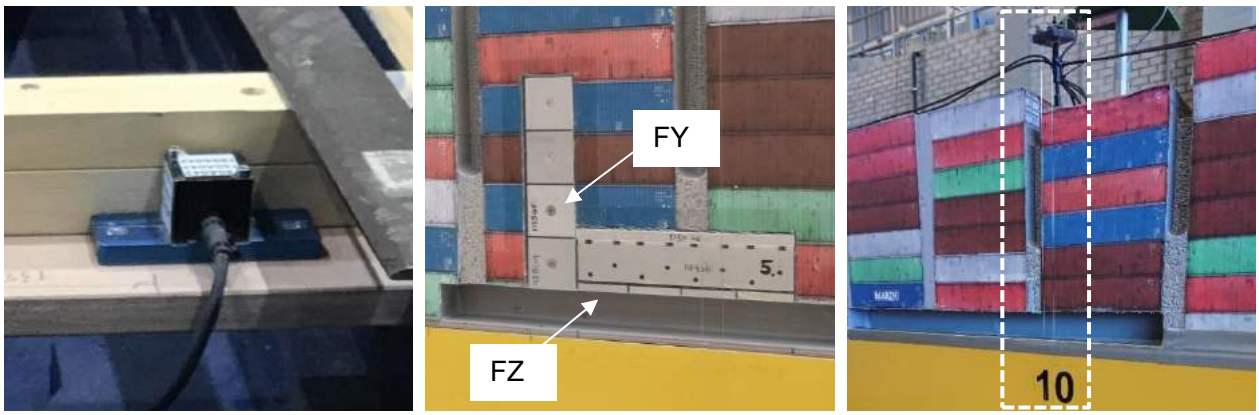

Figure 3-6: View of some of the instrumentation installed on the models (left: accelerometer, middle: force panels, right: resistive-type wave probes)

The force panels were square panels of 5 cm at model scale (1.65 m at full scale), located on the ship side and above the breakwater, see Figure 3-7. The number of panels measuring either a longitudinal (X), transverse (Y) or vertical (Z) force is indicated in between brackets. It should be borne in mind that in freeboard configurations 4 to 6 vertical forces were not measured.

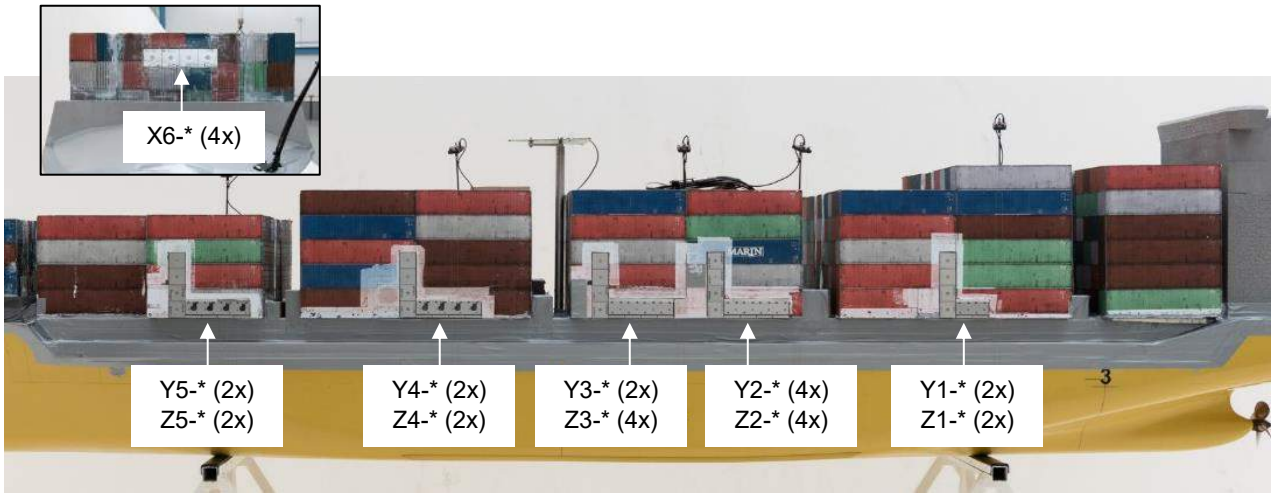

Figure 3-7: Force panel layout on the model

Not all quantities were measured during all green water load and parametric roll tests. Table 3-2 provides an overview of the measurands during the different tests.

Table 3-2: Measurands during the different tests

	Green water load tests	Parametric roll tests
6DOF motions	X	X
Ship speed	-	X
Accelerations	X	-
Wave loads	X	-
Rel. wave elevation	X	-
Rudder angle	-	X
Propeller revs	-	X
Incident wave elevation	X	X

3.3.4 Photo and video equipment

All tests were video-recorded from three different viewpoints:

- ship bow and ship stern, seen from port side, using two cameras fixed on the basin carriage (frame rate 25 frames per second, or 3.1 frames per second at full scale);
- ship windward side, using one camera fixed on the basin carriage (frame rate 238 frames per second, or 30.0 frames per second at full scale).

Digital photographs were also made during the tests from various viewpoints.

3.3.5 Data reduction

The results of the measurements were scaled up to full size values according to Froude's law of similitude. The scaling factors as applied are shown in Table 3-3.

Table 3-3: Data scaling[8]

Quantity	Scaling factor	Model	Prototype
Linear dimensions	$\lambda = 33.0$	1 m	33.0 m
Volumes	$\lambda^3 = 35{,}937$	1 dm^3	35.9 m^3
Forces	$\gamma\lambda^3 = 36{,}835$	1 kg	36.8 t
		1 N	36.8 kN
Angles	1	1 deg	1 deg
Linear velocities	$\lambda^{0.5} = 5.74$	1 m/s	5.74 m/s
Angular velocities	$\lambda^{-0.5} = 0.174$	1 deg/s	0.174 deg/s
Linear accelerations	1	1 m/s^2	1 m/s^2
Angular accelerations	$\lambda^{-1} = 0.030$	1 deg/s^2	0.030 deg/s^2
Time	$\lambda^{0.5} = 0.17$	1 s	0.17 s

3.3.6 Analysis and data-processing

Wave calibration

Most of the incoming waves were measured prior to the tests and calibrated so that the spectral shape showed a good agreement with specifications. Some waves were added in the course of the tests and were measured at the end of the test campaign, after the model had been removed from the basin.

Roll decay tests

Linear and quadratic roll damping coefficients were extracted from the roll decay tests. Based on these coefficients a linearised roll damping was derived.

Green water loads

Force panel dynamics

The dynamics of the force panels installed on the model were determined prior to the seakeeping tests by means of so-called "hammer tests". During these tests each panel was hit by a specific hammer. Because the impact force generated by the hammer is not only measured by the panel but also directly at the hammer, it is possible to determine the response characteristics of the force panel, namely its

[8] Note: γ is the ratio of the specific mass of seawater to that of the fresh water in the basin, with $\gamma = 1.025$. All measured pressures and loads refer to seawater conditions; in fresh water the loads reduce by 2.5%.

quasi-static amplification factor and natural period. A detailed description of the force panel dynamics is given by Van de Bunt et al.[9].

All panels are found to have a natural frequency comprised between 1.8 and 2.3 kHz model scale (approximately 350 Hz full scale, which make them among the stiffest force measuring systems available. The accuracy at which impact peaks are measured is very much dependent on the impact duration: while impacts of a few tenths of a second at full scale are very well captured, impacts of a few hundreds of a second lead to strong overshoot and resonance of the panel (see Figure 3-8). These different behaviours are observed when either more hydrostatic or more dynamic green water loads against the containers are observed, respectively.

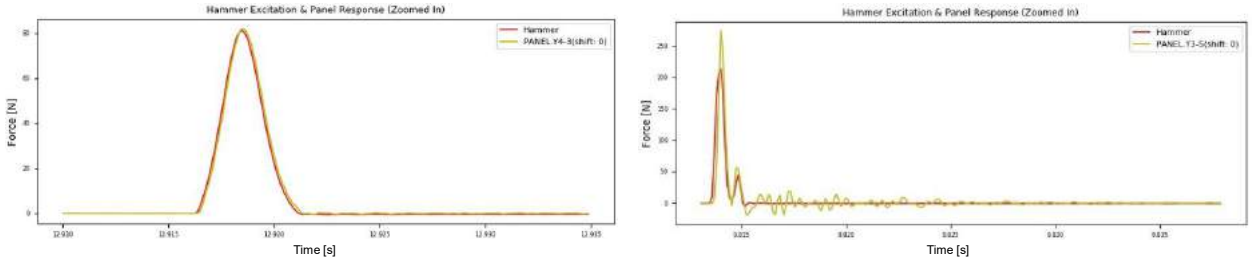

Figure 3-8: Hammer test analysis (left: hammer impact force vs measured force by panel for a long impact, right: hammer impact force vs measured force by panel for a short impact)

Post-processing of wave load measurement

Wave load measurements by means of panels were subject to signal treatment before further analysis could be conducted. The treatment mainly consisted in removing false positives caused by ship motions and vibratory behaviour linked to slamming or motor noise. Also, the signals showed high-frequency noise difficult to remove since low-pass filtering could affect the amplitude of the green water loads. This resulted in selecting the peaks in the measurements that were higher than 100 kN at full scale.

Although some of the measured impacts show resonant behaviour of the force panel, it was decided not to apply any filtering to the measured impact forces. This decision was motivated by the fact that filtering would not bring a significant improvement in the quality of the measurement quality.

The forces measured at the panels located on the windward side of the container stacks were further post-processed to determine in a first step a mean pressure, and subsequently a force equivalent to the side of a container. The mean pressure was assumed to be uniformly distributed over the panel and was calculated as follows:

$$P_{mean} = \frac{F_{meas}}{A_{panel}}$$

where F_{meas} is the full scale force measured over a given panel and A_{panel} the panel area at full scale being 2.7 m^2. The mean pressure was in turn translated into an equivalent force for the side of a container. The container panel areas considered in the calculation are listed in Table 3-4.

Table 3-4: Full scale container panel area

Side panel	Underside panel
12.2 x 2.6 **31.6 m²**	12.2 x 1.7 **20.0 m²**

[9] Van de Bunt et al., “Applying force panels for wave impact measurements”, Ocean Engineering 232(12):108857, 2021

Green water limit used in previous studies

To determine the capacity of present day containers against green water loading on container side surfaces, finite element calculations were carried out in our previous study[10]. The green water pressure was assumed as uniform over the front or side panel surface for both yielding and buckling analyses.

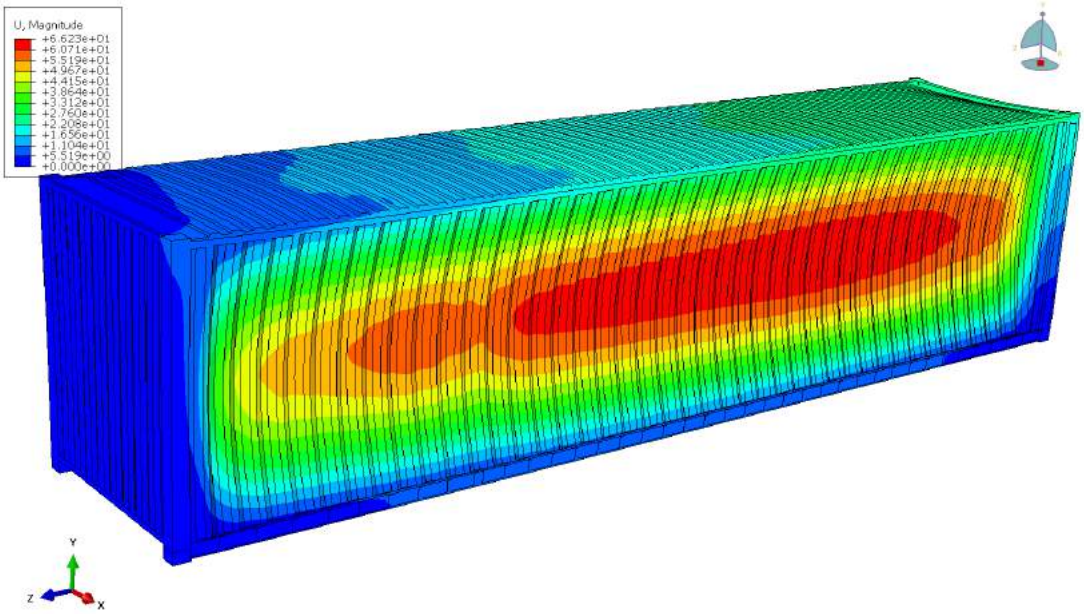

Figure 3-9: Max. full scale displacement in [mm] as determined by FE simulations in the previous study

The limiting yielding and buckling load pressure values are given in Table 3-5. Based on these low values (a side panel yield limit of 11 kPa), in our previous study we assumed that for the derivation of the preliminary limiting wave heights the criterion should be that green water does not touch the containers. This can be ensured based on the criterion that the extreme relative wave motions along the side of the ship do not exceed the threshold of the lowest container, as shown in Figure 3-10.

Table 3-5: Limiting pressure and load values at yielding and buckling limits for a 40 ft container

	Pressure at yielding limit	**Pressure at buckling limit**
Side panel	9.07 kPa	10.99 kPa
Front panel	21.26 kPa	22.71 kPa

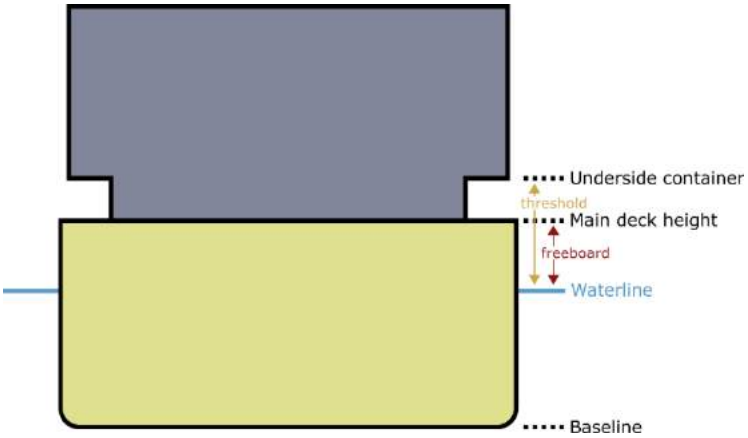

Figure 3-10: Definition of the freeboard (waterline to main deck level) and green water threshold for relative wave motions (waterline to underside container

[10] 'Further Investigations into the Behaviour of Container Ships in Storms above the Wadden Islands', Summary report, Report No. 32558-1-DIR, September 2020

Threshold wave height from measurement of relative wave elevation

Because of the low number of significant wave loads measured on the panels the relative wave elevation along the windward side of the model was used instead to estimate limiting significant wave heights regarding the occurrence of green water. The estimation consisted first in the determination of a most probable maximum (mpm) relative wave elevation for the duration of a standard test (3 hours full scale), obtained by a curve fitting of the tail of the cumulative distribution of the relative wave elevation (1% of highest events was considered). A reasonable fit was obtained using a negative exponential function:

$$P(X > X_A) = \alpha e^{\beta(X_A - X_0)}$$

where α and β are the fit parameters and X_0 the amplitude of relative wave elevation corresponding to a probability of exceedance of 1%. The fit parameters were obtained by minimising the cumulative sum of the absolute difference between the logarithms of the estimate and the realised distributions:

$$f(\alpha, \beta) = \sum_i \left| \log\left(\alpha e^{\beta(X_i - X_0)}\right) - \log(P(X > X_i)_{real} \right|$$

An impression of the realised fits for the three vessels is seen in Figure 3-11.

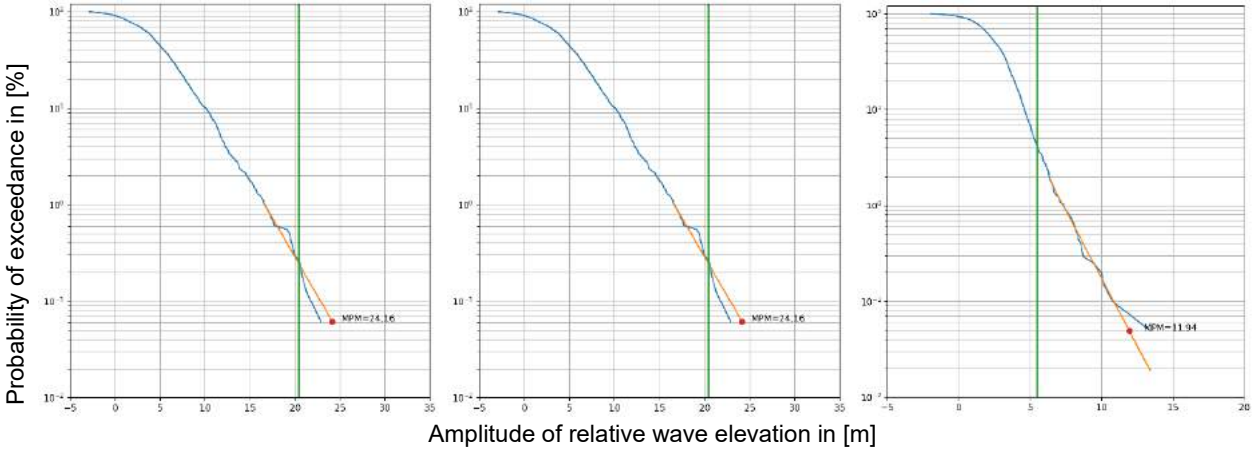

Figure 3-11: Negative exponential fit of the tail (1% highest amplitudes) of the cumulative distribution of the relative wave elevation

The mpm's and associated significant wave heights were subsequently fitted linearly (see Figure 3-12). The fit was interpolated or extrapolated to determine the threshold wave height. The threshold was defined as the wave height, for which the mpm is equal to the freeboard to lowest container tier. From the mpm's obtained at all measurement locations the lowest is selected as overall threshold.

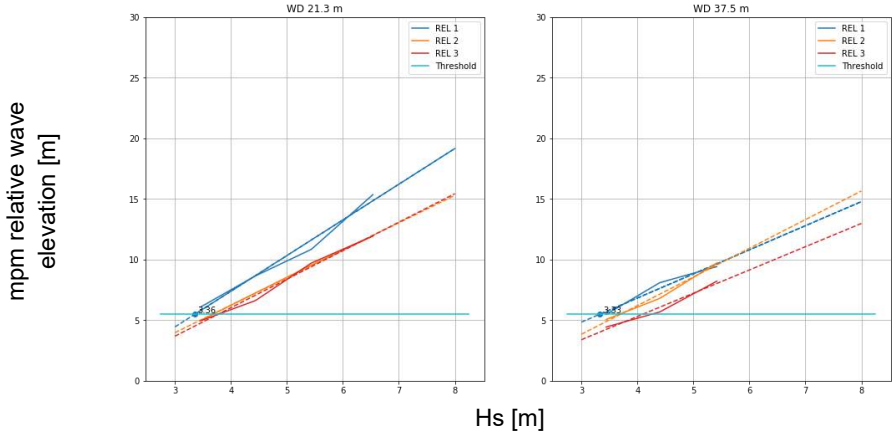

Figure 3-12: Linear fit through mpm estimates for the various measurement locations (REL 1 to REL 3) – feeder ship. The linear fit is interpolated (extrapolated) to determine the threshold wave height

3.4 Test programme

3.4.1 General considerations in the preparation of the test programme

The test programme consisted of two parts: one large part was dedicated to the prediction of green water loads in various combinations of ship arrangement and wave conditions, a second, more limited part aimed at quantifying the roll behaviour of the ship when sailing in wave conditions where parametric roll is likely to occur.

3.4.2 Green water load tests

Wave conditions

The wave conditions considered during the green water load tests are summarised in Table 3-6. The conditions listed under “main wave conditions” follow from a metocean analysis of the southern North Sea using the 40-year ERA-5 hindcast database. The other conditions, derived from the main conditions by applying a gain to the wave-maker, were used to determine wave height thresholds as explained further down.

Table 3-6: Wave conditions considered during the green water load tests

Hs	Tp	SC/LC	Seed	Water depth
[m]	[s]	[-]	[-]	[m]
Main wave conditions				
3.0	7.0	SC	X	21.3, 37.5, 100.0
3.0	9.0	SC		21.3
4.5	8.5	SC	X	21.3, 37.5, 100.0
4.5	10.0	SC		21.3
6.0	10.0	SC		21.3, 37.5, 100.0
6.0	12.0	SC		21.3
3.0	7.0	LC		21.3
4.5	8.5	LC		21.3
6.0	10.0	LC		21.3
Variations in wave height				
1.2	7.0	SC		21.3
1.2	9.0	SC		21.3
1.8	7.0	SC	X	21.3
1.8	9.0	SC		21.3
2.1	7.0	SC		21.3
2.4	7.0	SC		21.3
2.4	9.0	SC		21.3
3.6	7.0	SC		21.3
3.8	7.0	SC		21.3

SC/LC: short-crested or long-crested
Seed: variation in wave realisation, for same Hs and Tp

The heights of the main wave conditions were selected in a window ranging between 3.0 and 6.0 m. The lower limit of 3.0 m was selected based on the preliminary estimated limiting wave heights for feeders (3.3 m) as mentioned in report 32558-1-DIR and included in the Dutch Coast Guard’s

navigational warning issued to all ships[11]. The higher limit (6.0 m) is among the most severe wave conditions encountered in the area, occurring 7 hours per year in average.

For each wave height among the main conditions two peak periods were considered: the first relatively low in comparison with the distribution of periods observed for the given wave height, the second relatively high (see illustration in Figure 3-13). The low wave peak period yields short, steep waves with regular wave-breaking.

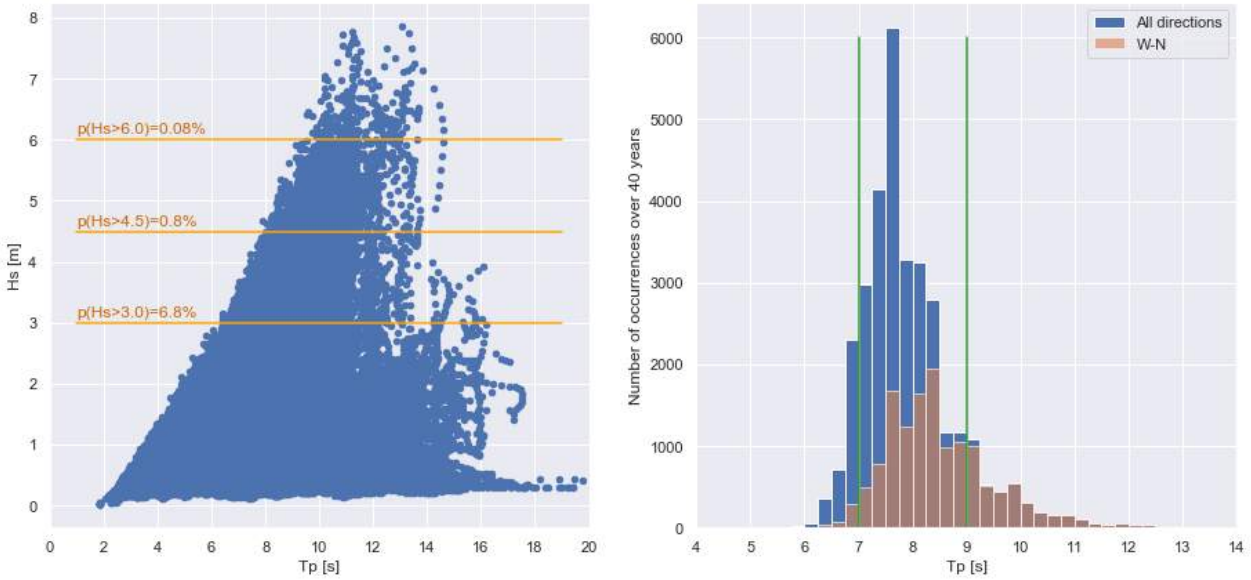

Figure 3-13: Left: wave scatter diagram of the southern North Sea (40-year ERA5 DB) with probabilities of exceedance of wave heights considered in Table 3-6. Right: Selection of peak periods (green lines) based on probability distribution for given wave height (here Hs=3m)

Effect of freeboard type and freeboard height

A large part of the test programme was dedicated to the quantification of the influence of freeboard type and freeboard height on the frequency of occurrence and amplitude of green water on the ship side. For each configuration at least two beam wave conditions were applied. For configurations 1, 2 and 3 (see Chapter 3 for further information) some additional variations in wave height were performed to estimate a threshold below which no occurrence green water would be reported.

Effect of wave heading relative to ship

By default all wave conditions shown in Table 3-6 were tested in beam wave conditions, as it was considered beforehand as the most critical wave heading. The influence of wave heading was nevertheless investigated for a selected number of conditions, mostly considering bow-quarter or stern-quarter. For one condition (Hs = 3.0 m, Tp = 7.0 s, short-crested) the wave heading was varied from following waves to head waves by steps of 30 deg.

Effect of water depth

Three wave conditions were carried out at three different water depths: 21.3, 37.5 and 100 m. The first depth is considered to be representative of those encountered along the Terschelling-German Bight Traffic Separation Scheme (so-called “southern route”), the second of those encountered along the East Frisian TSS (“northern route”) while the last corresponds to the deepest areas of the North Sea. It should be noted that a different wave realisation was considered and calibrated for each water depth, as depth was expected to affect the wave spectral shape.

[11] https://kustwacht.nl/en/route-advice-wadden-islands

Effect of short-crestedness

Experience from previous projects showed that the occurrence of green water is influenced by wave direction spreading: waves with little direction spreading, usually referred to as “long-crested” or “2D-waves”, yield more frequent and more intense occurrences of green water than short-crested waves. In order to evaluate such influence a selection of the above wave conditions was tested in both long-crested and short-crested forms. The spreading in wave direction of the short-crested waves was described by a $\cos^6$ function.

Figure 3-14: Long-crested waves (left) and short-crested waves (right). The dash lines underline the crest of the long-crested waves

Effect of wave realisation

For three of the wave conditions listed in Table 3-6 five different wave realisations were tested to determine the possible scatter in observed green water loads. The different wave realisations were obtained by changing the inner relation between the phases of the various wave components forming the irregular wave train. While the time traces of the wave realisations are different, the associated Hs, Tp and spectral shape remain the same.

Test duration

The adopted test duration was three hour full scale (standard for offshore model tests with focus on ship motions). As the model is kept at a fixed location by means of soft springs, the test can be done in one experiment since beaches on the side suppress all basin wave reflections. This ensures enough wave realisations, good statistical description of the ship motions and accelerations and a good estimate of the probability of a contact with the bottom. Three hours is approximately the duration of a typical wave condition at sea (before it evolves).

3.4.3 Parametric roll tests

The parametric roll tests consider wave conditions corresponding to moderate to strong gales (Beaufort 7 to 9), in which feeders are expected to take adaptive measures, such as weathervaning. In such condition the ship is expected to head into the waves, with zero to little forward speed (maximum assumed 4 kn). The test duration varied between 1 and 3 hours full scale.

Table 3-7: Wave conditions considered during the parametric roll tests

Hs	Tp	SC/LC	Water depth
[m]	[s]	[-]	[m]
4.5	11.8	LC	33.0
6.0	11.0	LC	33.0
6.0	11.8	LC	33.0
7.5	11.0	LC	33.0

3.5 Results and discussion

3.5.1 Green water loads

The measurement of the wave loads coupled with direct visual observations indicate that the dynamics of green water can be very different. In beam waves, impacts against the containers were very often caused by short, steep waves with relatively large horizontal velocity, which break against the side of the ship. On the measurements the associated loads are characterised by a very sharp peak, caused by the slamming of the breaking wave, followed by a relatively slow decay which denotes the subsequent hydrostatic loading induced by the mass of water. In other cases, less steep waves of relatively small velocity generate a mostly hydrostatic load, which is characterised by a longer-lasting peak. Another type of green water is observed at moments where the windward side of the ship undergoes a significant downward motion, as the result of combined heave and roll, following which the effective freeboard is so low that even moderate wave crests are able to reach the freeboard deck and containers. In oblique wave directions (waves originating from the bow-quarter and stern-quarter), the waves build up along the ship side, due to the combined effect of diffraction (reflection) and radiation from ship motions. Several occurrences of green water impacts are illustrated in Figure 3-16 and Figure 3-17.

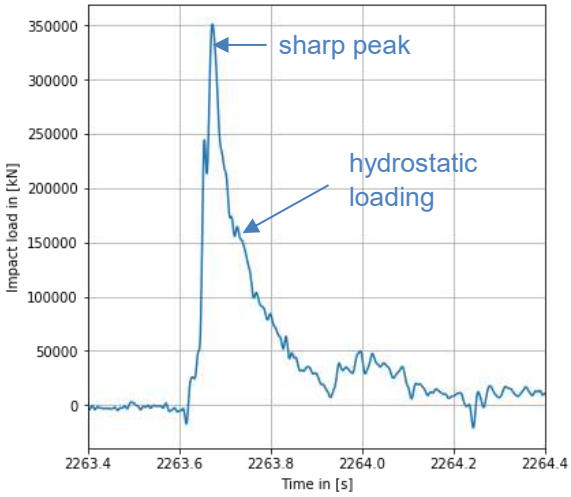

Figure 3-15: Wave load measurement

Figure 3-16: Green water load from steep, breaking beam waves

Figure 3-17: Green water load from in stern-quartering waves

The test campaign focused on two sea states: a significant wave height of 3 m with peak periods of 7 and 9 s and a significant wave height of 4.5 m and peak periods of 8.5 and 10 s. This selection was made in order to gain better insight in the wave loads that can be experience by feeder ships in waves close to the threshold currently considered by the Dutch Coast Guard (3.3 m) above which Navtex warnings are issued[12]. Other wave heights were also considered (from 1.2 to 6 m), depending on the adopted freeboard height.

Before entering into further detail in the analysis of the test results, it is important to stress that the wave loads measured are highly non-linear in nature in the first place. This means that the observed loads will not follow a linear relation with for instance the local relative wave elevation or relative wave velocity. Such non-linearity is related to the already present non-linearity of the incident wave, with interactions between different wave components and the presence of wave breaking, and by the complex dynamics of the water and air particles present at the impacted structure. In the second place, the wave loads are also extremely sensitive to the condition of the wave and ship at the moment of the impact: small deviations in observed ship motions (heave, roll, etc and wave crest elevation, for example, at the instant right before the impact will yield sensibly different results. This is why such loads are very difficult to reproduce when repeating a test. The same observation applies when different realisations of same wave characteristics are applied in the basin. By wave realisation is understood a unique train of waves representing a wave condition. Since irregular waves are generally described by statistical values (for instance the significant wave height, period of spectrum peak), a given combination of wave height and peak period can lead to an infinite number of wave realisations. In Figure 3-18 the largest pressure peaks and number of impacts is shown for five different realisations of three different wave conditions with significant heights 1.8, 3.0 and 4.5 m. For all these conditions it can be observed that the five realisations yield quite different measured top loads as well as number of impacts. Nevertheless, in the case of the lower wave all realisations tend towards the conclusion that in such condition there are either no loads measured or loads that are below the container side panel yield limit.

The very sensitive character of the wave loads may be illustrated by comparing the distributions of the incident wave elevation measured during the preliminary wave calibration phase (no ship model present in the basin) and that of the relative wave elevation measured along the ship during the test, see Figure 3-19. On the left side, the distribution of the wave crests from the calibrated wave is nearly identical for the three realisations considered, except the very tail (probabilities below 0.1) where some small scatter is observed. In this figure the distribution of the probability of exceedance (vertical axis) of a given amplitude of the relative wave elevation (horizontal axis) is given for all five wave realisations. It can be seen that for the moderate range of wave elevation, underlined by the dash rectangle, the distribution

[12] https://www.kustwacht.nl/nl/dossiers/routeadvies-waddeneilanden

is very similar for all five realisations, which highlight the rather linear character of the elevation. However, when looking at elevations close to the lower part of the lowest container tier, underlined by the dash circle, the distributions tend to diverge from each other, indicating that the frequency at which a wave will reach the lower containers will vary considerably from one realisation to another.

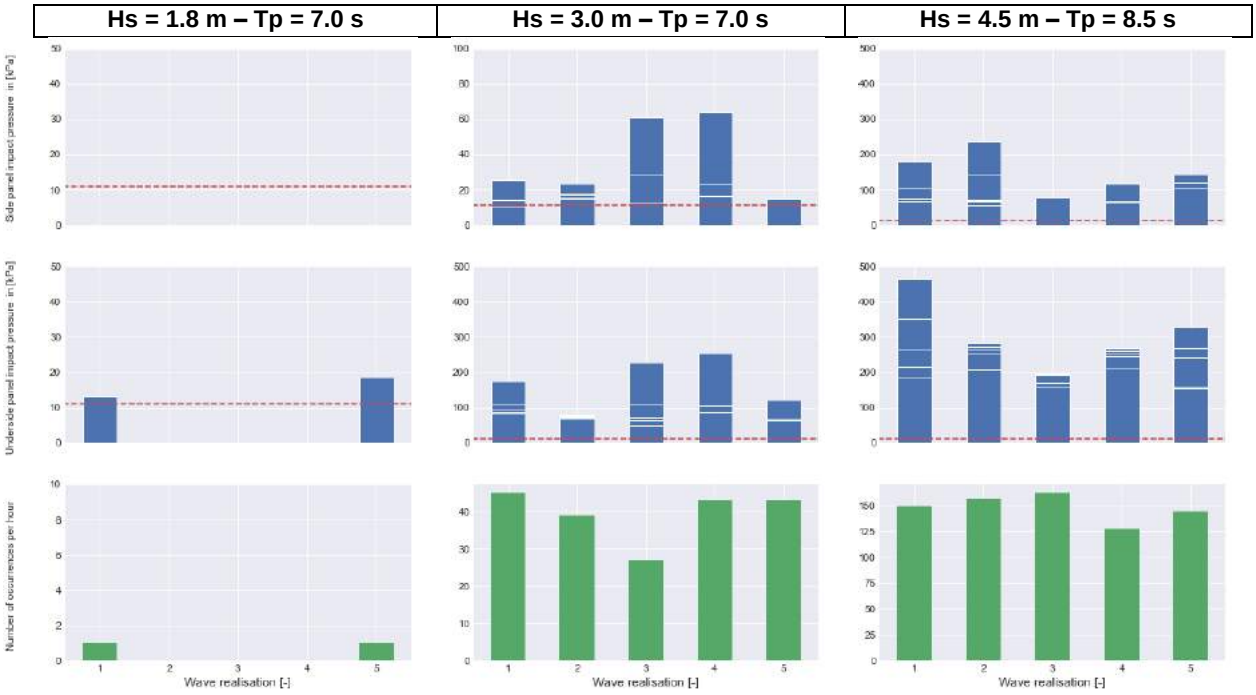

Figure 3-18: Stacked-up representation of the top five transverse wave load pressures (top), top five vertical wave load pressures (middle) and hourly number of occurrences (bottom)
Variation in wave realisation
Three different wave conditions, heading 270 deg, depth 21.3 m, short-crested waves

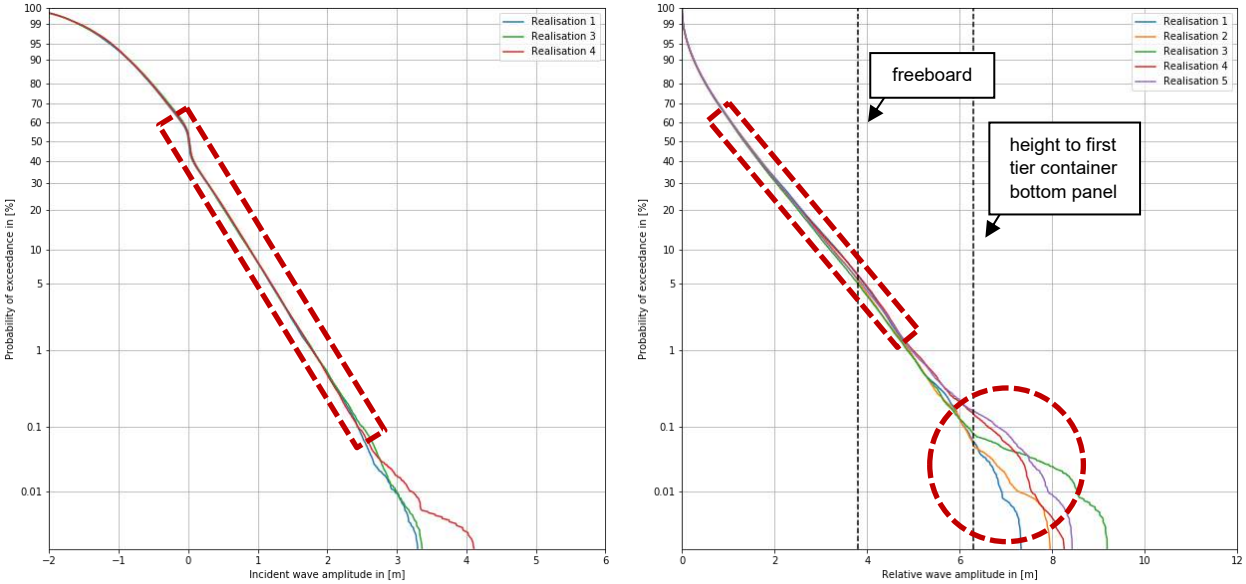

Figure 3-19: Cumulative distribution of the incident wave amplitude (left) and relative wave amplitude at location REL 2 (right)
Five realisations of beam wave condition Hs = 3.0 m – Tp = 7.0 s, short-crested waves
Water depth 21.3 m

In the light of the above, it can be said that a comparison of the different test results considering such non-linear phenomenon as green water remains a difficult exercise. In the following an attempt to do so is made, based on the following processed information: stacked-up representation of the top five transverse wave load pressures, top five vertical wave load pressures and number of occurrences per hour full scale, as shown in Figure 3-18 or Figure 3-20, relative wave elevation at the ship side at locations close to the wave load sensors and video and available photo and video material. For reference the container side panel yield limit as determined by means of finite element calculations[13] is indicated in the stacked up representations by the red dash line.

Effect of wave height, period and crestedness

The influence of wave parameters such as height, period and crestedness was estimated by performing a variation study. The main variation was carried out for the freeboard configuration 2, with a height to main deck of 3.8 m and height to container bottom panel of 6.3 m. It consists of a series of tests performed at wave heights 1.8, 2.1, 3.0 and 4.5 m. To estimate the effect of wave period the lower and higher waves are performed for two wave peak periods, shown at the bottom of Figure 3-20.

Figure 3-20: Stacked-up representation of the top five transverse wave load pressures (top), top five vertical wave load pressures (middle) and hourly number of occurrences (bottom) Different wave conditions, heading 270 deg, depth 21.3 m, short-crested waves

[13] For more information see MARIN report 32558-1-DIR.

Without much surprise it can be observed that the amplitude and frequency of green water loads increase with the wave height. Until a height of 2.1 m the loads are scarce, observed exclusively on the underside, with amplitudes at most matching the maximum yield limit pressure. This means that in such conditions the containers will not experience any green water loads that will cause damage. In wave heights of 3 m and higher the loads increase in both frequency and amplitude. Not only the underside of the bottom container experiences loading, but also the side panels of the lowest tiers. In Hs = 3 m the maximum transverse load pressure is about 25 kPa, equivalent to a force of 790 kN when considering the pressure uniformly applied to a container side panel, the maximum vertical load pressure 174 kPa (or 3,507 kN when applied to a container underside panel). Considering the wave height of 4.5 m the maximum pressures measured read 178 kPa (transverse pressure, or 5,637 kN) and 466 kPa (vertical pressure, or 9371 kN).

For both variations in wave peak period, performed at significant wave height of 1.8 m and 4.5 m the largest impact loads are encountered in the shorter wave condition. This is easily understandable as a good part of the impacts are generated by steep, breaking waves that are more present in the wave train of shorter peak period.

Finally, the effect of “wave crestedness” was studied considering two relatively short beam wave conditions: Hs = 3.0 m / Tp = 7.0 s and Hs = 4.5 m / Tp = 8.5 s. Both were realised considering a short-crested version and a long-crested version, see Section 3.4.2 for more detailed information. The measured maximum load pressures and number of occurrences are presented in Figure 3-21. Three observations can be made from these results: first the long-crested waves yield substantially more occurrences of green water loads (a nearly twofold multiplication of the number of occurrences in the lower wave condition and a 50% increase in the higher wave condition). Secondly, the transverse wave loads increase substantially in long-crested waves compared with those in short-crested waves. Finally, the largest loads obtained from the long-crested wave case seem to show less scatter. This last observation is particularly visible on the vertical loads. To summarise: more long-crested waves will lead more frequent and probably heavier wave loads than short-crested waves.

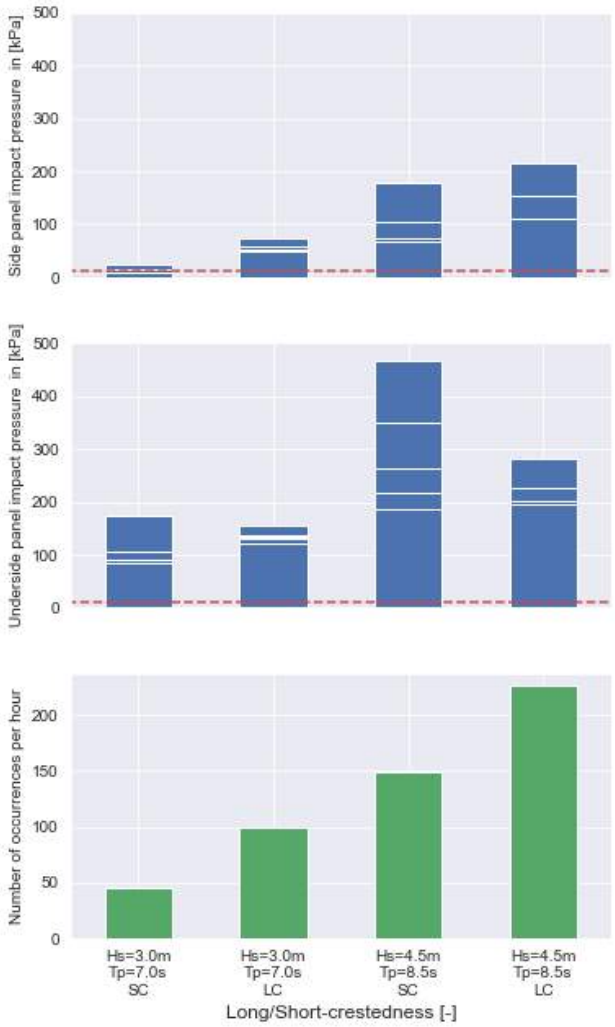

Figure 3-21: Stacked-up representation of the top five transverse wave load pressures (top), top five vertical wave load pressures (middle) and hourly number of occurrences (bottom) Variation in crest character Beam waves, depth 21.3 m

The same observations on the influence of wave height, peak period and effect of wave crestedness can also be made based on the analysis of the readings of the relative wave elevation, as illustrated in Figure 3-22.

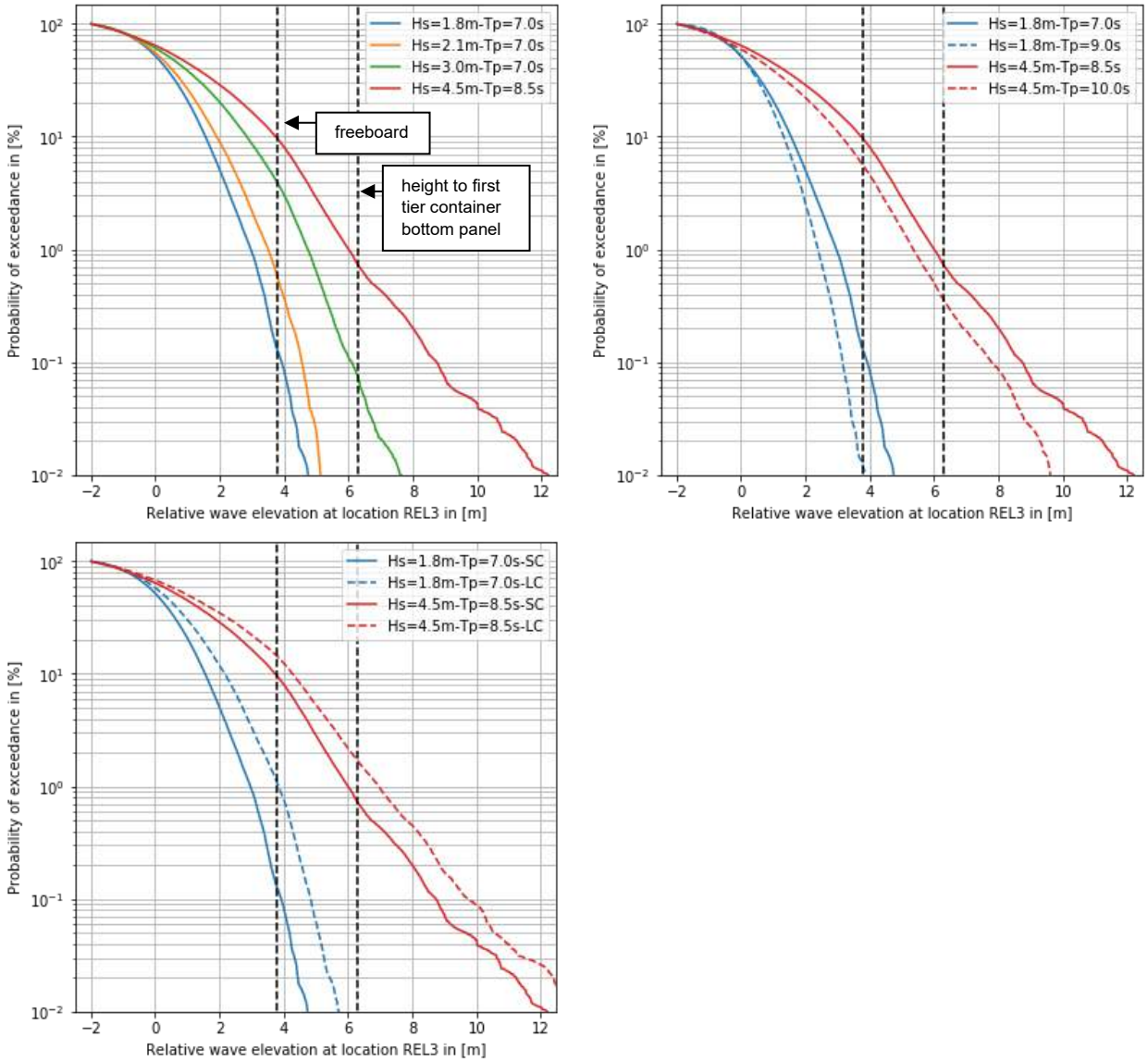

Figure 3-22: Cumulative distribution of the relative wave amplitude at REL 3 (amidships), configuration 2 Top left: variation in wave height, top right: variation in wave peak period, bottom left: variation in wave crestedness

Effect of freeboard height and type

The increase in freeboard height shows a largest effect on the number of occurrences: from freeboard configuration 1 to 2 (freeboard increase from 2.3 to 3.8 m) the number of occurrences per hour reduces from nearly 250 to less than 50 in the 3 m high beam wave condition and from more than 500 occurrences down to 150 in the condition 4.5 m high beam wave condition. In configuration 3 (freeboard height 5.3 m) no impact is observed in the 3 m wave condition and about 75 in the 4.5 m wave condition. A similar trend is observed for configurations 4, 5 and 6 (with all containers on deck). The difference in reported number of occurrences between configurations 1 and 4 may be explained by the absence of the contribution of exclusively vertical loads in the case of configuration 4.

Considering the 3 m beam wave condition the trend seen on the number of occurrences seems to apply also on both the largest horizontal and vertical loads. However this is not the case for the 4.5 m beam wave, where larger loads are observed in horizontal direction in configuration 6 than in configuration 5 and in vertical direction in configuration 2 than in configuration 3.

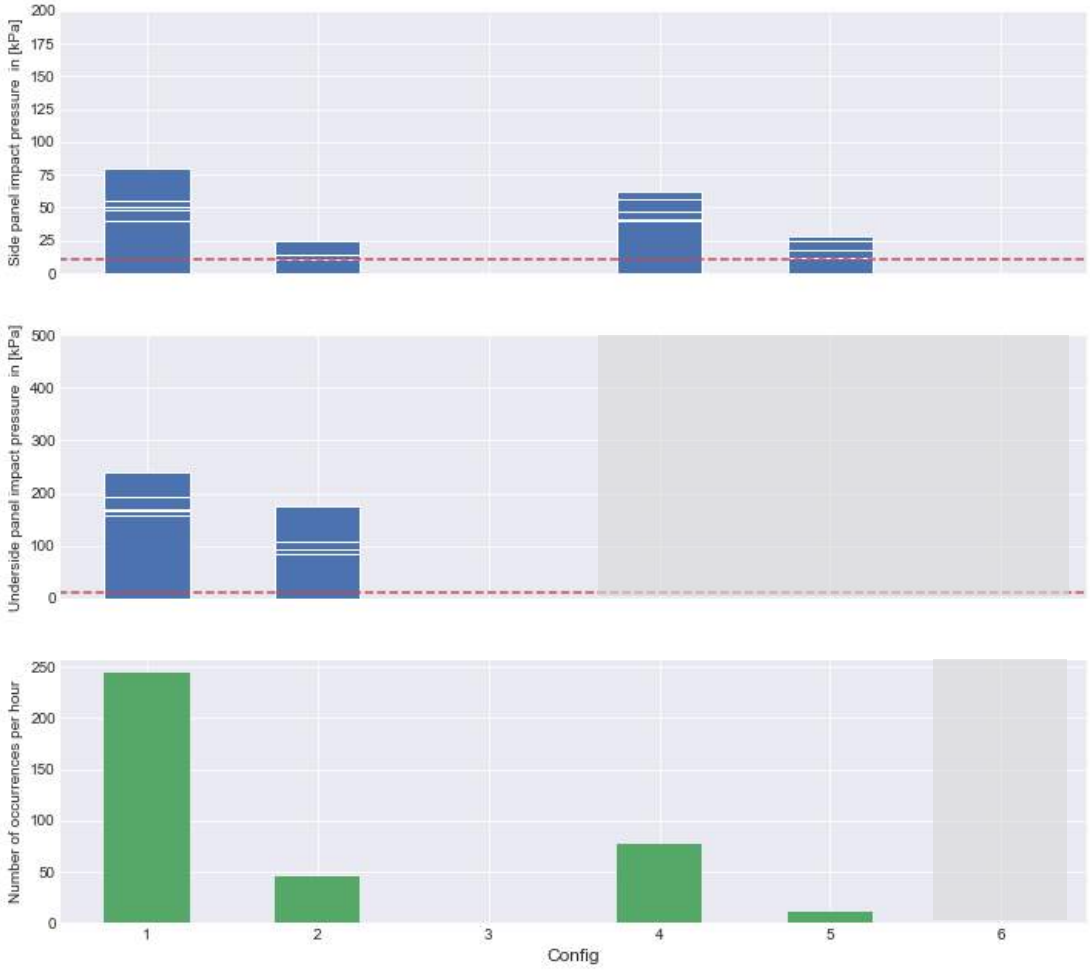

Figure 3-23: Stacked-up representation of the top five transverse wave load pressures (top), top five vertical wave load pressures (middle) and hourly number of occurrences (bottom) Hs = 3.0 m, Tp = 7.0 s, heading 90 deg, depth 21.3 m, short-crested wave

The cumulative distributions of the relative wave elevation on the ship side, such as presented for the REL 3 location in Figure 3-25, provides interesting insight in the influence of the freeboard on the green water dynamics. In general, the relative wave elevation is found not to be influenced significantly by either the freeboard height or the freeboard type, as the distribution lines remain close to each other. This is particularly visible in the case of the wave condition Hs = 3.0 m / Tp = 7.0 s. In the higher wave condition, Hs = 4.5 m / Tp = 8.5 s, some scatter is noted, particularly in the 1% highest amplitude range. Such scatter may partly be explained by the larger non-linearities that may affect the wave crests, but also by the fact that the ship motions are found to be slightly different from one configuration to another. Reasons for such deviations can be the slight variations in loading conditions (displacement, GM) caused by the change in configuration or different reactions to the largest waves previously encountered. The effect of water entrapped in the deck elements may also not be excluded, although best care was taken to minimise this effect. Nevertheless, it is interesting to note that despite the scatter, the distributions of the two freeboard types (configs 1 & 4, configs 2 & 5, configs 3 & 6) remain very similar.

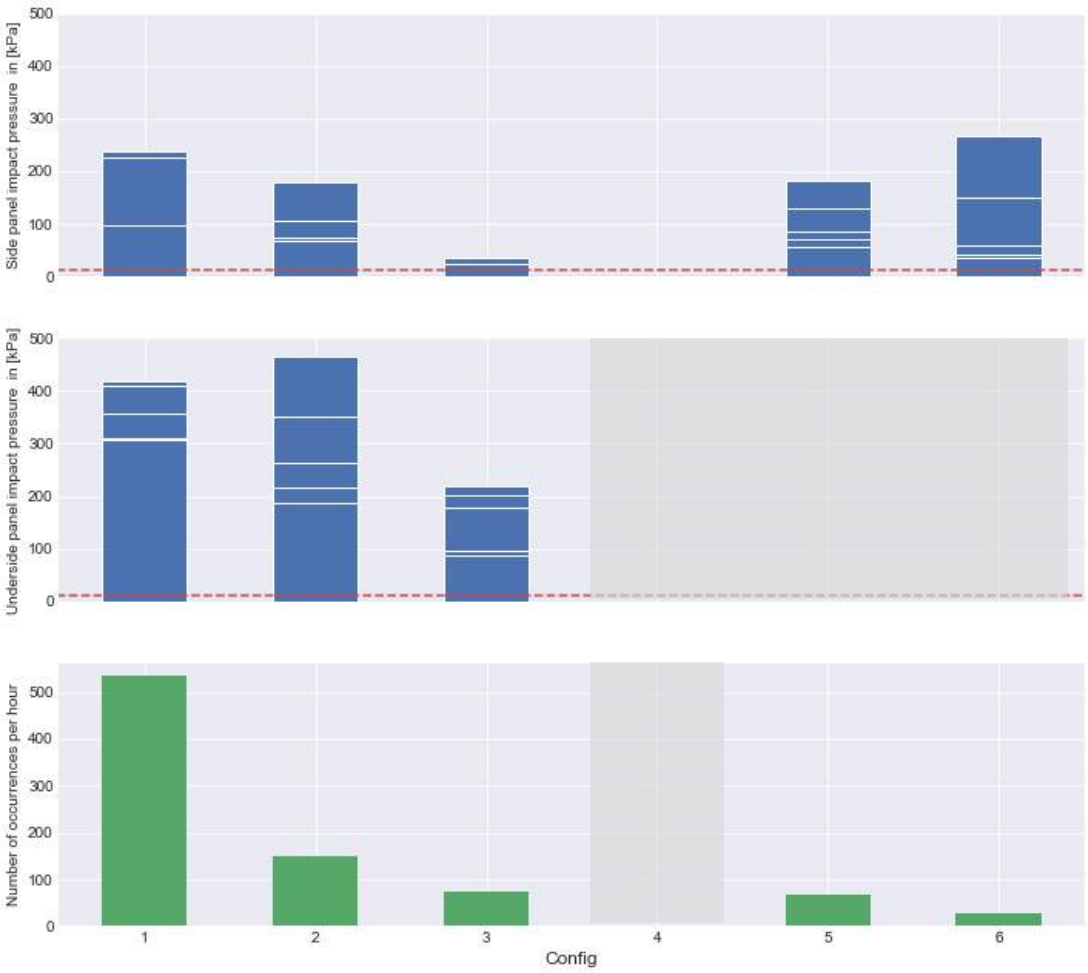

Figure 3-24: Stacked-up representation of the top five transverse wave load pressures (top), top five vertical wave load pressures (middle) and hourly number of occurrences (bottom) Hs = 4.5 m, Tp = 8.5 s, heading 90 deg, depth 21.3 m, short-crested waves

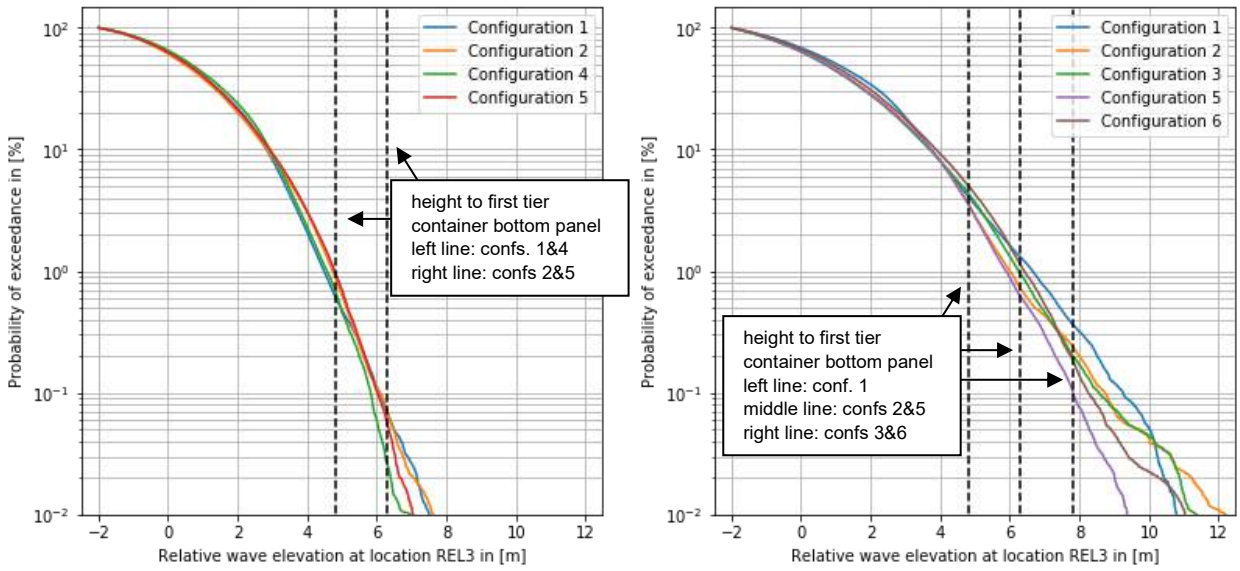

Figure 3-25: Cumulative distribution of the relative wave elevation at REL 3 (amidships) Left: Hs = 3.0 m / Tp = 7.0 s, right: Hs = 4.5 m / Tp = 8.5 s

From the available video records (as illustrated in Figure 3-26) it can be observed that freeboard type can have an effect on specific occurrences of green water. Whereas the largest wave elevations on the ship side breaking directly on the lower container tiers will not show any effect from the freeboard type, differences in green water patterns are noticed when the mass of water climbs along the ship wall after slamming on the hull. In the case of the outermost rows of containers hanging above the gangway (configurations 1, 2 and 3) the recess formed by the gangway acts as a sort of wave breaker, slowing down the progress of the water column. On the contrary, the absence of obstacles in the case where all containers are stowed on the hatch cover, is seen to give free way to the water to reach easily the container sides. Important to mention that such observation does not apply in the case of slow rise-up of the nearby water, due to a downward heave motion for instance.

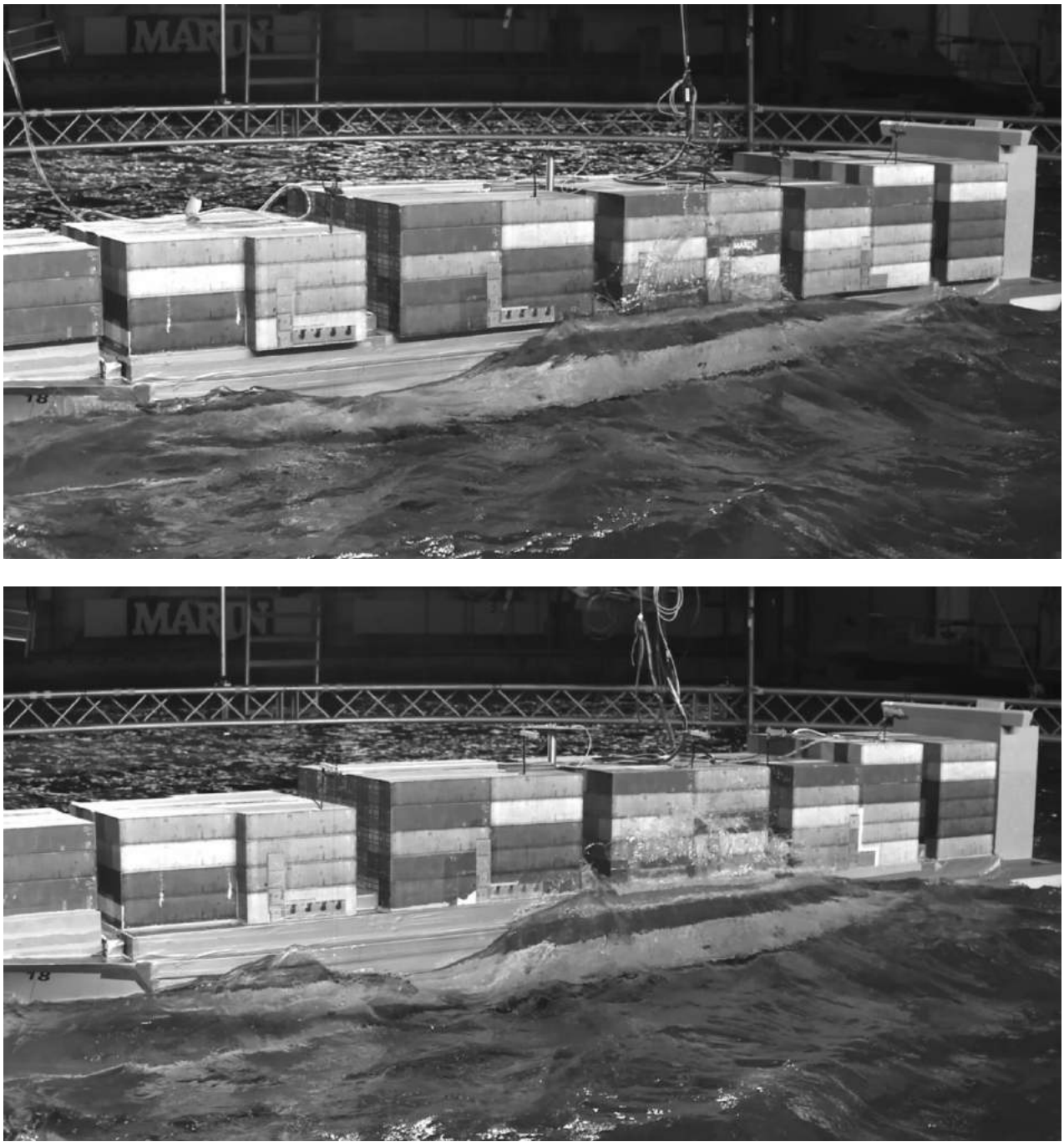

Figure 3-26: Wave impact observed in wave condition Hs = 4.5 m, Tp = 8.5 s, mu = 270 deg (beam waves), time stamp 479 s from start official measurement
Top: configuration 3, bottom: configuration 6

Effect of wave heading

From all tested headings beam waves may be regarded as the most unfavourable one from a green water perspective. Not only is the number of occurrences substantially larger in beam waves in comparison with oblique waves, the largest loads are in most tested conditions also higher. Although the peak vertical load in the 3.0 m high stern-quartering wave is noted to be larger than the largest peak in beam waves, it should be borne in mind that it is only applied to a smaller portion of the container side and bottom panels at one moment in time, compared with the extent of the load applied in beam waves. Where the model tests can only offer a very limited impression of the spatial distribution of the loads on a container stack, the CFD will provide a much better insight in it.

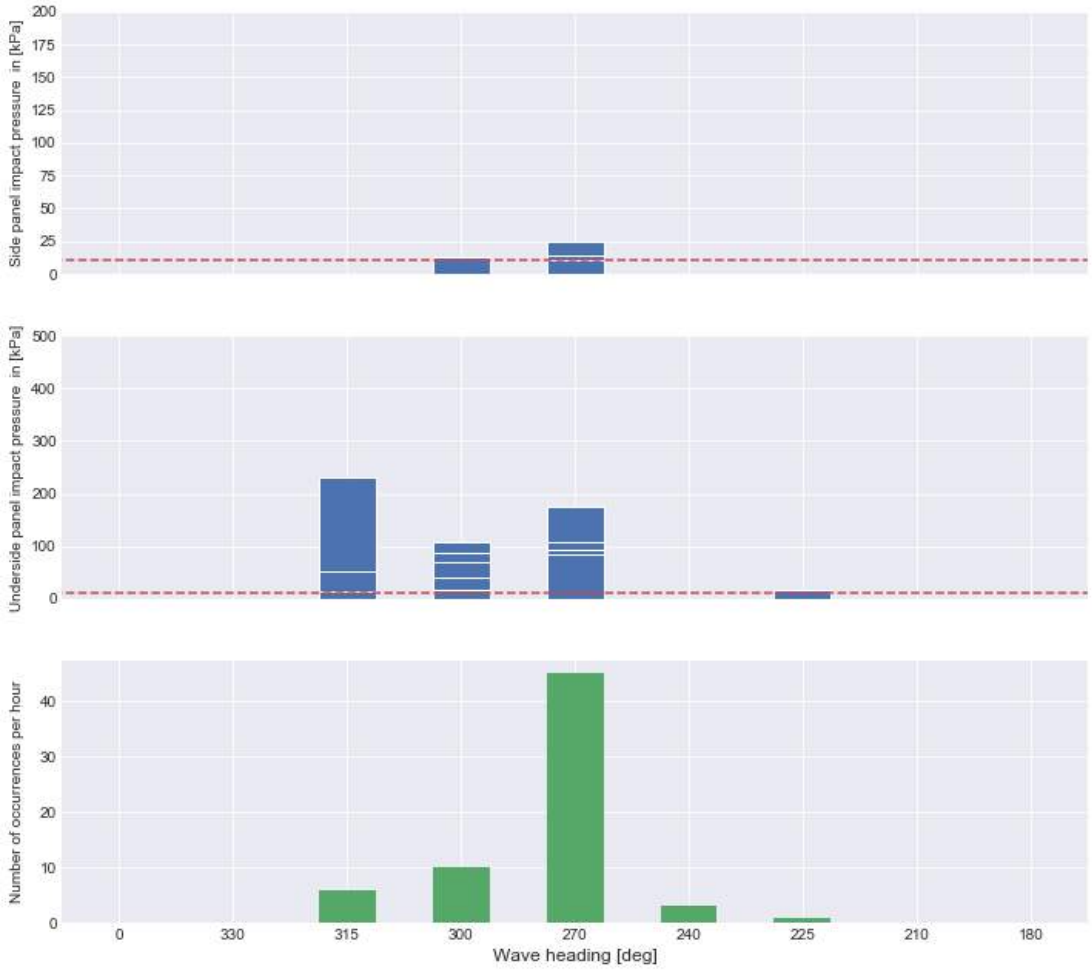

Figure 3-27: Stacked-up representation of the top five transverse wave load pressures (top), top five vertical wave load pressures (middle) and hourly number of occurrences (bottom) Variation in wave heading
Hs = 3.0 m, Tp = 9.0 s, depth 21.3 m, short-crested waves, configuration 2

The same trend is observed on the readings of the relative wave elevation on the ship side, which is highest in beam waves (Figure 3-29 and Figure 3-30). It is interesting to note that the distributions at midship are symmetrical between bow-quartering and stern-quartering waves. On the opposite, the distributions at locations closer to the bow or stern are noted to be asymmetric: the relative wave elevation is higher at the bow in stern-quartering waves and at the stern in bow-quartering waves, which reflect the effect of wave run-up.

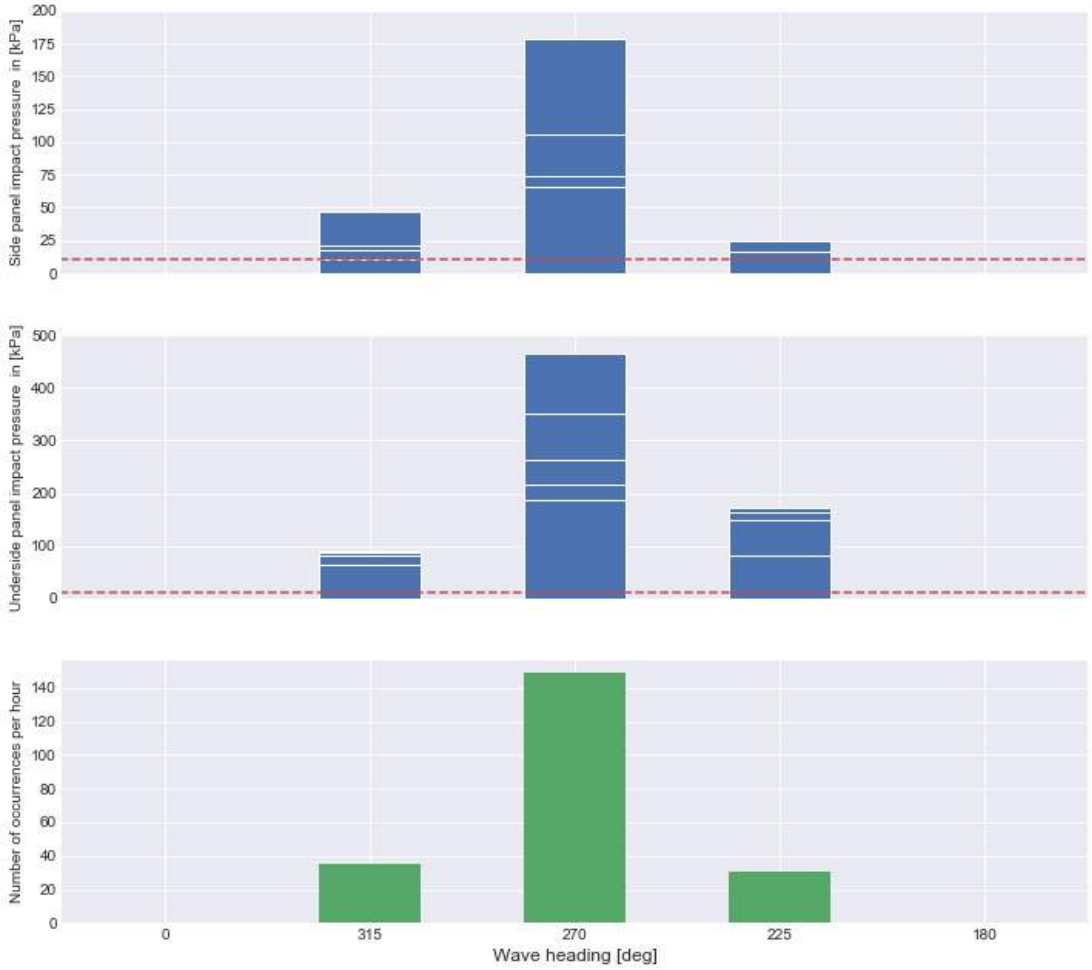

Figure 3-28: Stacked-up representation of the top five transverse wave load pressures (top), top five vertical wave load pressures (middle) and hourly number of occurrences (bottom) Variation in wave heading
Hs = 4.5 m, Tp = 8.5 s, depth 21.3 m, short-crested waves, configuration 2

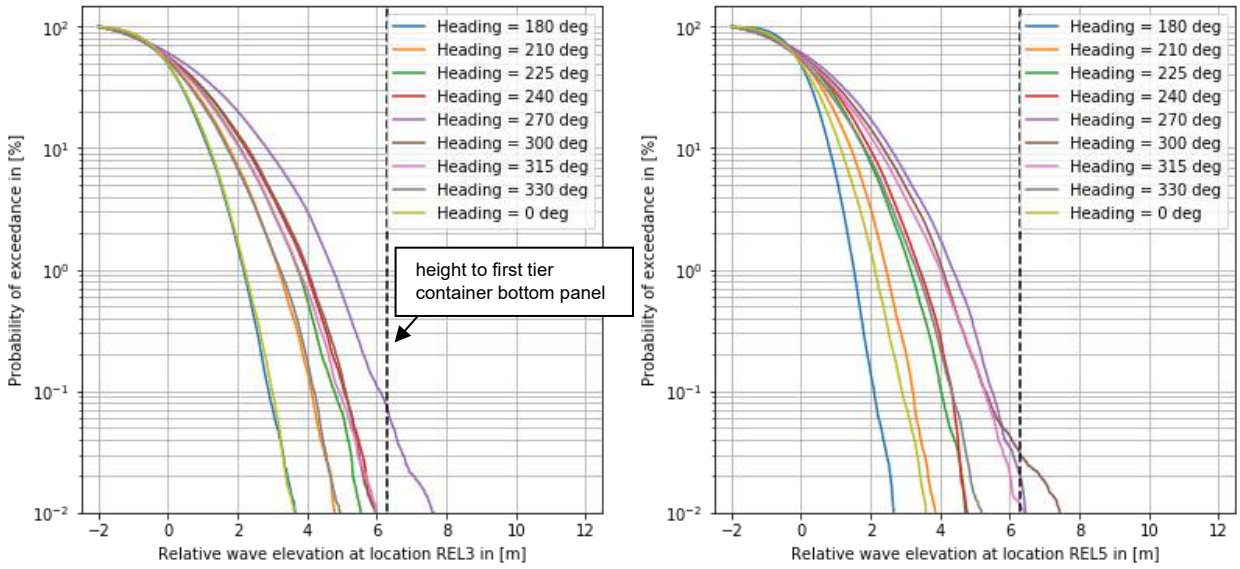

Figure 3-29: Cumulative distribution of the relative wave elevation, Hs = 3.0 m / Tp = 7.0 s, beam waves Configuration 2, left: location REL 3 (amidships), right: location REL 5 (bow)

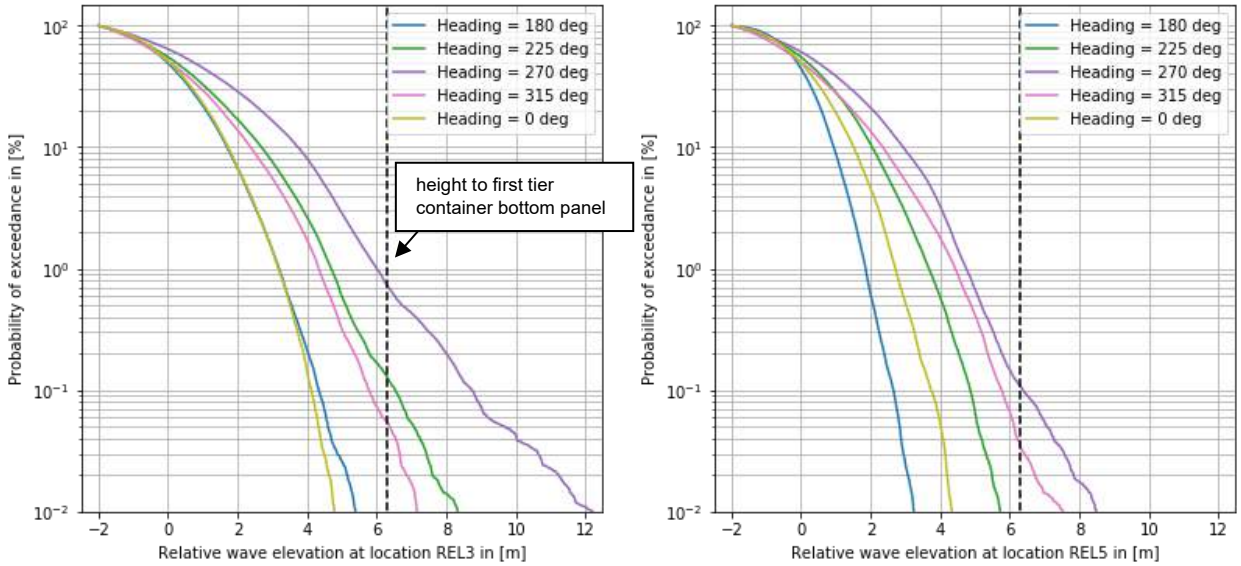

Figure 3-30: Cumulative distribution of the relative wave elevation, Hs = 4.5 m / Tp = 8.5 s, beam waves Configuration 2, left: location REL 3 (amidships), right: location REL 5 (bow). The vertical dash line denotes the height to freeboard deck and container bottom panel

The mechanics of green water change with the wave heading. In head and following waves the incident waves propagate along the hull and the wave crests are not high enough to reach the underside of the containers. In slightly oblique waves (within 30 deg from head of following waves) a growing contribution of wave run-up is observed, however not large enough for the wave crests to reach the containers.

In more oblique waves (incidence angle within 45 deg off beam waves: 225 to 315 deg) the combination of a larger run-up effect and a wave direction more and more perpendicular to the ship side yields significantly larger green water activity, described by larger impact amplitudes and number of occurrences. Because of the influence of run-up, the largest impacts are usually observed at the ship aft in bow-quartering waves and at the ship bow in stern-quartering waves.

In beam waves the largest impacts result from steep incident waves that collide against the ship side and lowest container tiers. Prior to the contact the high incident waves interact with the diffracted (reflecting) and radiated waves to form even higher waves that reach easily deck height and the containers.

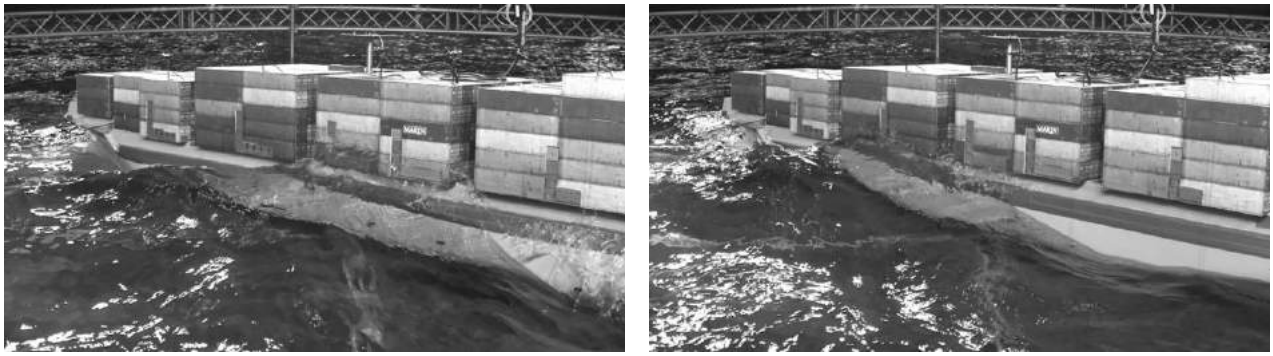

Figure 3-31: Takes of the largest transverse and vertical impact from green water taken shortly after each other, configuration 2, Hs = 4.5 m, Tp = 8.5 s, heading 315 deg

Figure 3-32: Takes of the largest transverse and vertical impact from green water taken shortly after each other, configuration 2, Hs = 4.5 m, Tp = 8.5 s, heading 270 deg

Effect of water depth

The comparison of the peak loads measured during tests performed at various water depths (Figure 3-34) does not allow to draw a formal conclusion on the influence of it on the load amplitude. It may nevertheless be said that an increase in water depth from 21.3 to 37.5 m (the depth observed in the southern route and northern route, respectively) will reduce substantially the frequency of occurrence of green water, as it was observed during previous studies. However, the tests performed in relatively deep water (100 m) show that the frequency does not further reduce, but rather stabilise. The comparison of the distributions (Figure 3-33) shows that in the wave condition Hs = 3.0 m they are rather similar. In the wave condition Hs = 4.5 m, the elevation in the shallowest condition is noted to be significantly higher, while the other two remain very similar to each other. From these results is may therefore be concluded that the influence of water depth on green water activity is function of the significant wave height: for Hs = 3.0 m there is hardly any significant effect of water depth observed, however for Hs = 4.5 m a higher green water activity may be expected in the very shallow condition.

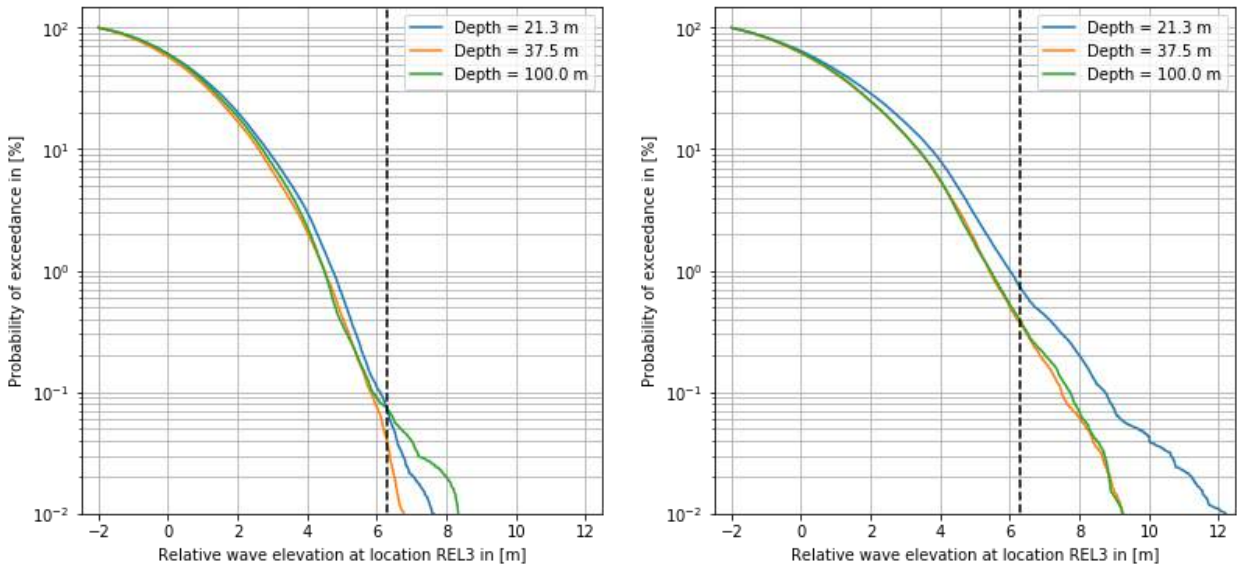

Figure 3-33: Cumulative distribution of the relative wave elevation at location REL 3 (amidships) Configuration 2, left: Hs = 3.0 m / Tp = 7.0 s, right: Hs = 4.5 m / Tp = 8.5 s, head. 270 deg

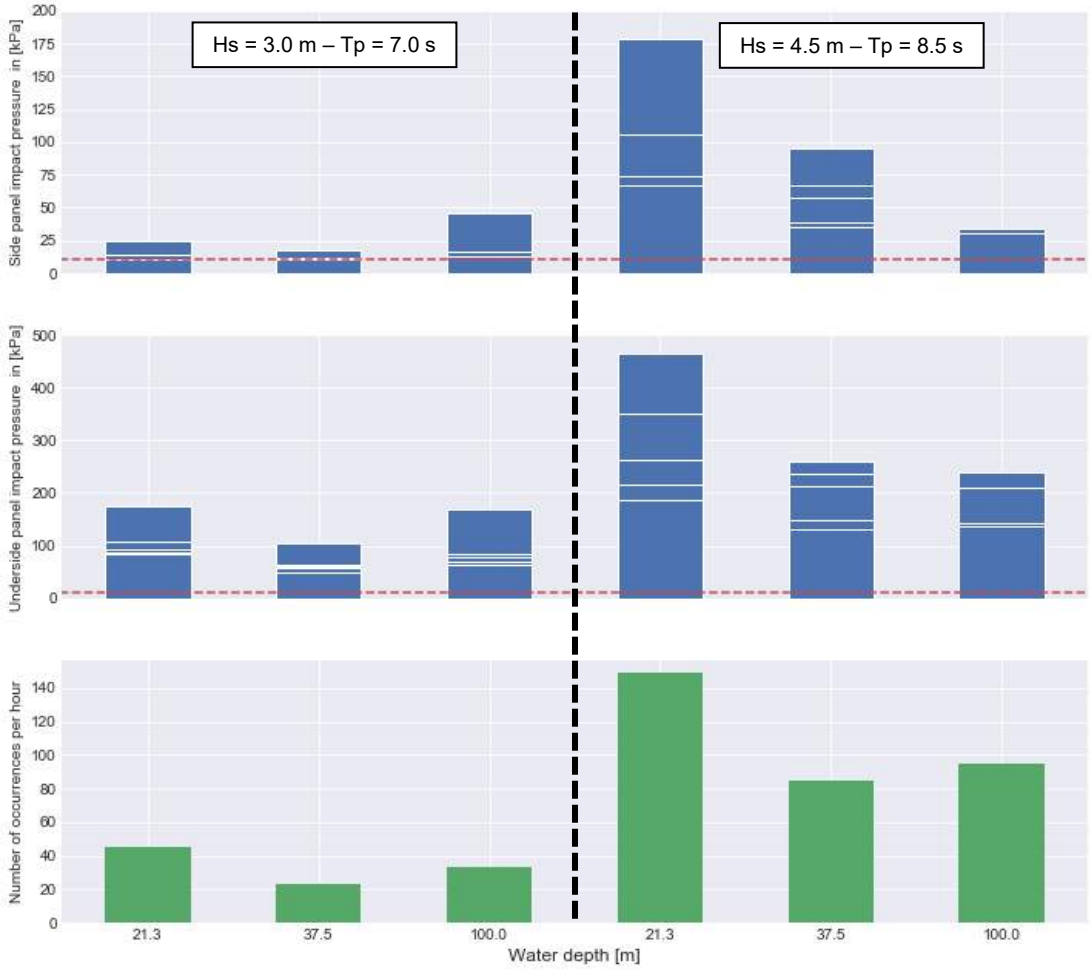

Figure 3-34: Stacked-up representation of the top five transverse wave load pressures (top), top five vertical wave load pressures (middle) and hourly number of occurrences (bottom) Variation in water depth Heading 270 deg, short-crested waves, configuration 2

Longitudinal wave loads

The longitudinal loads measured on the containers above the breakwater (arrangement in Figure 3-7) are presented for all wave conditions with significant height of 6.0 m and above in Figure 3-35.

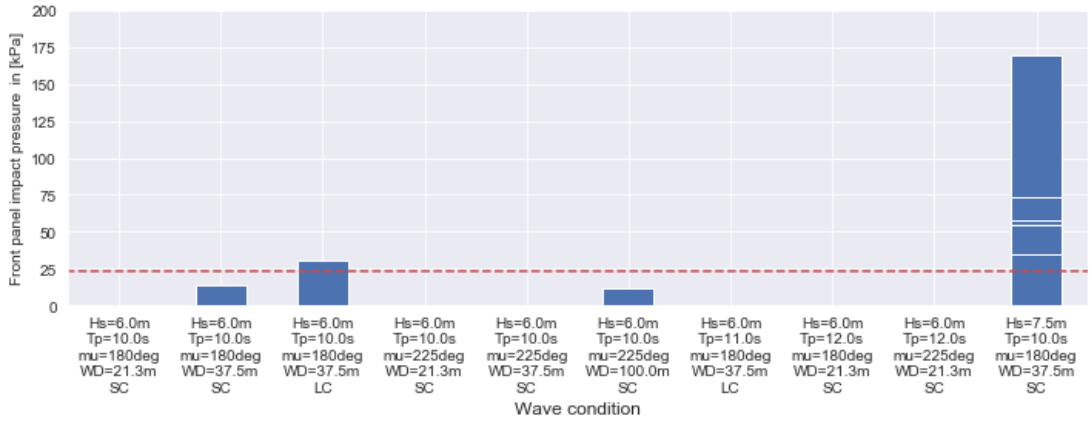

Figure 3-35: Stacked-up representation of the top five longitudinal wave load pressures Configuration 2

No wave loads were measured above the breakwater for waves with Hs ≤ 4.5 m, while either no occurrence or a single occurrence of relatively small amplitude were measured for Hs = 6 m. In waves with Hs = 7.5 m, the green water activity increases substantially and much higher loads were measured (impact pressure of approximately 175 kPa). Noteworthy that the conditions where impact loads were measured are not exclusively head sea conditions, but include also one bow-quartering wave condition.

Since the CFD and FE simulations in the present scope focused exclusively on wave impacts on the long side and bottom panels of the outermost containers, the only available criteria related to damage due to impacts on the container short side are the maximum yielding limit and maximum buckling limit from the previous study, given in Table 3-5. Comparing the obtained load pressures with these limits, as can be seen in Figure 3-35, yields the conclusion that no significant damage may be expected in significant wave heights of 6 m or lower.

Preliminary estimates of limiting wave heights

As mentioned in the introductory pages, the final objective of the model tests and numerical simulations is to determine the wave heights above which a feeder ship might experience green water loads that are too high to ensure safe container transport. While the final estimates require the combined analysis of model tests and simulations (addressed in chapter 6), it is interesting to proceed with a first estimate of these considering two low-level methods, similar to that applied in the previous study[14].

Method 1: determination based on relative wave elevation measurements

The first method relies on the use of the relative wave elevation readings at the different locations. Here a significant wave height is considered limiting when the relative wave elevation is high enough to reach the underside of the lower tier container bottom panel. The complete methodology is described in Section 3.3.6. The results are presented in Table 3-8, Table 3-9 and Figure 3-36 for all configurations. Since the ship is symmetric with respect to the centreline, the wave heights below apply to the headings to portside (225, 270 and 315 deg) as well as to startboard side (135, 90 and 45 deg).

Table 3-8: Limiting significant wave height for six freeboard configurations, water depth 21.3 m

	Config 1	**Config 2**	**Config 3**	**Config 4**	**Config 5**	**Config 6**
Freeboard	**2.3 m**	**3.8 m**	**5.3 m**	**2.3 m**	**3.8 m**	**5.3 m**
135/225 deg	2.1 m	2.7 m	3.5 m	N/A[15]	3.1 m	N/A
90/270 deg	1.7 m	2.3 m	2.8 m	1.6 m	2.1 m	2.9 m
45/315 deg	2.0 m	2.6 m	3.3 m	N/A	N/A	N/A

Table 3-9: Limiting significant wave height for three different water depths, configuration 2

	21.3 m	**37.5 m**	**100 m**
135/225 deg	2.7 m	2.6 m	3.2 m
90/270 deg	2.3 m	2.2 m	2.3 m
45/315 deg	2.6 m	2.4 m	2.9 m

Looking at the estimates for the six different configurations at water depth 21.3 m (Table 3-8), the limiting wave height is seen to increase with freeboard height, which is logical, however not as the same rate as the increase in freeboard: for example the limiting wave height increases by 0.6 m from configuration 1 to configuration 2, which is about one-third of the increase in freeboard height (1.5m). The height is approximately the same for the two freeboard types, at same freeboard height, which is consistent with the findings of the variation in freeboard configuration as reported earlier. A change in wave heading from beam seas to oblique waves yields also an increase in limiting wave height, in agreement with the previous findings on the sensitivity to the wave heading. There is, however, no effect of the water depth (Table 3-9), as found in the sensitivity study for low wave heights.

[14] For further information, see MARIN report 32558-1-DIR.

[15] Not Available: the limited number of tests did not allow the determination of the limiting wave height.

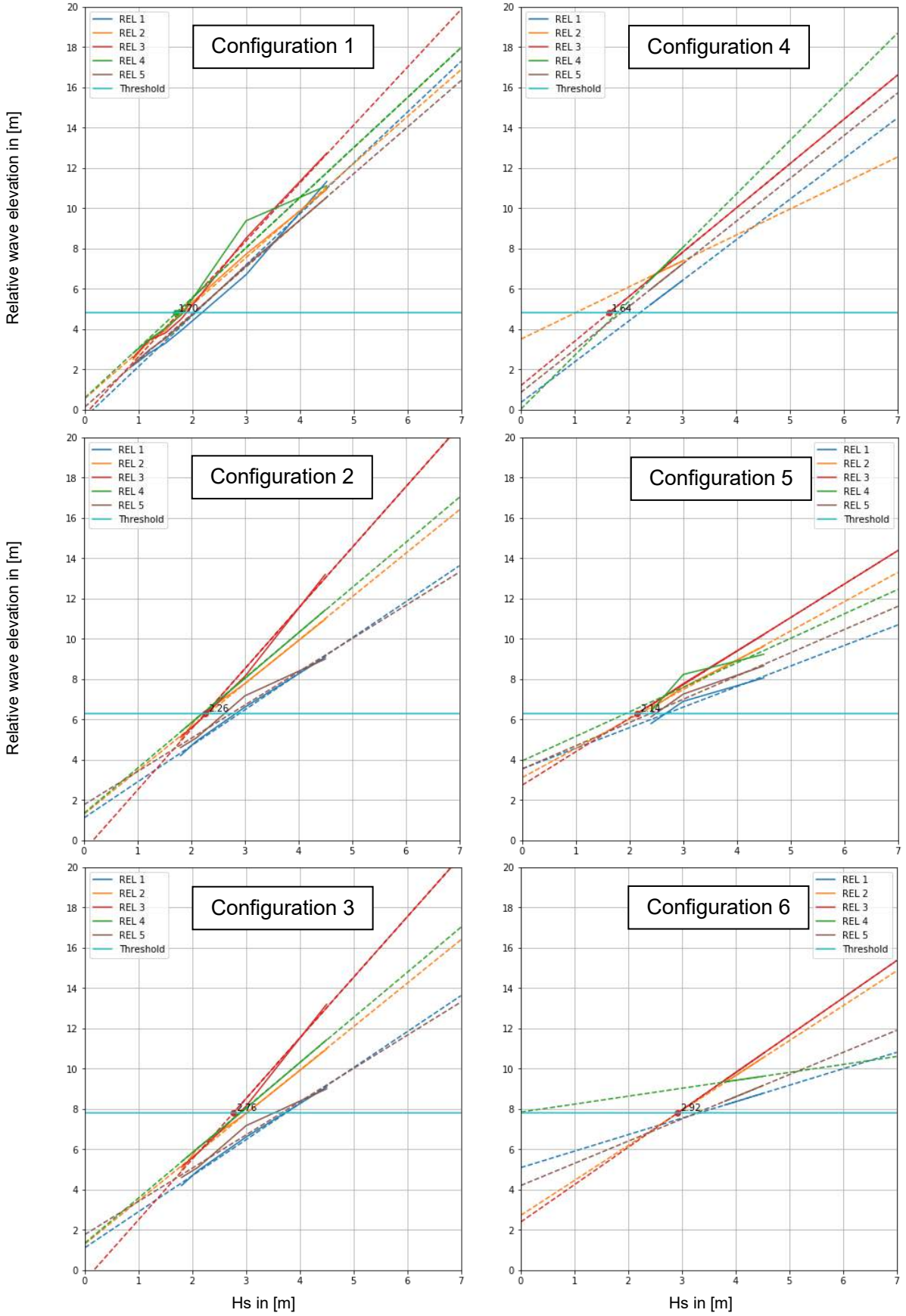

Figure 3-36: Determination of the limiting wave height from interpolation of mpm relative wave elevation at various locations
Heading 270 deg, water depth 21.3 m

Method 2: interpolation through force – wave height relation plots
In the second method, a given wave height is considered limiting when:

- the load pressure derived at any of the side force sensors (FY) exceeds the yield limit pressure of 15 kPa. This limit is slightly higher than the side panel yield limit of 11 kPa determined by means of finite element calculations applied on a typical container. The reason for such correction is explained by the noise bandwidth on the sensor that goes up to 12 kPa;

- or the load pressure derived at any of the underside force sensors (FZ) exceeds the side panel yield limit of 11 kPa, multiplied by a factor of 1.5.

The limiting significant wave height following this method is summarised in Table 3-10 and Table 3-11. The differences in method 1 are given in between brackets. These wave heights were obtained by considering the intersect of the maximum transverse and vertical pressures with the criterion values provided above. Associated plots are provided in Figure 3-37 to Figure 3-39. On these plots the criterion values are indicated by the red dash lines. As for the first method, the estimates hold for headings to port and starboard sides.

Table 3-10: Limiting significant wave height for six freeboard configurations, water depth 21.3 m

	Config 1	**Config 2**	**Config 3**	**Config 4**	**Config 5**	**Config 6**
Freeboard	**2.3 m**	**3.8 m**	**5.3 m**	**2.3 m**	**3.8 m**	**5.3 m**
135/225 deg	2.1 m *(+0.0)*	3.2 m *(+0.5)*	4.6 m *(+1.1)*	N/A	> 4.5 m *(+1.4)*	N/A
90/270 deg	1.6 m *(-0.1)*	2.2 m *(-0.1)*	2.8 m *(+0.0)*	2.3 m *(+0.7)*	3.0 m *(+0.9)*	~3.5 m *(+0.6)*
45/315 deg	2.1 m *(+0.1)*	2.5 m *(+0.1)*	3.7 m *(+0.4)*	N/A	N/A	N/A

Table 3-11: Limiting significant wave height for three different water depths, configuration 2

Depth	**21.3 m**	**37.5 m**	**100 m**
135/225 deg	3.2 *(+0.5)*	3.9 *(+1.3)*	3.7 *(+0.5)*
90/270 deg	2.2 *(-0.1)*	2.6 *(+0.4)*	2.5 *(+0.2)*
45/315 deg	2.5 *(+0.1)*	3.1 *(+0.7)*	3.6 *(+0.7)*

As observed for the estimates from the first method, the limiting wave height increases with freeboard height, although at a much lower rate than the increase in freeboard (maximum 1.1 m for 1.5 m increase in height). Besides, the comparison between the results obtained with the different freeboard types (configurations 1, 2 and 3 on the one side and configurations 4, 5 and 6 on the other side) show that the limiting wave height increases substantially (+0.7 m on average) when the containers all lie on deck (configurations 4 and higher). This is explained by the fact that the limiting wave height for the more classic freeboard type (configurations 1 to 3) is determined by the threshold on the vertical forces rather than by that on the transverse wave forces.

The results obtained with the second method are found to agree well with those of the first method overall, although some outliers are noted (bow-quartering wave case with configuration 5 for instance).

Comparison of the results with those obtained in the previous study (32558)

In comparison with the results presented and discussed in the previous study (MARIN report 32558-1-DIR), the limiting wave heights obtained based on the new basin tests are significantly lower (Method 1 gives 2.3 m with configuration 2 and freeboard height 3.8 m in beam waves against 3.3 m previously obtained with freeboard of 3 m). The main reason lies in the choice of the wave conditions used during the tests:

- In the previous tests the lowest significant wave height tested was 3.5 m. The preliminary limiting wave height had to be determined by extrapolation of the results to lower wave heights. The present test with even lower wave heights also showed green water events.
- The analysis conducted using the two methods above considered each significant wave height combined with the lowest peak period (Tp of 7-9s), since such condition was identified as most unfavourable, while being still realistic. However, the limiting wave heights that were obtained in the previous study were based on wave conditions with wave periods that were comparatively long (with peak period Tp of 10.2s).
- Another possible reason for the deviation lies in the adopted wave spectral shape, and more particularly the peak enhancement factor “gamma”. While in the previous study this factor was kept the same (gamma=2.0) for all conditions, it was varied in the present work between the short wave conditions (gamma=2.5) and the longer wave conditions (gamma=1.0). Decreasing the gamma factor yields a more present contribution of shorter waves, leading possibly to a higher relative wave elevation on the ship side.

For the reasons given above, the present more extensive and detailed model test scope with a larger model should be considered more reliable.

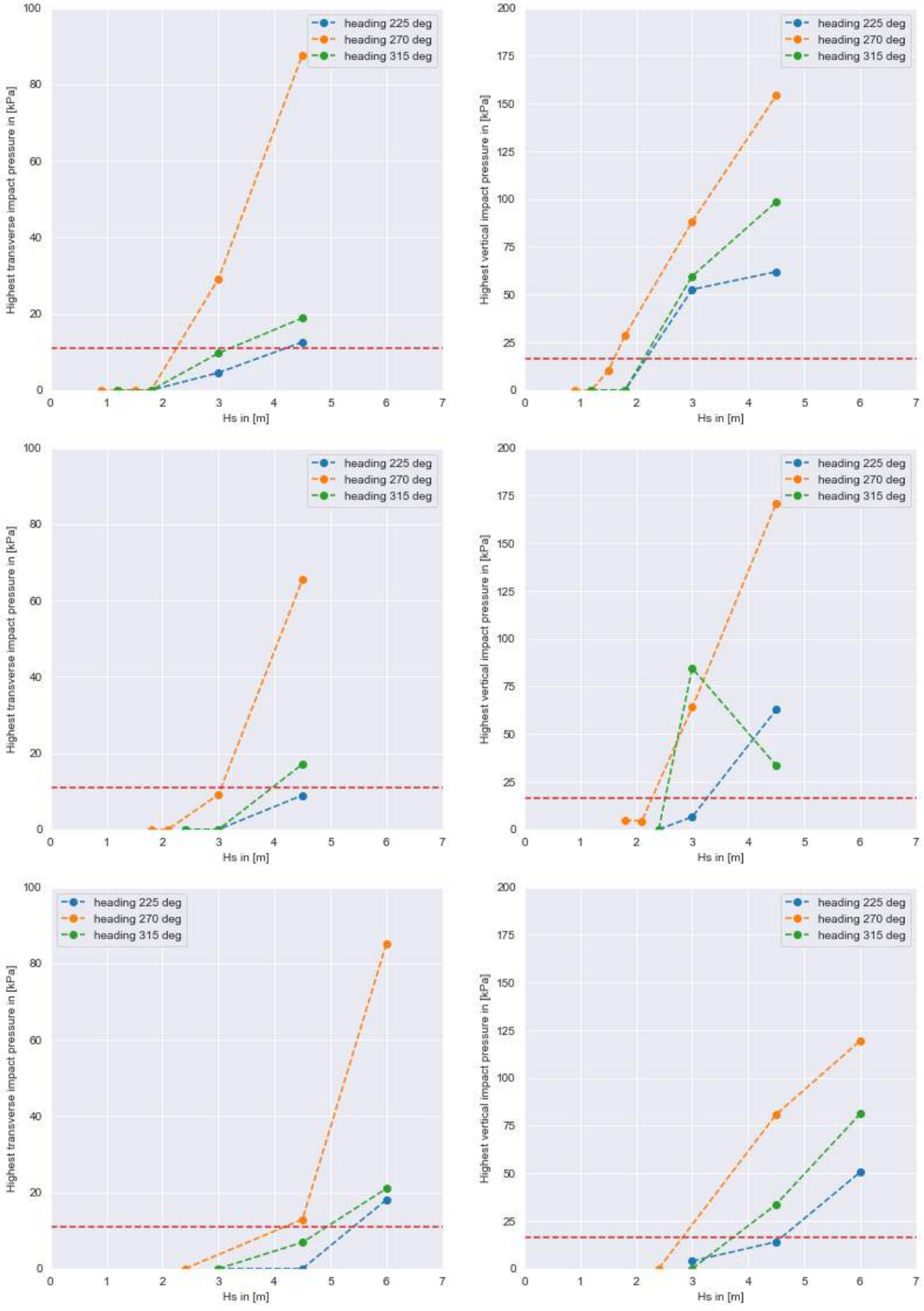

Figure 3-37: Highest transverse and vertical wave load pressures as a function of significant wave height. Left: transverse load pressures; right: vertical load pressures From top to bottom: configurations 1, 2 and 3; water depth 21.3 m

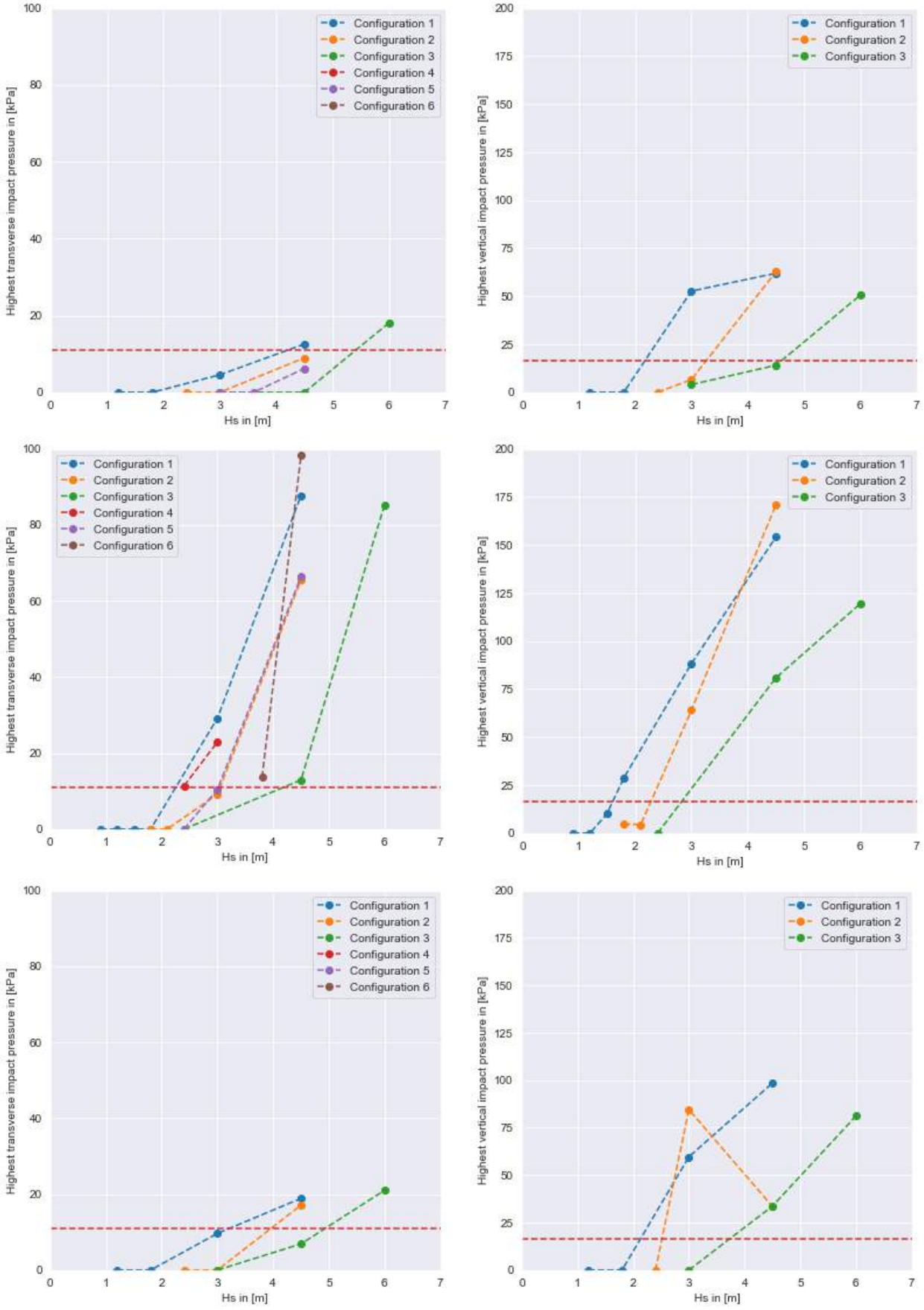

Figure 3-38: Highest transverse and vertical wave load pressures as a function of significant wave height. Left: transv. load pressures; right: vert. load pressures; all configs, water depth 21.3 m. From top to bottom: head. 225 deg (bow-quart.) 270 deg (beam) and 315 deg (stern-quart).

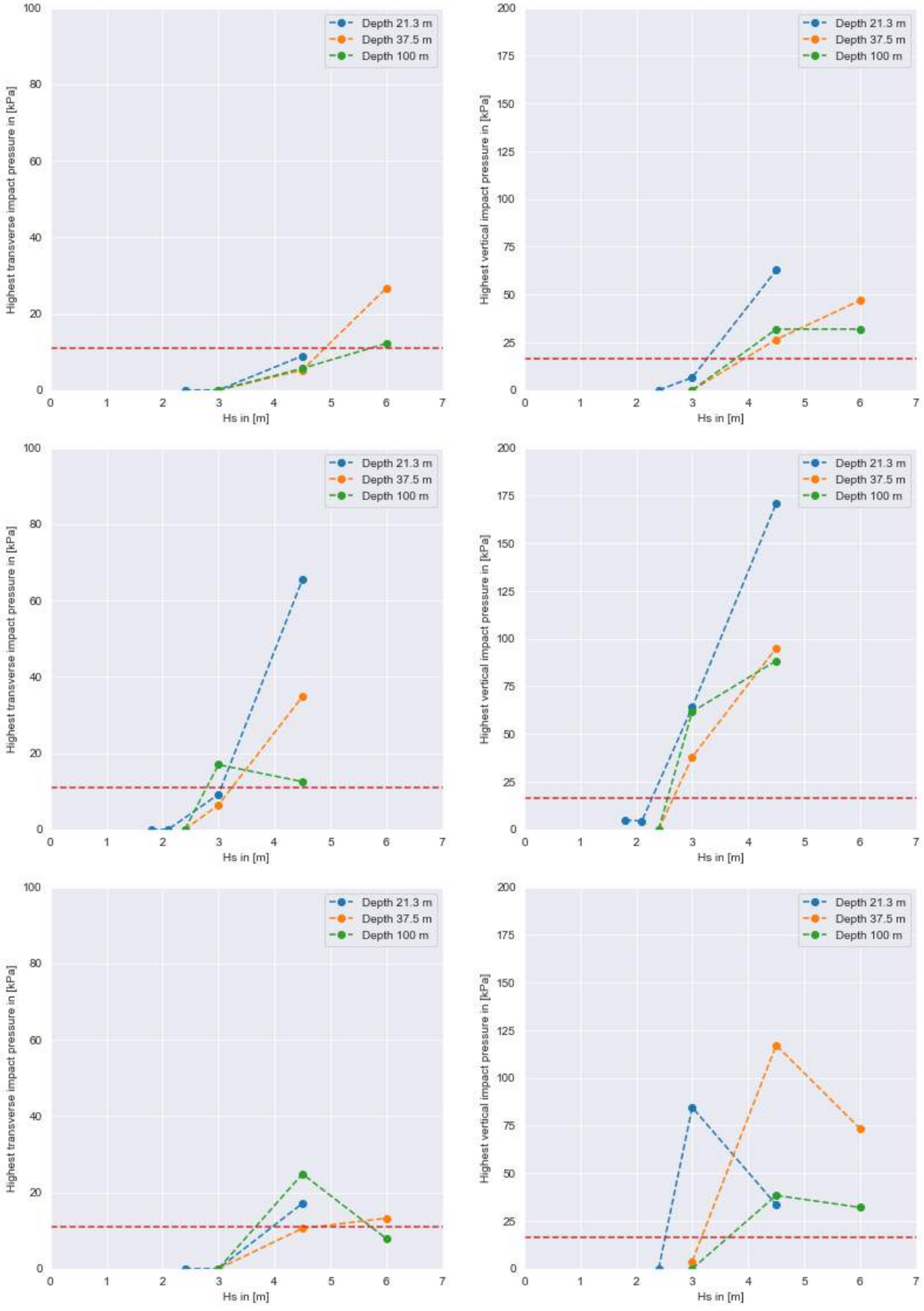

Figure 3-39: Highest transverse and vertical wave load pressures as a function of significant wave height. Left: transverse load pressures; right: vertical load pressures; configuration 2 From top to bottom: head. 225 deg (bow-quart.) 270 deg (beam) and 315 deg (stern-quart).

3.5.2 Occurrence of parametric roll

Preliminary time-domain calculations

A first prediction of the sensitivity of the feeder ship to parametric roll was obtained by means of time-domain calculations. These calculations were carried out using the CRNavies' code FREDYN, at the ship draught of 8.0 m, a water depth of 33 m and various head wave conditions.

A preliminary roll decay simulation showed that the ship natural period of roll was 21.5 s.

From the computations it was found that the ship may exhibit parametric roll in significant wave heights of 4.5 m or above, in combination with wave peak periods between 11 and 12.5 s.

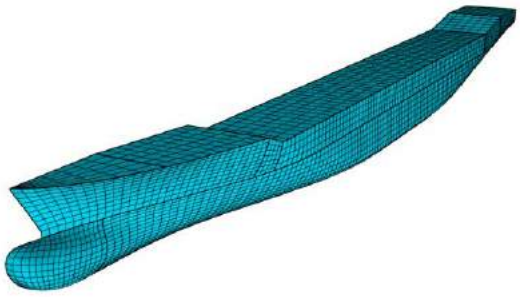

Figure 3-40: Hull form of the feeder used for the computations

Model test results

Based on the findings from the calculations, the test programme was engineered, see Table 3-7. The tests were carried out in long-crested head waves of significant height 4.5 to 7.5 m, combined with peak periods of 11 and 11.9 s. The mean ship speed varied per test between 1 and 4 kn, which was considered realistic. Prior to the tests in waves, a decay test conducted at zero speed indicated a natural period of roll of 20.9 s.

The maximum amplitudes of roll and transverse acceleration at a container located on the outermost row and on top tier (12.3 m from CL to portside and 25.2 m above BL) are provided in Table 3-12. It can be seen that the largest amplitude of roll measured during the tests is 12 deg, that of the transverse acceleration 0.4 m/s^2.

Table 3-12: Maximum amplitude of roll and transverse acceleration at container location

Hs [m]	Tp [s]	Vs [kn]	Max roll amplitude [deg]	Max AY container amplitude [m/s^2]
4.5	11.8	4	3.7	0.24
6.0	11.0	2	8.1	0.33
6.0	11.8	4	12.0	0.38
7.5*	11.0	2	11.6	0.41

**Measured wave height 7.1 m*

Figure 3-41: Occurrence of parametric roll during the test in head waves - Hs = 6 m, Tp = 11 s

The time traces of roll measured during all tests are provided in Figure 3-42. It can be seen that in Hs = 4.5 m no sign of parametric roll is observed, with relatively small amplitudes between the 3 and 4 deg. Increasing the wave height to 6 m yields the first occurrences of parametric roll, particularly visible in the case with the longer wave period. In 7.5 m high head waves (measured height 7.1 m) occurrences are also visible, but the amplitudes are not higher than the 6.5 m high wave condition.

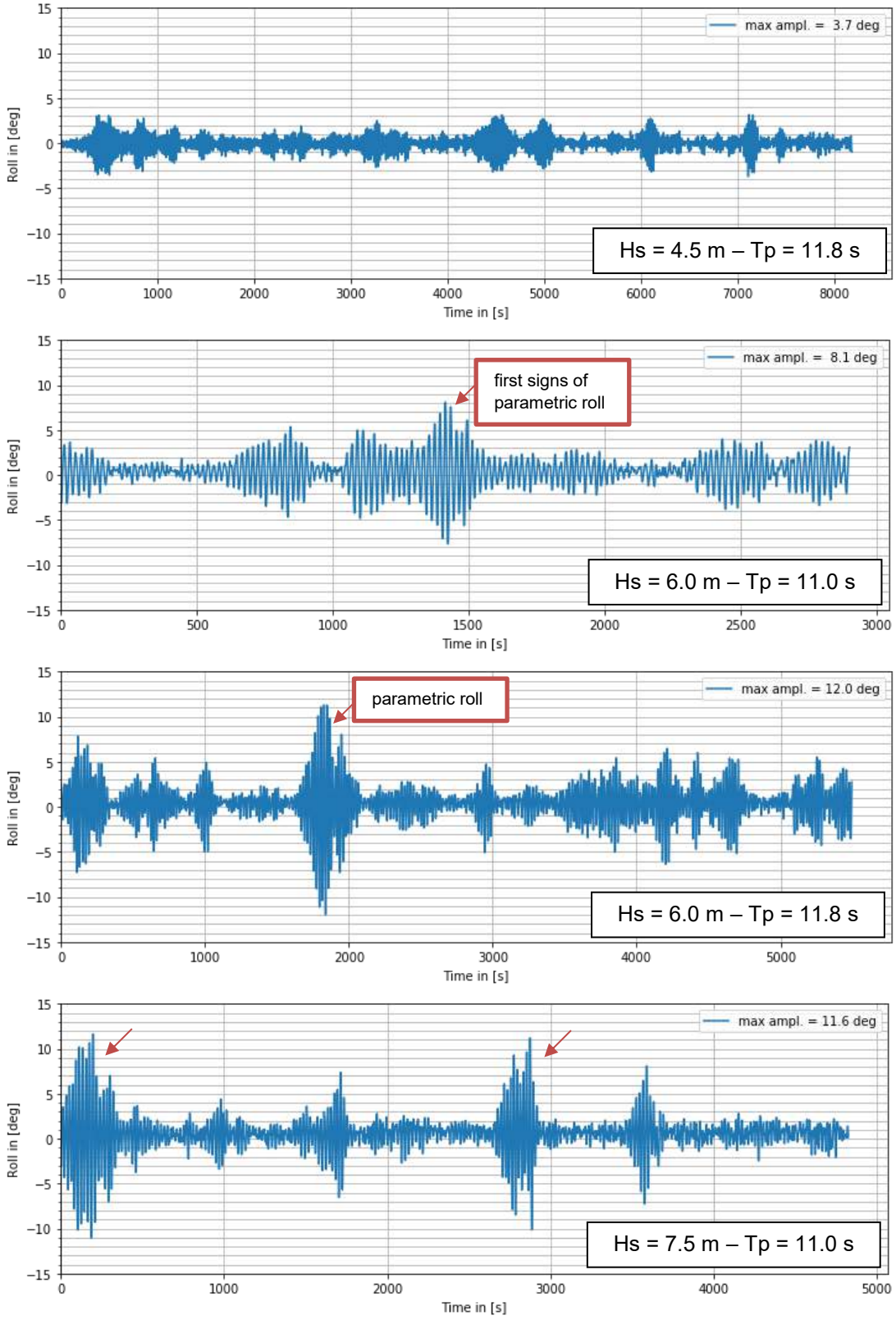

Figure 3-42: Occurrence of parametric roll during the tests in four head wave conditions

In order to determine whether the transverse accelerations applied on containers that are induced by parametric roll could be excessive, the most probable maximum (MPM) acceleration for a 3-hour exposure period was calculated, using the same approach as for the relative wave elevation described in 3.3.6. This MPM value was then compared to the design levels supplied by four classification societies for the previous study[16], see Table 3-13. The results are presented for the four test conditions under the form of cumulative distribution plots in Figure 3-43. The distribution and MPM value are those of the positive acceleration amplitudes or the negative ones, whichever was found most severe.

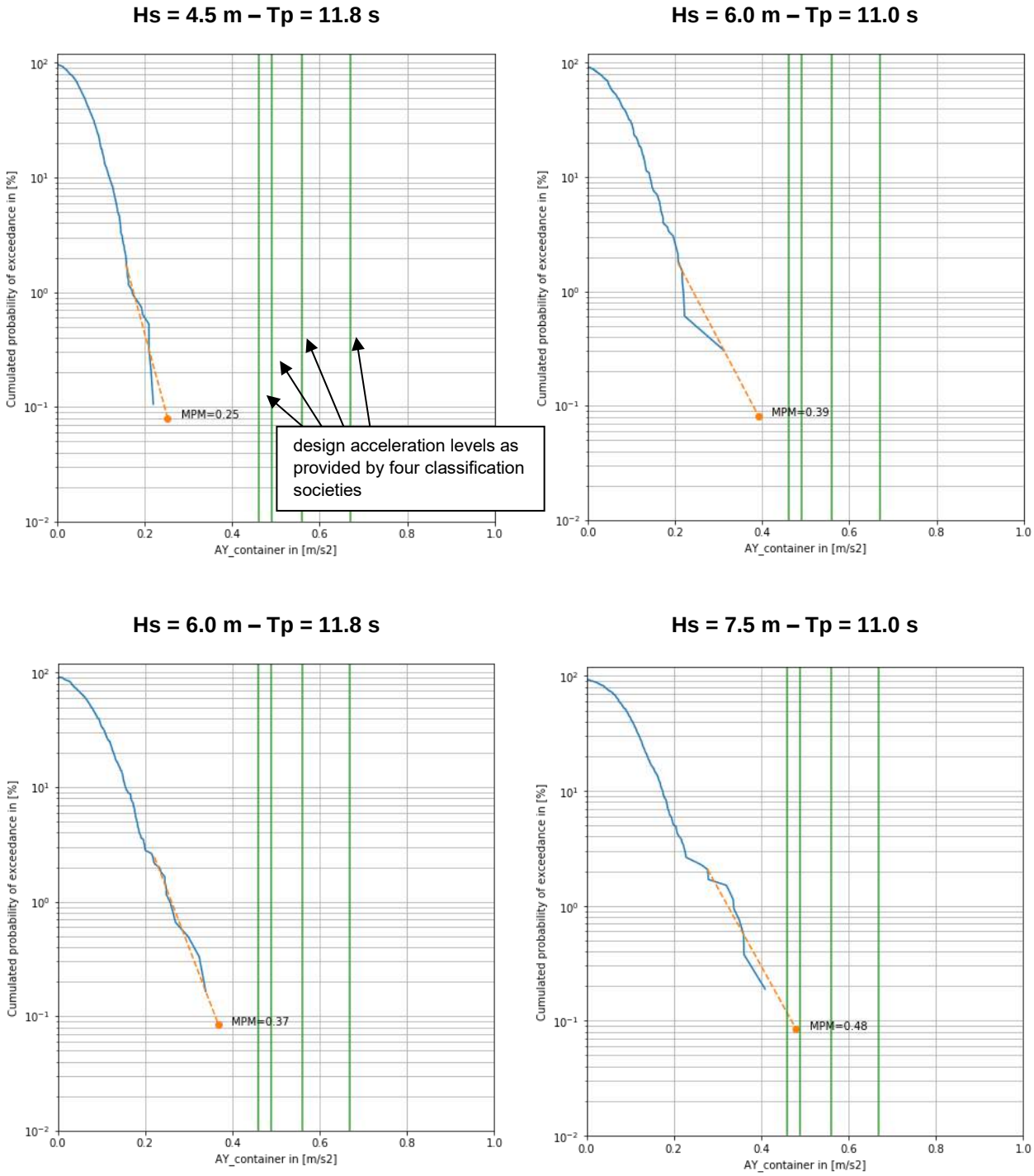

Figure 3-43: Cumulative distribution of the transverse acceleration at side container with mpm estimate

16 'Further Investigations into the Behaviour of Container Ships in Storms above the Wadden Islands', Summary report, Report No. 32558-1-DIR, September 2020

Table 3-13: Design transverse acceleration values as provided by four classification societies

	CR1	CR2	CR3	CR4
Design level [m/s^2]	0.67	0.46	0.49	0.56

From the results it can be seen that the MPM estimates in wave heights 4.5 and 6.0 m are at most 0.39 m/s^2 and therefore do not exceed any of the four design acceleration values. For Hs = 7.5 m, the MPM obtained is 0.48 m/s2, which is found to exceed the CR2 limit (0.46 m/s^2) and be very close to the CR3 limit (0.49 m/s^2). However it remains far from the CR4 (0.56 m/s^2) and CR1 limits (0.67 m/s^2).

Therefore, it may be concluded that occurrences of parametric roll in head waves is not expected to generate any excessive accelerations in significant wave heights up to 6.0 m. In 7.5 m the consequences of parametric roll on stack loss integrity remain unclear as only two out of the four design limits are exceeded.

4 GREEN WATER SIMULATIONS

In Section 3.5.1, limiting wave heights were estimated using the model test results and 2 different estimation methods; method 1 using a criterion of not allowing the underside of the bottom containers to get wet at all, method 2 using a criterion of measured force sensor loads on the containers not exceeding a (semi)-static yielding limit.

To come to more accurate estimations of the limiting wave heights, numerical simulations were performed after the model tests, using the model test results as necessary input. These numerical simulations consisted of a coupled CFD (Computational Fluid Dynamics) and FE (Finite Element) analysis. By coupling these 2 high-fidelity numerical models, accurate predictions of the behaviour of a container stack during actual green water events (that were encountered during the wave basin tests) could be made. For each of these green water events, the numerical simulation will provide a realistic prediction on whether a container (stack) will be lost or not. However, only a limited number of such simulations can typically be performed, as these simulations are very time consuming and computationally costly (many days per case on a High Performance Computer), depending on the simulation case. Therefore, a selection of to-be-simulated green water events was made from all the green water events that were encountered during the model tests, covering a broad range of conditions (such as vessel configuration, wave heading, and severity of the green water event). In total 12 events were selected. By assessing for these specific 12 events whether a container (stack) will be lost or not and relating this result back to quantities such as the relative wave height, wave heading and vessel configuration, more accurate estimations of the limiting wave heights can be made.

Table 4-1: The 12 simulated events, selected from the model tests. All events were taken from tests with a water depth of 21.3m, and a freeboard of 3.8m (time equals time in video)

Sim. #	Config	in wave cond. Hs / Tp	Heading	Impact class	Observations from model test
2-1	2	4.5m/8.5s (t≈7720s)	270	Low	Impact only on bottom panel, not side panel
2-2	2	3.0m/7.0s (t≈2292s)	270	Med	Impact on both bottom and side panel
2-3	2	4.5m/8.5s (t≈4326s)	270	High	Impact mostly hydrostatic (vertical run-up)
2-4	2	4.5m/8.5s (t≈6497s)	270	Extreme	Impact very dynamic (breaking wave)
2-5	2	4.5m/8.5s (t≈3960s)	315	Low	Impact on both bottom and side panel
2-6	2	4.5m/8.5s (t≈4327s)	315	Med-high	Impact on both bottom and side panel
5-1	5	4.5m/8.5s (t≈7720s)	270	Low	N/A
5-2	5	3.0m/7.0s (t≈2292s)	270	Med	N/A
5-3	5	4.5m/8.5s (t≈4326s)	270	High	N/A
5-4	5	4.5m/8.5s (t≈6497s)	270	Extreme	N/A
5-5	5	4.5m/8.5s (t≈3960s)	315	Low	N/A
5-6	5	4.5m/8.5s (t≈4327s)	315	Med-high	N/A

Table 4-1 lists the 12 selected events from the model tests that were reconstructed in the numerical simulations. For quick reference, these 12 events (and corresponding simulations) were given a simulation number, consisting of the freeboard configuration (see Figure 3-2) followed by a case number. So for example, sim. #5-2 corresponds to freeboard configuration 5, case 2. All simulations were performed at a water depth of 21.3m and a vessel freeboard of 3.8m. Table 4-1 shows that actually 6 distinct cases were selected, all from the model tests with freeboard configuration 2 (sim. #2-1 through 2-6). By assuming that the vessel motions are not influenced by the container configuration, these cases were then repeated with configuration 5 (sim. #5-1 through 5-6). This approach will make it possible to correlate the results of the two simulated configurations. Additionally, it is remarked that the first 4 cases

per configuration are beam-on conditions, while the last 2 cases are stern-quartering. This because from the model test results, the beam on conditions showed to be more critical in terms of green water events.

The reconstruction methodology used to replicate the selected green water events from the model tests within the numerical simulations was based on the use of CFD software “COMFLOW”, and is explained in detail in the attached “EXTReme event matching Analysis (‘EXTRA’)” leaflet. In short, both the incoming wave and vessel motions are taken from the selected model test events, and are accurately reconstructed within the CFD model using an iterative procedure. After the reconstruction, the selected events can be rerun in the CFD simulation, while monitoring all areas and quantities of interest. Figure 4-1 shows the vessel geometry used within the CFD model, for both configurations. As quantities of interest, the pressure distributions at either container stack locations 2 or 3 (close to midship) were considered, depending on the case number. These locations are accentuated in Figure 4-1.

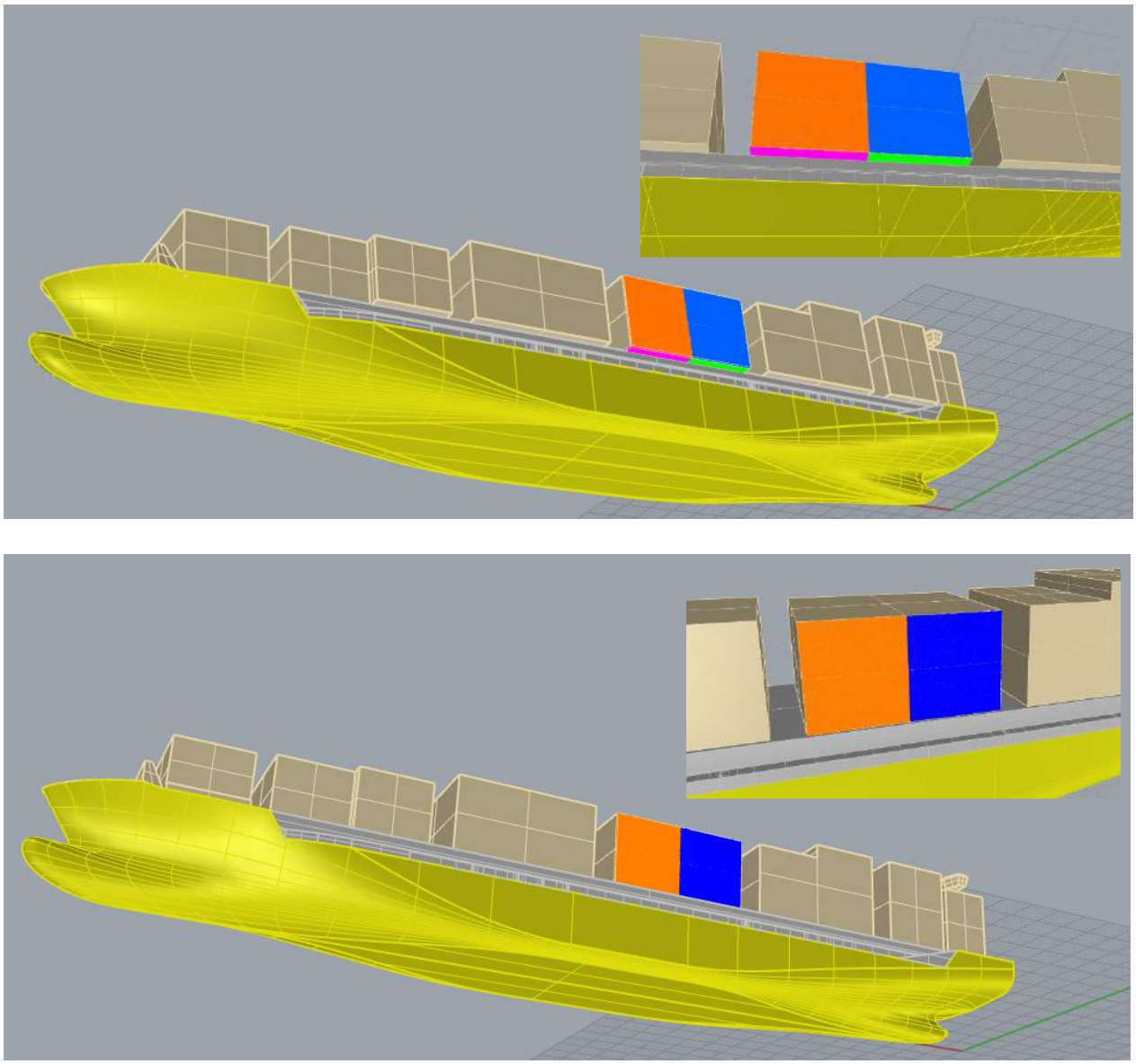

Figure 4-1: Location of the 2 container stacks that were considered in the numerical analysis. Top: configuration 2. Bottom: configuration 5. Container stack location 2 in blue (and green), container stack location 3 in orange (and pink).

For the final CFD simulations, a grid resolution of 12.5cm (dx=dy=dz) was applied at the free surface and container geometry, using adaptive mesh refinement. This resulted in a total number of computational cells ranging from 23M to 41M cells, and a total computational time ranging from 4 to 18 days, depending on the simulation case. All simulations were run on MARIN's latest HPCC solution Marclus5, consisting of over 9000 CPUs.

In Figure 4-2, typical results of the CFD simulations are depicted by means of snapshots, for both a beam-on and a stern-quartering case with configuration 2. Snapshots from the model test video at approximately the same time instances are added as reference.

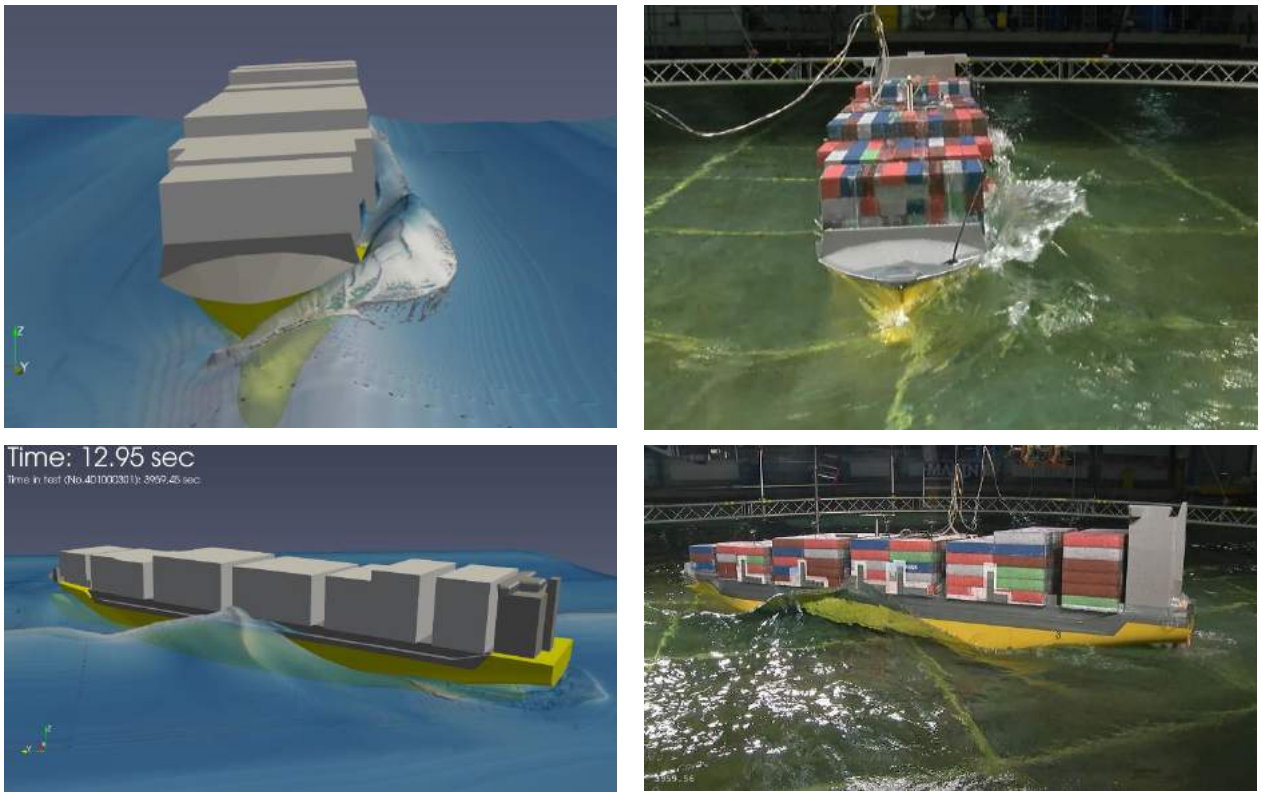

Figure 4-2: Snapshots of green water event #2-3 (top) and #2-5 (bottom). Next to the CFD simulation results (left), also a snapshot of the model test video (right) at approximately the same time instance is added as a reference.

As output of the 12 CFD simulations, detailed pressure distributions were produced to serve as input to the Finite Element model. Table 4-2 lists the container stack location for which these pressure distributions were outputted, together with the relative wave elevation at the stack location, for each of the simulations.

Table 4-2: Location of container stack for which pressures were outputted, together with the associated maximum relative wave elevation at that stack location, for each of the simulated cases.

Sim. #	**2-1**	**2-2**	**2-3**	**2-4**	**2-5**	**2-6**	**5-1**	**5-2**	**5-3**	**5-4**	**5-5**	**5-6**
Stack location [-]	2	2	3	2	3	3	2	2	3	2	3	3
Max rel. wave amplitude [m]	5.5	8.0	13.5	8.5	8.4	10.2	5.5	8.0	13.5	8.5	8.4	10.2

5 CONTAINER STACK BEHAVIOUR

Finite Element calculations were carried out on models of a 40-foot container and a container stack to determine their behaviour following an impact load caused by green water. In order to perform these calculations the FEM solver Abaqus was coupled to the CFD software COMFLOW (which results are presented in Chapter 4). The coupling was realised in one way (CFD to FEM), using a mapping method that was developed during the course of the project. In this method the pressures obtained from the CFD calculations were converted into FEM element surface pressures, in the time domain. The FE calculations were performed for all twelve cases run in CFD, as listed in Table 4-1.

5.1 Container and container stack modelling

The container geometry used in the modelling was based on the construction drawing of a 40-foot container available online[17]. Main and secondary steel structural components of the container were modelled including also the bottom plywood floor. End doors were neglected in the model but additional basic stiffness elements were added to include their effects.

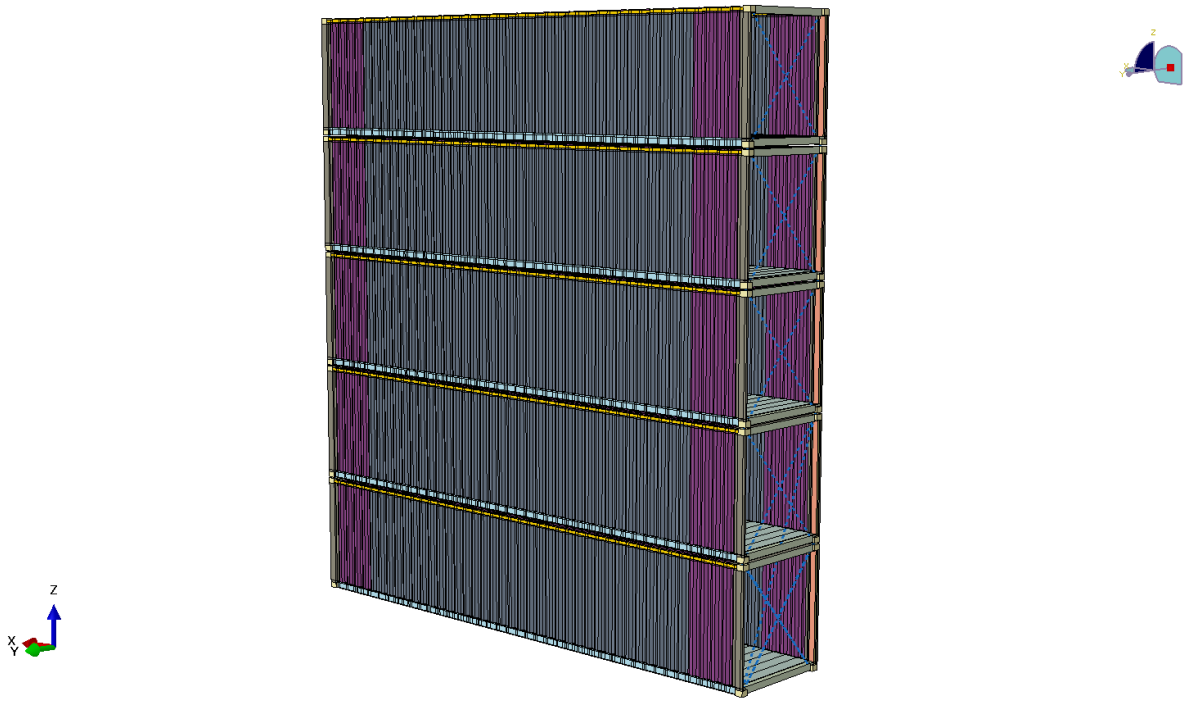

Figure 5-1: Geometry model of the container stack with 5 containers

The finite element mesh of the container stack can be seen in Figure 5-2 on the next page. The bottom two containers were finely meshed with characteristic element size of 30 mm, while the three containers above were meshed relatively coarsely, as it was observed during the tests and CFD that green water concentrates mostly on the bottom two containers. The resulting FEM model consists of approximately 200000 element in total.

The container FEM model was verified by performing a stiffness calculation check. Stiffness values were taken from the previous Lashing@Sea project report by GL[18]. Only the transverse stiffness values

[17] www.shipped.com
[18] Model Scale Desing of a 20' ISO-1CC Container Report No. NB-RA 2008.02 Version 2008-09-03/1

from that project were used by assuming that the 20-foot and 40-foot containers have the same transverse stiffness values. The longitudinal stiffness was verified based on the findings of Zha[19].
In order to obtain the similar stiffness value at the door end of the container, basic axial connector elements were added. These are marked by the red lines in Figure 5-4. The stiffness of these elements were calculated by ensuring that the container structure has the same stiffness value at the door end side. A stiffness comparison is given in Table 5-1.

Figure 5-2: FEM mesh of the container stack

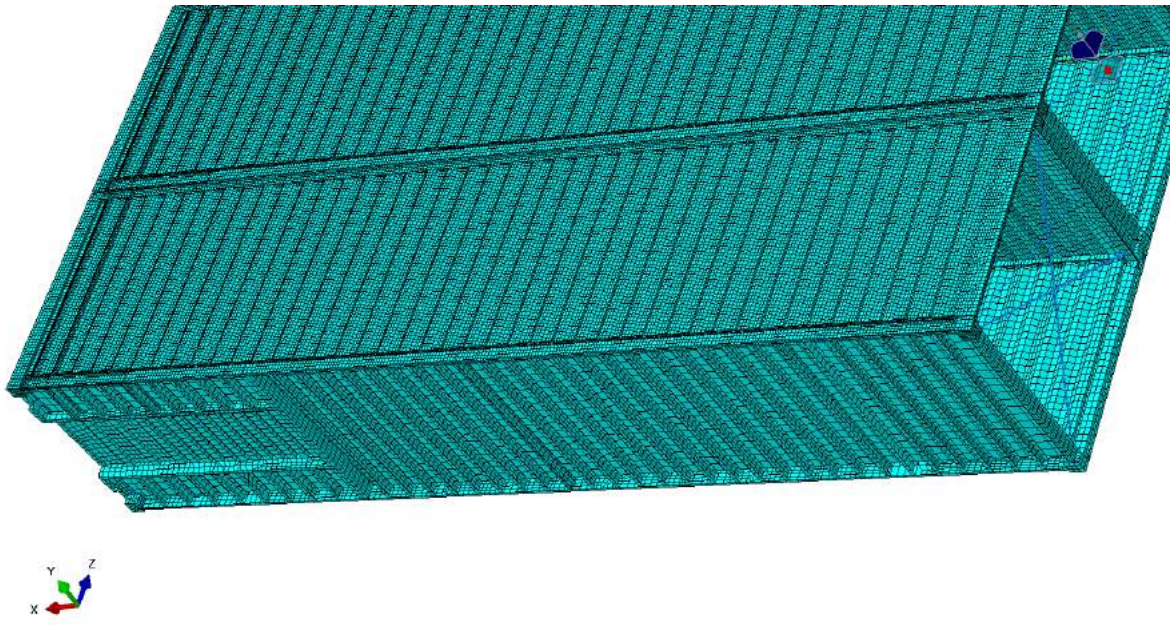

Figure 5-3: FEM mesh of the container stack

[19] Zha X and Zuo Y. Theoretical and experimental studies on in-plane stiffness of integrated container structure. Adv Mech Eng 2016; 8: 1–20.

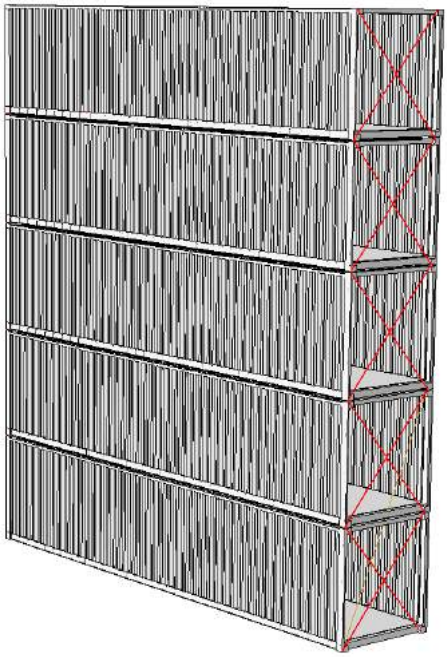

Figure 5-4: Additional axial connectors for end doors

Table 5-1: Stiffness verification of the FEM model of one container

	Literature	Calculated in FEM model
	kN/mm	kN/mm
Transverse Stiffness		
Closed end	57	60.41
Door end	3.4	3.38
Longitudinal stiffness	90	88

A basic lashing arrangement which was given in GL rules[20] was accepted as seen below Figure 5-5.

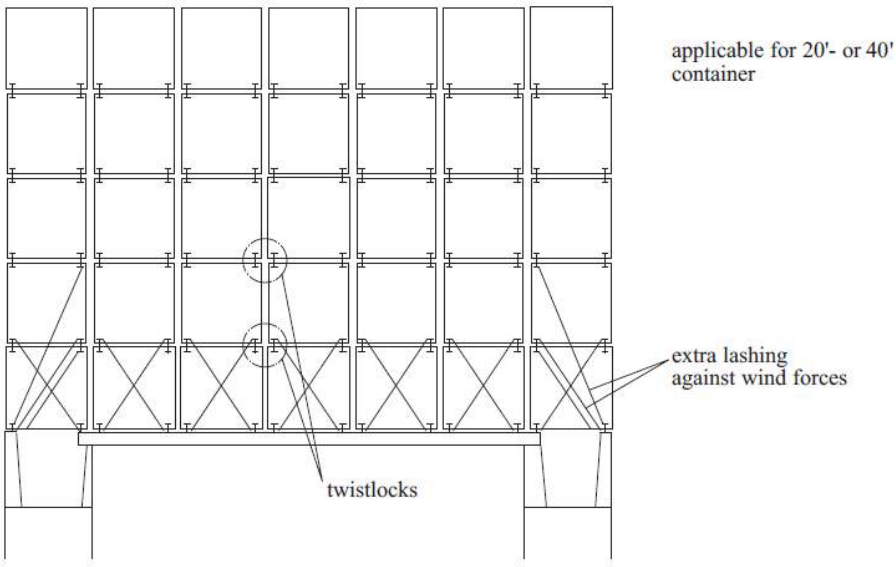

Figure 5-5: Basic lashing arrangement

[20] Stowage and Lashing of Containers GL Rules 2013

The applied lashing system in the FEM model can be seen in Figure 5-6. Four short crossing lashing rods were used to connect the lowest tier container bottom corners to the second tier container bottom corners. A long crossing lashing rod was used to connect the bottom container lower corner to the second tier container top corner. Stiffness values were calculated according to GL rules and applied to the model with a non-linear behaviour as can be seen in Figure 5-7. A 5,000 N pre-tension load was also applied.

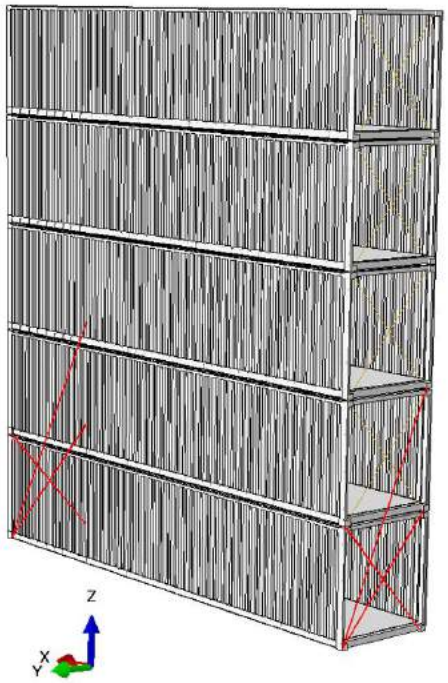

Figure 5-6: Applied lashing system

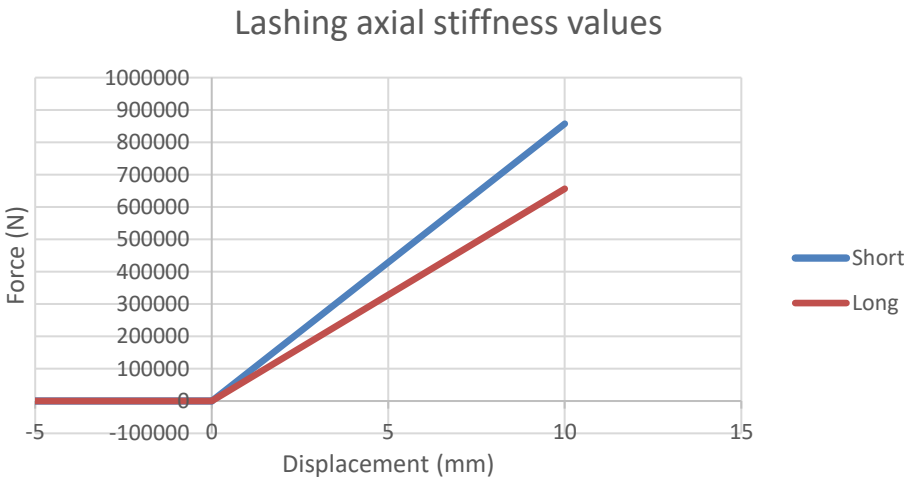

Figure 5-7: Lashing stiffness values

Containers are connected to each other's by using twist locks as can be seen in below figure. The stiffness values of the twist locks were obtained from the tensile test given by de Souza[21] as in Figure 5-9. The twist lock stiffness was modelled in a non-linear way, including gap values of 4 mm in vertical (Z) direction, 14 mm in longitudinal (X) direction and 6 mm in transverse (Y) direction. These gap values were taken from a Lashing@Sea project report[22].

[21] De Souza, Vinicius Aguiar Study on the Dynamic Response of Container Stacks Using Non-Linear Finite Element Analysis, PhD Thesis, The University of Tokyo, 2010.

[22] LASHING@SEA – MCS container tests - No 1 19717-14-TM Date : October 2009

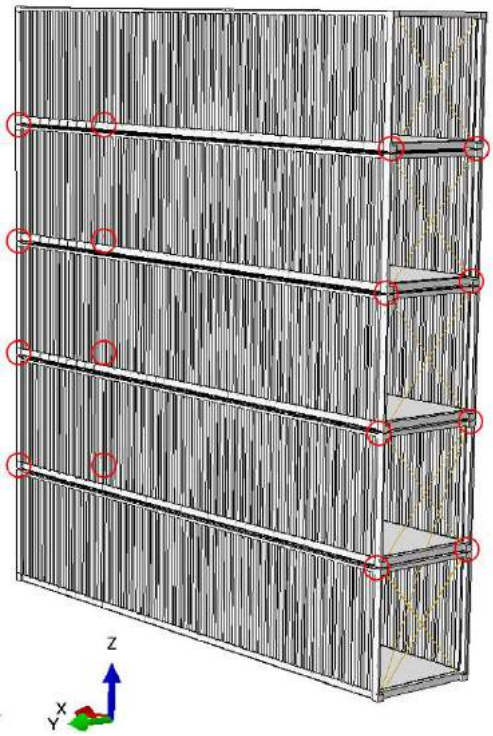

Figure 5-8: Twist lock arrangement

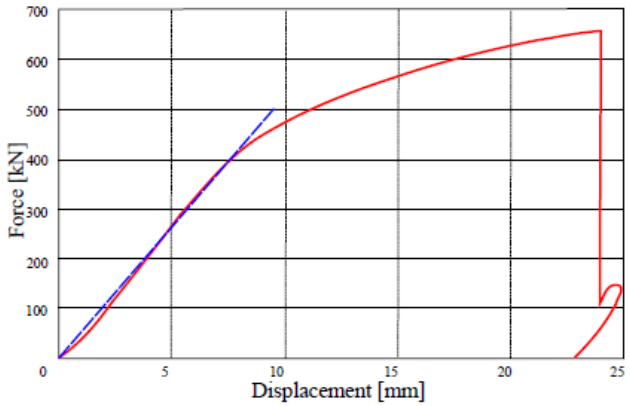

Figure 5-9: Tensile test results of twist locks. De Souza (2010)

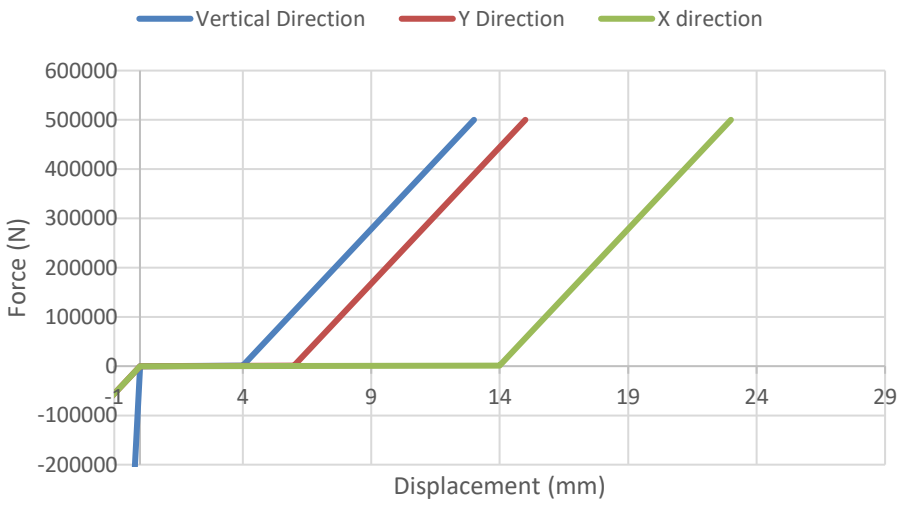

Figure 5-10: Stiffness values of twist locks

To observe damage or possible loss of a container or a container stack, breaking limits for lashing rods and twist locks were defined in the FEM model. They were taken from GL rules[23]. In order to account for limitations in the modelling, such as the absence of longitudinal loads on the two short sides of the containers, the limits were reduced by 5%. The original and corrected limits are seen in Table 5-2.

Table 5-2: Lashing system breaking limits

Equipment	Breaking limit from GL (kN)	Breaking limit applied (kN)
Twist lock vertical	500	475
Twist lock horizontal	420	400
Lashing rod	460	437

A point mass was defined for each container and connected to the bottom transverse beams. Each container mass and total value can be seen in Table 5-3.

Table 5-3: Mass distribution of the container stack

	Container Masses
	Tonnes
Tier 1	30.4
Tier 2	30.4
Tier 3	23.6
Tier 4	13.6
Tier 5	13.6
Total	**111.6**

Material properties were evaluated following Ehlers[24] (2009) and the report of the MarcolXMF[25] project. Tensile test results for S275 Mild steel were published by Ehlers. The applied S275 material property can be seen in Figure 5-11 below. An element failure plastic strain value of 0.2 was used, according to the element size used in the FEM model. Cowper-Symonds material deformation law was also applied for impact related strain-rate effects on the material, considering D and q coefficients of 40.4 and 5 respectively in the Cowper-Symonds equation for mild steel.

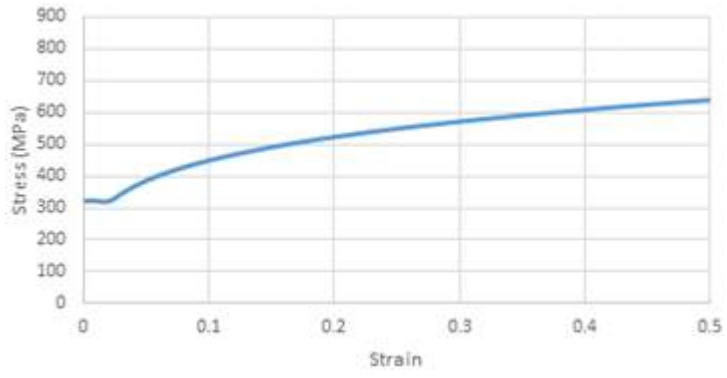

Figure 5-11: S275 Mild steel true stress strain curve

The bottom floor of a container is generally made from hard marine grade plywood. The material property of such plywood is taken from the 'Plywood Design Specification, 1997' book. An isotropic linear material property is used with an elasticity modulus of 7000 MPa and gravity of 900 kg/m^3.

[23] Stowage and Lashing of Containers GL Rules 2013

[24] Ehlers, S., Varsta, P., 2009. Strain and stress relation for non-linear finite element simulations. Thin-Walled Struct. 47 (11), 1203–1217.

[25] Tensile Test Simulation in Abaqus, 30703-HSS-01, Levent Kaydihan, MARIN, December 8, 2020

5.2 FEM calculation results

The time dependent pressure distributions obtained from the twelve CFD calculations as listed in Table 4-1 were mapped and applied to the FEM model by using a Radial Basis Function - based mapped algorithm. The results from the FEM analyses are summarised in Table 5-4.

Table 5-4: Results summary of FEM analyses

Sim	Conf	Mu	Impact class	Cont. stack loss	Cont. damage	Side panel deform. after Impact	Damage to bottom floor	Horiz. load on twist locks	Axial load on lashing rods
[-]	*[-]*	*[deg]*	*[-]*	*[y/n]*	*[y/n]*	*[mm]*	*[y/n]*	*[% max capacity]*	*[% max capacity]*
2-1	2	270	Low	No	No	0	No	9.6%	2%
2-2	2	270	Med	No	No	0	No	30%	42%
2-3	2	270	High	No	Yes	544	Yes	65%	65%
2-4	2	270	Extreme	**Yes**	**Yes**	558	Yes	**>100%**	54%
2-5	2	315	Low	No	No	0	No	3%	7%
2-6	2	315	Med-high	No	No	0	No	4%	10%
5-1	5	270	Low	No	No	0	No	0%	0%
5-2	5	270	Med	No	No	0	No	20%	41%
5-3	5	270	High	No	**Yes**	569	Yes	56%	64%
5-4	5	270	Extreme	No	**Yes**	404	No	37%	35%
5-5	5	315	Low	No	No	0	No	3%	7%
5-6	5	315	Med/high	No	No	7.5	No	2%	10%

In the present summary two failure criteria are defined: container damage and container stack loss. In the case of container damage, it is considered that the container structure has residual deformations that are so large that the container content may be damaged and the container may not be used anymore. Considerations of damage to the bottom floor are also included here. Regarding container stack loss, attention is paid not only to the damage brought to the containers but also to the integrity of the lashing system. In the case the lashing system (with twist locks and lashing rods) is broken, the stack stability is deemed lost and stack loss is likely to occur.

Table 5-4 also indicates the load applied on twist locks and lashing rods as fraction of their breaking limit, see Table 5-2. It should be noted that only horizontal loads are considered here as they were found more critical than vertical loads. For lashing rods, used axial loading capacity values are given.

As can be seen from the Table 5-4, beam on cases 2-3 and 2-4 are the worst cases and in both cases the bottom container is lost. In case 2-4, twist locks were also damaged and therefore, stack loss stability is lost anymore and container stack lost likely happens. The stern-quartering cases 2-5 and 2-6 were not severe cases because the applied pressures are acting locally and moving with the wave crest over the side of the container while in beam on cases those pressures are effective on whole side panel at once. For configuration 5, similar responses were obtained except 5-4 case.

For the extreme case in configuration 2 simulation 2-4, deformation results can be seen below in Figure 5-12. The detailed pictures of all cases can be seen on pages F21 to F44.

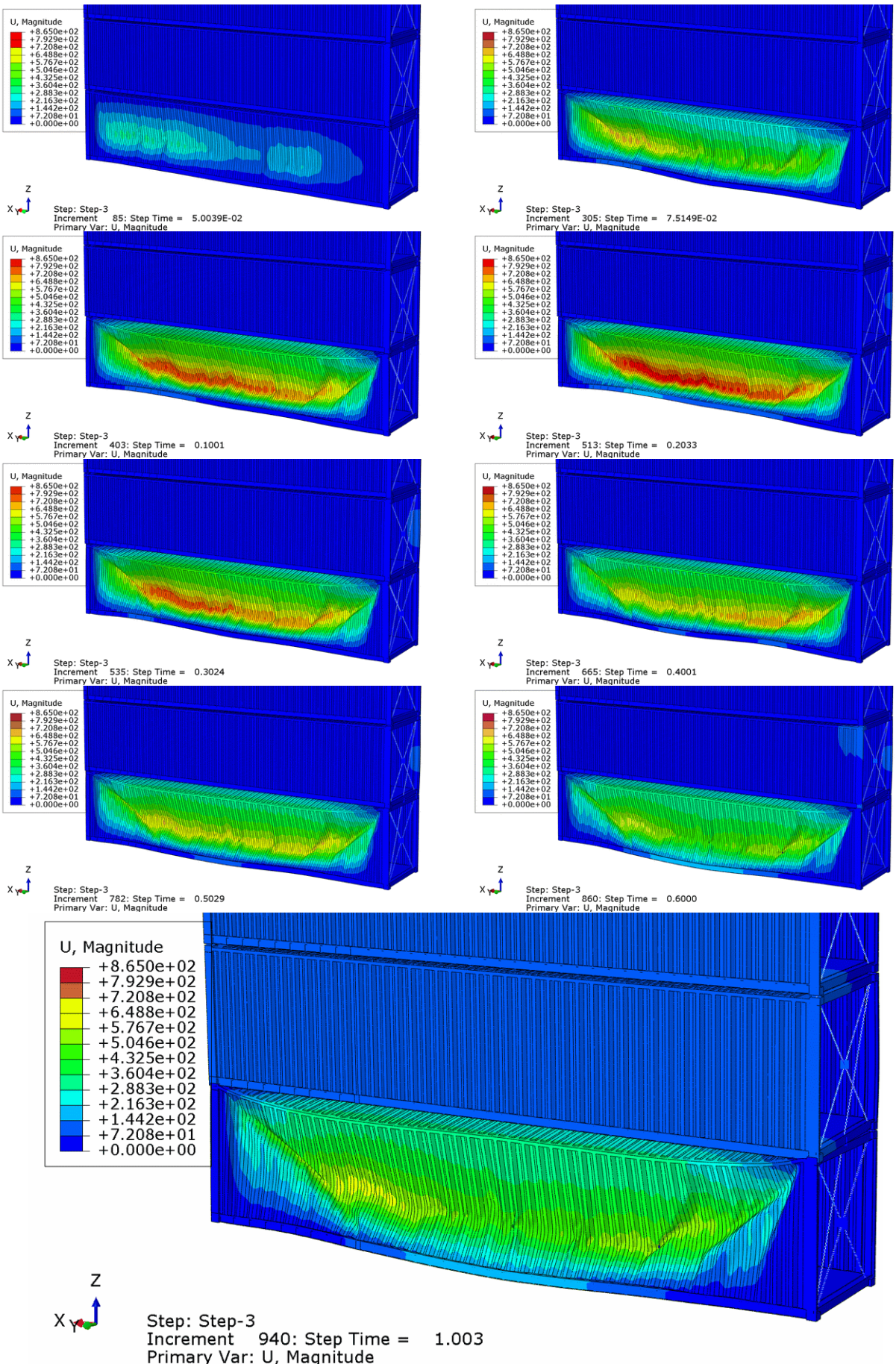

Figure 5-12: Simulation 2-4 (Beam seas), Deformation of the container at different time steps (top) and residual damage and displacement values at the end (bottom)

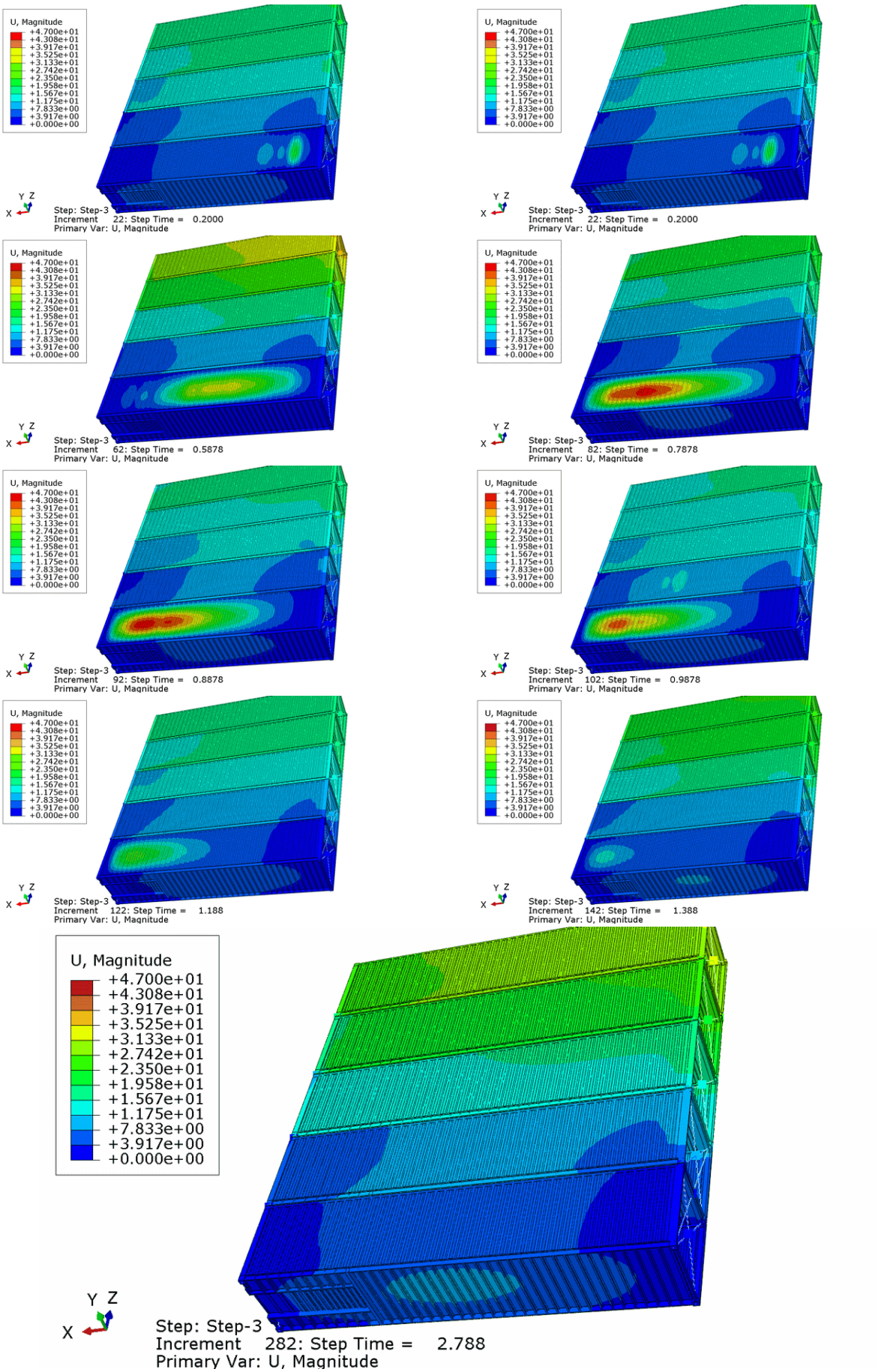

Figure 5-13: Simulation 2-6 (stern-quartering seas), Deformation of the container at different time steps (top) and residual damage and displacement values at the end (bottom)

6 LIMITING WAVE HEIGHTS

6.1 Followed methodology

The results of model tests (Chapter 3), CFD simulations (Chapter 4) and FE simulations (Chapter 5) were combined to determine the limiting wave heights, above which green water loads on deck containers are deemed excessive (leading to severe container damage and loss of stack). The methodology followed is summarised in Figure 6-1.

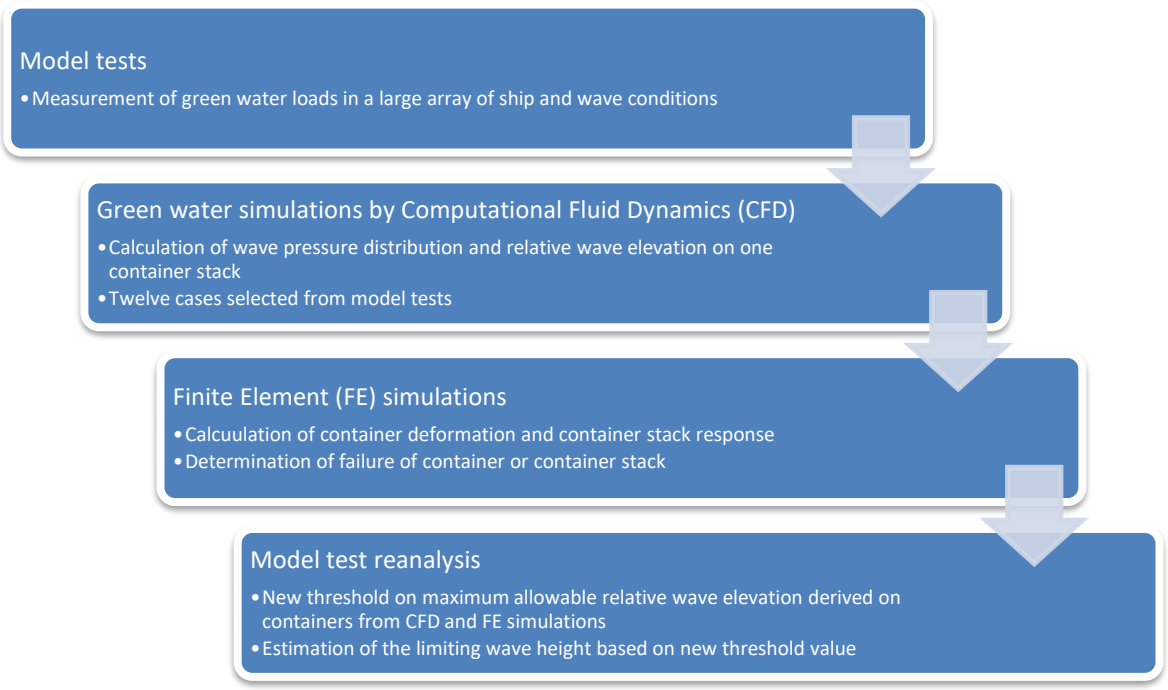

Figure 6-1: Overview of the methodology followed to determine the limiting wave heights

The model tests served a dual purpose. First, they provided a good overview of the influence of several ship and wave parameters on the occurrence and amplitude of green water loads on side and front containers. Second, they allowed to estimate the limiting wave heights by comparing mpm estimates of the relative wave elevation with a suitable threshold, following the approach as described in Section 3.3.6 and already applied as “first method” in Section 3.5.1. On their side, the CFD and FE simulations aimed at “re-evaluating” the threshold value, after a first estimation was obtained in the previous study[26].

The process of determining the new threshold value for the relative wave elevation based on the CFD and FE simulations is described in Section 6.2, the estimation of the limiting wave heights is presented and discussed in Section 6.3.

6.2 Threshold to container failure and container stack failure

As mentioned earlier, a first determination of a criterion for container failure was undertaken in the previous study based on finite element analysis. By considering maximum yield and buckling limits of the side panel of a container, a maximum transverse load pressure of 11 kPa was derived, assuming constant pressure over the complete side or front panel. Comparing this value to the green water loads measured during the tests led to the conclusion that a contact of water with the container was already enough to generate damage, and therefore should be avoided. The initially adopted threshold on the maximum relative wave amplitude was thus the vertical distance between the still water line and the

[26] MARIN report 32558-1-DIR

bottom panel of the lowest tier container. This is a conservative criterion as it is logical that the containers can withstand some water impact loading before structural collapse will occur.

Because this simple criterion was considered not adequate for the determination of the final limiting wave heights, a larger number of CFD and FE simulations was carried out to refine the threshold. This was done by drawing a relation between the peak of the relative wave elevation close to the container stack (obtained from the CFD simulations) and the failure of the container or whole container stack (obtained from the FE simulations), as shown in Table 6-1. Out of the many impacts seen in the model tests, twelve events were carefully selected for CFD and adjacent FE analysis.

Table 6-1: Overview of container failure study for the twelve cases

Sim	Conf	Mu	Impact class	Peak relative wave ampl.	Description of impact during model tests	Container stack loss	Container damage
[-]	*[-]*	*[deg]*	*[-]*	*[m]*	*[-]*	*[y/n]*	*[y/n]*
2-1	2	270	Low	5.5	only on bottom panel, not side panel	No	No
2-2	2	270	Med	8.0	on both bottom and side panels	No	No
2-3	2	270	High	13.5	mostly hydrostatic (vertical run-up)	No	Yes
2-4	2	270	Extreme	8.5	very dynamic (breaking wave)	**Yes**	**Yes**
2-5	2	315	Low	8.4	on both bottom and side panels	No	No
2-6	2	315	Med-high	10.2	on both bottom and side panels	No	No
5-1	5	270	Low	5.5	-	No	No
5-2	5	270	Med	8.0	-	No	No
5-3	5	270	High	13.5	-	No	**Yes**
5-4	5	270	Extreme	8.5	-	No	**Yes**
5-5	5	315	Low	8.4	-	No	No
5-6	5	315	Med/high	10.2	-	No	No

When looking at the four results for configuration 2 in beam waves (simulations 2-1 to 2-4), it is noted that no damage occurs on the container stack for low and medium impacts, with associated peak relative wave amplitude of 5.5 and 8.0 m. In this situation the wave crests do not go higher than two-thirds of the bottom container. The other two simulations, namely with high and extreme impacts, show different results. In the high impact case (sim 2-3), the wave load yields an important inward bending of the side panel, hence it is concluded that the container (and its content) is so damaged that it may be considered as lost. Nevertheless, the container structure and overall lashing arrangement, and therefore the whole stack integrity, are deemed still good. The peak relative wave amplitude is in this case the highest: 13.5 m, meaning a wave crest reaching the top of the third container tier. In the extreme impact case (sim 2-4) the inward bending of the bottom container side panel and longitudinal beams is such that the twistlocks are expected to break. In this case it is expected that the stack will be eventually lost. In this simulation the peak relative wave amplitude is 8.5 m, meaning a wave crest reaching the top of the bottom container. A comparison with the medium impact case (8.0 m relative wave elevation) shows a rather logical trend:an increase of 0.5 m represents indeed one fifth of the container height and the overall pressure field is expected to increase significantly between the two cases.

Comparing the result with the high load gives a rather confusing picture, as the trends of impact (and resulting failure on the container stack) and relative wave elevation are found to be opposite, with a very large different in peak amplitude (5 m). This different behaviour is explained by the nature of the loads: the high load of simulation 2-3 is mainly of hydrostatic character, whereas the extreme load of simulation 2-4 is definitely dynamic. Because the relative velocities of the water particles are much lower in the case of a hydrostatic load than in a dynamic load, a much higher crest elevation is needed to come to the same fluid pressure. This is why dynamic loads are deemed more dangerous than hydrostatic loads, and therefore the result of simulation 2-4 is very meaningful. In the light of the above, a threshold relative wave amplitude of 8.0 m, meaning a wave crest reaching two-thirds of the bottom container height, is considered for the configuration 2 in beam waves.

The determination of the threshold for configuration 2 in stern-quartering waves followed the same approach, however based on a smaller number of cases. From the two cases considered, one low and one medium-high, no significant damage was observed to either a single container or the whole container stack structure. Therefore, the threshold is set to the highest relative wave elevation determined from the calculations, being 10.2 m.

Threshold applied to other freeboard heights

Since the adopted approach for the determination of the threshold uses a relation between the relative height of the wave crest with respect to the bottom container and container (stack) damage, the threshold is adjusted to other freeboard heights by simply adding or subtracting the difference in freeboard height to it.

Threshold applied to other freeboard type

The simulations performed for configuration 5, the configuration with same freeboard height as configuration 2 but a different layout (all containers on deck) give the same peak relative wave amplitude and same failure indicator as for configuration 2. Therefore it is considered that the difference in freeboard type does not affect the determination of the threshold value.

Summary

The process in Figure 3-36 was repeated for the new threshold values. The final threshold values to the relative wave elevation, applied to the six freeboard configurations considered in the present study, are summarised in Table 6-2. Compared with the previous threshold values they are higher by 1.7 m.

Table 6-2: New threshold values for relative wave height

	Config.1	**Config.2**	**Config.3**	**Config.4**	**Config.5**	**Config.6**
Freeb. type [-]	**Outer row above gangway**			**All on hatch covers**		
Freeb. hght [m]	**2.3**	**3.8**	**5.3**	**2.3**	**3.8**	**5.3**
Old threshold [m]	4.8	6.3	7.8	3.8	6.3	7.8
New threshold [m]	6.5	8.0	9.5	6.5	8.0	9.5

6.3 Limiting wave heights

Similarly to the analysis presented in the last part of Section 3.5.1, limiting wave heights are derived considering the new relative wave height threshold values. They are listed in Table 6-3 and Table 6-4.

Table 6-3: Limiting significant wave height for six freeboard configurations, water depth 21.3 m

	Config 1	**Config 2**	**Config 3**	**Config 4**	**Config 5**	**Config 6**
Freeboard	**2.3 m**	**3.8 m**	**5.3 m**	**2.3 m**	**3.8 m**	**5.3 m**
135/225 deg	3.4 m	4.5 m	5.6 m	N/A	4.6 m	N/A
90/270 deg	2.4 m	3.0 m	3.4 m	2.4 m	3.2 m	3.8 m
45/315 deg	3.5 m	4.9 m	6.0 m	N/A	N/A	N/A

Table 6-4: Limiting significant wave height for three different water depths, configuration 2

Depth	**21.3 m**	**37.5 m**	**100 m**
135/225 deg	4.5 m	6.4 m	6.4 m
90/270 deg	3.0 m	3.1 m	3.1 m
45/315 deg	4.9 m	5.8 m	6.4 m

As observed previously, the wave heights determined are approximately the same for both freeboard types, the small differences being explained by slight deviations in the distributions of the relative wave elevations. Noteworthy that limiting wave heights are also determined for bow-quartering waves, whereas no threshold value was estimated for this heading explicitly. For this heading the same threshold values as those derived for stern-quartering waves were applied. It should be underlined, however, that such assumption is based on the fact that a similar ship behaviour and green water activity was observed during the tests in bow-quartering waves and those in stern-quartering waves, which in turn is mainly explained by the zero speed. When forward speed will be taken into account, the interaction between the incident waves and the ship will change, for instance due to a different wave celerity relative to the ship, leading to different green water activity and eventually variations in limiting wave heights.

7 CONCLUSIONS

Green water load impact model tests, CFD (Computational Fluid Dynamics) simulations and FE (Finite Element) calculations were conducted on a 163 m long feeder ship. Based on the results the following conclusions may be drawn:

- Green water load impacts are sensitive to the environmental wave conditions: they are found to be largest in wave conditions with high significant height and low peak period Long-crested yield larger wave loads than realistic short-crested waves.
- The distribution of the relative wave elevation along the windward side was found to be fairly similar for the different freeboard heights and freeboard types tested. Therefore, the green water activity is expected to be dominated by freeboard height. Direct visualisations indicate that the recess formed by the gangway in configurations 1 to 3 can reduce the intensity of green water in some cases.
- Beam waves are the most unfavourable waves from a green water point of view. In such heading the frequency of occurrence and the loads associated to green water are found to be largest. Although comparable loads are measured in stern-quartering waves, beam wave impacts cover a larger container panel area than those from stern-quartering waves at one moment in time, leading to a larger load overall.
- For the lower wave heights the wave loads are similar for the different water depths (21.3m southern route, 37.5m northern route, 100 m deep North Sea). For the higher wave heights the largest wave loads were observed in the lowest water depth (21.3 m southern route).
- The results of model tests, CFD and Finite Element simulations have led to the determination of the following limiting wave heights from the perspective of green water loads applied on side containers. Because of the symmetry of the ship with respect to the centreline the following estimates hold for wave headings from both port (225, 270 and 315 deg) and starboard (135, 90 and 45 deg) sides.

	Config 1	**Config 2**	**Config 3**	**Config 4**	**Config 5**	**Config 6**
Freeboard	**2.3 m**	**3.8 m**	**5.3 m**	**2.3 m**	**3.8 m**	**5.3 m**
135/225 deg	3.4 m	4.5 m	5.6 m	N/A	4.6 m	N/A
90/270 deg	2.4 m	3.0 m	3.4 m	2.4 m	3.2 m	3.8 m
45/315 deg	3.5 m	4.9 m	6.0 m	N/A	N/A	N/A

Depth	**21.3 m**	**37.5 m**	**100 m**
135/225 deg	4.5 m	6.4 m	6.4 m
90/270 deg	3.0 m	3.1 m	3.1 m
45/315 deg	4.9 m	5.8 m	6.4 m

- The estimates given above are lower than the preliminary limiting wave height of 3.3 m obtained for a freeboard of 3 m in the previous study for the Ministry (MARIN report 32558-1-DIR). This can be explained by the wider range of realistic wave conditions that is used for present study and increased insight from the CFD and FE calculations.
- Investigations in head waves have shown that green water loads on the foremost container bay can (only) occur in wave heights of 6 m and higher. The loads measured for Hs = 6 m remain relatively small in comparison with those observed on the side containers in beam waves, however for Hs = 7.5 m they are found to reach relatively high levels.
- Parametric roll is observed in wave heights of 6 m and higher. The transverse accelerations on side containers during parametric roll in waves up to Hs = 6 m remain below the design values supplied by four classification societies. In Hs = 7.5 m the transverse accelerations exceeded the design values given by two classification societies.

8 RECOMMENDATIONS

The Dutch Coast Guard gives by waves higher than 3.3 m the advice to “take necessary measures and/or to sail a different course”. This advice is based on the results of MARIN’s previous study conducted in beam waves (considering a freeboard of 3.0 m).

The objective of the present study was to refine the above limiting wave height by including the influence of wave direction and freeboard. When one considers the most encountered freeboard type (containers over the whole breadth of the ship, configurations 1-3) then the following limiting wave heights are estimated:

Limiting wave height as a function of freeboard height

Freeboard height	**2.3 m**	**3.8 m**	**5.3 m**
135/225 deg (bow-quartering waves)	3.4 m	4.5 m	5.6 m
90/270 deg (beam waves)	*2.4 m*	*3.0 m*	*3.4 m*
45/315 deg (stern-quartering waves)	3.5 m	4.9 m	6.0 m

From the table above it can be seen that beam waves yield the lowest limit. For the range of freeboard heights investigated **the limiting wave height** is 2.4 to 3.4 m.

The results obtained at various wave heights show that this advice is independent of the water depth:

Limiting wave heights as a function of water depth (configuration 2 with freeboard height 3.8 m)

Water depth	**21.3 m (southern route)**	**37.5 m (northern route)**	**100 m (deep North Sea)**
90/270 deg (beam waves)	3.0 m	3.1 m	3.1 m

When the wave height exceeds 3.0 m the situation degrades in shallow water faster than in deep water.

In quartering waves (heading 225 and 315 deg), the situation gets better. The (relative) waves around the ship are lower than in purely beam waves and the loads on the containers are more local and moves together with the wave crest that propagates along the ship. In beam waves, the wave crest collide directly over the whole side panel in a short amount of time.

Nevertheless, the safest measure is to sail at low speed in head waves. Until significant wave heights of 6 m the loads on containers at the bow in head waves are limited and no critical parametric roll is observed.

Wageningen, March 2022
MARITIME RESEARCH INSTITUTE NETHERLANDS

Ir. G. Gaillarde
Head Ships Business Unit

TABLES

Table 1 Main particulars and stability data of the vessel – LC 1 – Tests in OB

Model No. 10246 Model scale ratio λ = 33

Designation	Symbol	Magnitude specified *(realised*)*		Unit
Main particulars				
Length between perpendiculars	L_{PP}	163.00		m
Length on waterline	L_{WL}	165.76		m
Length overall submerged	L_{OS}	171.60		m
Breadth moulded on WL	B_{WL}	27.00		m
Draught moulded on FP (relative to baseline)	T_F	8.70		m
Draught moulded on AP (relative to baseline)	T_A	8.70		m
Displacement volume moulded	∇	27788		m^3
Displacement mass in seawater	Δ_1	28511		t
Wetted surface area bare hull	S	5909		m^2
Longitudinal position of centre of gravity				
LCB position aft of FP	FB	83.58		m
LCB position from amidships	-	-1.27		%
LCG position from AP	LCG	79.42	*(79.42)*	m
Vertical position of cog and stability				
Transverse metacentric height (incl. free surface correction)	GMt_{WET}	*(0.76 – 1.37**)*		m
Vertical position centre of gravity (dry)	KG	*(11.02 – 11.63**)*		m
Vertical position centre of buoyancy	KB	4.69		m
Transverse metacentre above base	KM	12.39		m
Mass radius of gyration around X-axis	K_{XX}	9.99 – 11.34**		m
Mass radius of gyration around Y-axis	K_{YY}	42.38		m
Mass radius of gyration around Z-axis	K_{ZZ}	17.93		m
Natural period of roll (incl. added mass, target value provided by calculations)	$T\phi$	19.0 – 23.0	*(19.6)*	s
Coefficients				
Block coefficient	C_B	0.720		-
Amidships section coefficient	C_M	0.993		-
Prismatic coefficient	C_P	0.725		-
Length-Breadth ratio	L_{PP}/B_{WL}	6.037		-
Breadth-Draught ratio	B_{WL}/T	3.103		-
Length-Draught ratio	L_{PP}/T	18.736		-

**: when measurable*

*** the GMtwet, KG and Kxx differed slightly from one freeboard configuration to another.*

Table 2 Main particulars and stability data of the vessel – LC 2 – Tests in BT

Model No. 10246 Model scale ratio λ = 33

Designation	Symbol	Magnitude specified *(realised*)*		Unit
Main particulars				
Length between perpendiculars	L_{PP}	163.00		m
Length on waterline	L_{WL}	166.32		m
Length overall submerged	L_{OS}	166.96		m
Breadth moulded on WL	B_{WL}	27.00		m
Draught moulded on FP (relative to baseline)	T_F	8.00		m
Draught moulded on AP (relative to baseline)	T_A	8.00		m
Displacement volume moulded	∇	24917		m^3
Displacement mass in seawater	Δ_1	25564		t
Wetted surface area bare hull	S	5573		m^2
Longitudinal position of centre of gravity				
LCB position aft of FP	FB	83.07		m
LCB position from amidships	-	-0.96		%
LCG position from AP	LCG	79.93	*(79.95)*	m
Vertical position of cog and stability				
Transverse metacentric height (incl. free surface correction)	GMt_{WET}	1.20	*(1.23)*	m
Vertical position centre of gravity (dry)	KG	11.48.30		m
Vertical position centre of buoyancy	KB	4.30		m
Transverse metacentre above base	KM	12.48		m
Mass radius of gyration around X-axis	K_{XX}	10.50		m
Mass radius of gyration around Y-axis	K_{YY}	42.38		m
Mass radius of gyration around Z-axis	K_{ZZ}	-		m
Natural period of roll (incl. added mass, target value provided by calculations)	$T\phi$	21.0	*(20.9)*	s
Coefficients				
Block coefficient	C_B	0.708		-
Amidships section coefficient	C_M	0.992		-
Prismatic coefficient	C_P	0.713		-
Length-Breadth ratio	L_{PP}/B_{WL}	6.037		-
Breadth-Draught ratio	B_{WL}/T	3.375		-
Length-Draught ratio	L_{PP}/T	20.375		-

**: when measurable*

Table 3 Main particulars of propellers

Designation	Symbol	Magnitude	Unit
Propeller model No. 5108R Centre			
Diameter	D	5.56	m
Direction of rotation	Clockwise looking ahead		

Table 4 Main particulars of rudders and control settings

Designation	Symbol	Magnitude	Unit
Rudder particulars			
Number of rudders	-	1	-
Average height	b_R	7.71	m
Average chord	c_R	4.08	m
Geometric aspect ratio	λ	1.89	-
Thickness / chord	T / C_R	18.14	%
Projected area	A_R	31.46	m^2
Longitudinal position of rudder axis from AP	X_R	0.00	m
Offset of rudder axis from centreline	Y_R	0.00	m
Angle of the rudder with horizontal	β_R	90	deg
Total rudder area ratio, $A_R / (L_{PP}*T_{mean})$ LC1	-	2.22	%
Total rudder area ratio, $A_R / (L_{PP}*T_{mean})$ LC2	-	2.41	%
Rudder settings for autopilot in waves – Tests in BT			
max rudder angle	δ_{MAX}	35	deg
rudder angle per deg course deviation	C_Ψ	3.00	deg/deg
rudder angle per deg/s rate of turn	B_Ψ	17.25	deg/(deg/s)
rudder angle per m transverse course deviation	C_Y	0.30	deg/m
rudder rate of application	$\dot{\delta}$	2.32	deg/s

Table 5 Main particulars of bilge keels

Designation	Symbol	Magnitude	Unit
Bilge keels – LC 1			
Total length	L_{BK}	48.69	m
Height	H_{BK}	0.50	m
Location: between station 6 and station 13 (29.87% of Lpp)			
Bilge keels – LC 2			
Total length	L_{BK}	48.69	m
Height	H_{BK}	0.40	m
Location: between station 6 and station 13 (29.87% of Lpp)			

Table 6 Designation, notation, sign convention and measuring devices of measured quantities

Sample frequency 100 Hz.

Designation	Notation	Positive for	Measured by
Motions of ship at COG:			
Surge Sway Heave Roll Pitch Yaw	SURGE SWAY HEAVE ROLL PITCH YAW	Ship forwards Ship to port side Ship upwards Starboard down Bow down Bow to port side	Optical tracking system
Position and velocity of carriage – BT basin:			
X position on north rail	XCarrNRel	Carriage moving east	SSI encoder
Speed X-direction on north rail	VX-Carr-N		
Y position	YCarrRel	Carriage moving north	SSI encoder

Sample frequency 200 Hz.

Designation	Notation	Positive for	Measured by
Wave elevation – OB basin during wave calibrations:			
Beam seas:		**WAVE: 212.5 m forward of station 10, at CL** **WAVE SC: Centre of model in soft mooring setup**	
Wave elevation – OB basin during tests:			
Head and bow-quartering seas:		**WAVE: Next to centre model and 212.5 m to starboard**	
Beam seas:		**WAVE: 212.5 m forward of station 10, at CL**	
Stern-quartering and following seas:		**WAVE: Next to centre model and 212.5 m to port side**	
Wave elevation – BT basin during wave calibrations:			
Head seas:		**WAVE: 287.4 m forward of station 10, at CL**	
Wave elevation – BT basin during tests:			
Head seas:		**WAVE: 287.4 m forward of station 10 and 132 m to starboard**	
Incident wave elevation, wave sort crested (WAVE SC)	WAVE.CL WAVE.MF WAVE.SBF WAVE.SBA WAVE.PSA WAVE.PSF	Wave elevation upwards	Resistance type wave probe
Incident wave elevation	WAVE	Wave elevation upwards	Resistance type wave probe

Table 7 Designation, notation, sign convention and measuring devices of measured quantities (continued)

Sample frequency 200 Hz.

Designation	Notation	Positive for	Measured by
Accelerations of the ship – Tests in OB			
Longitudinal acceleration portside for	AX PSF	Ship forwards	Accelerometers
Transverse acceleration portside for	AY PSF	Ship to port side	
Vertical acceleration portside for	AZ PSF	Ship upwards	
Longitudinal acceleration starboard for	AX SBF	Ship forwards	
Transverse acceleration starboard for	AY SBF	Ship to port side	
Vertical acceleration starboard for	AZ SBF	Ship upwards	
Longitudinal acceleration portside aft	AX PSA	Ship forwards	
Transverse acceleration portside aft	AY PSA	Ship to port side	
Vertical acceleration portside aft	AZ PSA	Ship upwards	
Longitudinal acceleration starboard aft	AX SBA	Ship forwards	
Transverse acceleration starboard aft	AY SBA	Ship to port side	
Vertical acceleration starboard aft	AZ SBA	Ship upwards	
Wave elevation – Tests in OB			
Incident wave heights	REL 1 AFT REL 2 REL 3 REL 4 REL 5 REL 6 BOW	Wave elevation upwards	Resistance type wave probe

Table 8 Designation, notation, sign convention and measuring devices of measured quantities (continued)

Sample frequency 9602 Hz.

Designation	Notation	Positive for	Measured by
Impact forces – Tests in OB (*see* Figure 3 to Figure 8 *for details of locations)*:			
Vertical impact force panel	PANEL Z1-1	Inward force	Force transducers
Vertical impact force panel	PANEL Z1-2		
Transverse impact force panel	PANEL Y1-3		
Transverse impact force panel	PANEL Y1-4		
Vertical impact force panel	PANEL Z2-1		
Vertical impact force panel	PANEL Z2-2		
Vertical impact force panel	PANEL Z2-3		
Vertical impact force panel	PANEL Z2-4		
Transverse impact force panel	PANEL Y2-5		
Transverse impact force panel	PANEL Y2-6		
Transverse impact force panel	PANEL Y2-7		
Transverse impact force panel	PANEL Y2-8		
Vertical impact force panel	PANEL Z3-1		
Vertical impact force panel	PANEL Z3-2		
Vertical impact force panel	PANEL Z3-3		
Vertical impact force panel	PANEL Z3-4		
Transverse impact force panel	PANEL Y3-5		
Transverse impact force panel	PANEL Y3-6		
Vertical impact force panel	PANEL Z4-1		
Vertical impact force panel	PANEL Z4-2		
Transverse impact force panel	PANEL Y4-3		
Transverse impact force panel	PANEL Y4-4		
Vertical impact force panel	PANEL Z5-1		
Vertical impact force panel	PANEL Z5-2		
Transverse impact force panel	PANEL Y5-3		
Transverse impact force panel	PANEL Y5-4		
Longitudinal impact force panel	PANEL X6-1		
Longitudinal impact force panel	PANEL X6-2		
Longitudinal impact force panel	PANEL X6-3		
Longitudinal impact force panel	PANEL X6-4		

Table 9 Designation, notation and sign convention of calculated quantities

Sample frequency 100 Hz.

Designation	Notation	Positive for
Motions at COG:		
Low-frequent longitudinal motion	SURGE LF	Ship forwards
Wave-frequent longitudinal motion	SURGE WF	
Low-frequent transverse motion	SWAY LF	Ship to port side
Wave-frequent transverse motion	SWAY WF	
Low-frequent rotation around the vertical axis	YAW LF	Bow to port side
Wave-frequent rotation around the vertical axis	YAW WF	
Speed of ship at COG – Tests in BT:		
Speed	VX SHIP	Sailing ahead

Table 10 Analysis of force panels

Impact forces	**Amplification factor** [-]	**Frequency** [Hz]	**Threshold** [kN]
PANEL Z1-1	0.99	2191	25
PANEL Z1-2	0.99	2236	25
PANEL Y1-3	0.99	1845	25
PANEL Y1-4	0.99	1850	25
PANEL Z2-1	0.99	1920	25
PANEL Z2-2	0.99	1917	25
PANEL Z2-3	1.01	2011	25
PANEL Z2-4	1.01	1924	25
PANEL Y2-5	0.99	1900	25
PANEL Y2-6	0.98	1985	25
PANEL Y2-7	0.98	1980	25
PANEL Y2-8	0.99	1900	25
PANEL Z3-1	0.99	1911	25
PANEL Z3-2	0.98	2000	25
PANEL Z3-3	0.99	2006	25
PANEL Z3-4	0.98	1913	25
PANEL Y3-5	0.99	1840	25
PANEL Y3-6	0.99	1836	25
PANEL Z4-1	1.01	1837	25
PANEL Z4-2	1.00	-	25
PANEL Y4-3	0.99	1877	25
PANEL Y4-4	0.99	1871	25
PANEL Z5-1	0.99	1770	25
PANEL Z5-2	1.00	2280	25
PANEL Y5-3	0.99	1862	25
PANEL Y5-4	0.99	1864	25
PANEL X6-1	0.99	1900	25
PANEL X6-2	1.00	1970	25
PANEL X6-3	1.01	1976	25
PANEL X6-4	0.99	1897	25
Analysis impact forces		Band-pass filter lower limit (rad/s)	Band-pass filter upper limit (rad/s)
All force panels		0.50	400

Table 11 Spring settings

Spring settings	Stiffness (kN/m)	Pretension (kN)
Springs	66.8	1808.5

Table 12 Filter frequencies of calculated quantities – specified by test condition

Test condition	**Filter frequencies**		
	Low frequent signals	Wave frequent signals	
	Low-pass filter upper limit [rad/s]	Band-pass filter lower limit [rad/s]	Band-pass filter upper limit [rad/s]
Zero speed tests	0.30 – 0.50	0.30 – 0.50	2.70
Tests in transit in head seas	0.30	0.30	1.90

Table 13 Overview of calibrated irregular waves

Model scale ratio $\lambda = 33$

JONSWAP wave spectrum

MARIN test ID 33327_01OB_	Test duration [s]	Wave conditions				Water depth [m]	Remarks
		Significant Height [m]	Peak Period [s]	Heading [deg]	Gamma [-]		
03_003_004_01	10800	1.2	7.0	270	2.5 SC	21.3	
03_003_006_01		1.8					
03_301_001_02							Different wave realisation 1
03_302_001_01							Different wave realisation 2
03_003_007_01		2.4					
03_003_002_02		3.0					
03_303_001_01							Different wave realisation 3
03_304_001_01							Different wave realisation 4
03_003_009_01		3.6					
03_003_008_01		3.8					
03_004_002_01		4.5	8.5				
03_401_001_01							Different wave realisation 1
03_402_001_02							Different wave realisation 2
03_005_002_01		6.0	10.0				
03_003_005_01		1.2	9.0		1.0 SC		
03_006_004_01		1.8					
03_006_005_01		2.4					
03_006_002_01		3.0					
03_007_002_01		4.5	10.0				
03_008_003_01		6.0	12.0				
03_009_002_01		3.0	7.0		2.5 LC		
03_010_002_01		4.5	8.5				
03_011_002_01		6.0	10.0				
03_033_002_01		3.0	7.0		2.5 SC	37.5	
03_034_002_01		4.5	8.5				
03_035_002_01		6.0	10.0				
03_041_002_01					2.5 LC		
03_063_002_01		3.0	7.0		2.5 SC	100.0	
03_064_002_01		4.5	8.5				
03_065_002_01		6.0	10.0				
MARIN test ID 33327_02BT_	Test duration [s]	Wave conditions				Water depth [m]	Remarks
		Significant Height [m]	Peak Period [s]	Heading [deg]	Gamma [-]		
02_080_001_01	7200	6.0	11.8	180	1.0 LC	33.0	
02_081_001_01			11.0		2.0 LC		

Table 14 Overview of tests in calm water (including decay tests)

Model scale ratio λ = 33

MARIN test ID 33327_01OB_	Type of test	Mean Speed [knots]	Water depth [m]	Remarks
LC 1 – GM = 1.19 m – Configuration 1				
04_001_011_01	Surge decay	0	21.3	Soft mooring
04_001_010_01	Sway decay			
04_001_009_01	Roll decay			
04_001_012_01	Yaw decay			
MARIN test ID 33327_02BT_	Type of test	Mean Speed [knots]	Water depth [m]	Remarks
LC 2 – GM = 1.23 m – Configuration 2A – Bilge keels 0.4 m				
03_001_001_02	Calm water	4	33.0	Free sailing
03_004_001_01	Roll decay	0		Free floating
03_004_002_01				
03_005_001_01		4		Free sailing

Table 15 Overview of zero speed tests in irregular waves

Model scale ratio λ = 33
JONSWAP wave spectrum

MARIN test ID 33327_01OB_	Test duration [s]	Wave conditions				Water depth [m]	Remarks
		Significant Height [m]	Peak Period [s]	Heading [deg]	Gamma [-]		
LC 1 – GM = 1.19 m – Configuration 1							
Bow-quartering seas							
04_003_006_01	10800	1.2	7.0	225	2.5 SC	21.3	
04_003_007_01		1.8					
04_006_004_01			9.0		1.0 SC		
04_003_008_01		3.0	7.0		2.5 SC		
04_004_002_01		4.5	8.5				
04_007_002_01			10.0		1.0 SC		
Beam seas							
04_003_002_01	10800	0.9	7.0	270	2.5 SC	21.3	
04_003_005_01		1.2					
04_006_003_01			9.0		1.0 SC		
04_003_004_01		1.5	7.0		2.5 SC		
04_003_003_01		1.8					
04_003_001_02		3.0					
04_006_001_01			9.0		1.0 SC		
04_004_001_04		4.5	8.5		2.5 SC		
04_007_001_01			10.0		1.0 SC		

Table 15 Overview of zero speed tests in irregular waves (continued)

Model scale ratio λ = 33
JONSWAP wave spectrum

MARIN test ID 33327_01OB_	Test duration [s]	Wave conditions				Water depth [m]	Remarks
		Significant Height [m]	Peak Period [s]	Heading [deg]	Gamma [-]		
LC 1 – GM = 1.19 m – Configuration 1							
Stern-quartering seas							
04_003_010_01	10800	1.2	7.0	315	2.5 SC	21.3	
04_003_009_02		1.8					
04_006_005_01			9.0		1.0 SC		
04_003_011_01		3.0	7.0		2.5 SC		
04_004_003_01		4.5	8.5				
04_007_003_01			10.0		1.0 SC		
LC 1 – GM = 0.82 m – Configuration 2							
Bow-quartering seas							
04_003_017_01	10800	2.4	7.0	225	2.5 SC	21.3	
04_006_008_01			9.0		1.0 SC		
04_003_018_01		3.0	7.0		2.5 SC		
04_004_007_02		4.5	8.5				
04_007_006_01			10.0		1.0 SC		
Beam seas							
04_003_016_01	10800	1.8	7.0	270	2.5 SC	21.3	
04_006_007_01			9.0		1.0 SC		
04_003_014_01		2.1	7.0		2.5 SC		
04_003_015_01		3.0					
04_004_016_01		4.5	8.5				GM = 1.20 m
04_007_005_01			10.0		1.0 SC		
Stern-quartering seas							
04_003_013_01	10800	2.4	7.0	315	2.5 SC	21.3	
04_006_006_01			9.0		1.0 SC		
04_003_012_01		3.0	7.0		2.5 SC		
04_004_005_01		4.5	8.5				
04_007_004_01			10.0		1.0 SC		
LC 1 – GM = 0.90 m – Configuration 3							
Bow-quartering seas							
04_003_019_01	10800	3.0	7.0	225	2.5 SC	21.3	
04_006_009_01			9.0		1.0 SC		
04_004_008_01		4.5	8.5		2.5 SC		
04_007_007_01			10.0		1.0 SC		
04_005_001_01		6.0			2.5 SC		
04_008_001_01			12.0		1.0 SC		

Table 15 Overview of zero speed tests in irregular waves (continued)

Model scale ratio λ = 33
JONSWAP wave spectrum

MARIN test ID 33327_01OB_	Test duration [s]	Wave conditions				Water depth [m]	Remarks
		Significant Height [m]	Peak Period [s]	Heading [deg]	Gamma [-]		
LC 1 – GM = 0.90 m – Configuration 3							
Beam seas							
04_003_020_01	10800	2.4	7.0	270	2.5 SC	21.3	
04_006_010_01			9.0		1.0 SC		
04_004_009_01		4.5	8.5		2.5 SC		
04_007_008_01			10.0		1.0 SC		
04_005_002_02		6.0			2.5 SC		
04_008_002_02			12.0		1.0 SC		
Stern-quartering seas							
04_003_021_01	10800	3.0	7.0	315	2.5 SC	21.3	
04_006_011_01			9.0		1.0 SC		
04_004_010_01		4.5	8.5		2.5 SC		
04_007_009_01			10.0		1.0 SC		
04_005_003_01		6.0			2.5 SC		
04_008_003_01			12.0		1.0 SC		
LC 1 – GM = 1.12 m – Configuration 4							
Beam seas							
04_003_024_01	10800	2.4	7.0	270	2.5 SC	21.3	
04_003_023_01		3.0					
LC 1 – GM = 1.37 m – Configuration 5							
Bow-quartering seas							
04_003_027_01	10800	3.0	7.0	225	2.5 SC	21.3	
04_003_028_01		3.6					
04_004_013_01		4.5	8.5				
Beam seas							
04_003_025_01	10800	2.4	7.0	270	2.5 SC	21.3	
04_003_026_01		3.0					
04_004_012_03		4.5	8.5				
LC 1 – GM = 0.87 m – Configuration 6							
Beam seas							
04_003_022_01	10800	3.8	7.0	270	2.5 SC	21.3	
04_004_011_01		4.5	8.5				

Table 15 Overview of zero speed tests in irregular waves (continued)

Model scale ratio $\lambda = 33$
JONSWAP wave spectrum

MARIN test ID 33327_01OB_	Test duration [s]	Wave conditions				Water depth [m]	Remarks
		Significant Height [m]	Peak Period [s]	Heading [deg]	Gamma [-]		
LC 1 – GM = 1.20 m – Configuration 2							
Head seas							
04_003_029_01	10800	3.0	7.0	180	2.5 SC	21.3	
04_004_014_01		4.5	8.5				
04_005_004_01		6.0	10.0				GM = 0.76 m
04_008_004_01			12.0		1.0 SC		
Bow-quartering seas							
04_003_030_01	10800	3.0	7.0	210	2.5 SC	21.3	
04_009_001_01				225	2.5 LC		
04_010_001_01		4.5	8.5				
04_003_031_01		3.0	7.0	240	2.5 SC		
Beam seas							
04_301_001_01	10800	1.8	7.0	270	2.5 SC	21.3	Different wave realisation 1
04_302_001_01							Different wave realisation 2
04_303_001_01							Different wave realisation 3
04_304_001_01							Different wave realisation 4
04_009_002_01					2.5 LC		
04_301_002_01		3.0			2.5 SC		Different wave realisation 1
04_302_002_01							Different wave realisation 2
04_303_002_01							Different wave realisation 3
04_304_002_01							Different wave realisation 4
04_009_003_01					2.5 LC		
04_401_001_01		4.5	8.5		2.5 SC		Different wave realisation 1
04_402_001_01							Different wave realisation 2
04_403_001_01							Different wave realisation 3
04_404_001_01							Different wave realisation 4
04_010_002_01					2.5 LC		
Stern-quartering seas							
04_003_032_01	10800	3.0	7.0	300	2.5 SC	21.3	
04_009_004_01				315	2.5 LC		
04_010_003_01		4.5	8.5				
04_003_033_02		3.0	7.0	330	2.5 SC		
Following seas							
04_003_034_01	10800	3.0	7.0	0	2.5 SC	21.3	
04_003_035_01		3.8					
04_004_015_01		4.5	8.5				

Table 15 Overview of zero speed tests in irregular waves (continued)

Model scale ratio $\lambda = 33$
JONSWAP wave spectrum

MARIN test ID 33327_01OB_	Test duration [s]	Wave conditions				Water depth [m]	Remarks
		Significant Height [m]	Peak Period [s]	Heading [deg]	Gamma [-]		
LC 1 – GM = 1.20 m – Configuration 2							
Bow-quartering seas							
05_033_004_01	10800	3.0	7.0	225	2.5 SC	37.5	
05_034_003_01		4.5	8.5				
05_035_002_01		6.0	10.0				
Beam seas							
05_033_003_01	10800	2.4	7.0	270	2.5 SC	37.5	
05_033_002_01		3.0					
05_034_002_01		4.5	8.5				
Stern-quartering seas							
05_033_001_01	10800	3.0	7.0	315	2.5 SC	37.5	
05_034_001_01		4.5	8.5				
05_035_001_02		6.0	10.0				
Bow-quartering seas							
06_063_001_01	10800	3.0	7.0	225	2.5 SC	100.0	
06_064_001_01		4.5	8.5				
06_065_001_01		6.0	10.0				
Beam seas							
06_063_003_01	10800	2.4	7.0	270	2.5 SC	100.0	
06_063_002_01		3.0					
06_064_002_02		4.5	8.5				
Stern-quartering seas							
06_063_004_01	10800	3.0	7.0	315	2.5 SC	100.0	
06_064_003_01		4.5	8.5				
06_065_002_01		6.0	10.0				
LC 1 – GM = 0.76 m – Configuration 2							
Head seas							
05_035_003_01	10800	6.0	10.0	180	2.5 SC	37.5	Parametric roll
05_041_001_01					2.5 LC		
05_042_001_01			11.0				
05_035_004_01		7.5	10.0		2.5 SC		

Table 16 Overview of parametric roll tests in transit in irregular waves

Model scale ratio $\lambda = 33$
JONSWAP wave spectrum

MARIN test ID 33327_02BT_	Test duration [s]	Wave conditions				Mean Speed [knots]	Water depth [m]	Remarks
		Significant Height [m]	Peak Period [s]	Heading [deg]	Gamma [-]			
LC 2 – GM = 1.23 m – Configuration 2A – Bilge keels 0.4 m								
Head seas								
04_002	8178	4.5	11.8	180	1.0 LC	4	33.0	
04_003	7455	6.0	11.0		2.0 LC	2		
04_006	7254		11.8		1.0 LC			
04_001	8345					4		
04_005	8075	7.5	11.0		2.0 LC	2		
04_004	8164		11.8		1.0 LC			
04_007	9701				3.3 LC			
04_008	3867	8.5	11.0		2.0 LC			
06_002	5496	6.0	11.0					
06_001	2902		11.8		1.0 LC	4		
06_003	4826	7.5	11.0		2.0 LC	2		

FIGURES

Figure 1 General arrangement and small scale body plan

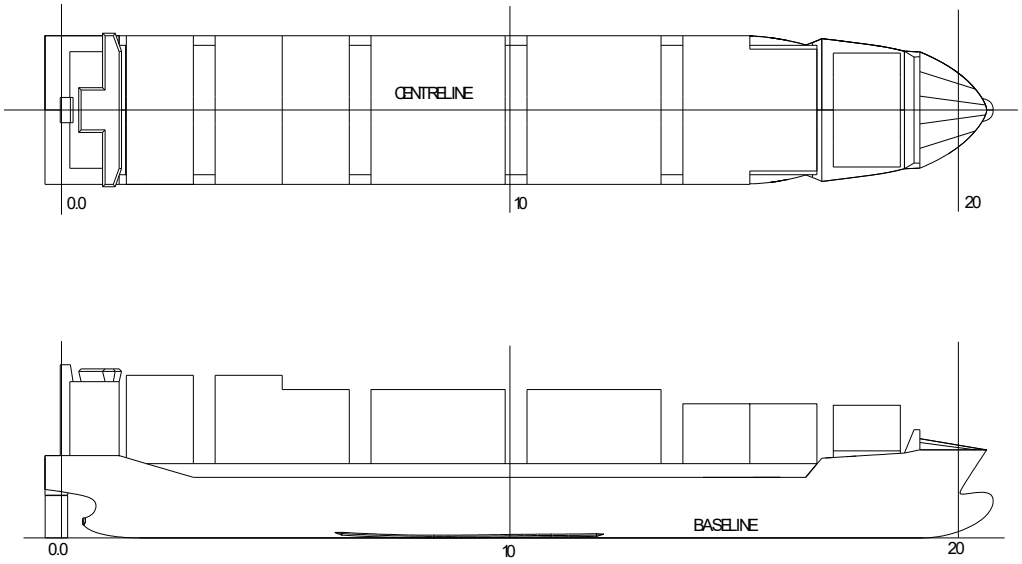

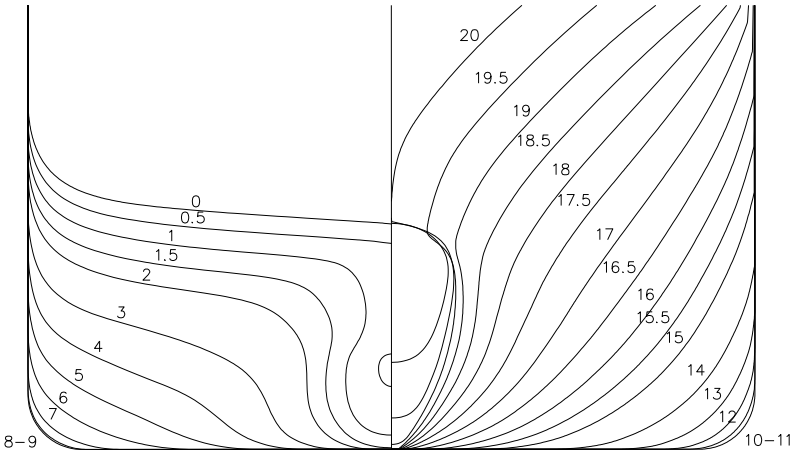

OVERVIEW OF SHIP MODEL No. 10246
DIMENSIONS ARE GIVEN IN mm FOR SHIP

Figure 2 Location of measuring devices

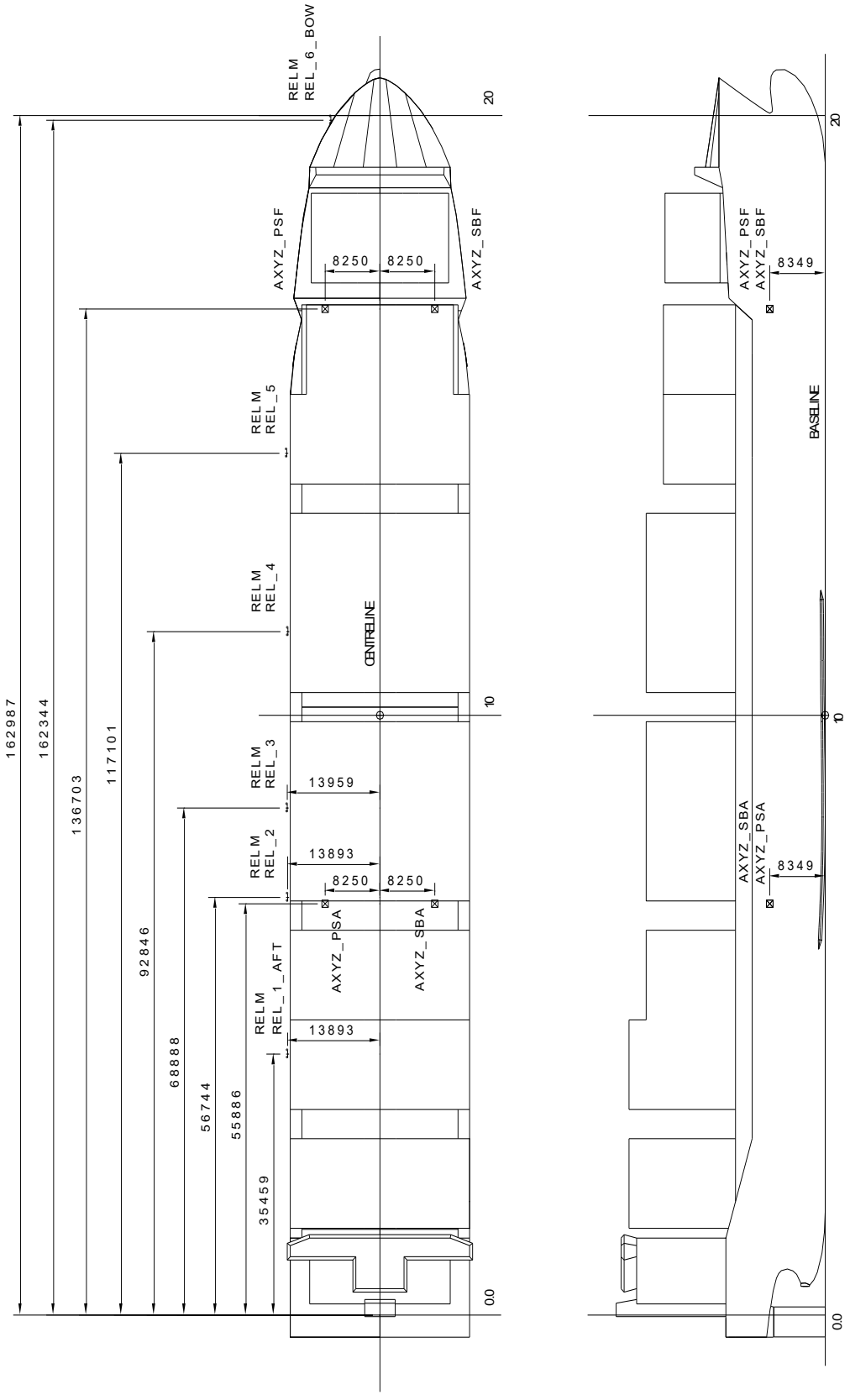

MEASURING DEVICES I FOR SHIP MODEL No. 10246
DIMENSIONS ARE GIVEN IN mm FOR SHIP

Figure 3 Location of measuring devices – Configuration 1

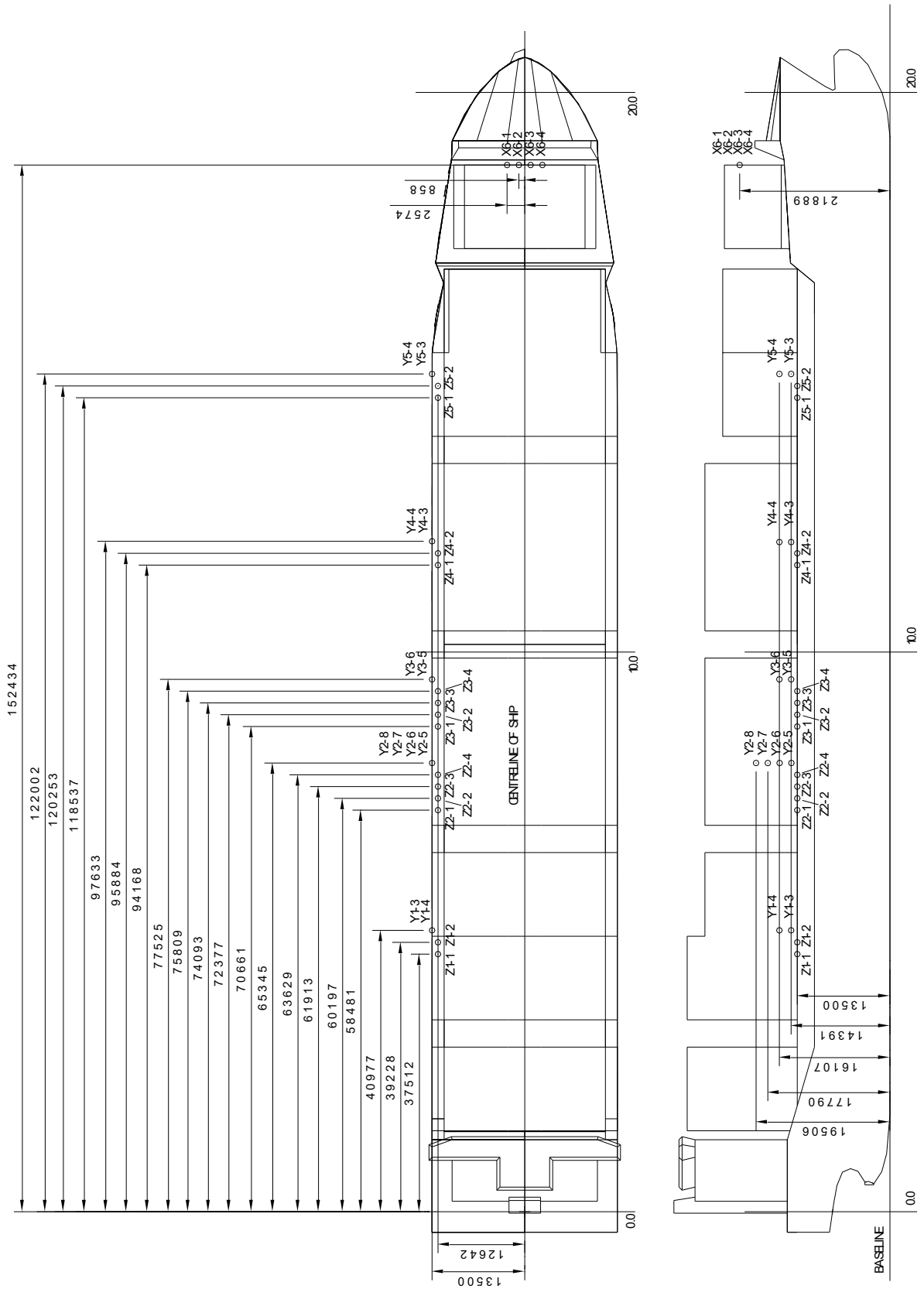

CONFIGURATION SUPERSTRUCTURE I WITH HEIGHT 0 WITH 30 PRESSURE PANELS
ON SHIP MODEL No. 10246
DIMENSIONS ARE GIVEN IN mm FOR SHIP

Figure 4 Location of measuring devices – Configuration 2

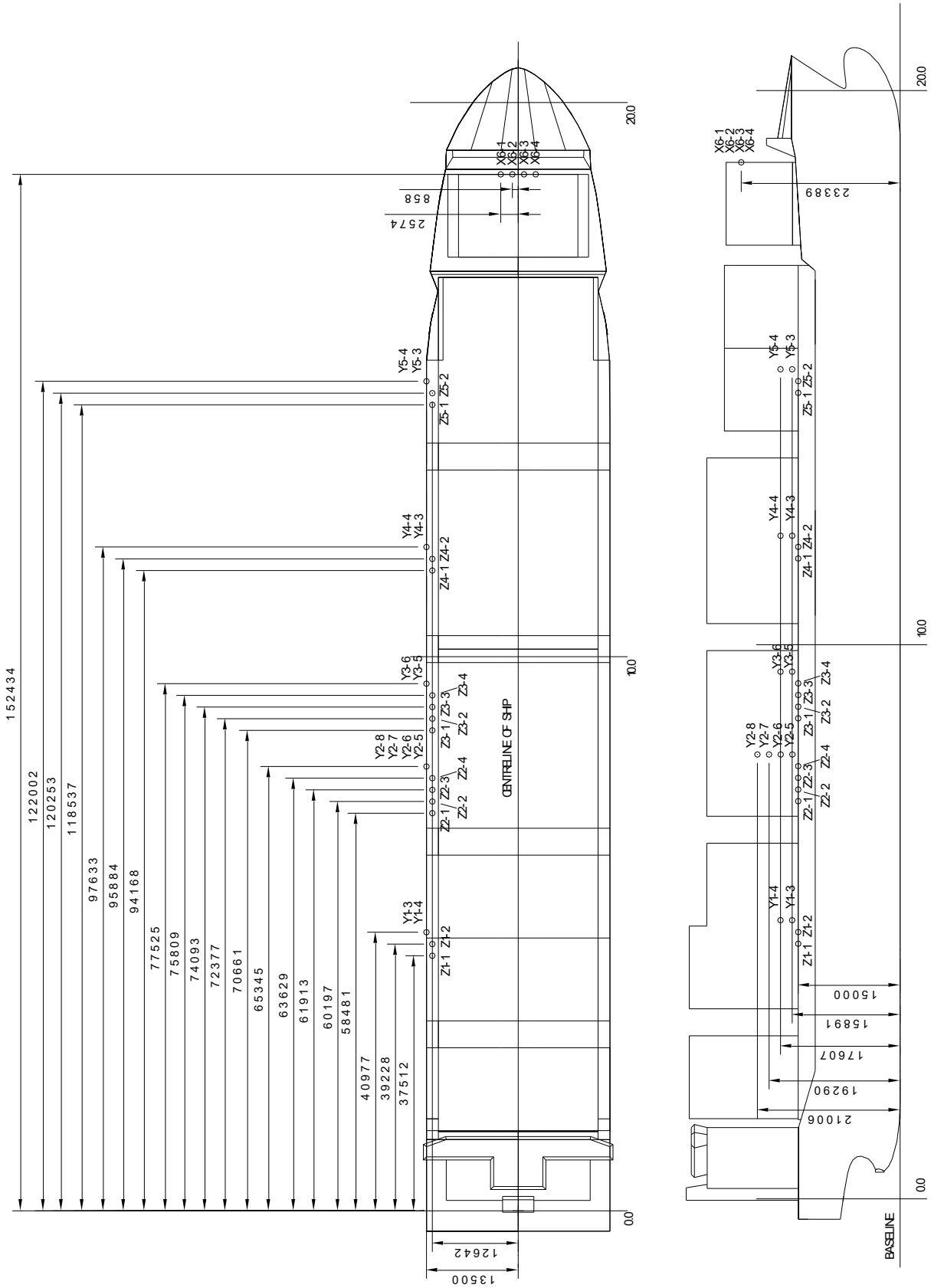

CONFIGURATION SUPERSTRUCTURE I WITH HEIGHT 1,5 WITH 30 PRESSURE PANELS
ON SHIP MODEL No. 10246
DIMENSIONS ARE GIVEN IN mm FOR SHIP

Figure 5 Location of measuring devices – Configuration 3

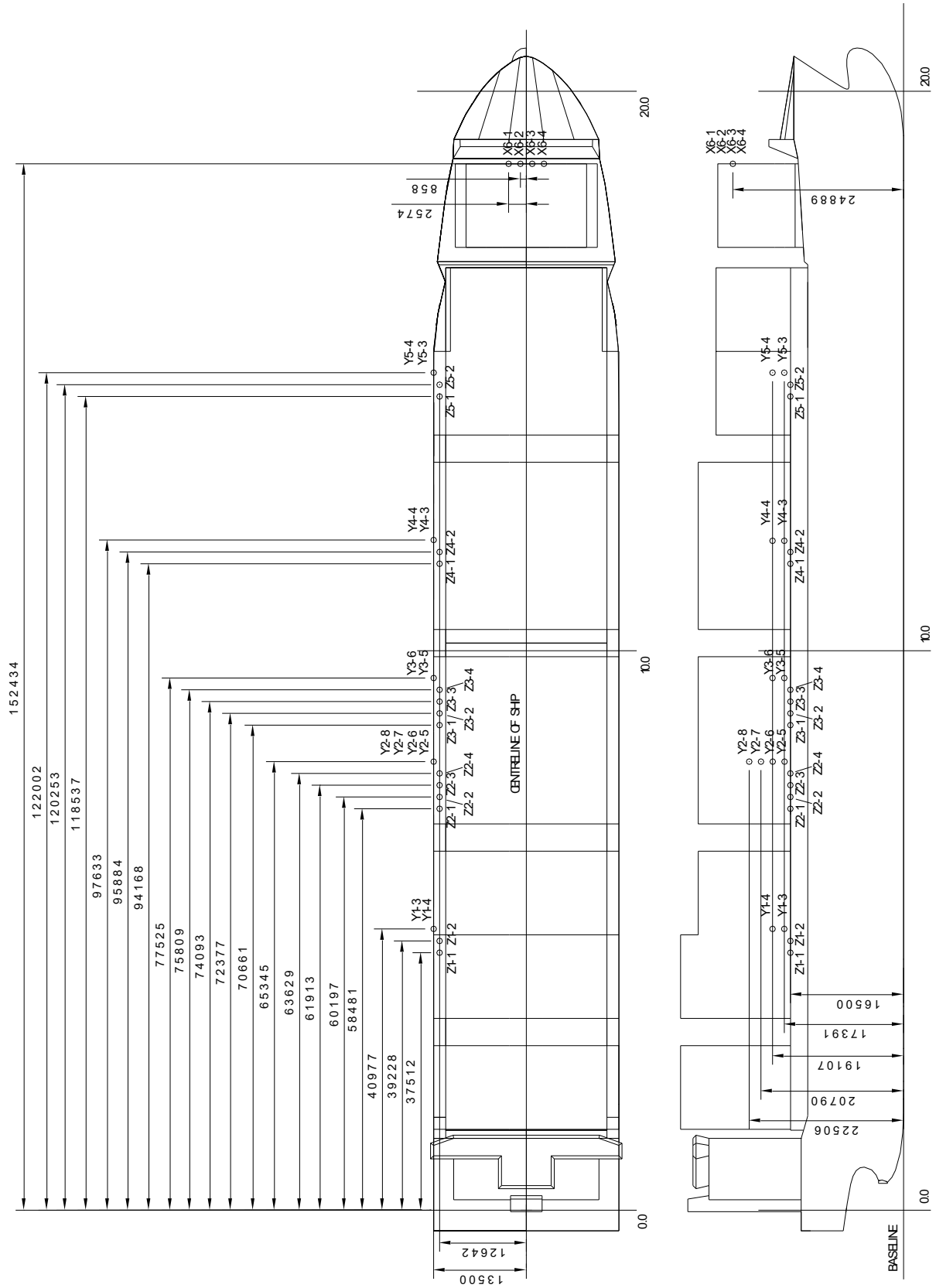

CONFIGURATION SUPERSTRUCTURE I WITH HEIGHT 3 WITH 30 PRESSURE PANELS
ON SHIP MODEL No. 10246
DIMENSIONS ARE GIVEN IN mm FOR SHIP

Figure 6 Location of measuring devices – Configuration 4

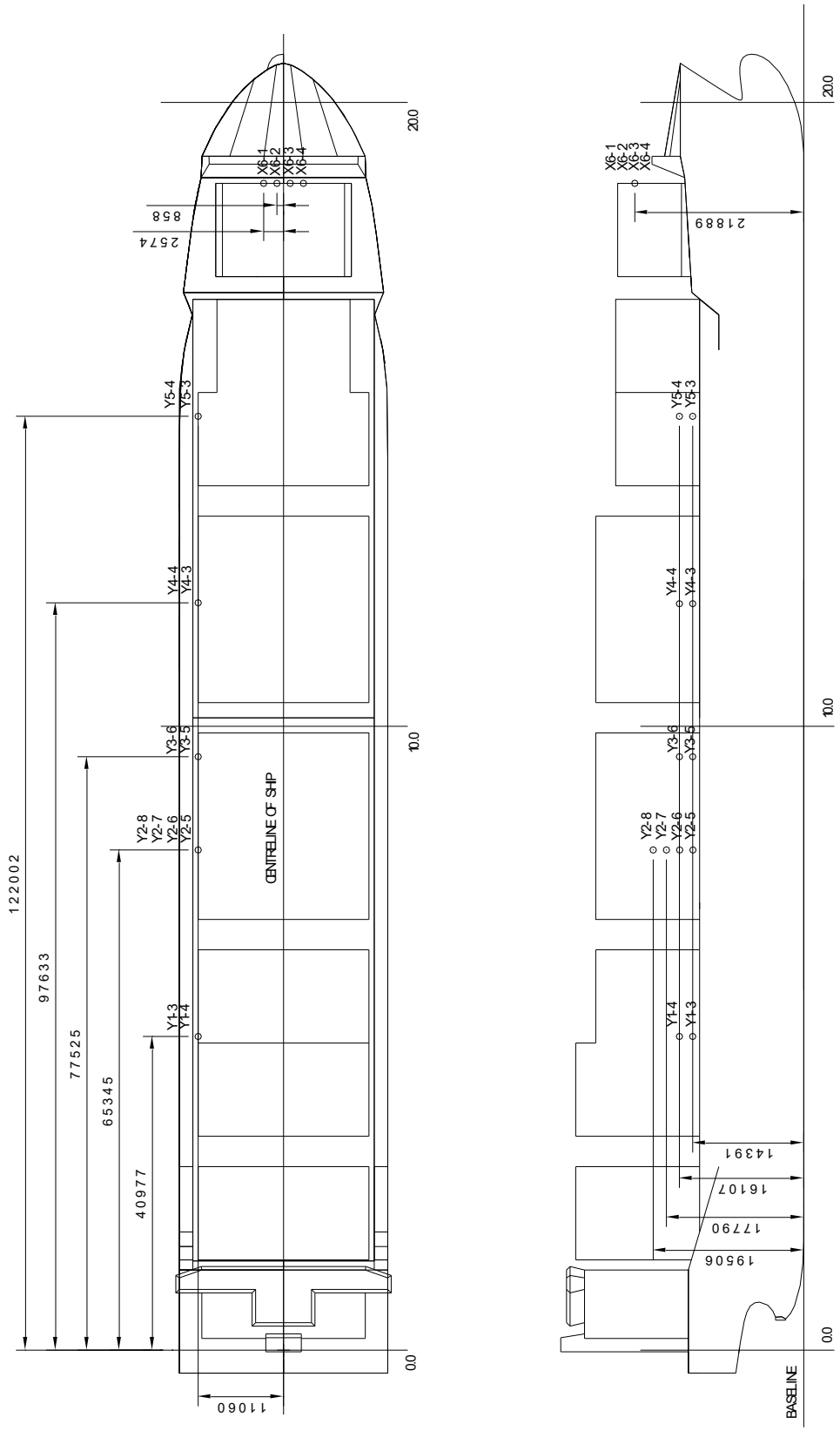

CONFIGURATION SUPERSTRUCTURE II WITH HEIGHT 0 WITH 16 PRESSURE PANELS ON SHIP MODEL No. 10246
DIMENSIONS ARE GIVEN IN mm FOR SHIP

Figure 7 Location of measuring devices – Configuration 5

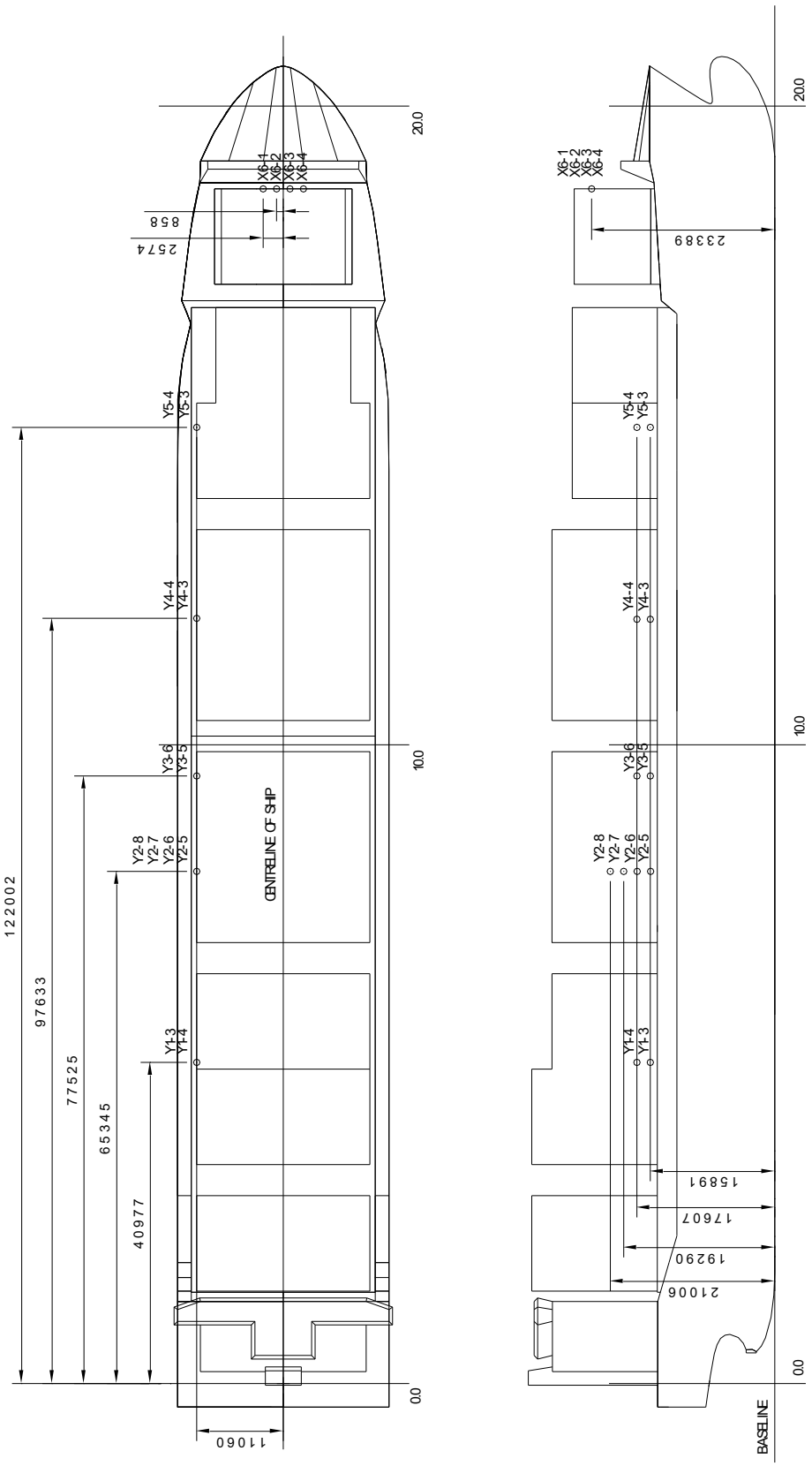

CONFIGURATION SUPERSTRUCTURE II WITH HEIGHT 1,5 WITH 16 PRESSURE PANELS ON SHIP MODEL No. 10246
DIMENSIONS ARE GIVEN IN mm FOR SHIP

Figure 8 Location of measuring devices – Configuration 6

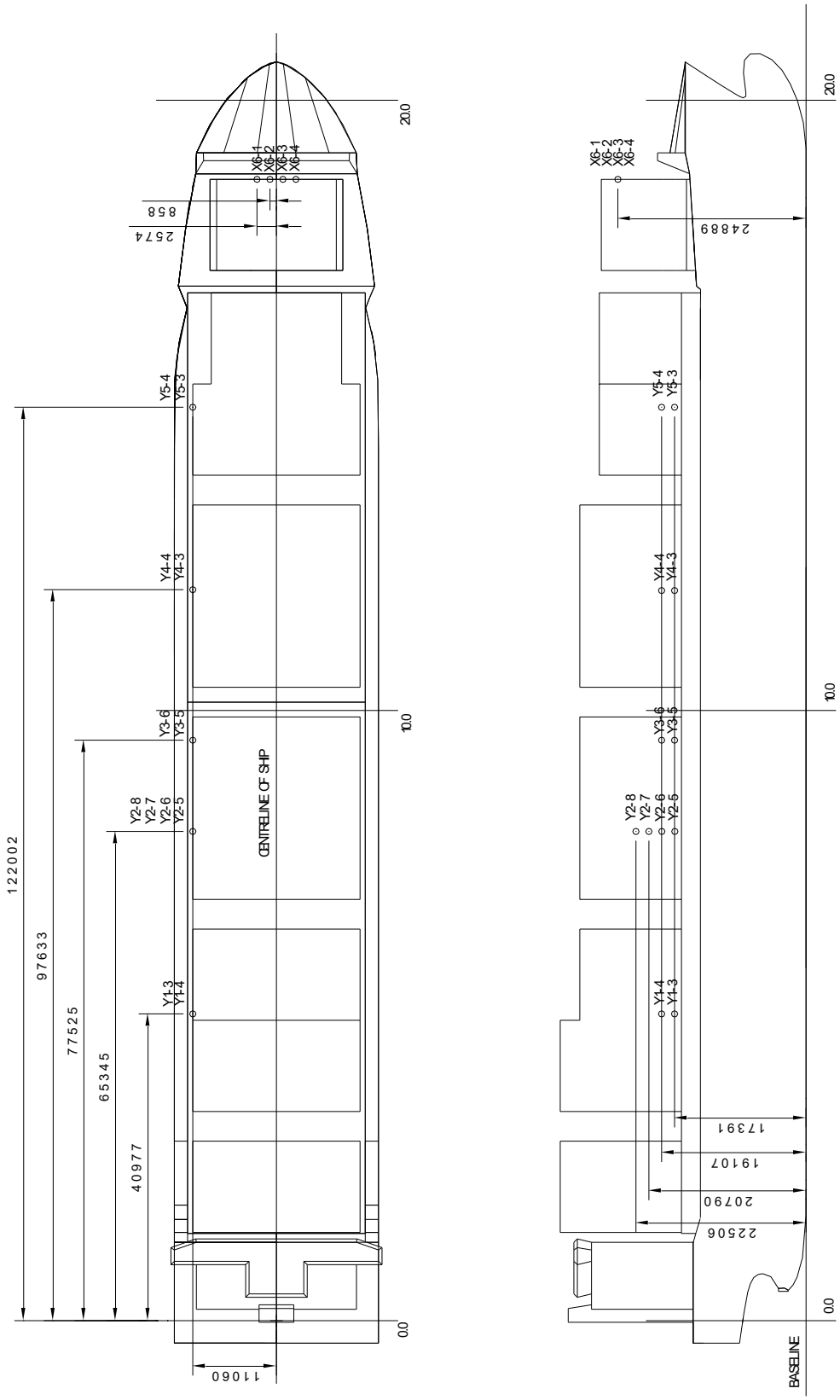

CONFIGURATION SUPERSTRUCTURE II WITH HEIGHT 3 WITH 16 PRESSURE PANELS ON SHIP MODEL No. 10246
DIMENSIONS ARE GIVEN IN mm FOR SHIP

Figure 9 Close-up view on panel set

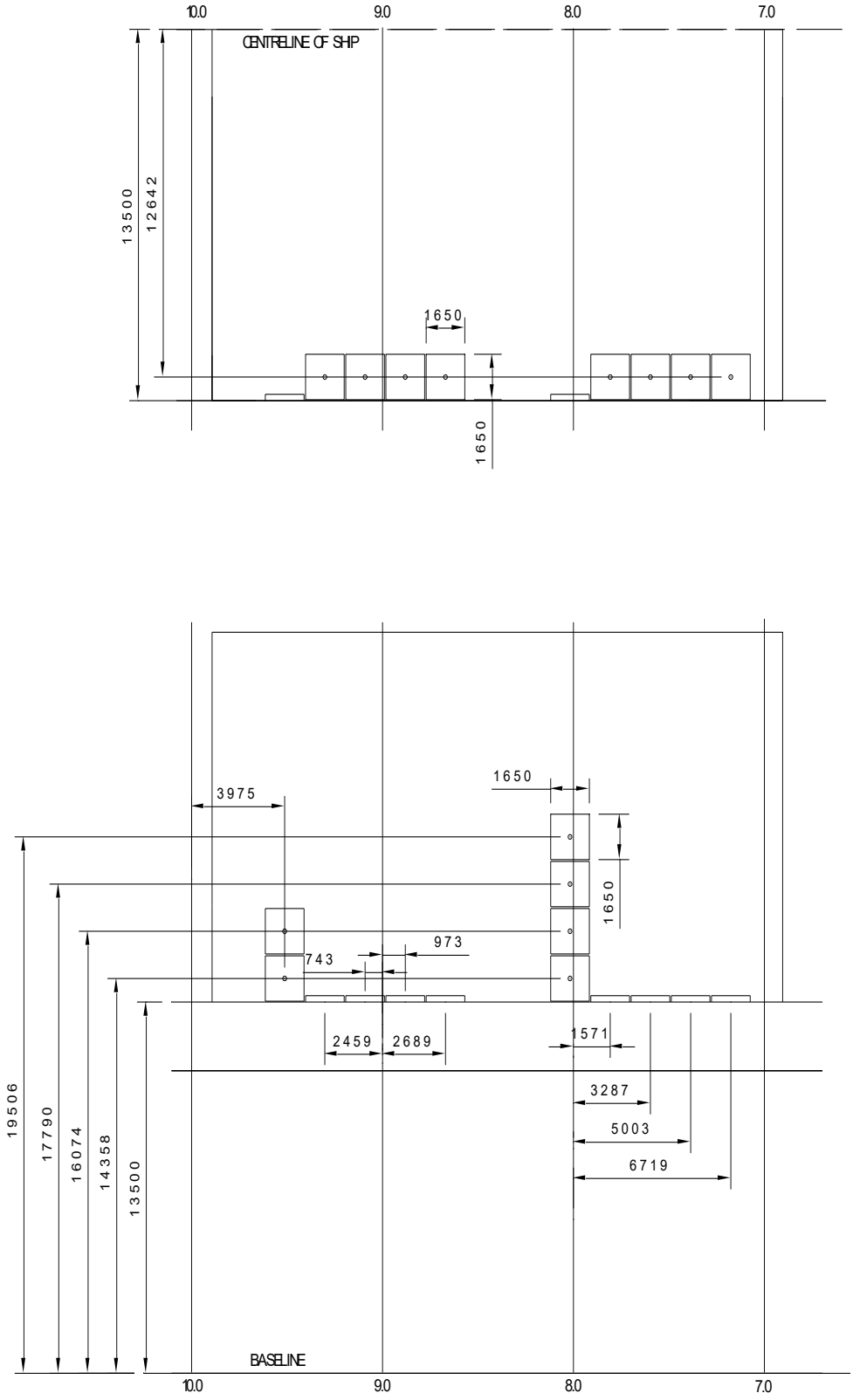

CLOSE UP VIEW PANEL SET FOR SHIP MODEL No. 10246
DIMENSIONS ARE GIVEN IN mm FOR SHIP

Figure 10 Rudder and propeller arrangement

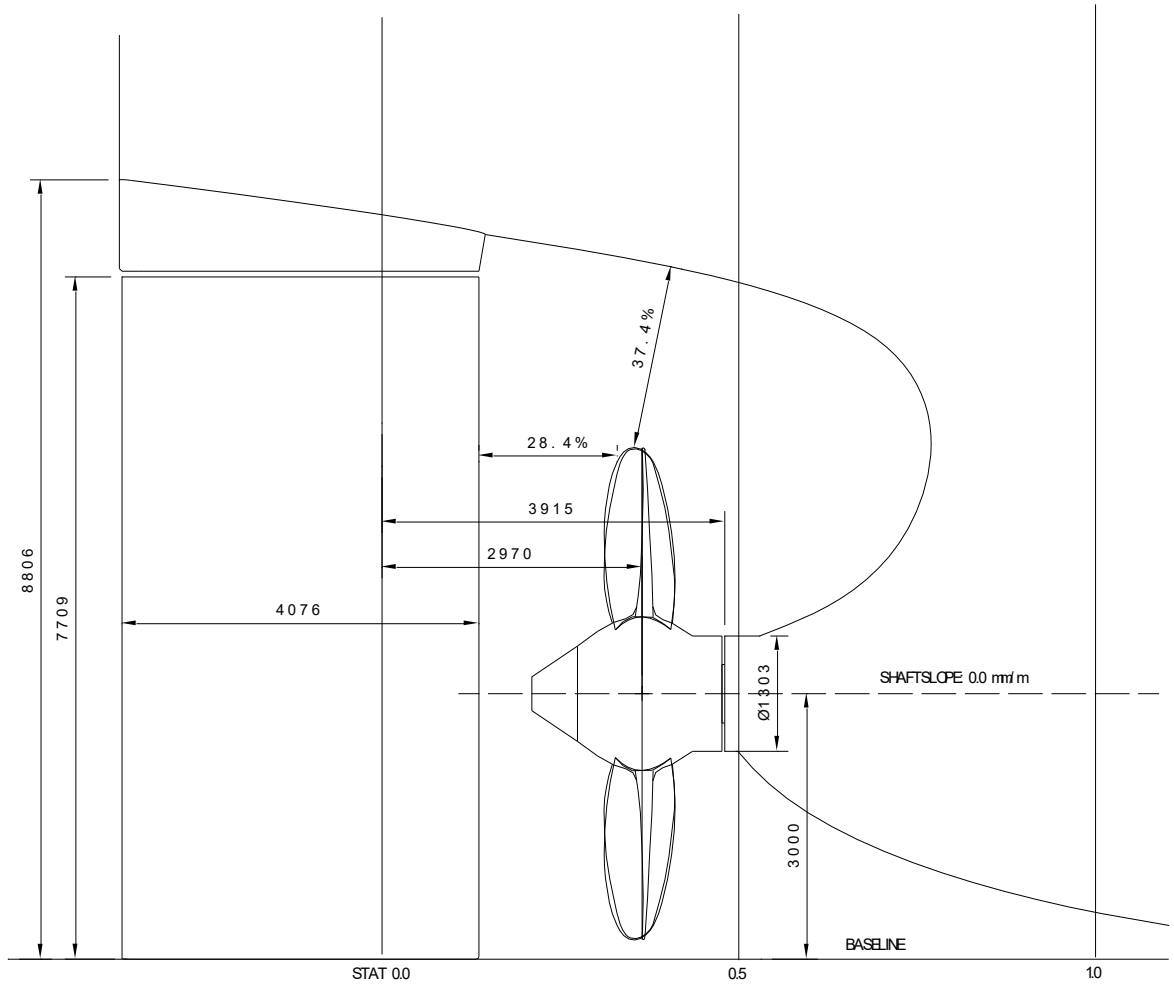

SCREW APERTURE I WI TH RUDDER I, RUDDER HEADBOX I AND PROPELLER MODELS No. 5108R FOR SHI P MODEL No. 10246
DI MENSI ONS ARE GI VEN I N mm FOR SHI P

Figure 11 Particulars and location of the bilge keels – LC 1

Station	Distance measured along the stations from WL 8m to bilge keel
6	7331
End BK	7363
7	7638
8	7832
9	7812
10	7676
11	7584
12	7546
Start BK	7539

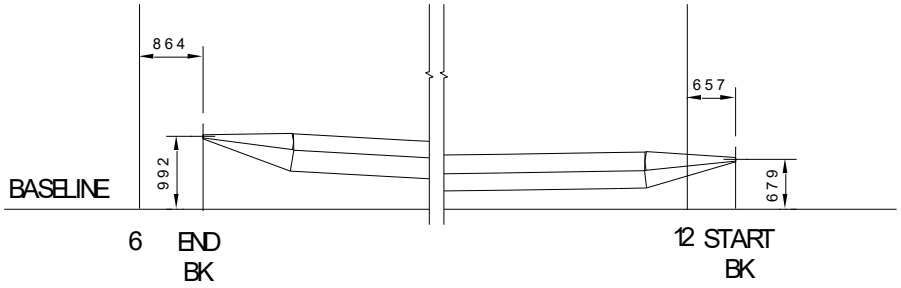

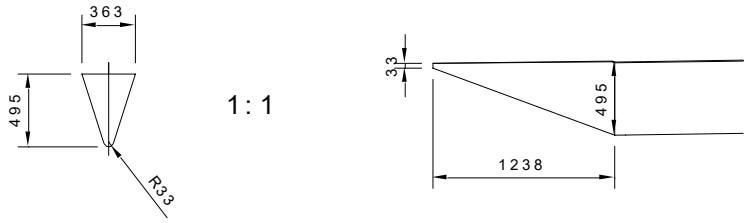

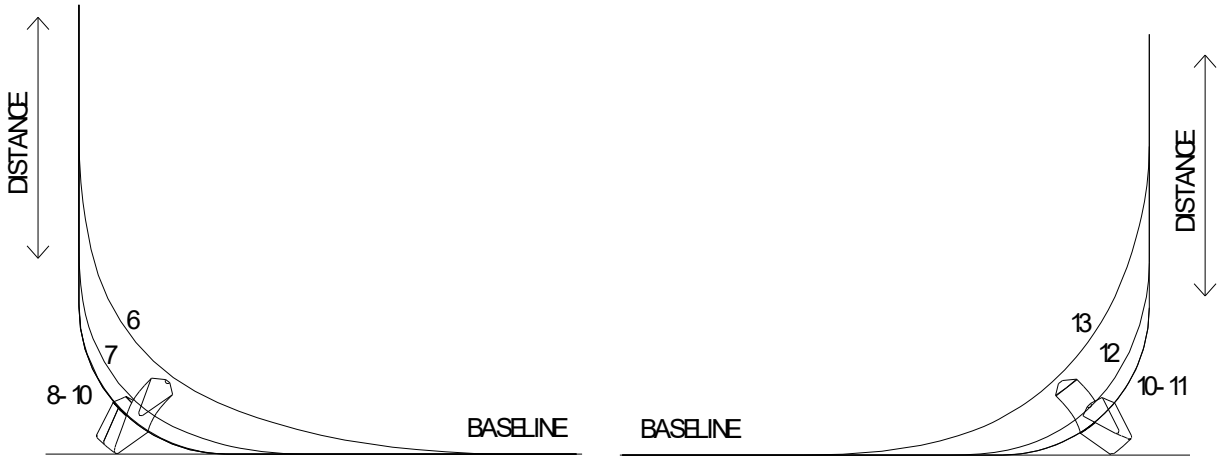

2 BILGE KEELS I FOR SHIP MODEL No. 10246
DIMENSIONS ARE GIVEN IN mm FOR SHIP

Figure 12 Particulars and location of the bilge keels – LC 2

Station	Distance measured along the stations from WL 8m to bilge keel
6	7331
End BK	7363
7	7638
8	7832
9	7812
10	7676
11	7584
12	7546
Start BK	7539

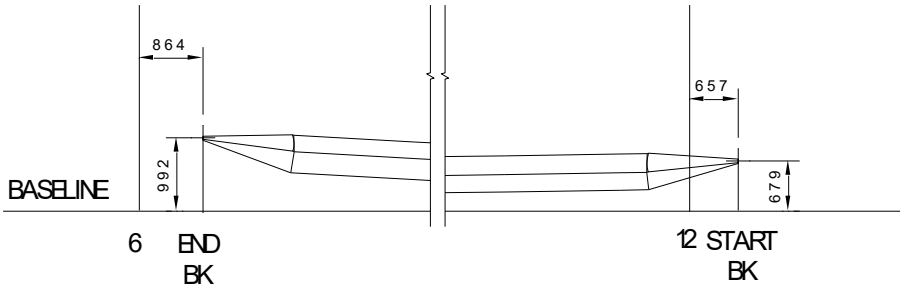

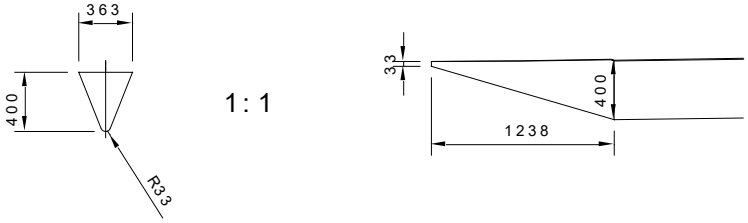

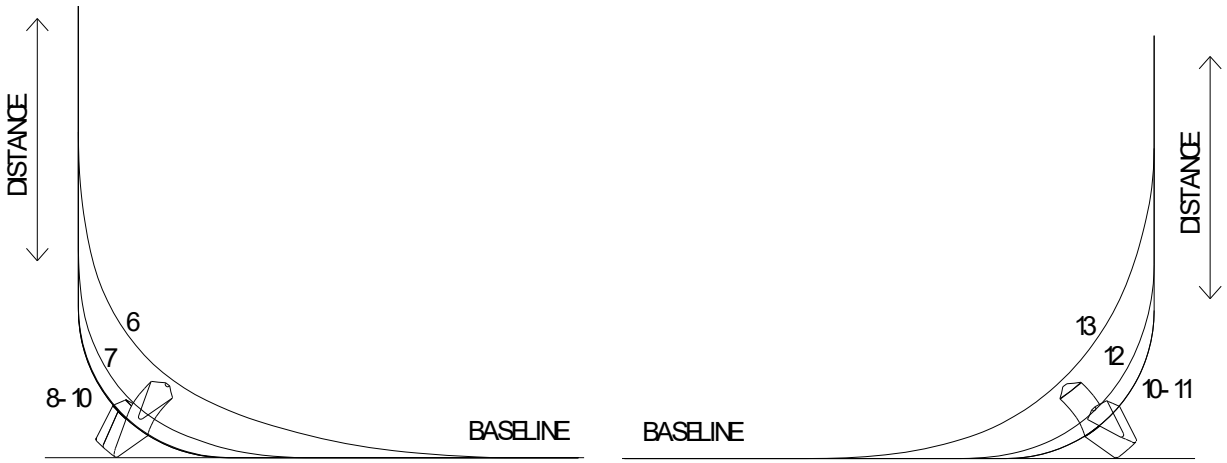

2 BILGE KEELS II FOR SHIP MODEL No. 10246
DIMENSIONS ARE GIVEN IN mm FOR SHIP

Figure 13 Soft mooring setup – Tests in OB

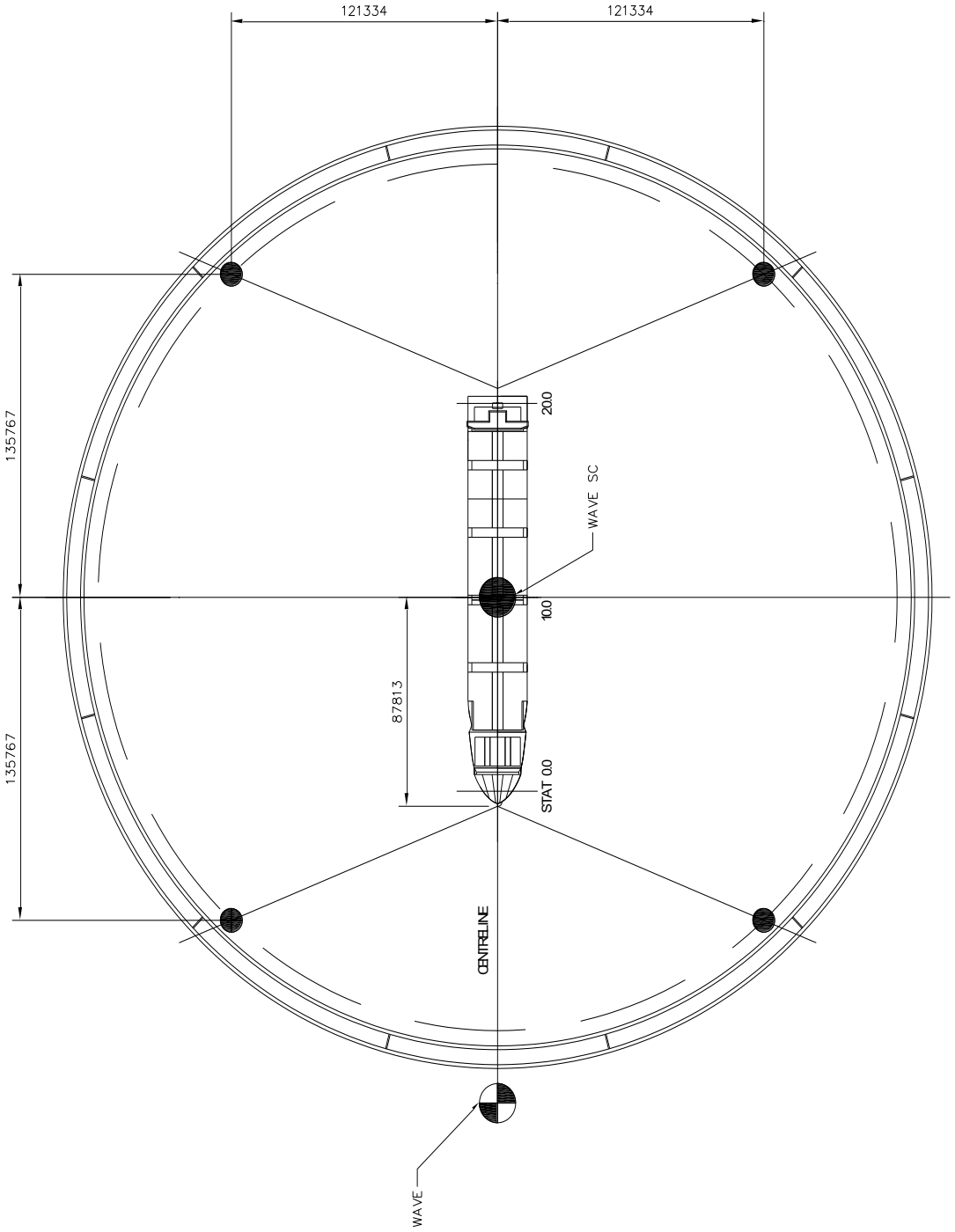

SOFT MOORING SETUP I WITH HEADING 0 DEG FOR SHIP MODEL No. 10246
DIMENSIONS ARE GIVEN IN mm FOR SHIP

Figure 14 Configuration 2 - Simulation 2-1, Displacement values in [mm]

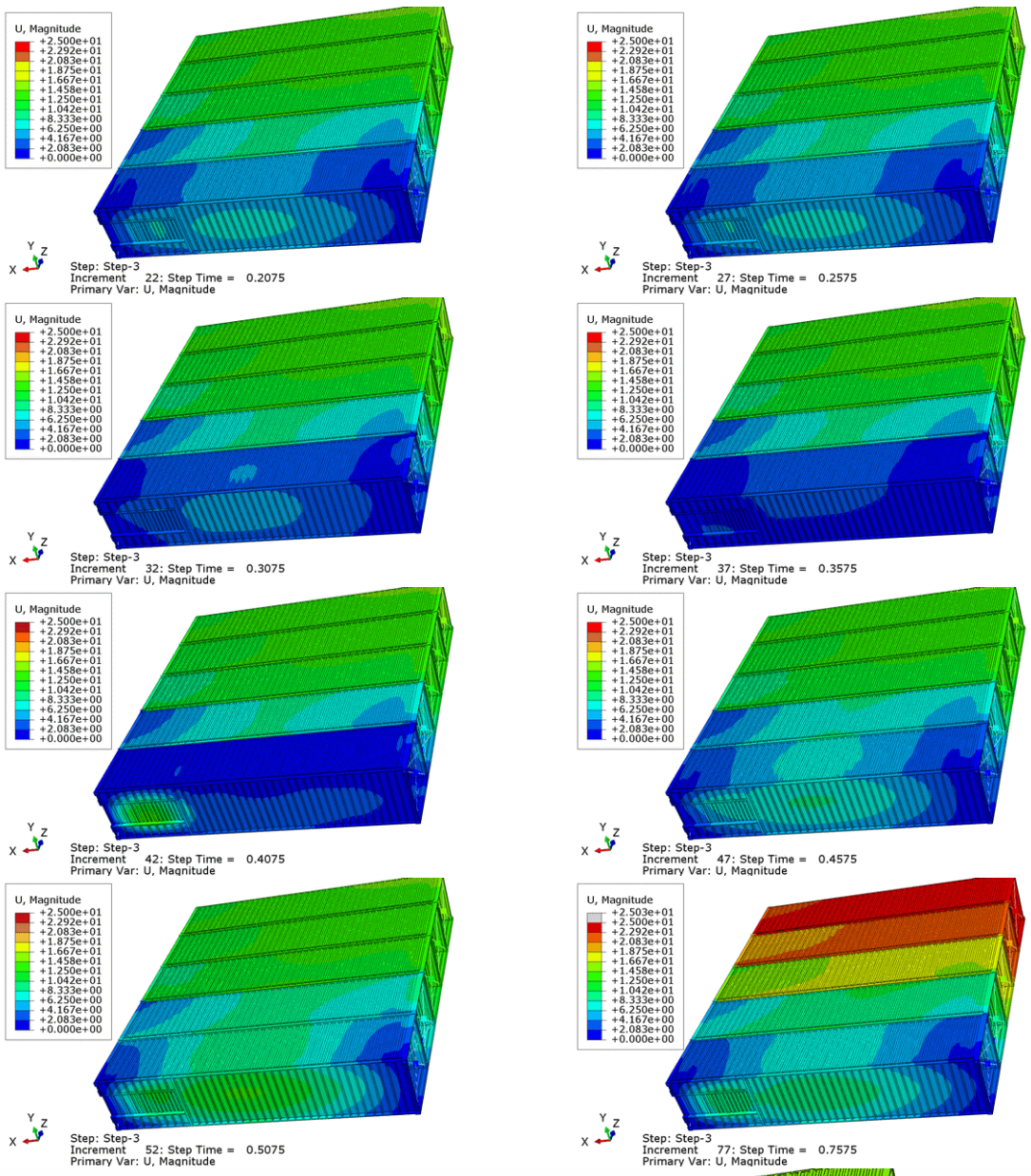

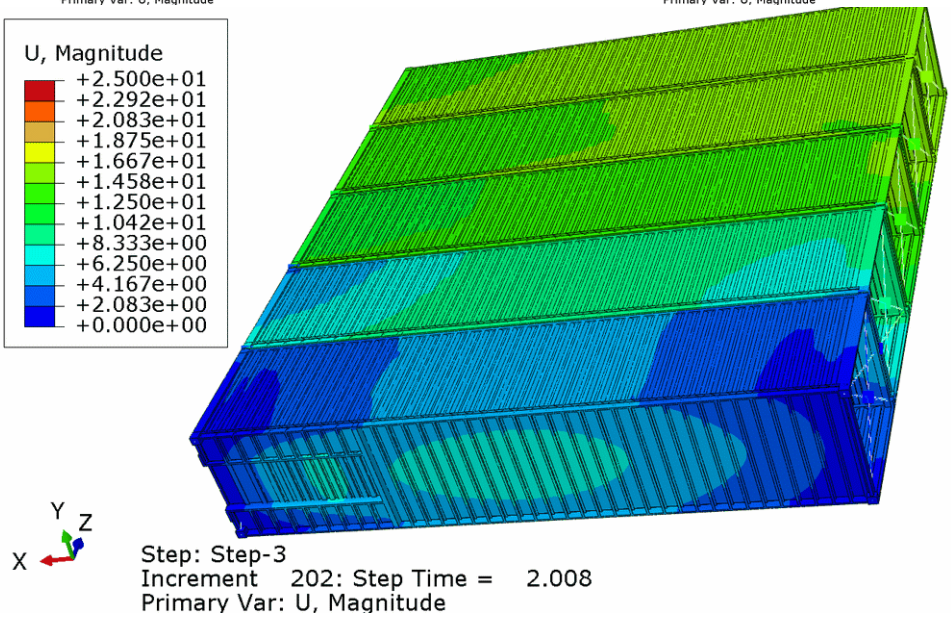

Figure 15 Configuration 2 - Simulation 2-1, Von Mises stress values in [MPa]

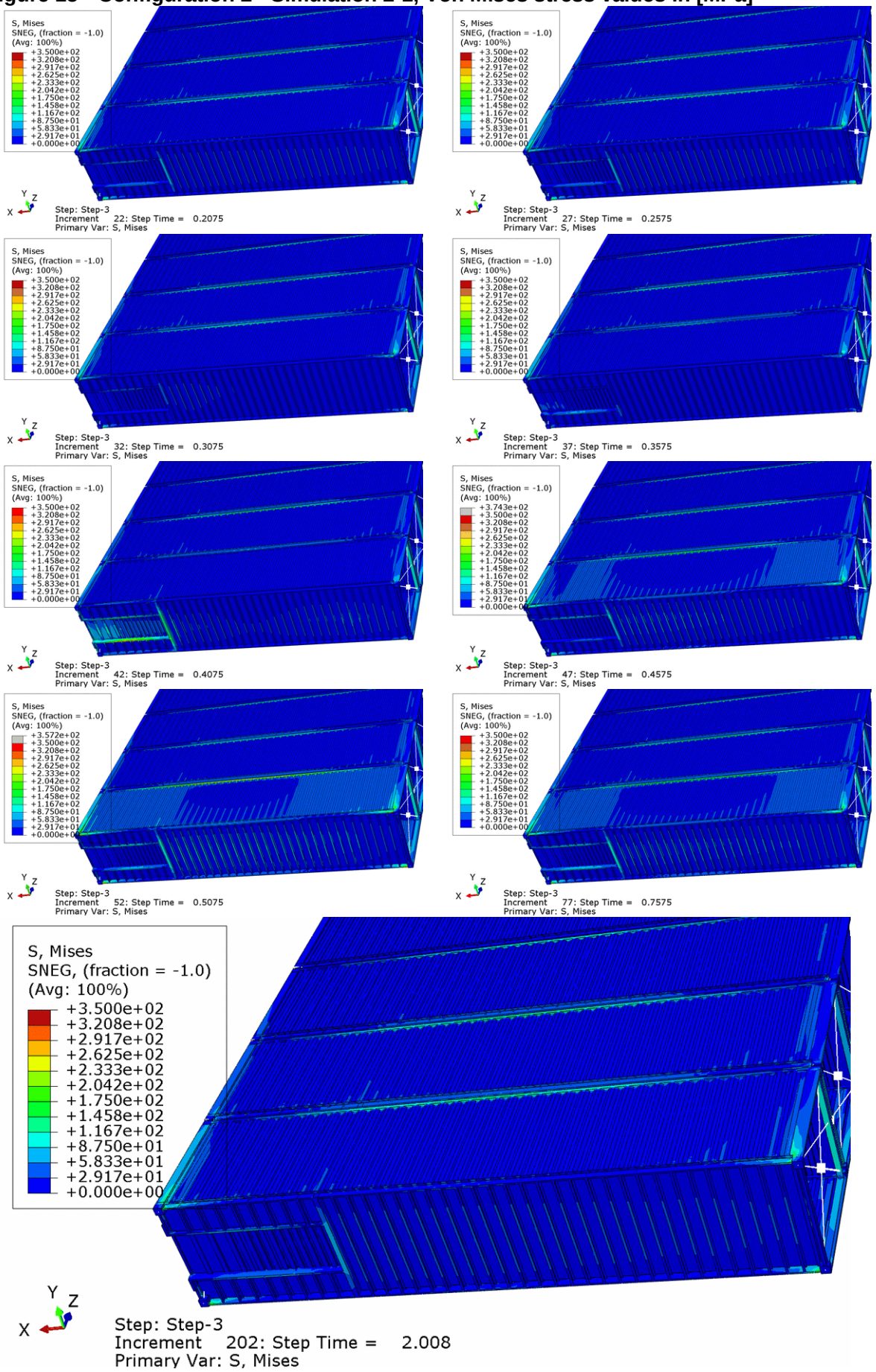

Figure 16 Configuration 2 - Simulation 2-1, Pressure values in [MPa]

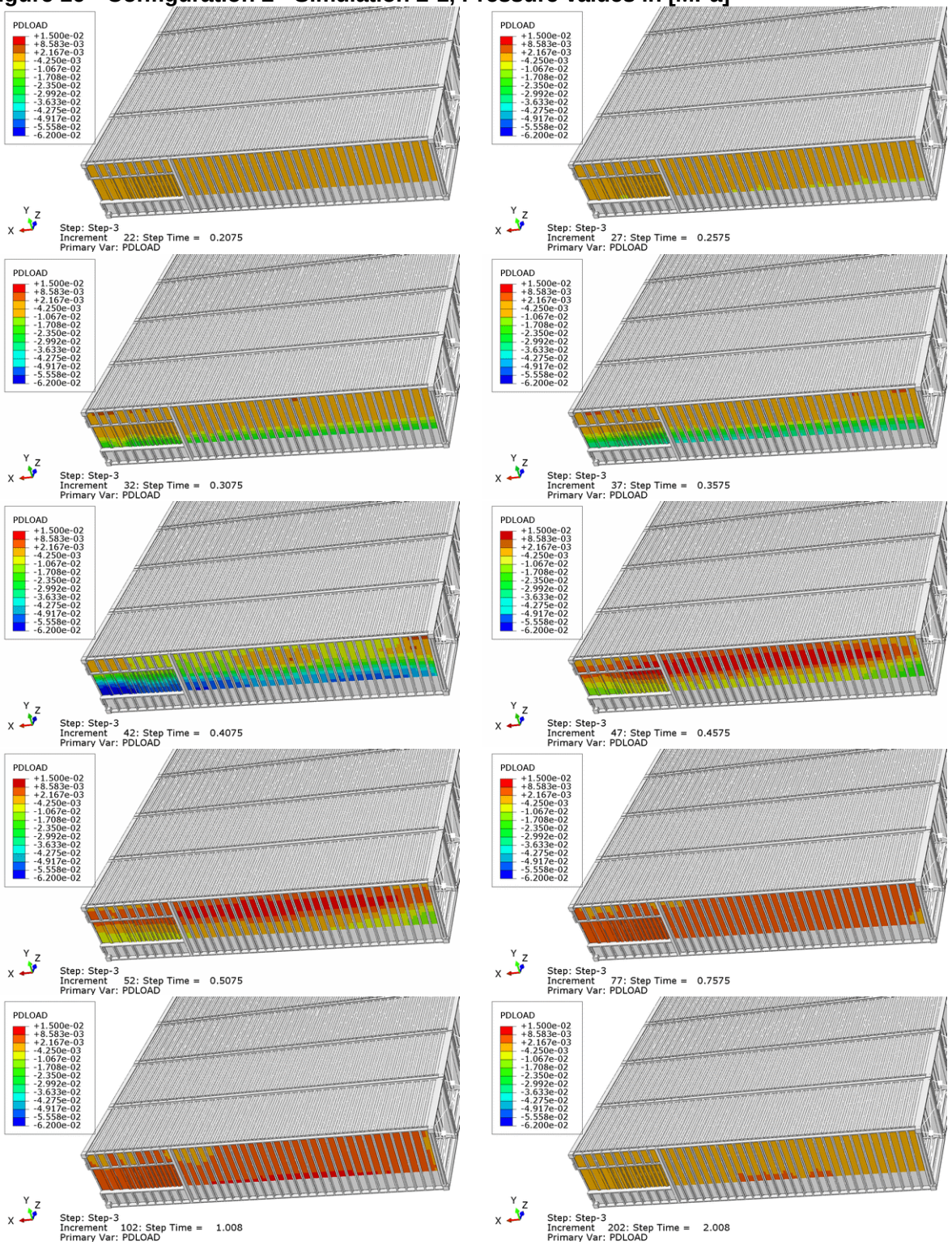

Figure 17 Configuration 2 - Simulation 2-2, Displacement values in [mm]

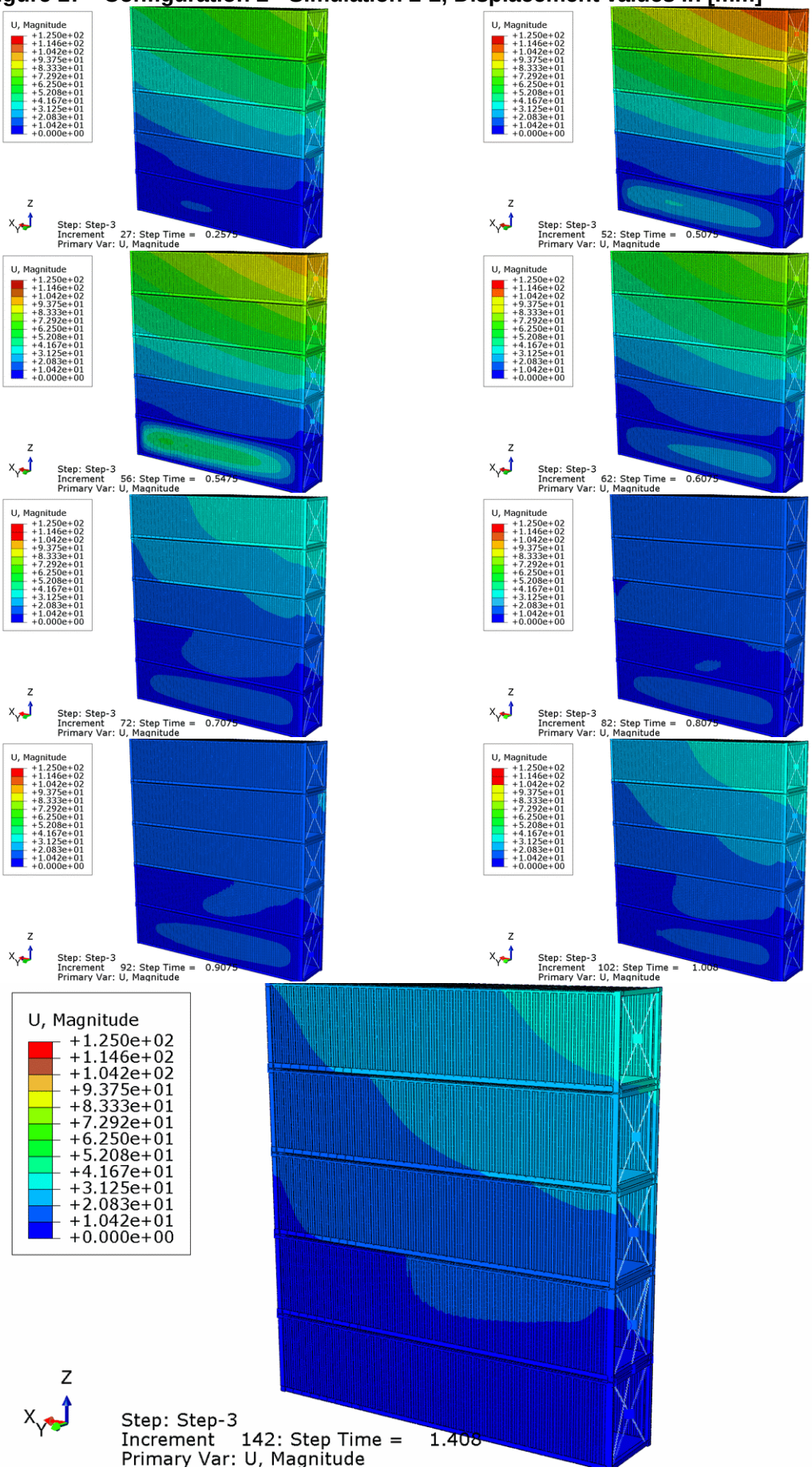

Figure 18 Configuration 2 - Simulation 2-2, Von Mises stress values in [MPa]

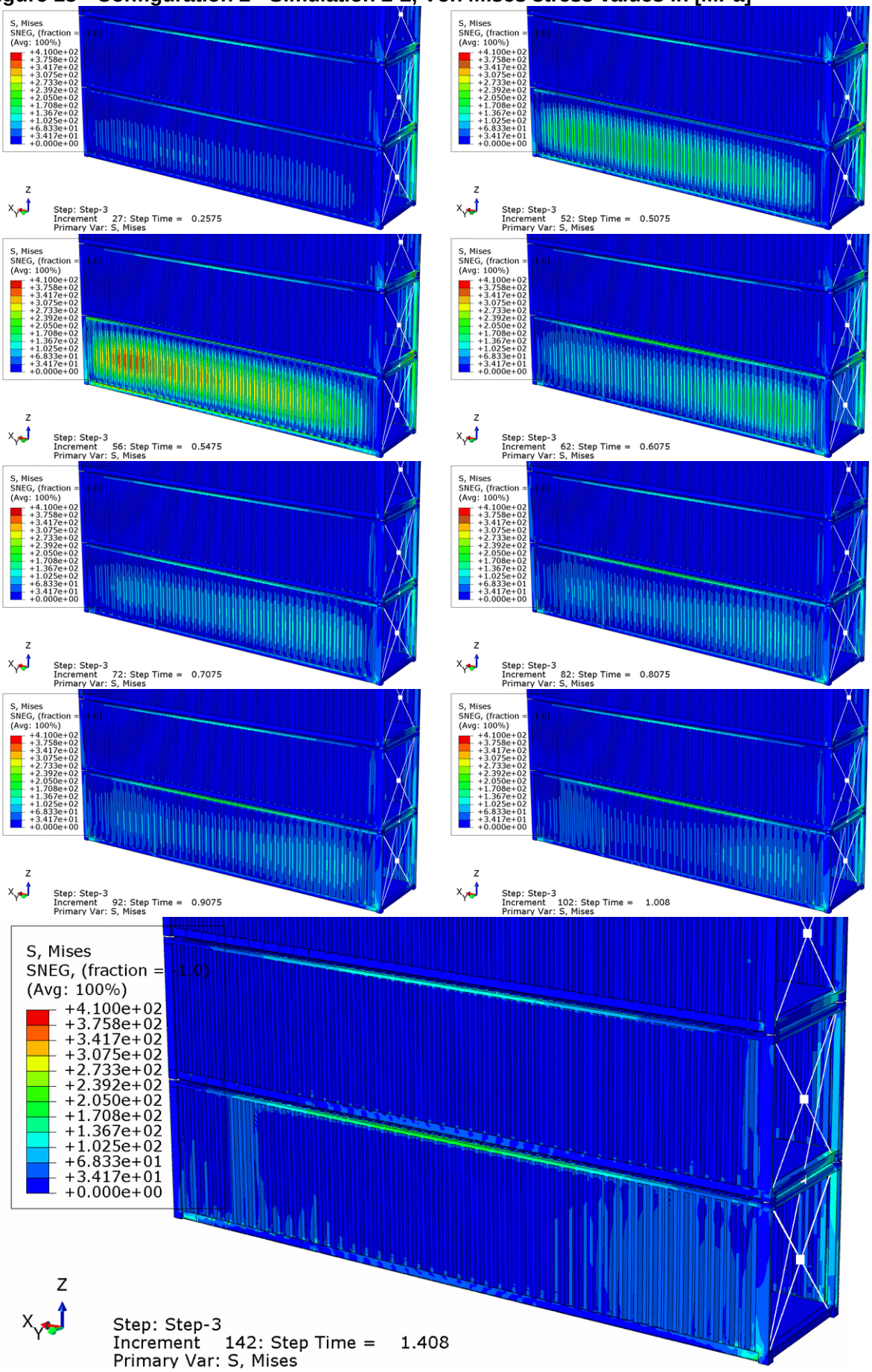

Figure 19 Configuration 2 - Simulation 2-2, Pressure values in [MPa]

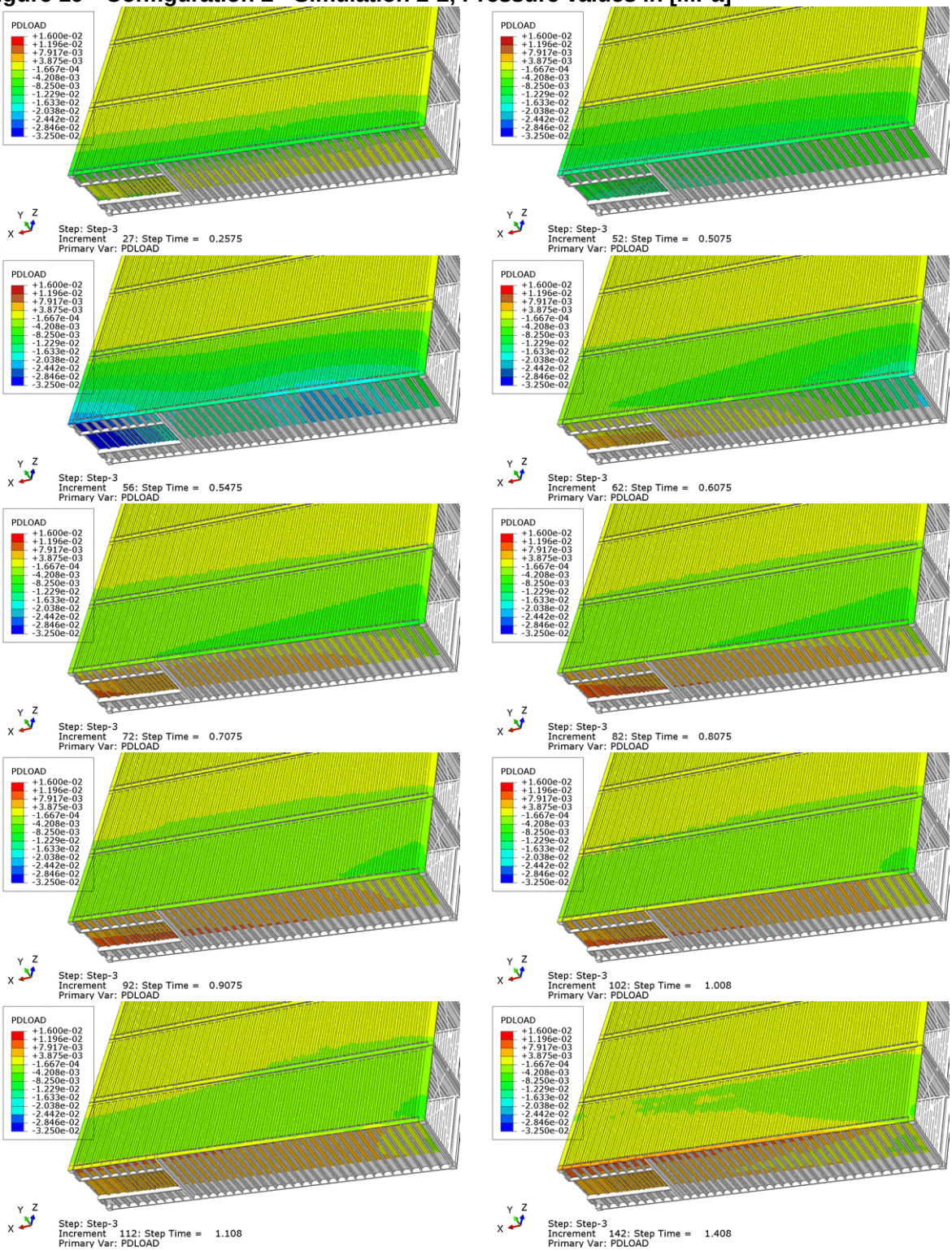

Figure 20 Configuration 2 - Simulation 2-3, Displacement values in [mm]

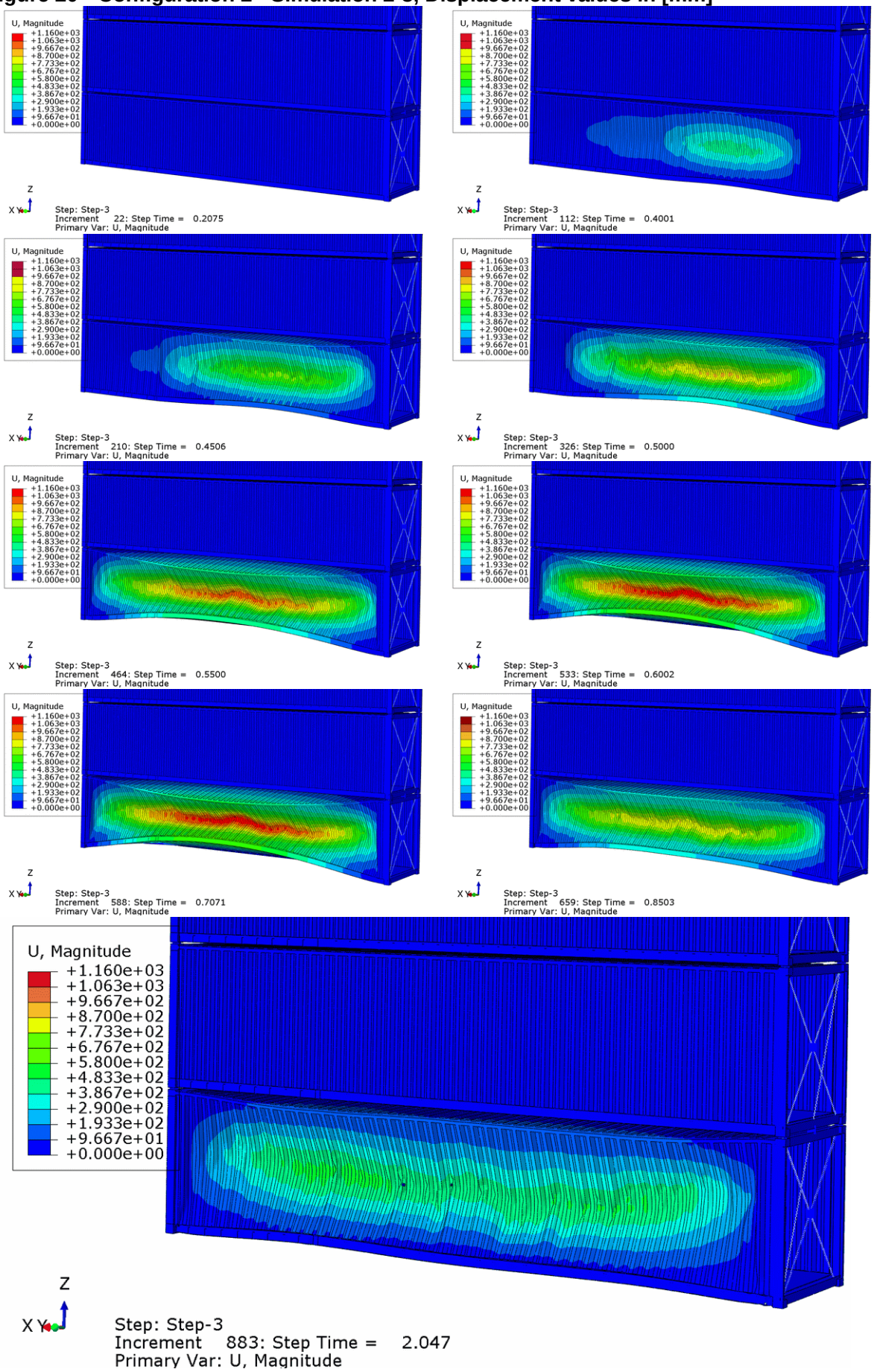

Figure 21 Configuration 2 - Simulation 2-3, Von Mises stress values in [MPa]

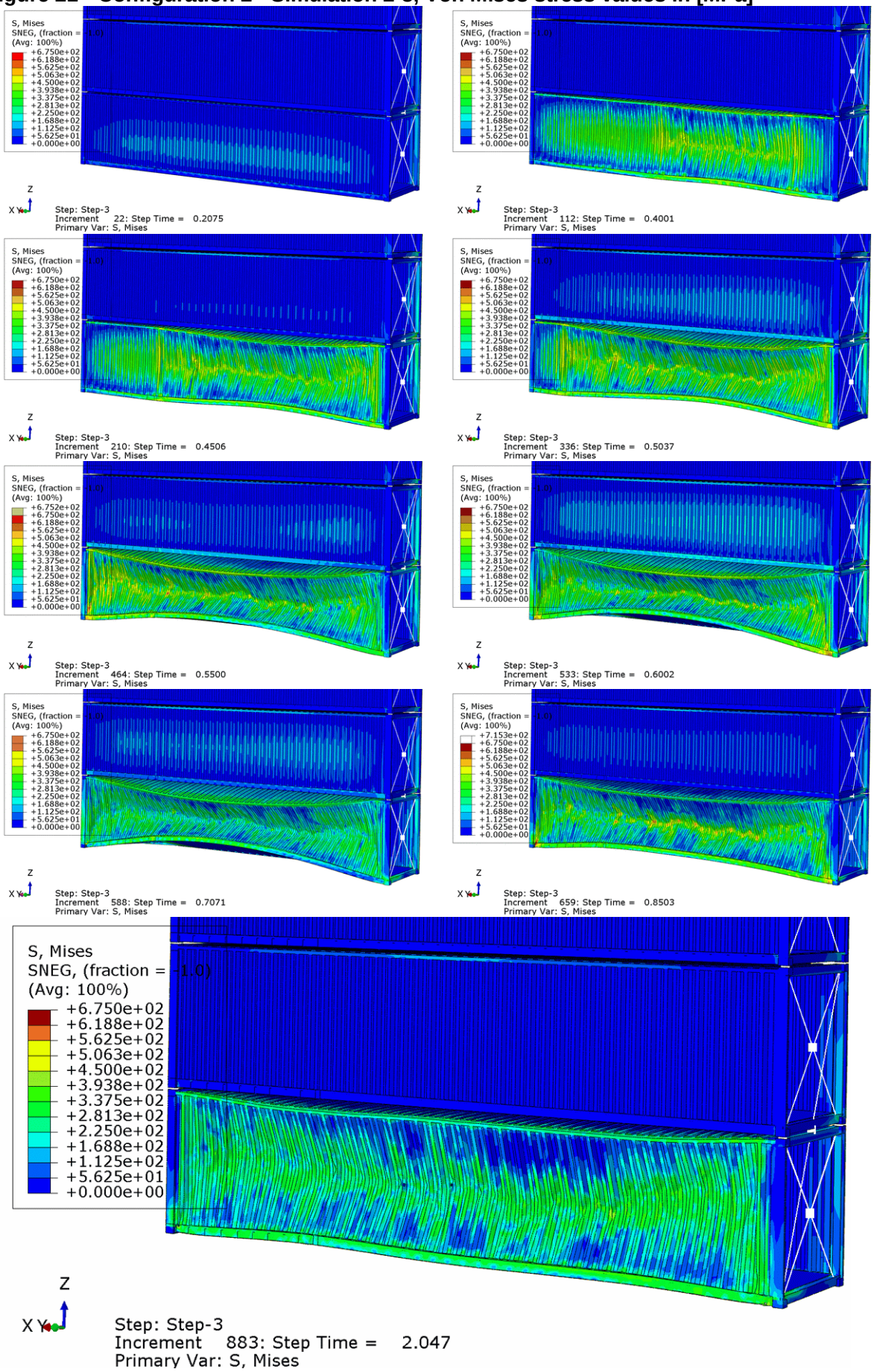

Figure 22 Configuration 2 - Simulation 2-3, Pressure values in [MPa]

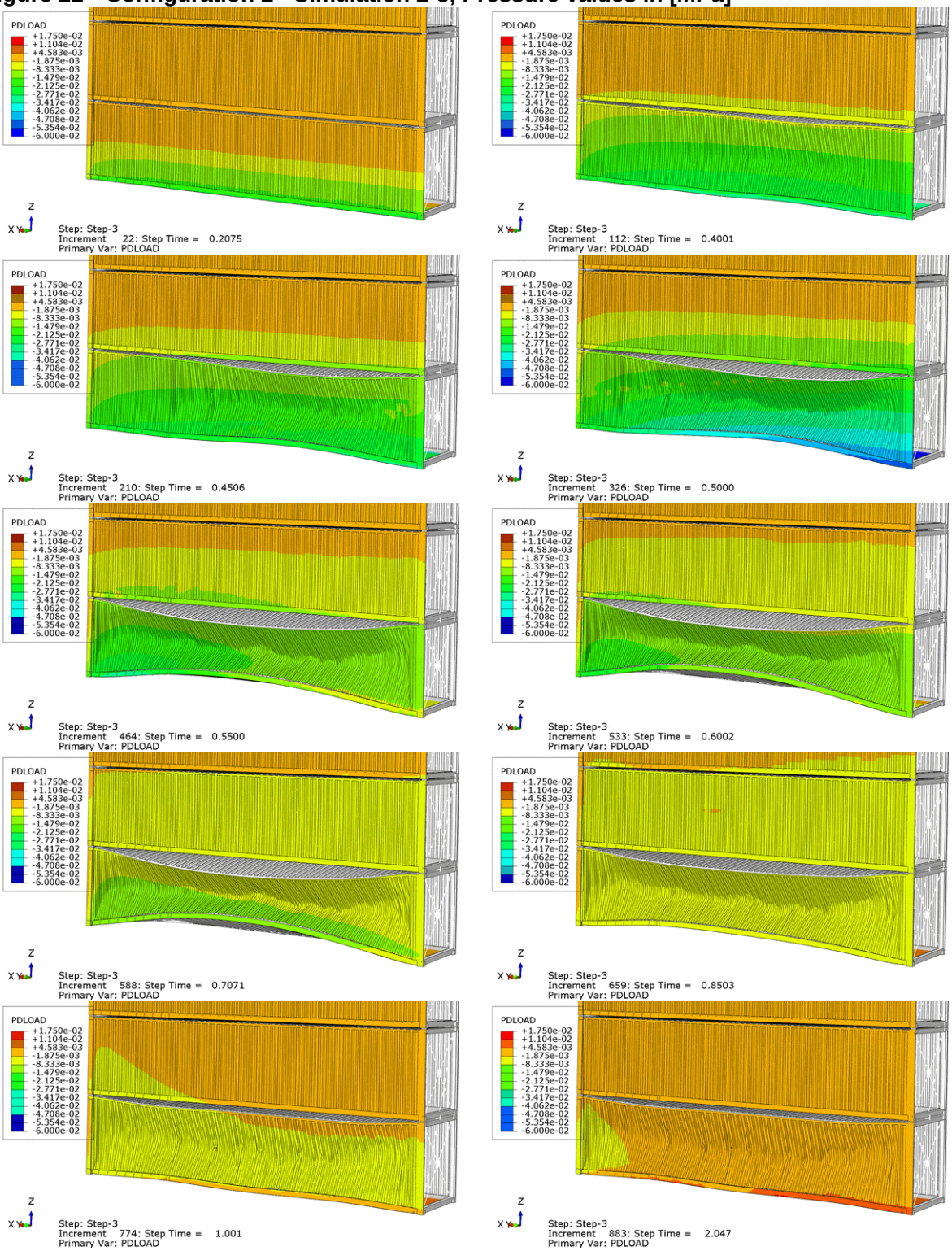

Figure 23 Configuration 2 - Simulation 2-4, Displacement values in [mm]

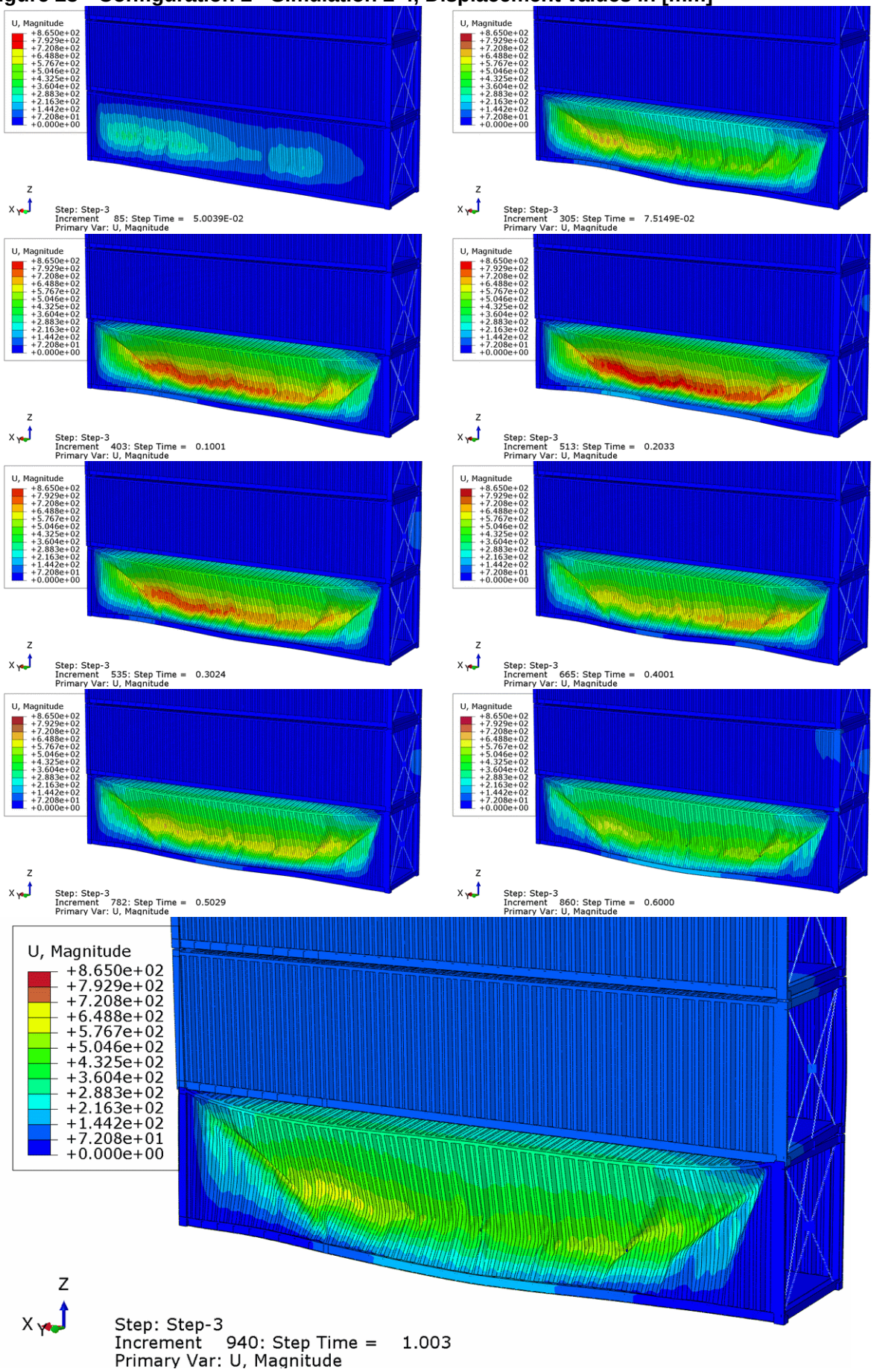

Figure 24 Configuration 2 - Simulation 2-4, Von Mises stress values in [MPa]

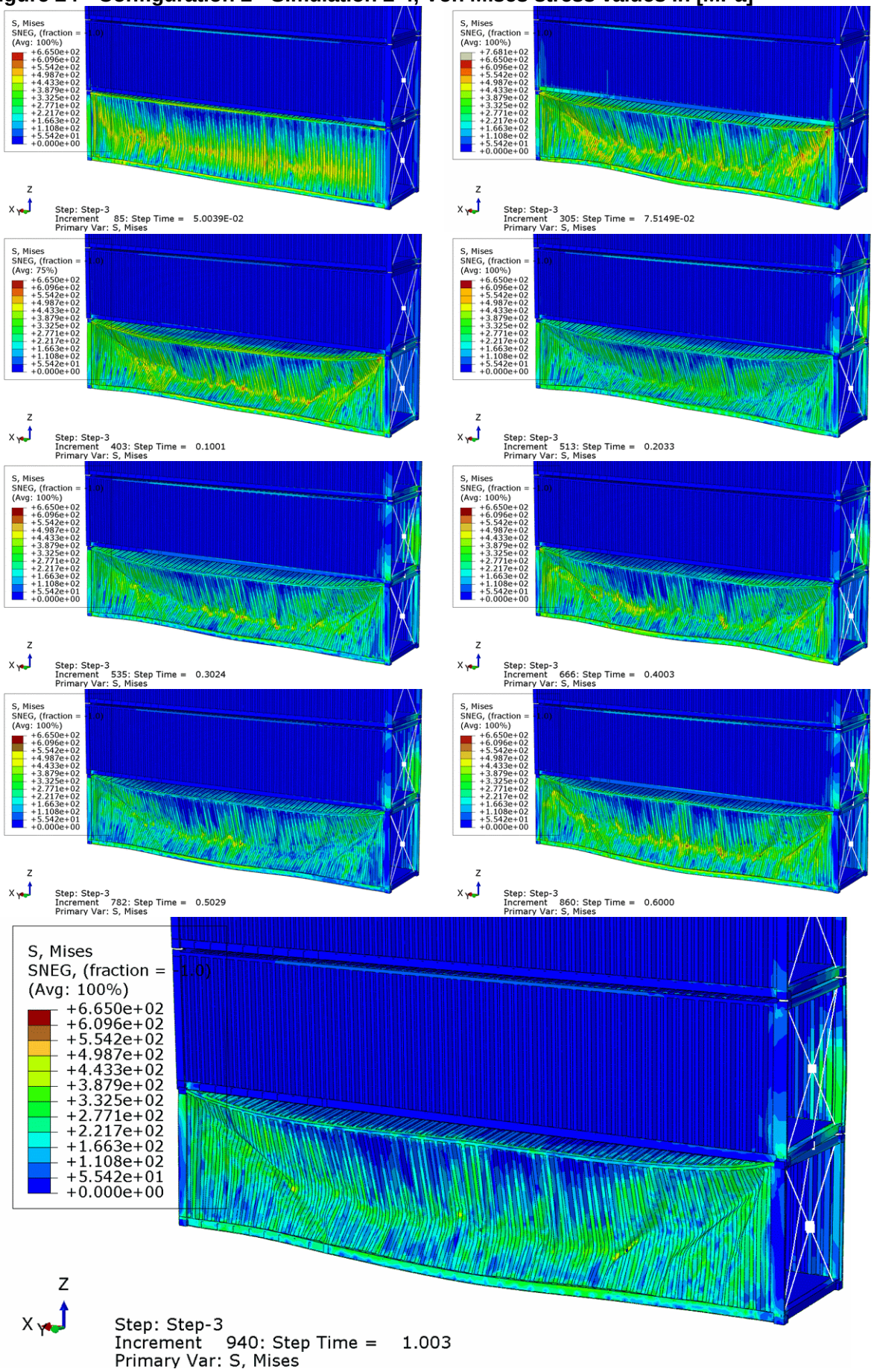

Figure 25 Configuration 2 - Simulation 2-4, Pressure values in [MPa]

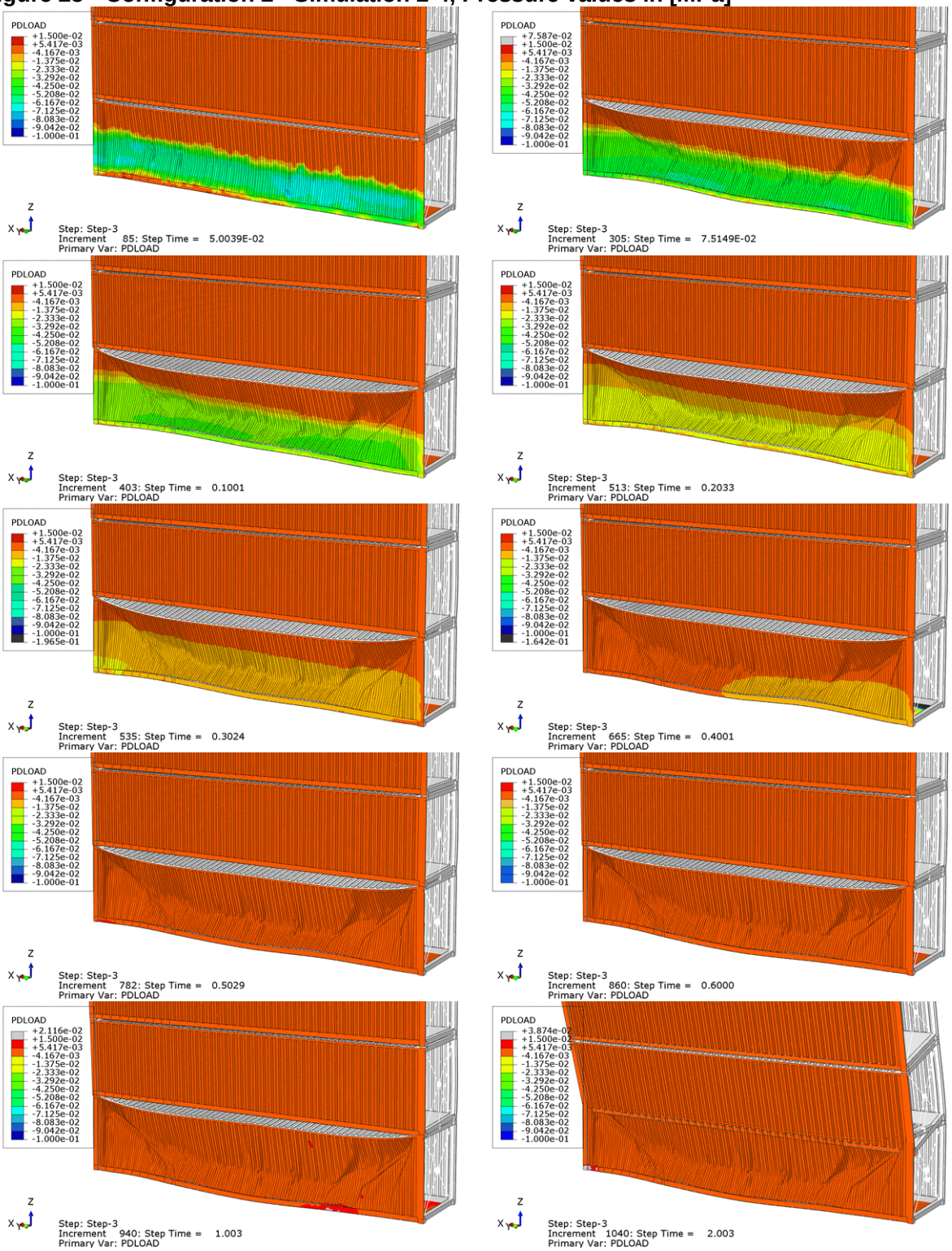

Figure 26 Configuration 2 - Simulation 2-5, Displacement values in [mm]

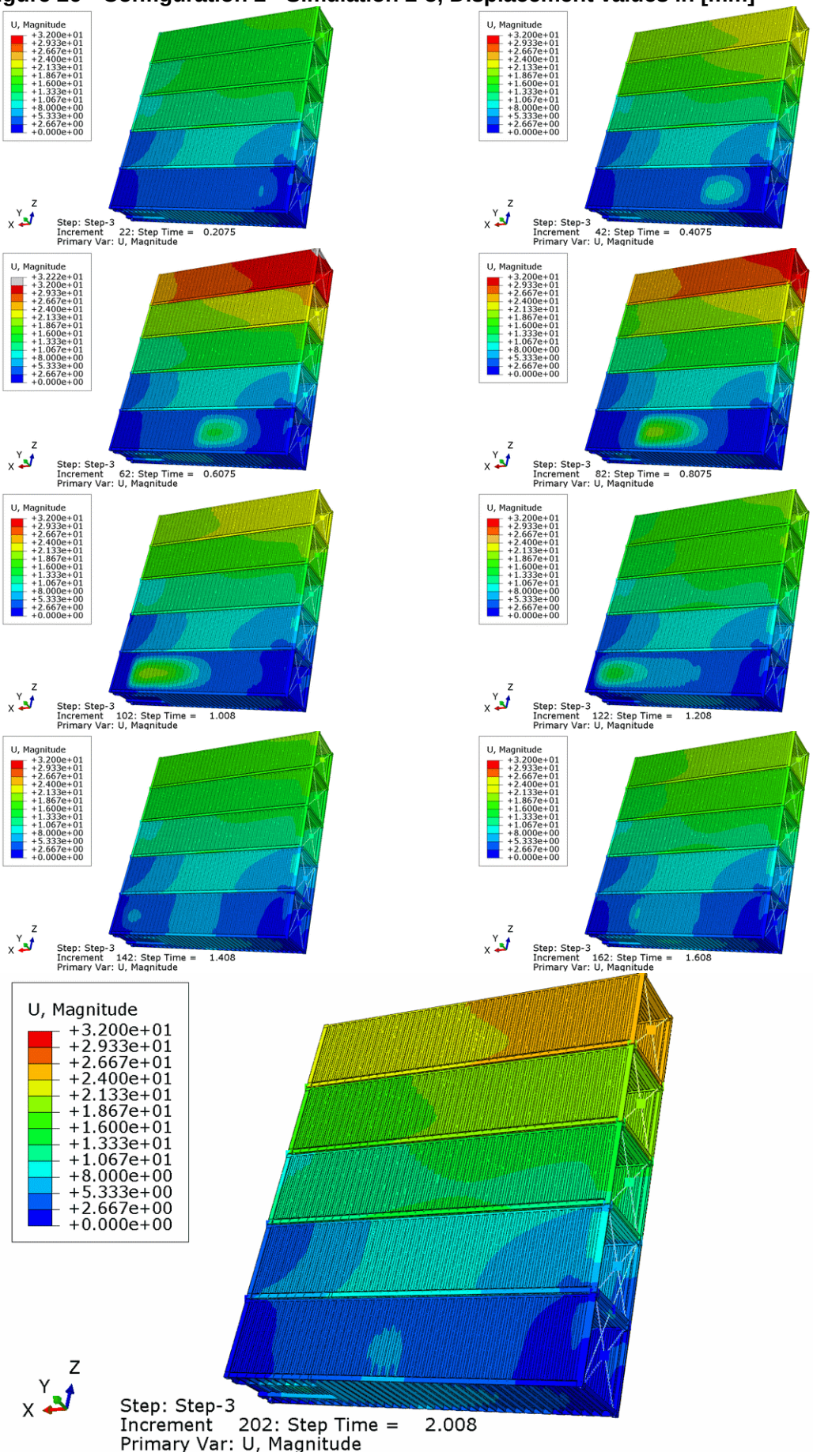

Figure 27 Configuration 2 - Simulation 2-5, Von Mises stress values in [MPa]

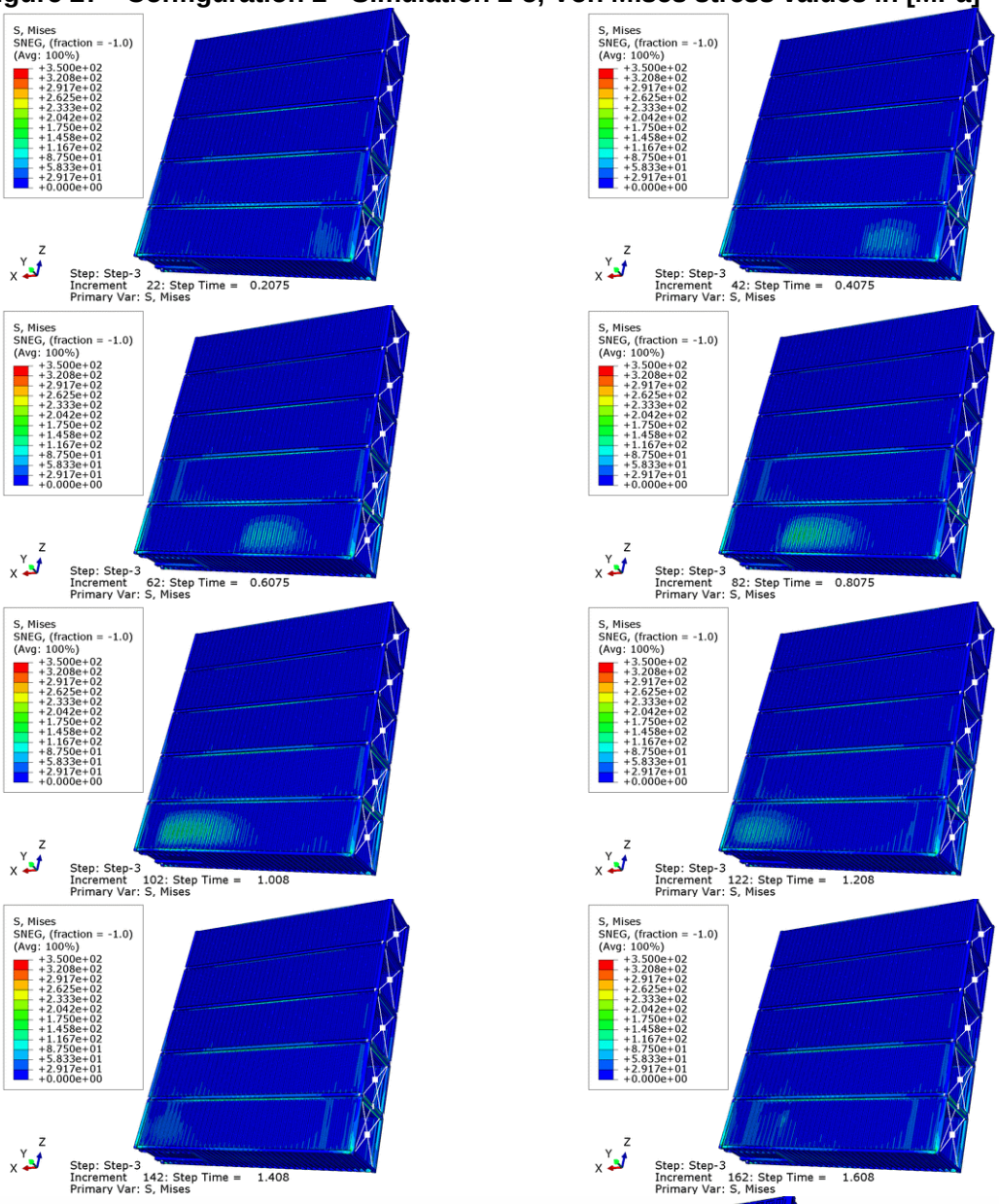

Figure 28 Configuration 2 - Simulation 2-5, Pressure values in [MPa]

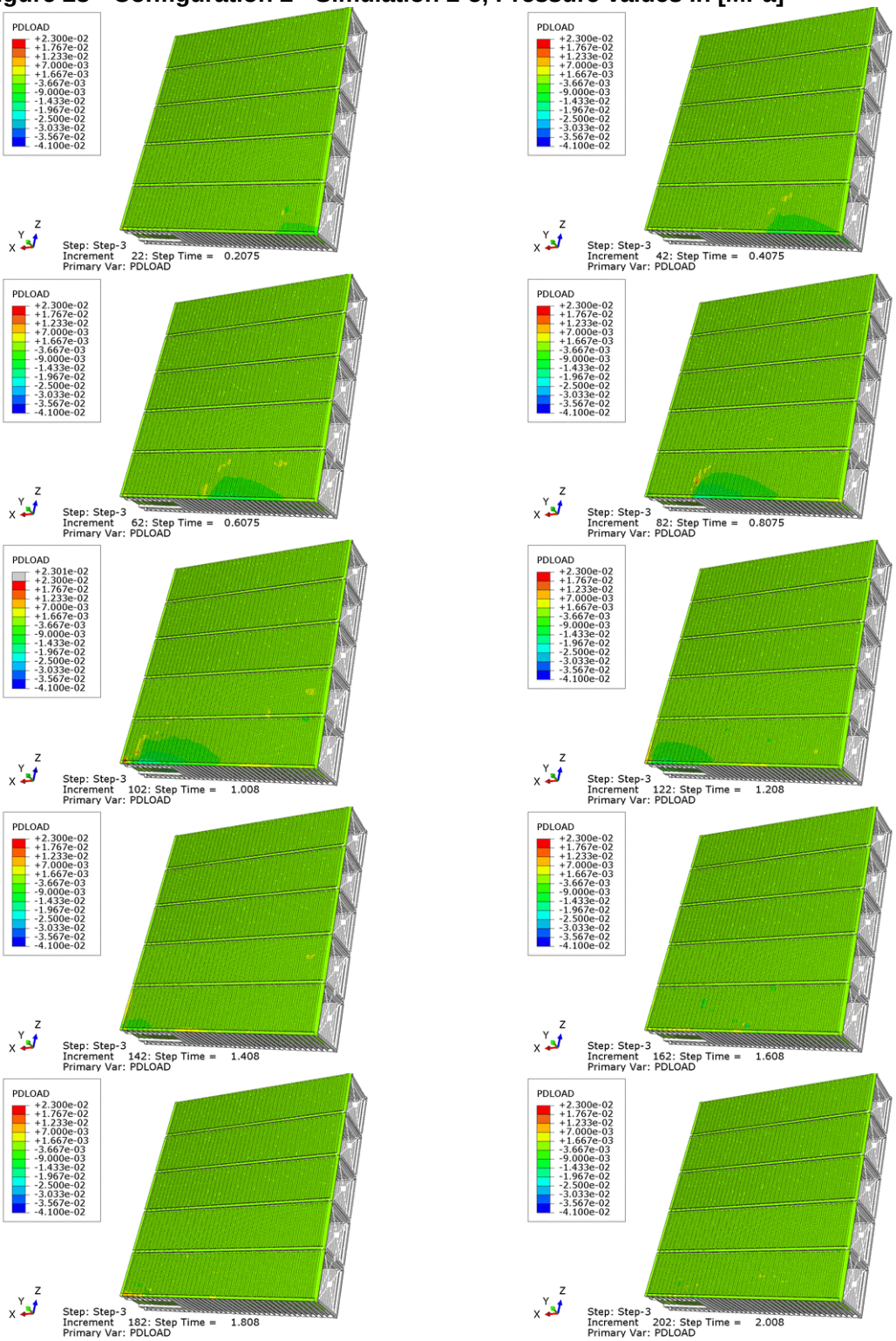

Figure 29 Configuration 2 - Simulation 2-6, Displacement values in [mm]

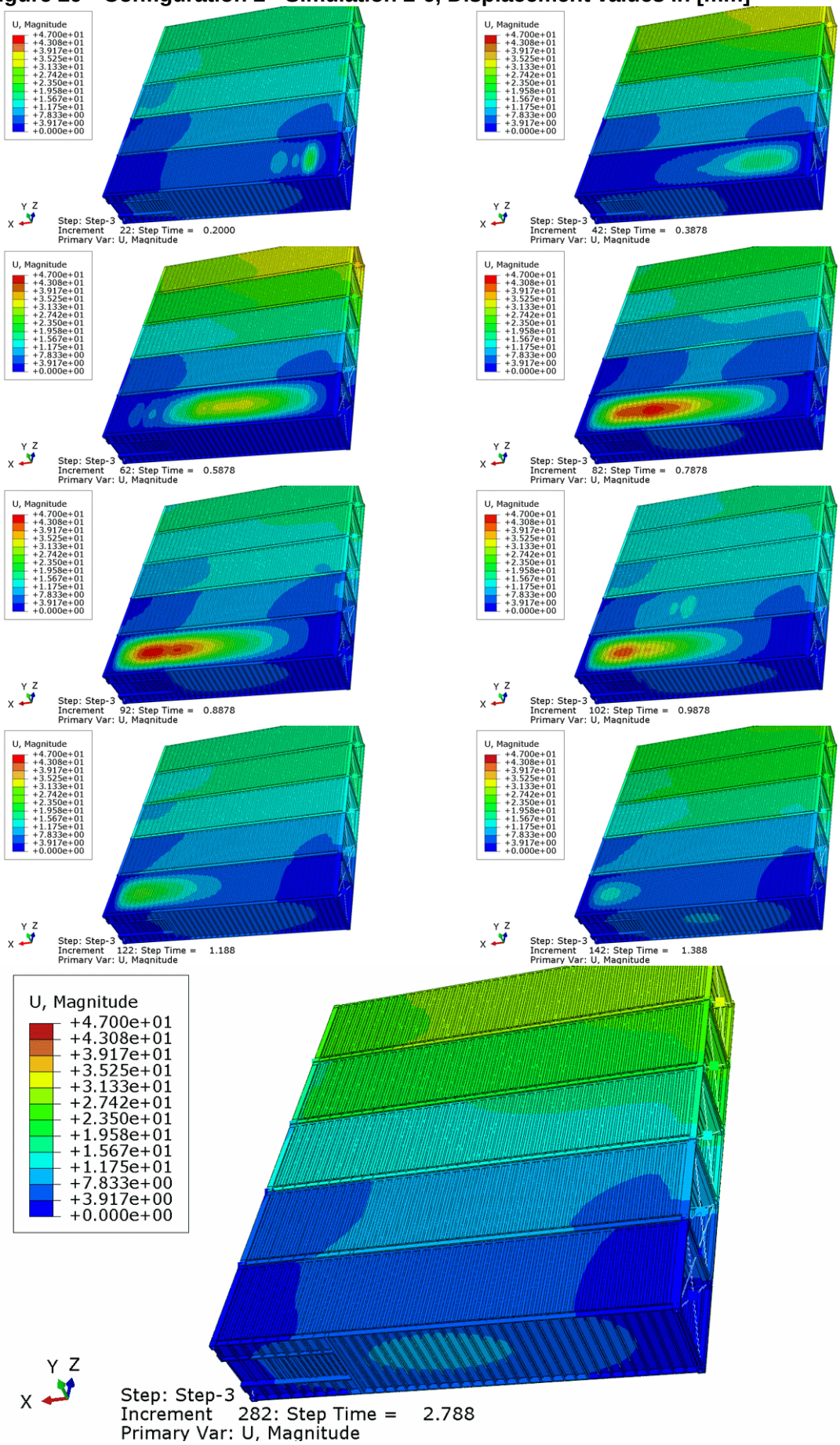

Figure 30 Configuration 2 - Simulation 2-6, Von Mises stress values in [MPa]

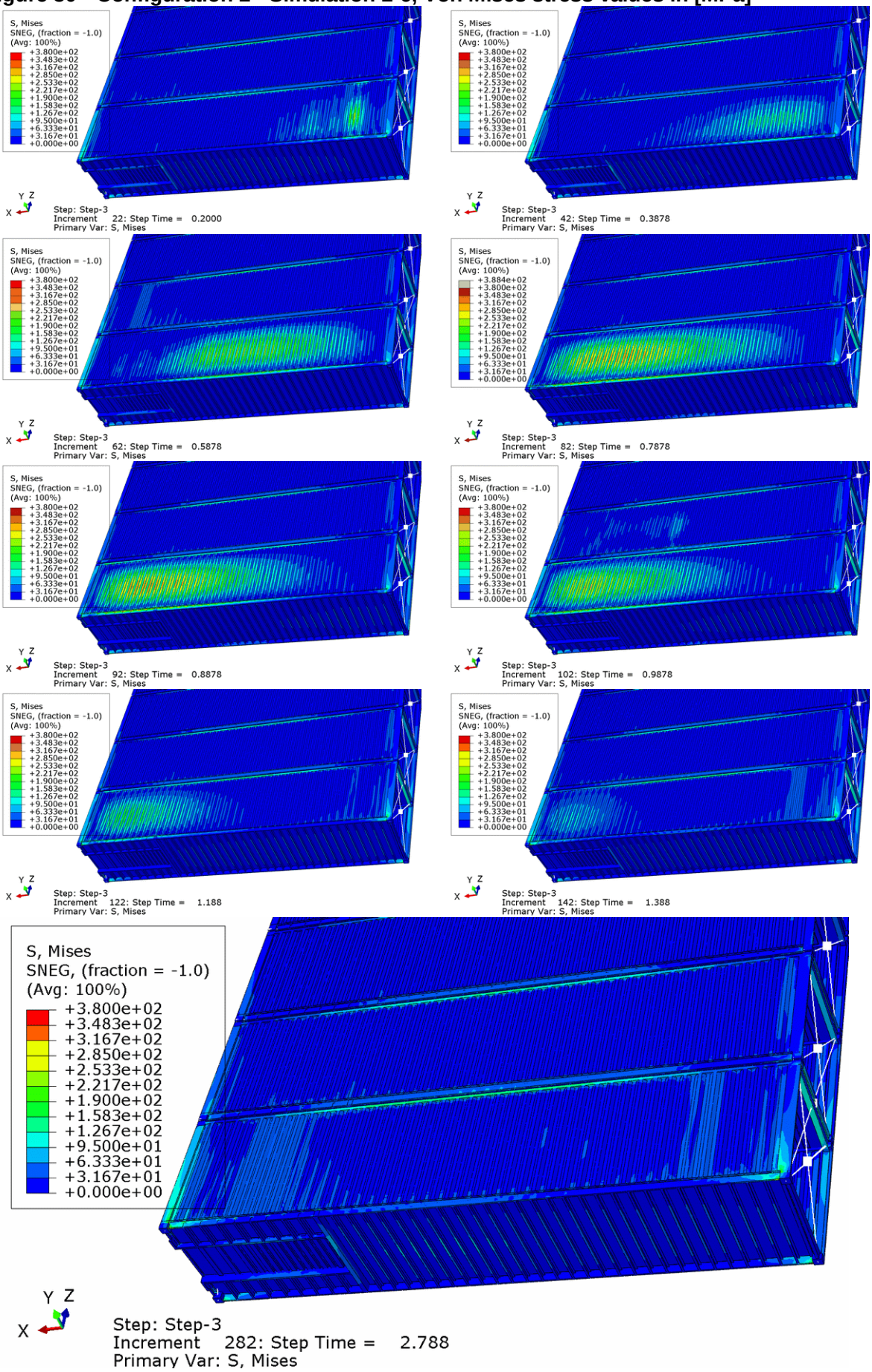

Figure 31 Configuration 2 - Simulation 2-6, Pressure values in [MPa]

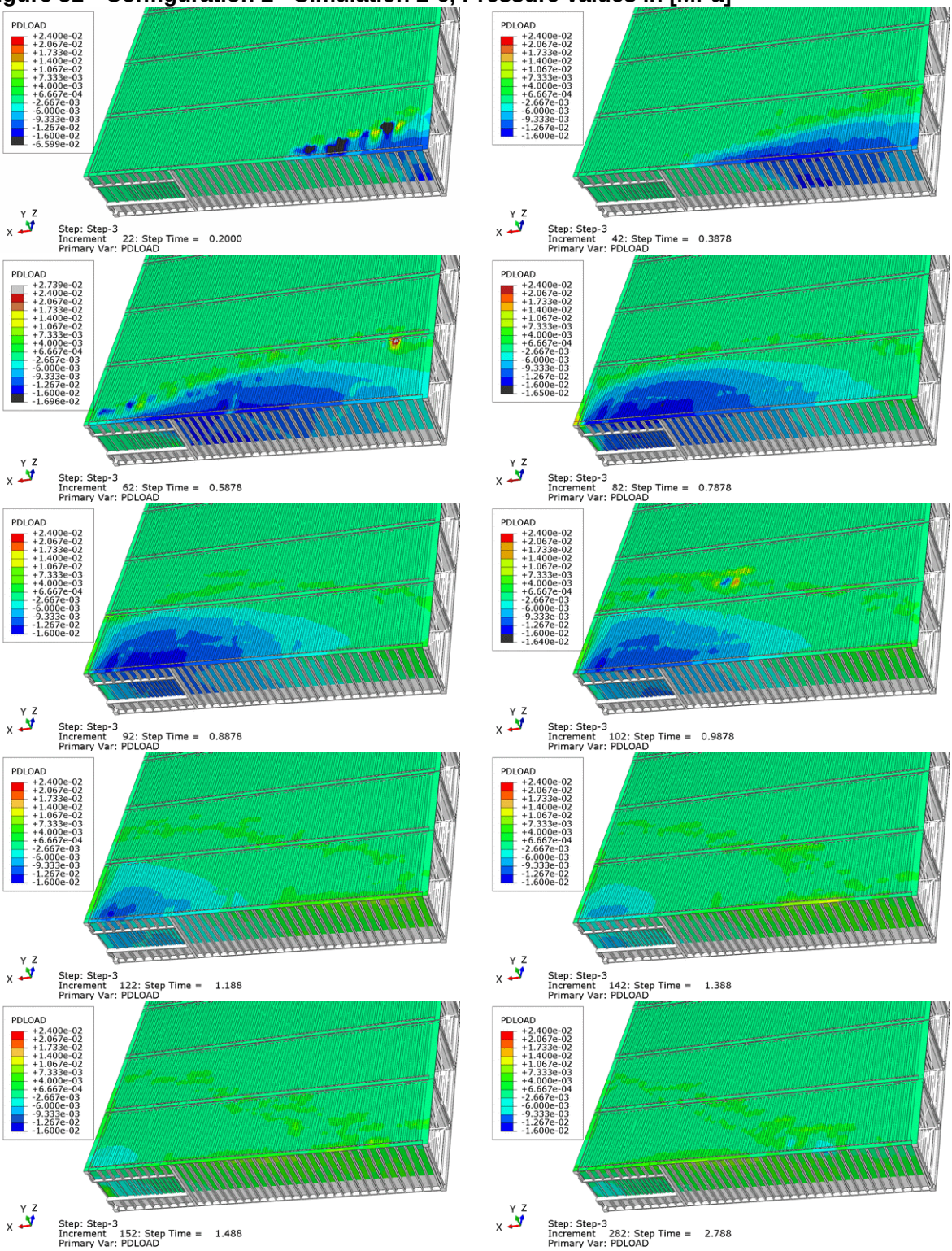

Figure 32 Configuration 5 - Simulation 5-2, Displacement values in [mm]

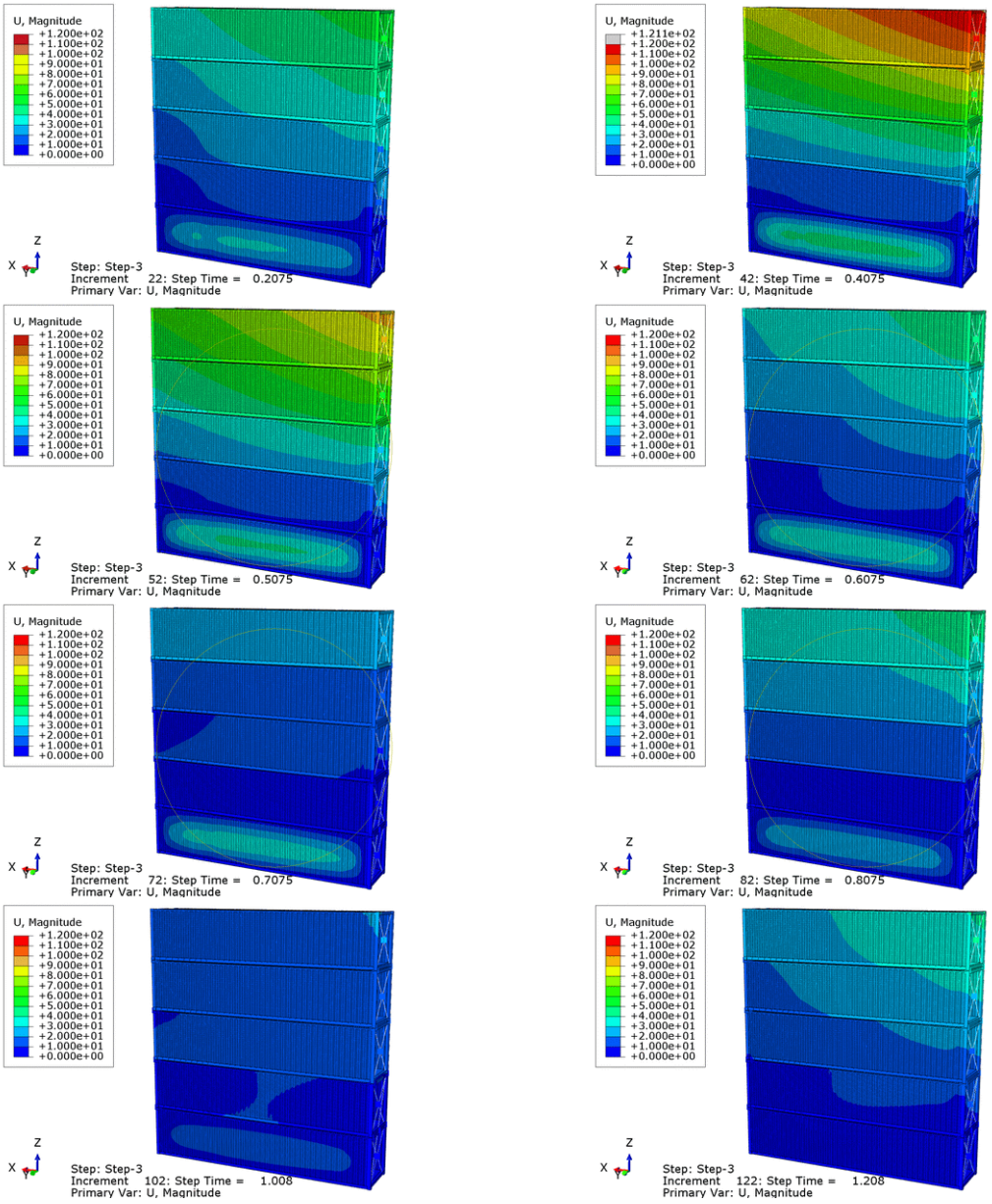

Figure 33 Configuration 5 - Simulation 5-2, Von Mises stress values in [MPa]

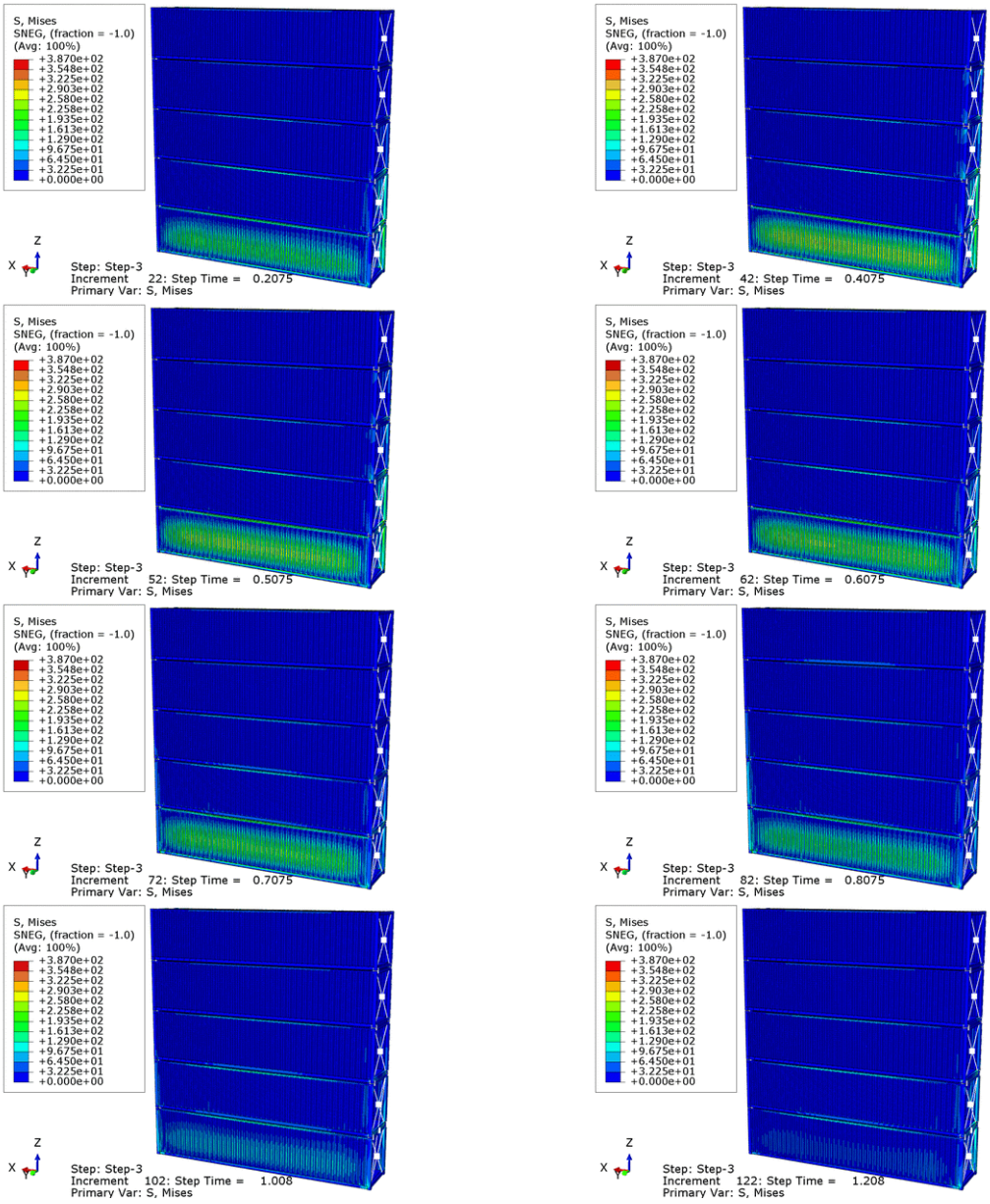

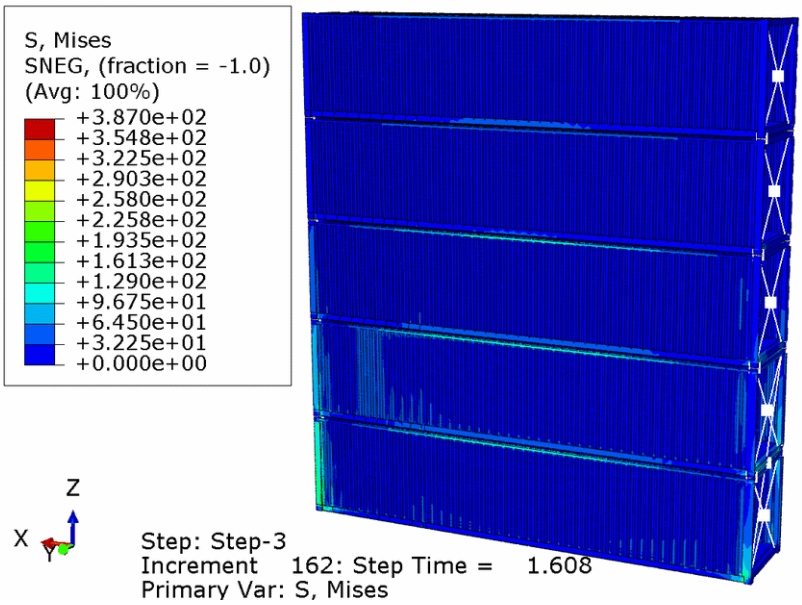

Figure 34 Configuration 5 - Simulation 5-2, Pressure values in [MPa]

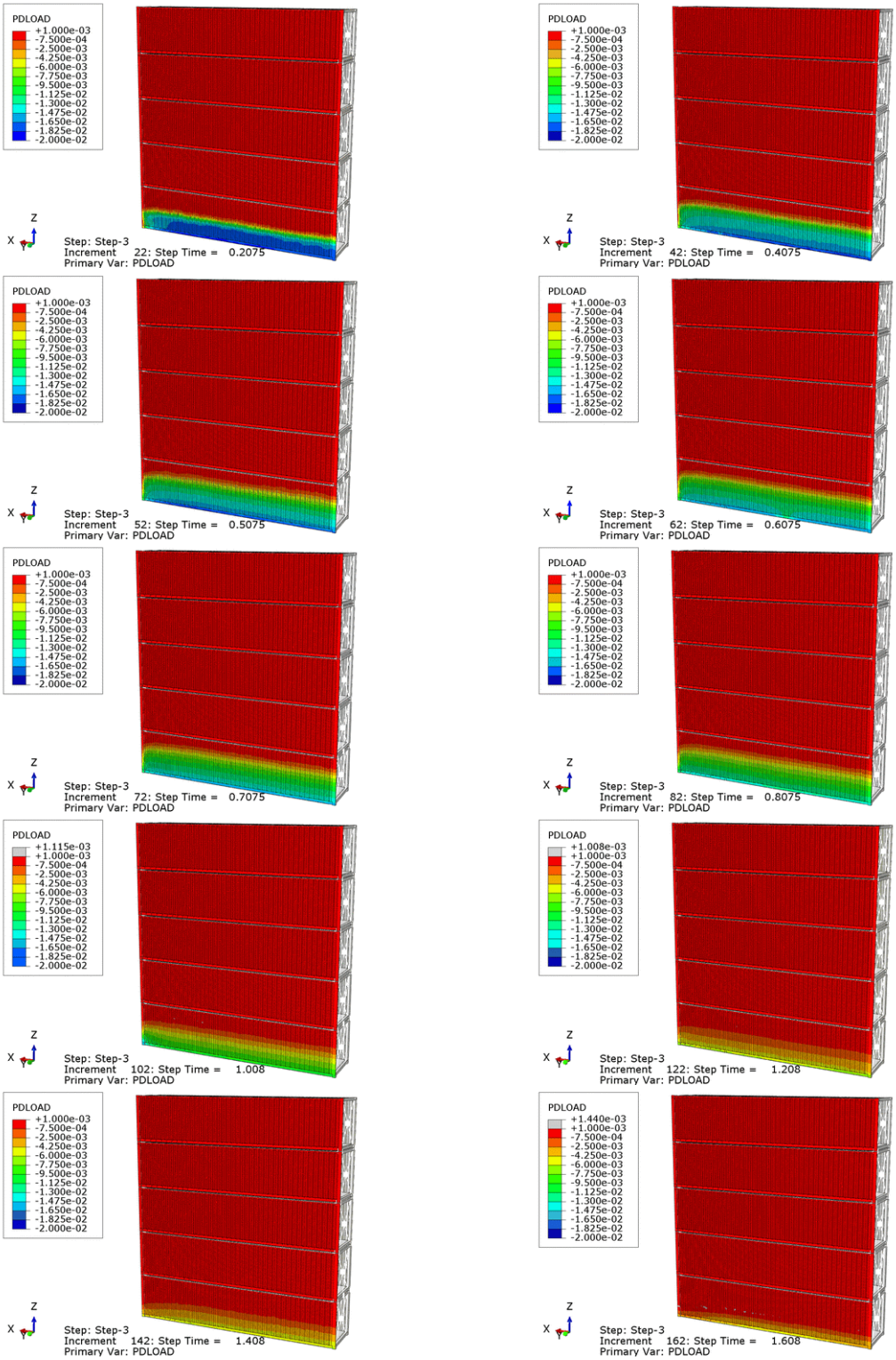

Figure 35 Configuration 5 - Simulation 5-3, Displacement values in [mm]

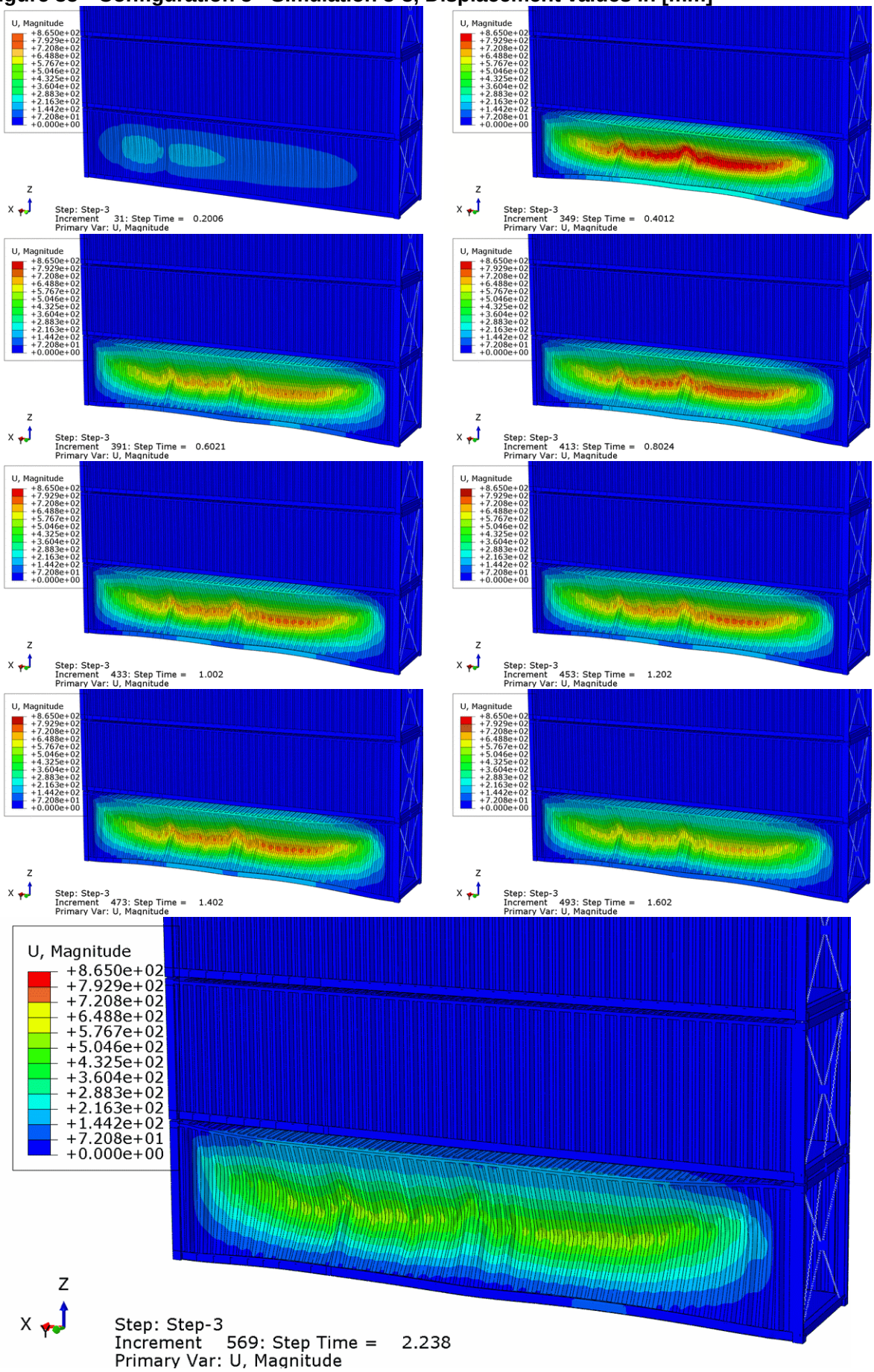

Figure 36 Configuration 5 - Simulation 5-3, Von Mises stress values in [MPa]

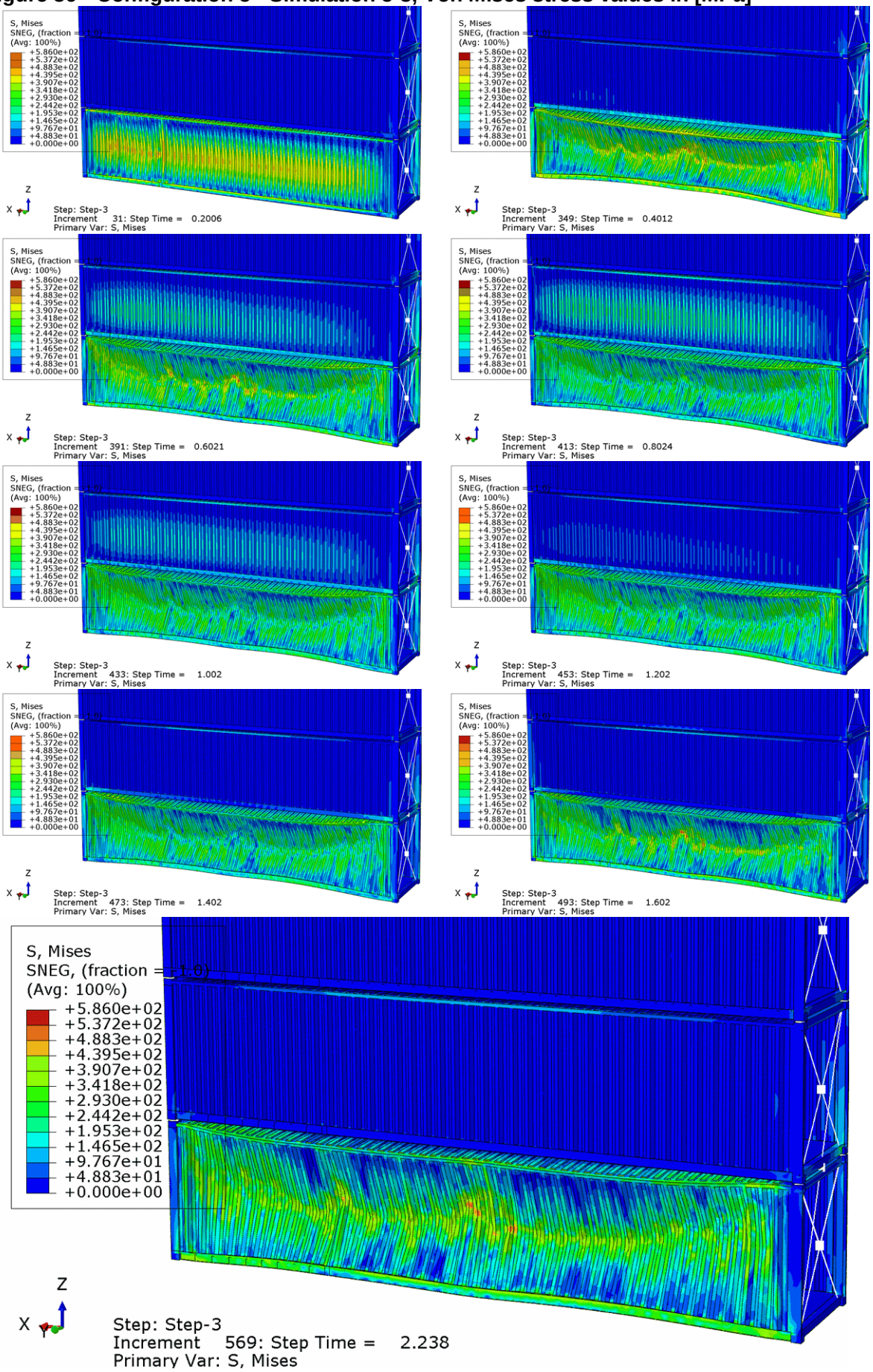

Figure 37 Configuration 5 - Simulation 5-3, Pressure values in [MPa]

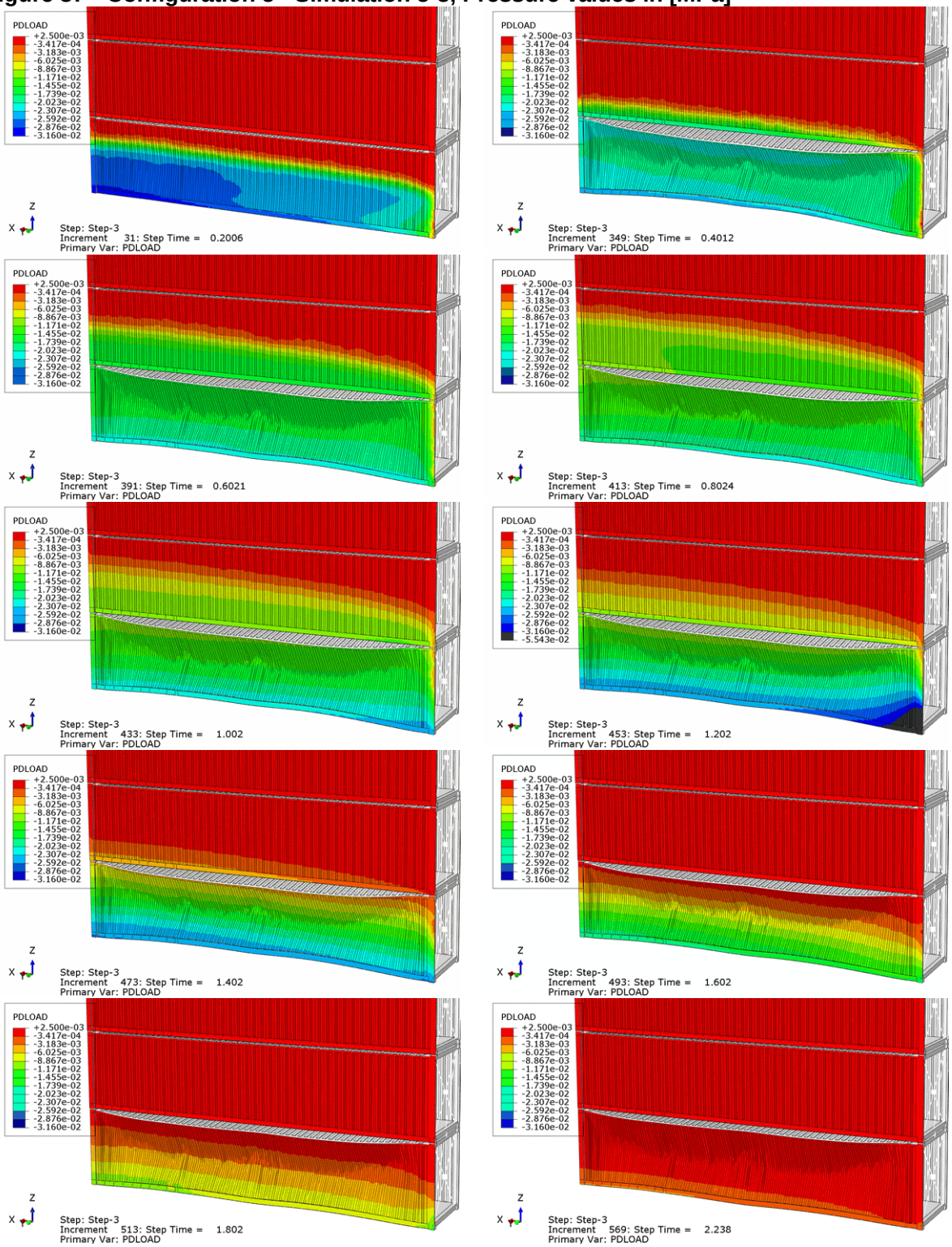

Figure 38 Configuration 5 - Simulation 5-4, Displacement values in [mm]

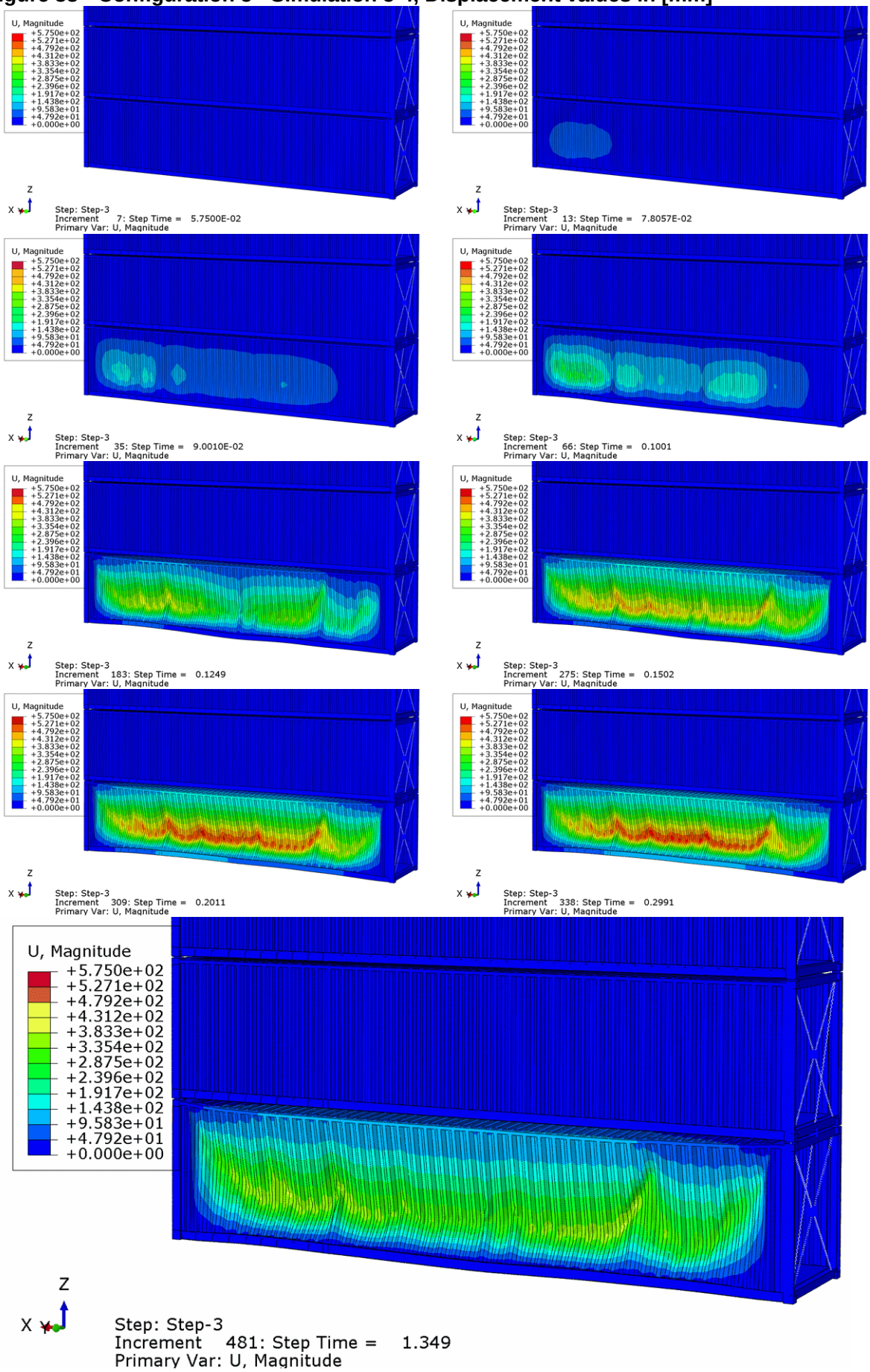

Figure 39 Configuration 5 - Simulation 5-4, Von Mises stress values in [MPa]

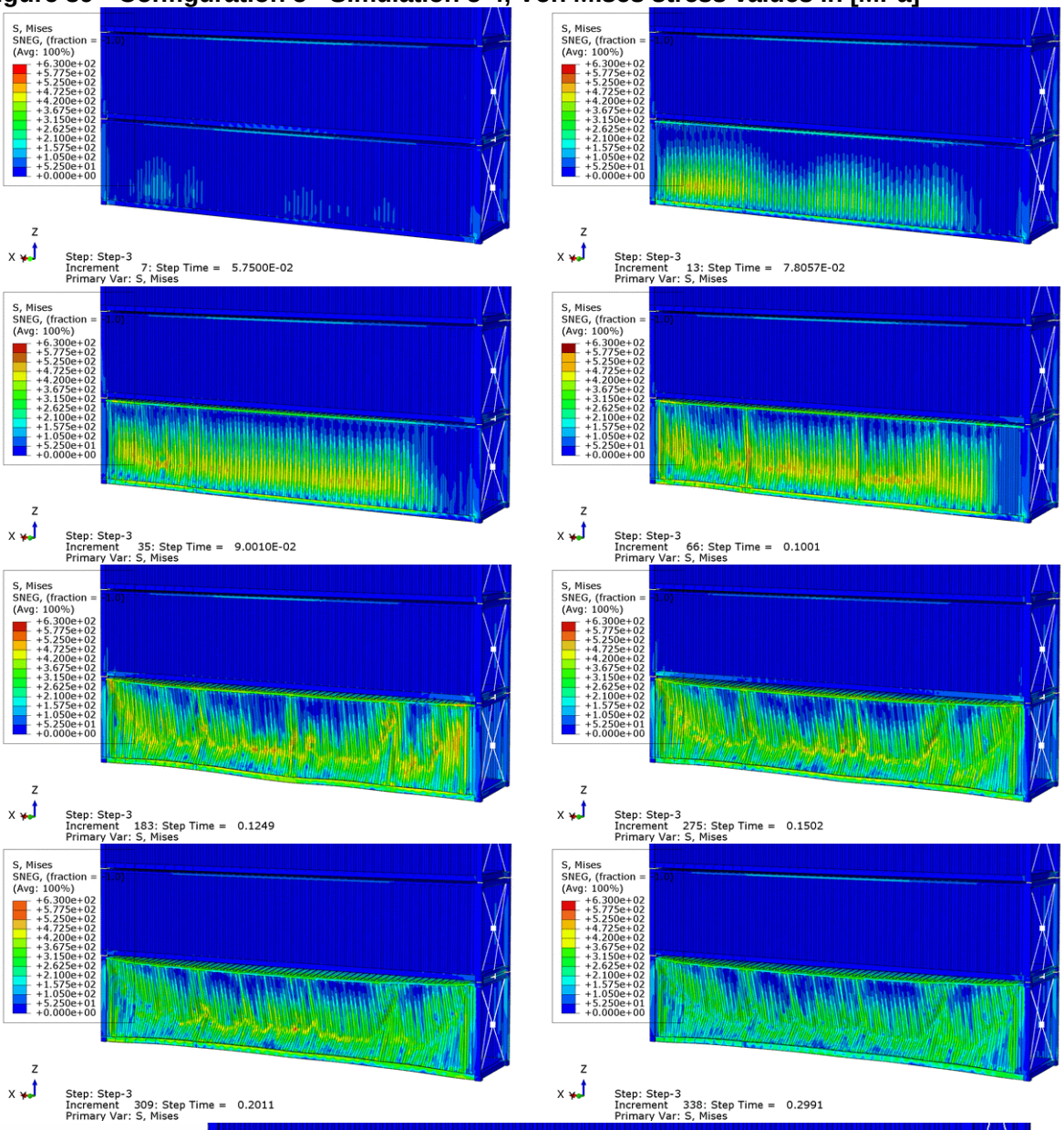

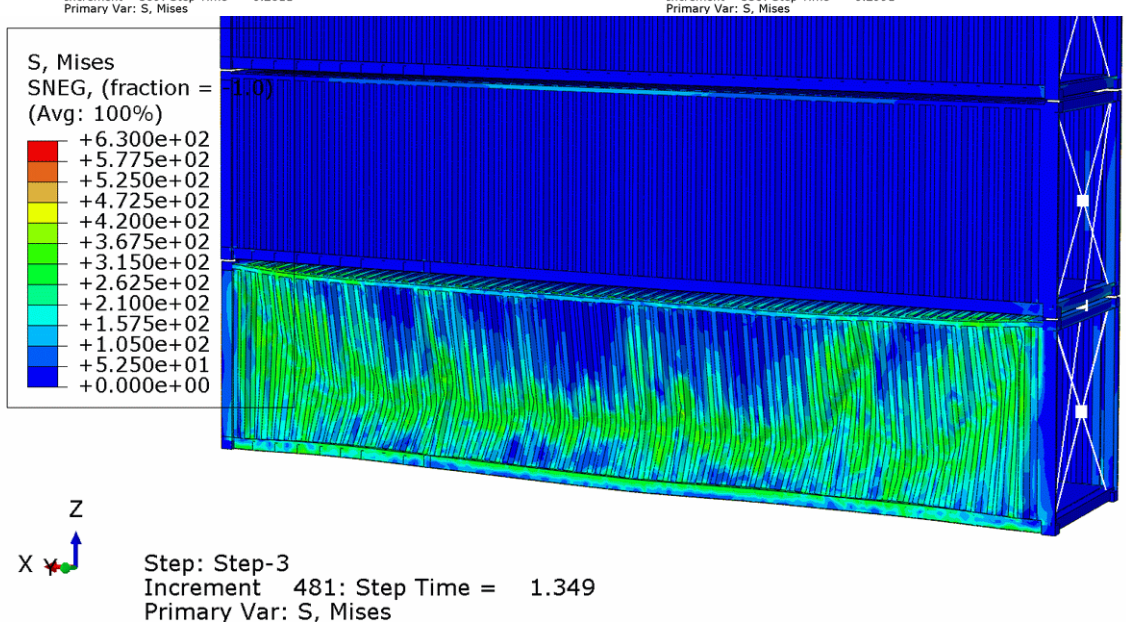

Figure 40 Configuration 5 - Simulation 5-4, Pressure values in [MPa]

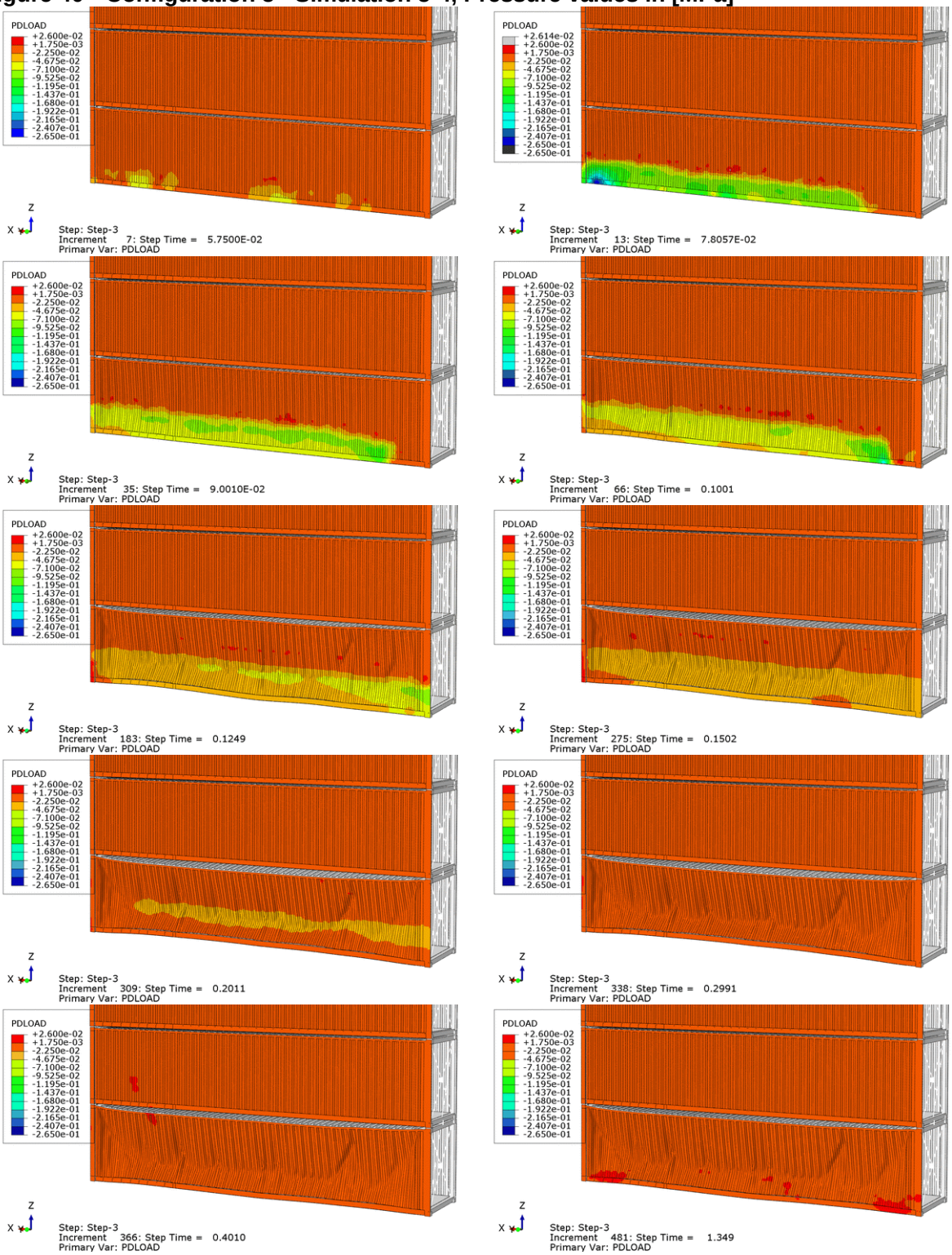

Figure 41 Configuration 5 - Simulation 5-5, Displacement values in [mm]

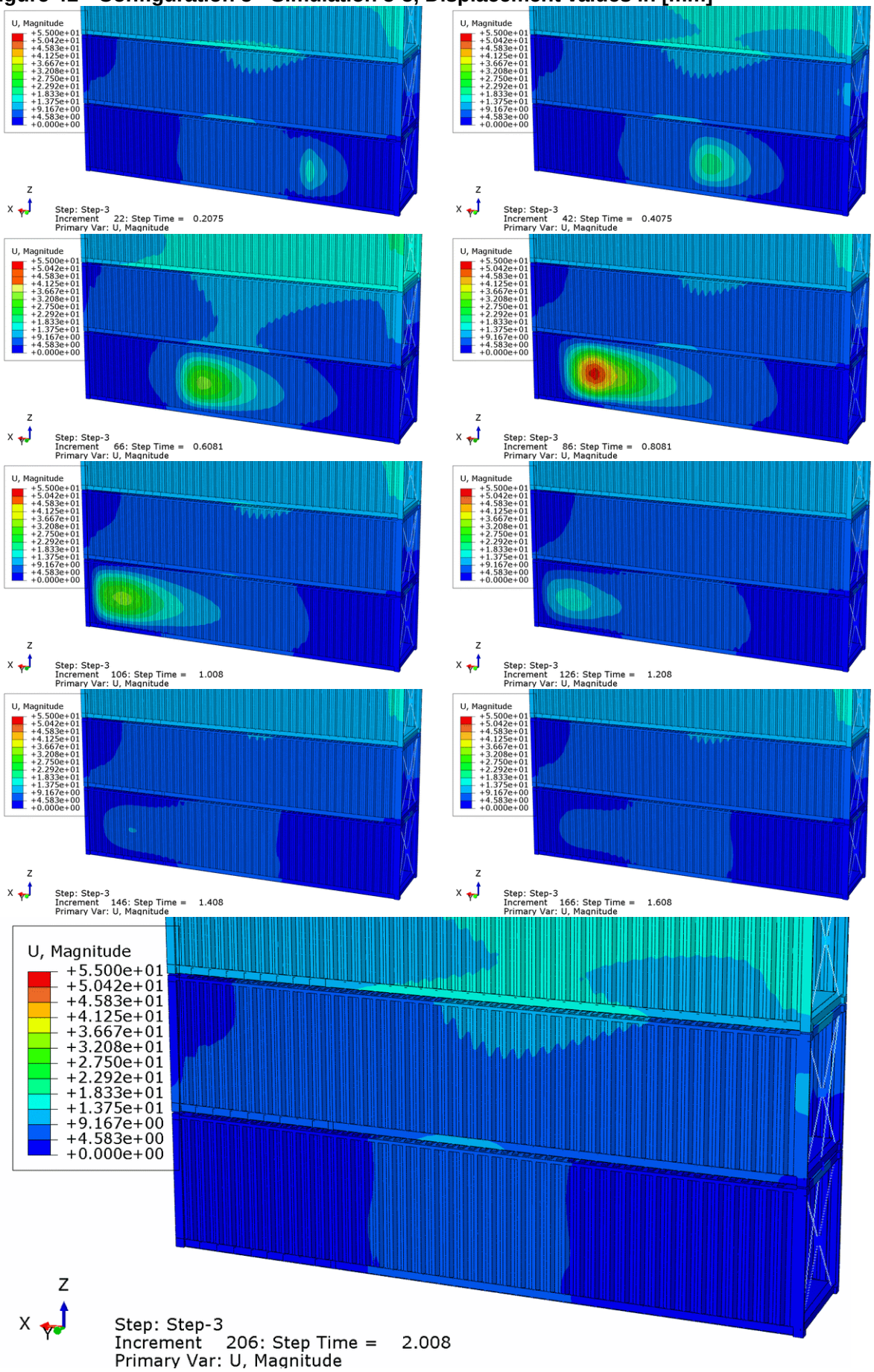

Figure 42 Configuration 5 - Simulation 5-5, Von Mises stress values in [MPa]

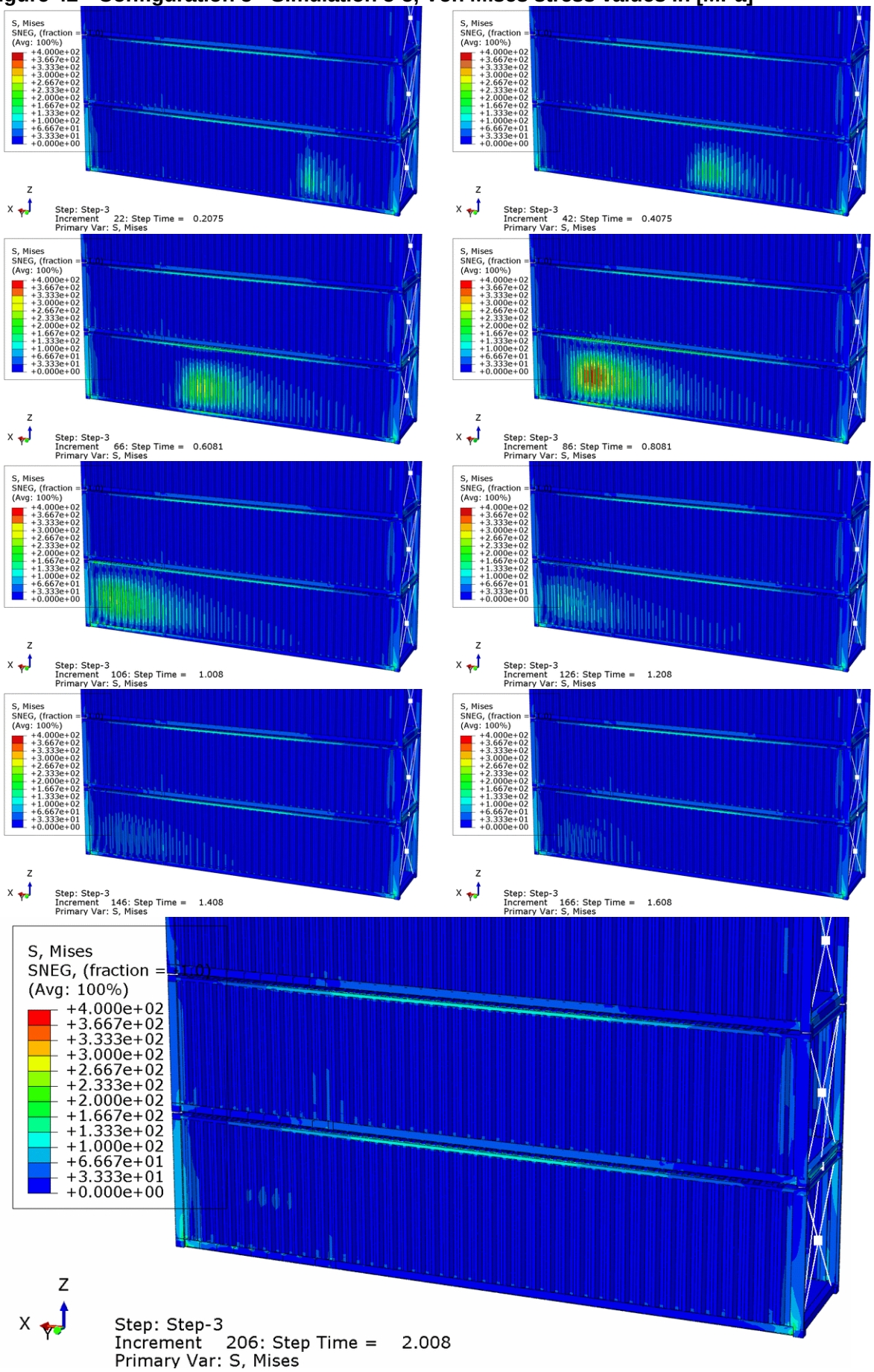

Figure 43 Configuration 5 - Simulation 5-5, Pressure values in [MPa]

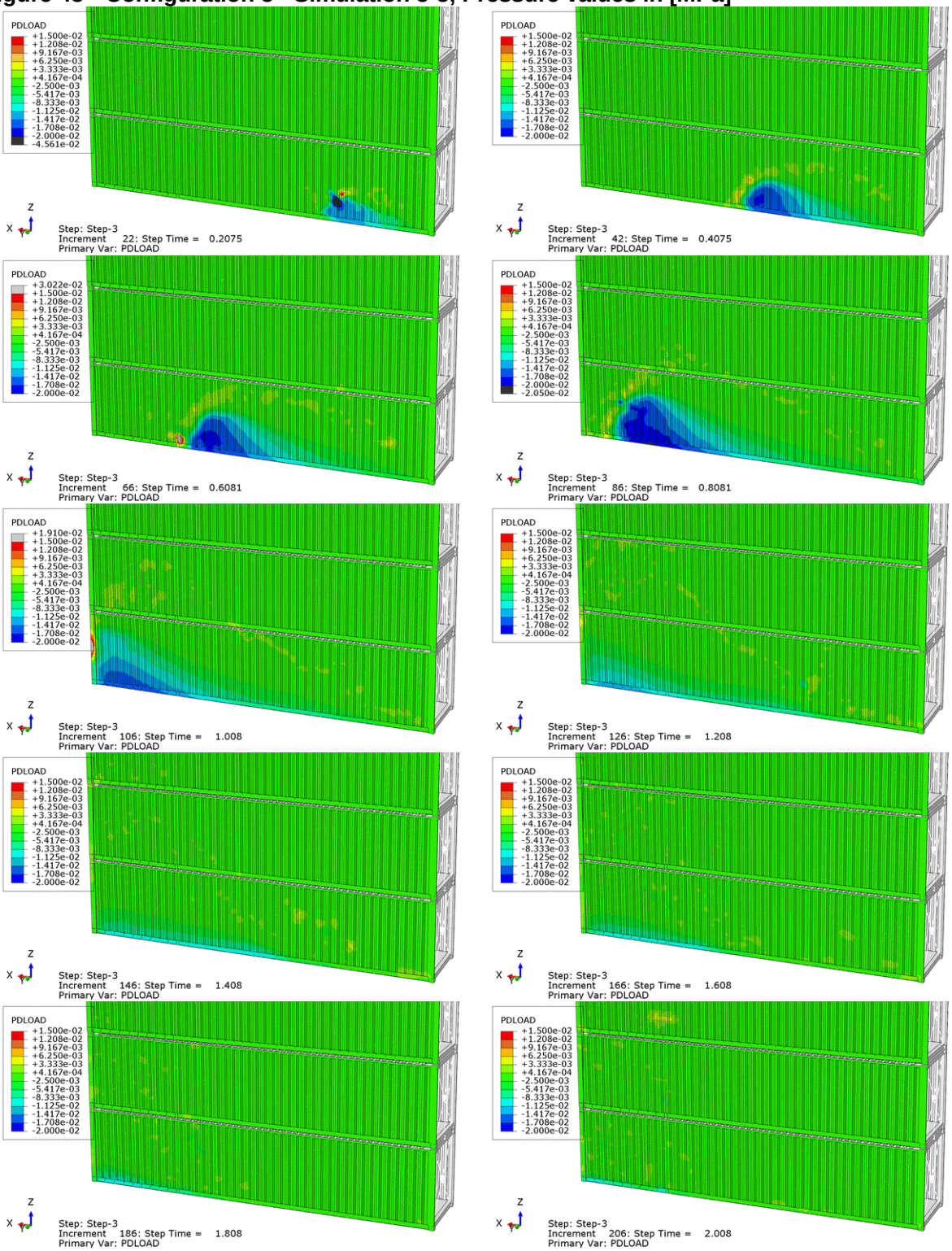

Figure 44 Configuration 5 - Simulation 5-6, Displacement values in [mm]

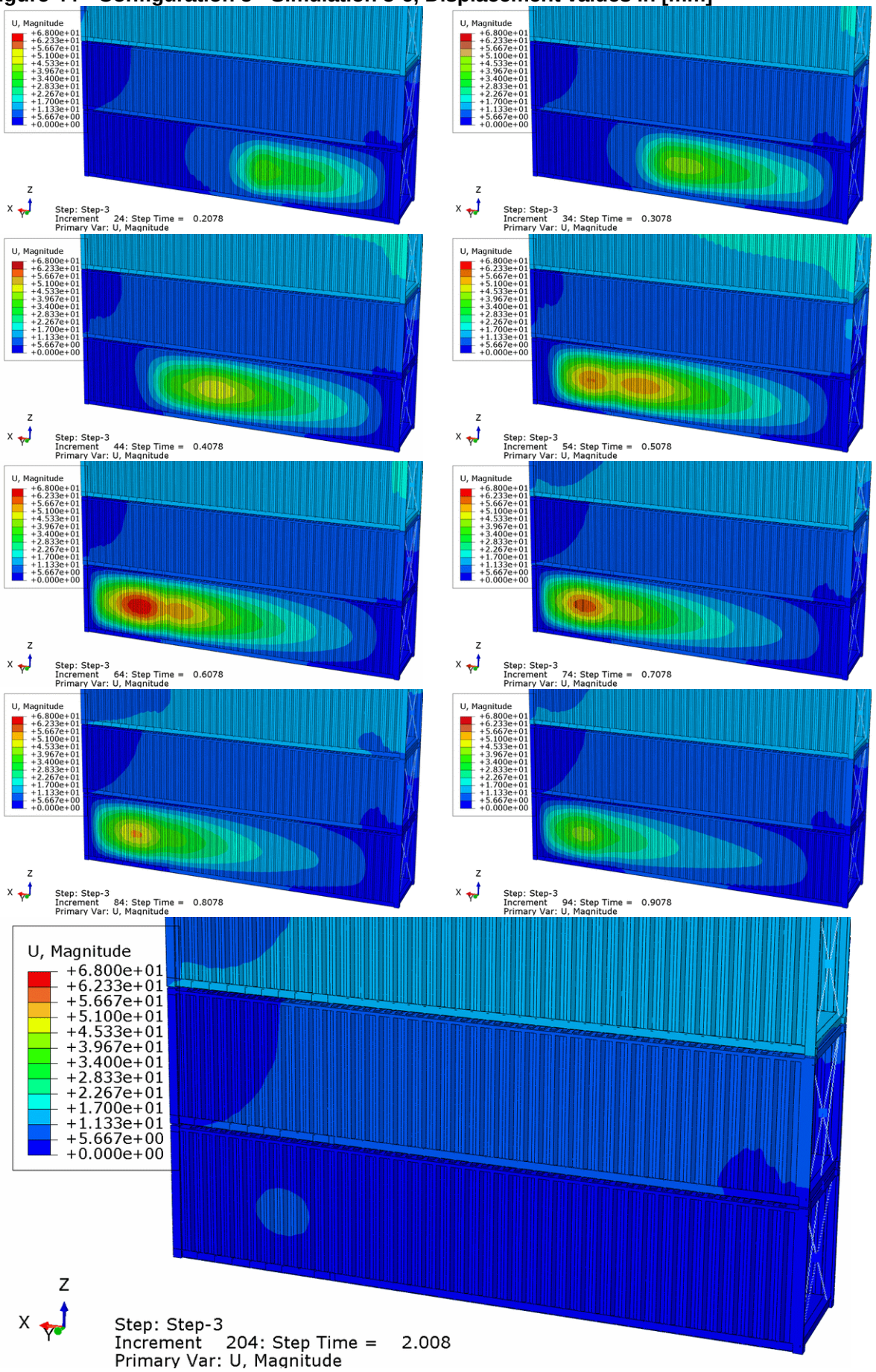

Figure 45 Configuration 5 - Simulation 5-6, Von Mises stress values in [MPa]

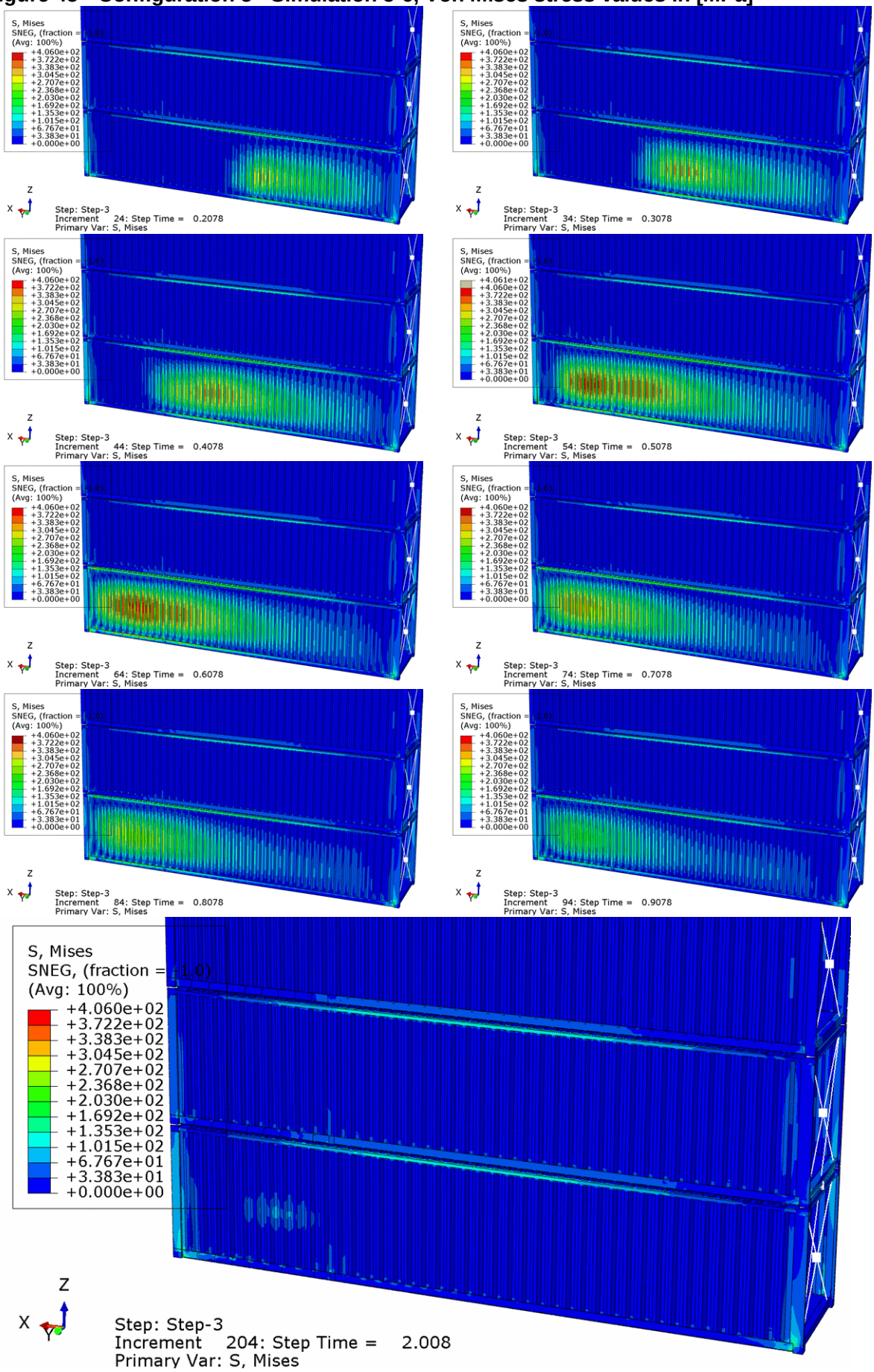

Figure 46 Configuration 5 - Simulation 5-6, Pressure values in [MPa]

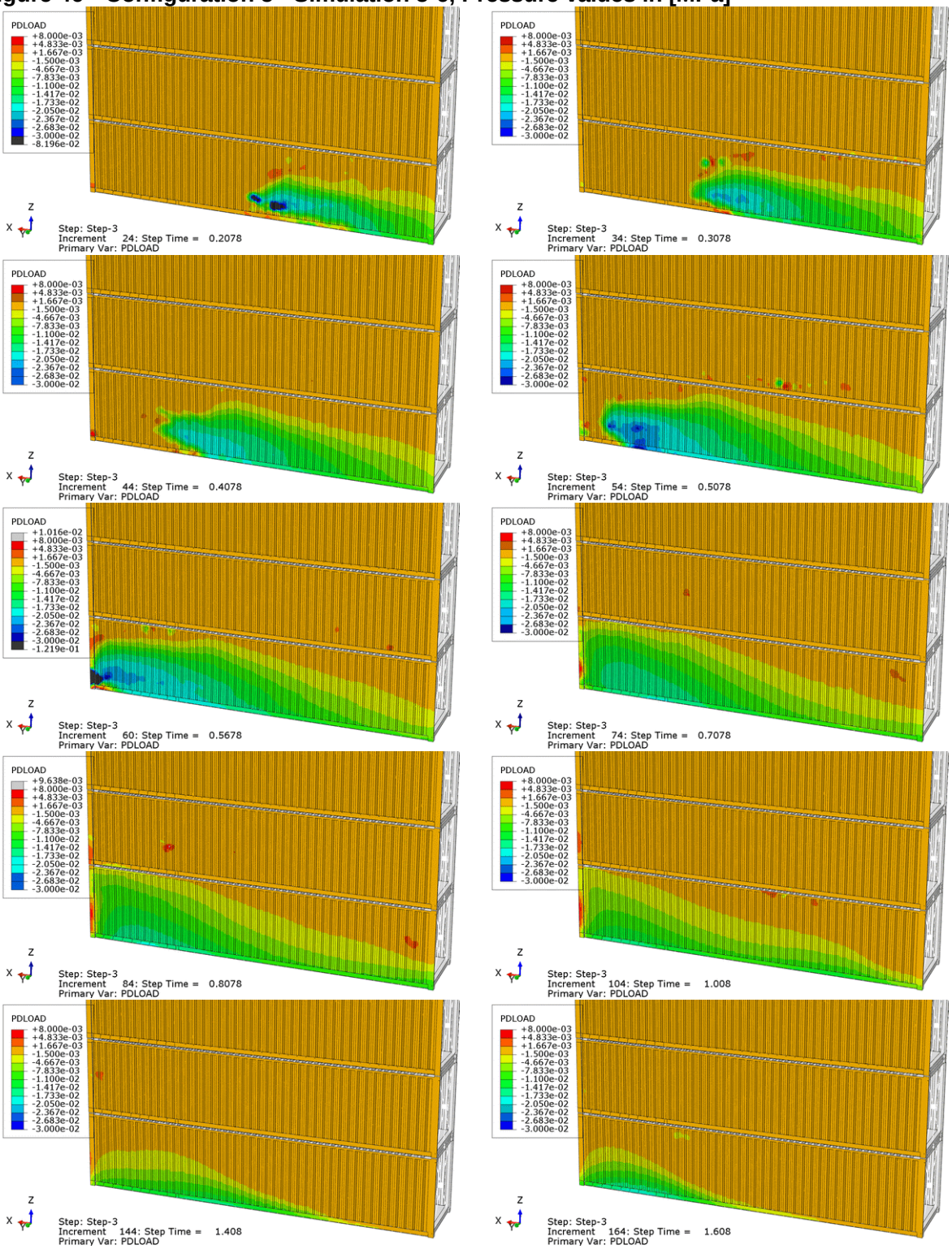

PHOTO PAGES

Photo 1 Side view of the model

Photo 2 Side view of the model

Photo 3 Bow view of the model

Photo 4 Aft view of the model

Photo 5 Details of the rudders and propellers

Photo 6 Details of the rudders and propellers

Photo 7 Details of the bilge keels – LC 1

Photo 8 Details of the bilge keels – LC 2

Photo 9 Details of the force panels

Photo 10 Details of the force panels

Photo 11 Details of the force panels

Photo 12 Details of the force panels

Photo 13 Test 33327_01OB_04_004_009_01: Mu = 270 deg – Hs = 4.5 m – Tp = 8.5 s

Photo 14 Test 33327_01OB_04_004_009_01: Mu = 270 deg – Hs = 4.5 m – Tp = 8.5 s

Photo 15 Test 33327_02BT_04_001: Mu = 180 deg – Hs = 6.0 m – Tp = 11.8 s – Vs = 4 kn

Photo 16 Test 33327_02BT_04_001: Mu = 180 deg – Hs = 6.0 m – Tp = 11.8 s – Vs = 4 kn

APPENDICES

APPENDIX I

MEAN TOP 5 WAVE PRESSURE LOADS AS A FUNCTION OF SIGNIFICANT WAVE HEIGHT

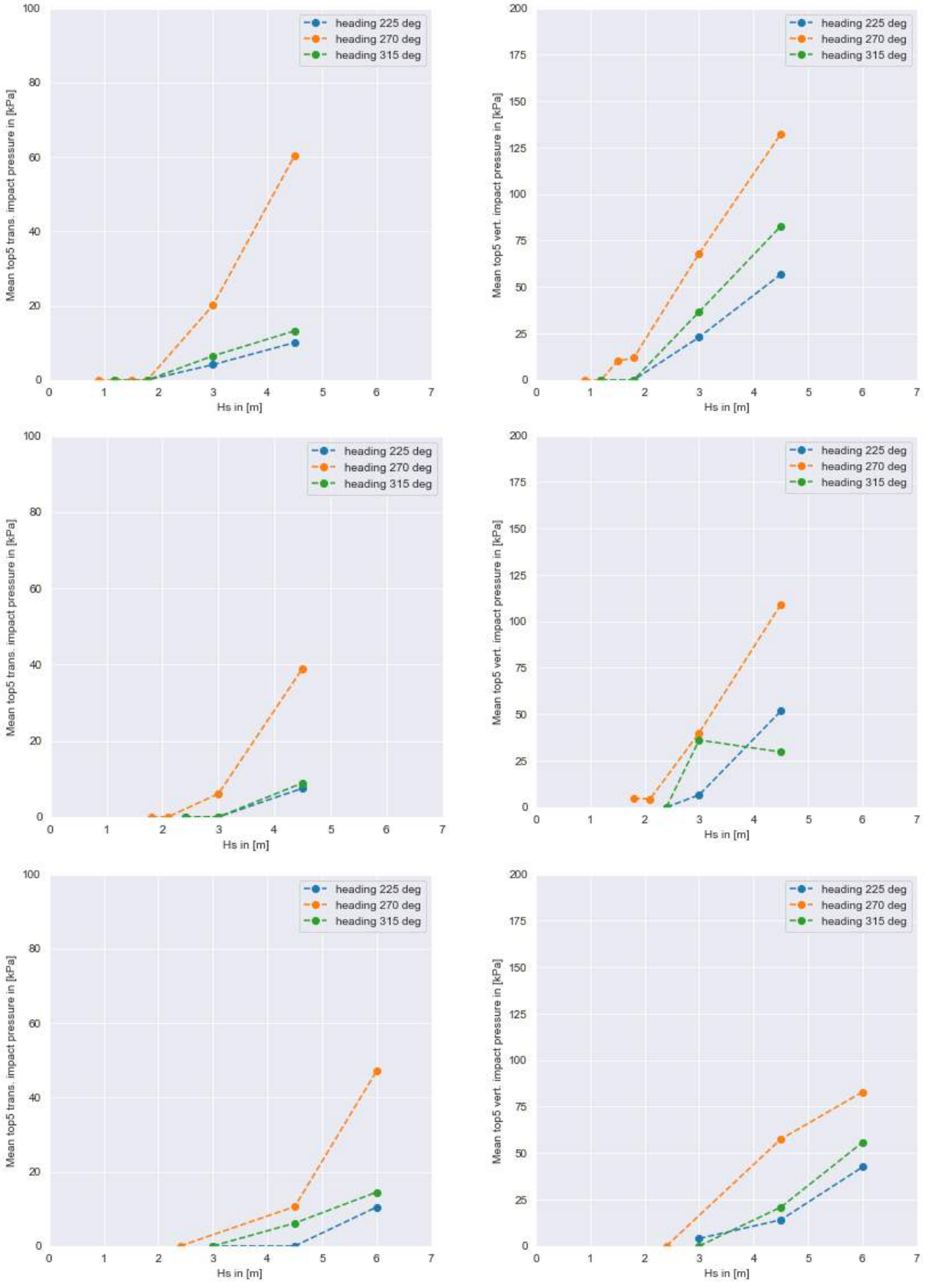

Mean top 5 wave pressure loads;
From top to bottom: configurations 1, 2 and 3

WIND-WAVE CLIMATOLOGY AND AREA OF OPERATIONS

Wind statistics

The oldest and simplest way to characterise an offshore environment is to characterise the wind climate, for instance in terms of the frequency of occurrence of various Beaufort numbers. These wind classes are related to area dependent “average” wave conditions. The tables below summarises some commonly used relations.

Example of wave conditions as a function of Beaufort number

BEAUFORT NUMBER	WIND VELOCITY	OBSERVED AVERAGE SIGNIFICANT WAVE HEIGHT							
		NORTH ATLANTIC OCEAN Roll [1953]a)			NORTH SEA Petri [1958]b)			FULLY ARISEN SEA (THEORETICAL)	
		Sign.Wave Height	Stage of Dev.	Zero up-crossing period	Sign.Wave Height	Stage of Dev.	Zero up-crossing period	Bhattacha-ryya, 1978	Komen
	V_W [m/s]	$H_{1/3}$ [m]	Π [-]	T2 [s]	$H_{1/3}$ [m]	Π [-]	T2 [s]	$H_{1/3}$ [m]	$H_{1/3}$ [m]
2	2.6				0.9	5.4	5.9	0.15	0.2
3	4.4	1.4	3.0	6.3	0.9	1.9	4.4	0.4	0.5
4	6.9	1.7	1.5	5.8	1.3	1.1	4.7	1	1.2
5	9.8	2.15	0.9	5.8	1.9	0.8	5.3	2.01	2.4
6	12.6	2.9	0.7	6.4	2.9	0.7	6.4	3.2	3.9
7	15.7	3.75	0.6	6.9	3.7	0.6	6.9	5.15	6.0
8	19	4.85	0.5	7.6	5.2	0.6	8.0	7.58	8.8
9	22.7	6.2	0.5	8.3				10.73	12.6
10	26.6	7.45	0.4	8.8				14.73	17.3
11	30.6	8.4	0.4	9.0				19.63	22.9
12	>33.0								

Sea state definition according to NATO Stanag 4194 Annex D

Sea State Number	Percentage Probability of Sea State	Significant Wave Height [m]		Sustained Wind Speed [kn]		Model (peak) Wave Period [s]	
		Range	Mean	Range	Mean	Range	Most probable
1	0	0 - 0.1	0.05	0 - 6	0.5	-	-
2	7.2	0.1 - 0.5	0.30	7 - 10	3.5	3.3 - 12.8	7.5
3	22.4	0.5 - 1.25	0.88	11 - 16	8.5	5.0 - 14.8	7.5
4	28.7	1.25 - 2.5	1.88	17 - 21	19.0	6.1 - 15.2	8.8
5	15.5	2.5 - 4	3.25	22 - 27	24.5	8.3 - 15.5	9.7
6	18.7	4 - 6	5.00	28 - 47	37.5	9.8 - 16.2	12.4
7	6.1	6 - 9	7.50	48 - 55	51.5	11.8 - 18.5	15
8	1.2	9 - 14	11.50	56 - 63	59.5	14.2 - 18.6	16.4
8	<0.05	>14	>14	>63	>63	15.7 - 23.7	20

Although often used in ship operations this approach fails to recognise the fact that one wind speed can come with a wide range of wave heights and periods, strongly depending on the fetch and duration (or

more generally the history) of the wind. Since wind speed and direction are highly variable this means that in practice, the waves are never in equilibrium with the wind.

In the situation of a relatively high wind speed (a “young”, growing wave) most of the energy input will take place at the high frequency tail of the wave spectrum. The result is a short, steep wave.
If the wind speed drops relatively quickly the continuing non-linear transfer of wave energy from shorter to longer wave components as well as frequency segregation (long waves travel faster than short waves) yields swell type wave conditions.

The fact that one wave height can show very different period characteristics has serious consequences because, as will be shown in the following, the motion characteristics of ships strongly depend on the wave period. This implies that wave height statistics only provide a rather narrow basis for design.

Wave scatter diagrams

In the offshore industry, the availability of wave measurements has led to the introduction of so-called scatter diagrams, reflecting the joint statistics of significant wave height and average zero-upcrossing period. Work by BMT (Hogben[27] and BMT[28]) has provided a practical basis for the design of ships.

Wind speed

The added resistance and total mean environmental loads are the sum of a wind- and a wave- (or motion-) induced component. This means that the joint statistics of wind and waves are of interest. Empirical information used in earlier wave models (Janssen *et al.*[29]), which relates a peak period T_p to the wave height and wind speed v_w at 10 m height, was therefore used to describe average non-stationary wind-wave relations. Their work can be expressed as:

$$T_p = \frac{9.25 \cdot {H_{1/3}}^{0.688}}{{v_w}^{0.376}}$$

Systematic calculations based on this work (accounting for the varying spectral shape) suggest for the zero-upcrossing period the following relation with wind speed:

$$v_w = A \cdot {T_2}^{B} \cdot {H_{1/3}}^{C \cdot {T_2}^{D}}, \text{with: } A = 80.443;\ \mathrm{B} = -1.8421;\ \mathrm{C} = 1.6012 \text{ and } \mathrm{D} = -0.0474$$

v_w in this formulation is the wind speed at 10 m height in m/s, T_2 is the average zero-upcrossing period in seconds as defined in Appendix 3 and $H_{1/3}$ is the significant wave height in metres. The values of the coefficients A to D depend on atmospheric conditions (like stability), where the field data suggest the values given above. Results from these formulations show that high wind speeds occur in combination with short, steep waves.

Although no wind is modelled during the tests in the SMB, the above relation is used in the post-processing to predict the sustained speed including wind added resistance.

---

27 Hogben, N., Dacuhna, N.M.C. and Olliver, G.F.; “Global Wave Statistics”, BMT, London, 1986.
28 BMT; PC Global Wave Statistics - User Manual.
29 Janssen, P.A.E.M., Komen, G.J. and Voogt, W.J.P.; “An Operational Coupled Hybrid Wave Prediction Model”, Journal of Geophysical Research, Vol. 89, pp. 3635-3684, 1984.

Wave spectra

A wave spectrum is characterised by the significant wave height, peak enhancement factor and information on the wave period. The latter can refer to the peak of the spectrum (T_p), the average value from the spectrum (T_1) and the average time between two zero-upcrossings (T_2). Their mutual relations are indicated in the table below for two types of wave spectrum. Details of the statistical description of an irregular sea can be found in Appendix III.

Wave spectral parameters

	JONSWAP	Pierson-Moskowitz / Bretschneider
T_p / T_2	1.287	1.405
T_p / T_1	1.198	1.296
T_1 / T_2	1.072	1.086

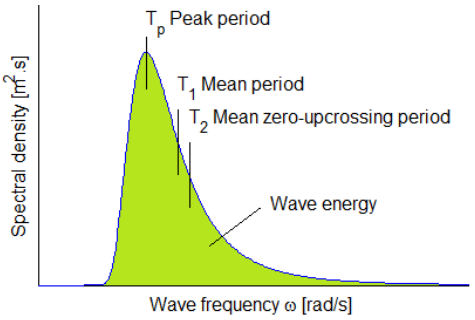

Spectral wave period definitions

APPENDIX II

DATA ANALYSIS

Statistical analysis

The statistical analysis performed on the various motions, relative motions, forces and accelerations, and on the wave elevation, is as given on below, based on the following general picture of a record.

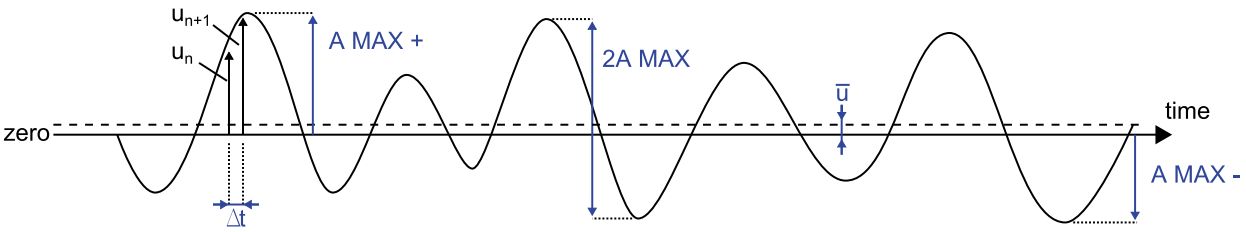

Example of signal record

For the wave elevation the mean equals zero.

1. *Mean value*: $\bar{u}$ (MEAN)

   $\bar{u} = \frac{1}{N}\sum_{n=1}^{N} u_n$ (N is number of samples)

2. *Standard deviation*: σ_u (ST.DEV.)

   $\sigma_u = \sqrt{\frac{1}{N}\sum_{n=1}^{N}(u_n - \bar{u})^2}$

3. *Maximum value*: A MAX +
   Highest crest value, positive unless stated otherwise

4. *Maximum value*: A MAX -
   Highest trough value, negative unless stated otherwise

5. *Maximum double amplitude*: 2A MAX
   This is the maximum crest to trough value.

6. *Significant peak value*: A 1/3 +
   This is the mean of the one-third highest zero to crest values, positive unless stated otherwise

7. *Significant trough value*: A 1/3 -
   This is the mean of the one-third highest zero to trough values, negative unless stated otherwise

8. *Significant double amplitude*: 2A 1/3
   This is the mean of the one-third highest crest to trough values.

9. *Number of oscillations*: NO
   This is the total number of oscillations in the record.

Response functions in irregular seas

Apart from the statistical analysis, another result of the tests in irregular seas is the spectral density of a signal. The response functions are calculated from the spectral densities in the following way:

$$H_u = \frac{u_a(\omega_e)}{\zeta_a(\omega_e)} = \sqrt{\frac{S_{uu}(\omega_e)}{S_{\zeta\zeta}(\omega_e)}}$$

in which:

H_u	=	response function of a signal u
$u_a(\omega_e)$	=	amplitude at frequency (ω_e) of signal u
$\zeta_a(\omega_e)$	=	amplitude at frequency (ω_e) of wave elevation ζ
$S_{uu}(\omega_e)$	=	spectral density of signal u
$S_{\zeta\zeta}(\omega_e)$	=	spectral density of wave elevation ζ

The frequency ω_e at which these spectral densities and response functions are calculated represents the true frequency of the ship motions. Transformation of ω_e to ω takes place according to:

$$\omega_e = \omega - kV\cos\mu$$

or for deep water:

$$\omega_e = \omega - \frac{\omega^2}{g} V\cos\mu$$

or:

$$\omega = \frac{1 - \sqrt{1 - 4\omega_e \frac{V\cos\mu}{g}}}{2\frac{V\cos\mu}{g}}$$

in which:

ω	=	wave frequency	in rad/s
ω_e	=	frequency of wave encounter	in rad/s
k	=	wave number = $2\pi/\lambda$	in m^{-1}
λ	=	wave length	in m
V	=	speed of ship (to be taken negative when sailing astern)	in m/s
μ	=	heading of the ship	(defined in Section 3.3.1)
g	=	acceleration due to gravity	in m/s^2.

After these manipulations, the results are plotted on base of ω, the wave frequency.

Response functions in regular waves

From the tests in regular waves the amplitude of the first harmonic component, the mean value and phase angles were derived. The phase relationship was determined with respect to the wave height at a location in a transverse plane through the CoG. From the amplitudes, RAOs are derived by dividing the motion amplitude by the wave amplitude:

$$\frac{u_a}{\zeta_a} = \frac{\text{motion amplitude}}{\text{wave amplitude}}$$

From the thrust increase as given in the tables, the thrust response function is derived by dividing this thrust increase by the squared wave amplitude:

$$\frac{\Delta T}{\zeta_a^2} = \frac{\text{thrust increase}}{\text{squared wave amplitude}}$$

Natural periods and motion decay tests

Motion decay tests are performed to determine the damping coefficients, damped period and natural period of a vessel or system. Decaying signals are characterised by a decaying oscillation around a mean value, with an approximately constant period. An example of a decaying signal is shown in the figure on the right. It is assumed that the decaying system can be accurately described by the following equation:

$$a\ddot{x} + b(\dot{x}) + cx = 0$$

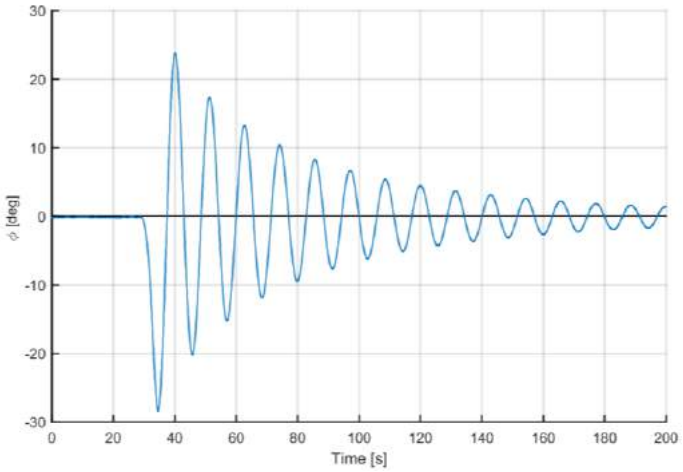

Example time series of decaying roll signal

Where:

x	=	a motion signal (e.g. roll, pitch or heave)
$\dot{x}$	=	the first derivative of the motion signal (e.g. roll velocity)
$\ddot{x}$	=	the second derivative (e.g. roll acceleration)
a	=	the mass or inertia of the vessel (including added mass or added inertia)
c	=	the restoring term of the vessel
b	=	the damping term

The damping is assumed to consist of various terms. The following terms are implemented for analysis at MARIN:

$$b(\dot{x}) = B_1\dot{x} + B_2\dot{x}|\dot{x}| + B_3\dot{x}^3$$

Where:

B_1	=	the linear damping coefficient
B_2	=	the quadratic damping coefficient
B_3	=	the cubic damping coefficient (disregarded within this project)

The system damping can be analysed by three methods. First, it can be solved by inserting the measured motion, velocity and acceleration and solving in a least squared sense. This is called the “least squares fit”. Secondly, a classic “PQ analysis” can be performed. PQ analysis sets out all individual crests and troughs as a function of amplitude and fits a polynomial. The polynomial coefficients are denoted by P and Q (and R in the cubic damping case). Lastly, the motion signal itself can be fit in an optimal sense by varying the relative damping and natural period of the system until an optimum is found. This is called “motion optimised”.

All three methods determine the same damping values, but with different approaches to what is optimal. The classic PQ analysis works very well for lightly damped systems, but has difficulties to provide accurate values for highly damped systems (e.g. ships sailing at speed). The least squares fit and motion optimised methods are closely related. The motion optimised method actually removes the need for fitting velocity and acceleration in the system of equations, which sometimes causes irregularities in the fitting.

In the present report, the damping values resulting from a motion optimised fitting are provided and the cubic damping coefficient is disregarded. From the P and Q polynomial coefficients, the equivalent damping is obtained as:

$$B_{eq} = \frac{P + Q \cdot \phi_{amp}}{2\pi} B_{crit} \qquad \text{With:} \qquad B_{crit} = \frac{2g\Delta GM}{2\pi / T_{\phi}}$$

Where ϕ_{amp} is the roll amplitude for which B_{eq} is linearised, g is the gravity constant, Δ is the ship mass and T_{ϕ} the ship natural period.

More details regarding the analysis of motion decay tests can be found in Appendix IV.

Thrust increase and sustained speed in wind and waves

The total thrust necessary for a vessel to advance in a certain wind and wave climate is assumed to be built from three components: the thrust in calm water, the added thrust due to waves and the added thrust due to wind.

$$T_{total} = T_{calm} + T_{waves} + T_{wind}$$

Calm water thrust

The calm water thrust is the mean thrust required for propulsion of the seakeeping model. At a certain speed this thrust was determined using the thrust derived from the calm water runs at that speed (from force measurements on the pods).

Added thrust in waves

The thrust increment due to wave action is evaluated from the test results by subtracting the thrust in calm water from the mean thrust in waves at the same ship speed (see figure below). The tests were performed without correction for scale effects. The mean thrust increment was scaled up with the third power of the scale. In order to determine the total required thrust in a seaway, this increment is added to the still water thrust curve as measured during the still water tests.

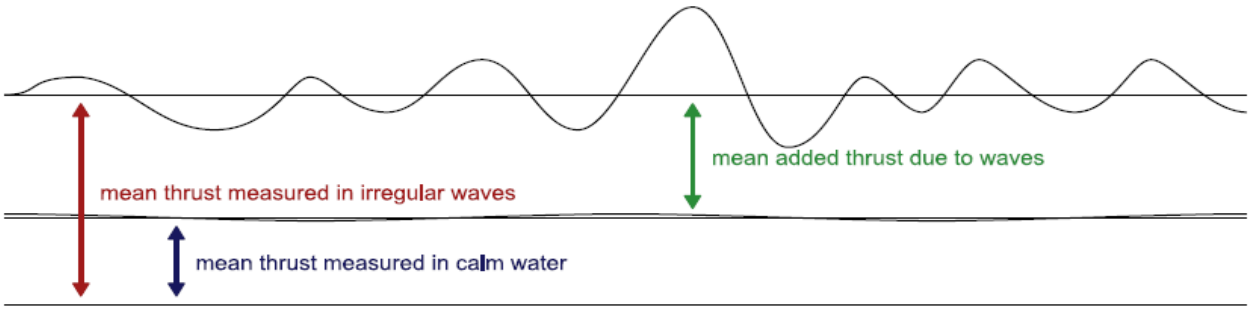

Example time series of mean wave added thrust

Added thrust in wind

The resistance added due to the wind is derived using frontal wind coefficients. The relation between frontal wind coefficients and resistance is:

$$F_{wind} = \frac{1}{2} \cdot c_x \cdot \rho_{air} \cdot A_x \cdot V_{w_{rel}}^2$$

where:

c_x	is the frontal wind coefficient
A_x	is the frontal wind exposed area
$V_{w_{rel}}$	is the relative wind velocity with respect to the vessel
ρ_{air}	is the air density

This relative wind speed (with respect to the vessel) is calculated using the relations between H_s/T_p and the wind speed at 10 m altitude given in Appendix I. Wind and waves are assumed to have the same direction and only the component of the wind force in x-direction is taken into account.

It should be noted that the air resistance due to ship forward speed was not included in the calculation as it is already included in the calm water resistance. The translation from wind resistance to wind added thrust is done

Sustained speed

To obtain the average speed that can be maintained under the prevailing wave and wind conditions ("sustained speed"), the required thrust curve derived in the foregoing from the wave, wind and calm water components is compared to the available thrust. The latter was estimated on the basis of the calm water tests performed previously at MARIN. The measured thrust figures were extrapolated towards the maximum available thrust in each condition, in order to find the sustained speed (see figure on the right). The extrapolation method used is based on empirical formulations derived from model tests performed with similar vessels.

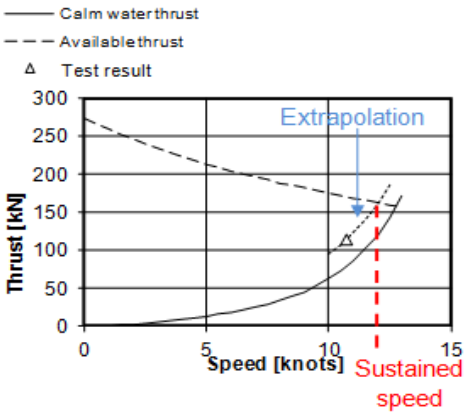

Sustained speed analysis

Drift forces

At zero speed, the longitudinal and transverse wave forces applied to the vessel are measured at the bow and at the transom, which, after post-processing, are translated into longitudinal and transverse wave forces and yaw moment at CoG. The mean of the wave force represents the wave drift force applied to the vessel.

The wave drift force applied to the vessel is commonly used as input or reference material for further Dynamic Positioning (DP) calculations.

Cumulative probability distribution functions

Some measurements were subjected to an additional statistical analysis yielding the cumulative distribution function of the peaks and troughs of the signal. These distributions can be used to predict the probability that the crest or trough of the measured signal exceeds a given magnitude. Multiplication of this probability by a factor $3600/T^*$, in which T^* is the average period between successive crests (or troughs) of the relative motion, gives the number of times per hour that a crest or trough exceeds the given magnitude.

The following figure present what typical distributions look like, for signals such as wave elevation or wave induced motions, velocities or accelerations.

Fitting a general theoretical distribution (like Rayleigh or Weibull distributions) allows extrapolation of the results to more extreme values than the ones that were measured during the test duration. The 3-hour most probable maximum (MPM) single amplitude is for instance a good measure for the short-term “maxima”. However, for the long-term “maxima” the varying weather conditions should be taken into account.

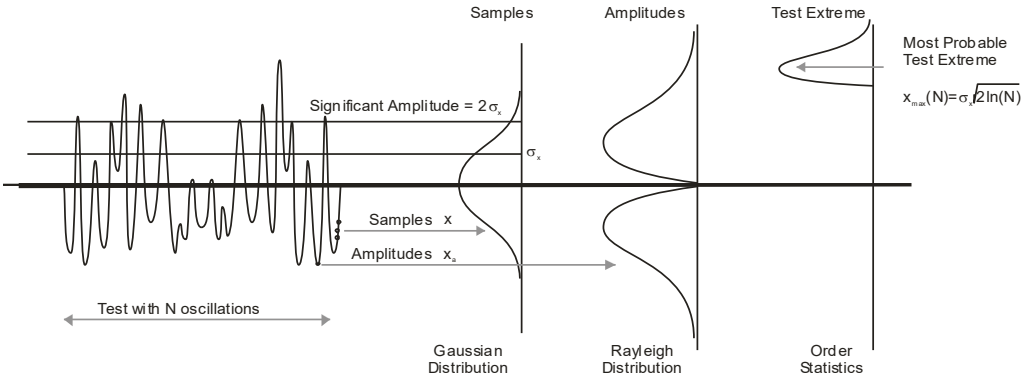

Typical distributions of signals like wave elevation or wave induced motions

Rayleigh distributed signals

In case of linear quantities, like relative motions, the estimate of the most probable extreme value can be based on Rayleigh distribution.

$$P\left(x > x^*\right)_{rayleigh} = e^{-\frac{1}{2}\left(\frac{x^*}{RMS}\right)^2}$$

When N (the number of expected events) is large, the MPM can be approximated by:

$$MPM_{rayleigh} = RMS\sqrt{2\ln(N)}$$

Weibull distributed signals

In case of non-linear quantities, like slamming, the estimate of the most probable extreme value cannot be based on the RMS of the signal as the peaks are not Rayleigh distributed. The cumulative 3-parameter Weibull probability density function is often used to fit the data.

$$P\left(x > x^*\right)_{weibull} = e^{-\left(\frac{x^*-\Theta}{\alpha}\right)^{\beta}}$$

The governing parameters are the scale parameter α, shape parameter β and offset θ. Note that no Weibull fit is made in the case of less than 13 peaks.

If the outcome of the analysis yields a shape factor β of around 2 and offset 0, the results correspond to a Rayleigh distribution. For processes which are governed by quadratic values of the underlying motions (like the relative velocity which determines an impact pressure) the value of β is often close to 1 (corresponding to a negative exponential distribution).

When N (the number of expected events) is large, the MPM can be approximated by:

$$MPM_{weibull} = \Theta + \alpha\sqrt[\beta]{-\ln\frac{1}{N}}$$

Comfort analysis

Effective gravity angle

The "effective gravity angle" (EGA) is the angle between the horizontal accelerations and the sum of the vertical acceleration and gravity (see figure and formula) and contains not only the static roll angle but also the dynamic components. The EGA is direct measure of the need to look for support for standing persons, but also for tipping or sliding of for instance glasses. Tipping will occur when the EGA is pointing outside the base of the subject. Sliding is dependent on the friction between the subject and the surface on which it is standing.

$$\mathrm{EGA}(t) = \arctan\left(\frac{\mathrm{AY}(t)}{\mathrm{AZ}(t)+g}\right)$$

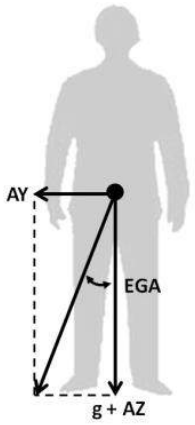

Definition of EGA

Motion illness rating

The EU Compass project[30] resulted in the Illness Rating (IR), which accounts for the combined effect of vertical and horizontal accelerations on seasickness. It is based on Motion Sickness Incidence (MSI) as defined by ISO 2631-1:1997(E) Annex D[31] but extended to also account for:

- The effect of longitudinal and transverse accelerations
- Susceptibility to ship motions

The Illness Rating is given by: $IR = a_v \cdot h \cdot S'$

Where a_v is the effective acceleration, h the habituation function and S' the susceptibility function. The IR is limited between 0 and 100.

Effective acceleration
The effective acceleration is given by:

$$a_v = \sqrt{k_h^2\left(a_{wx}^2 + a_{wy}^2\right) + a_{wz}^2}$$

Where a_{wx}, a_{wy} and a_{wz} are the RMS of the frequency-weighted longitudinal, transverse and vertical accelerations in [m/s^2]. k_h is the weighting factor for the horizontal and vertical accelerations and ranges between 0 (vertical accelerations only) and 1 (equal weighting for all acceleration components). The RMS of the frequency-weighted accelerations is calculated by:

$$a_{wx}^2 = \int_0^\infty S_x \cdot w_f^2 \, d\omega$$

Where S_x is the response spectrum of the vertical accelerations and w_f the frequency weighting for the vertical accelerations. The calculation of the frequency-weighted longitudinal and transverse accelerations is identical, except that the horizontal weighting factors (w_h) are different. The weighting factors are shown in below plots and are taken from the EU Compass project. Note that the frequency weighting for the vertical accelerations is identical to ISO 2631-1:1997(E) Annex D.

[30] EU Compass project G3RD-CT-2002-00809 Final Publishable Report "A rational approach for reduction of motion sickness & improvement of passenger comfort & safety in sea transportation"

[31] ISO 2631-1:1997(E) Mechanical vibration and shock –Evaluation of human exposure to whole body vibration Part 1: General requirements

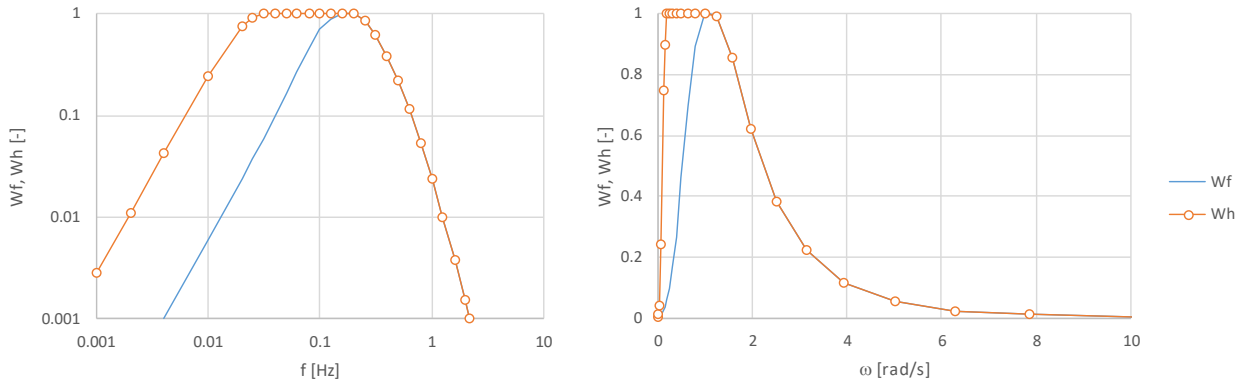

Frequency weighting for vertical (w_f) and horizontal (w_h) accelerations

Habituation function

For short exposure (say ≤ 3 h) the habituation function (*h*) can be approximated by $\sqrt{t}$ with *t* in [s]. For longer exposure, it the can be taken from the plot below. This habituation function is growing in the first hours and declining afterwards due to habituation. It has been developed after the EU Compass project and is not public yet.

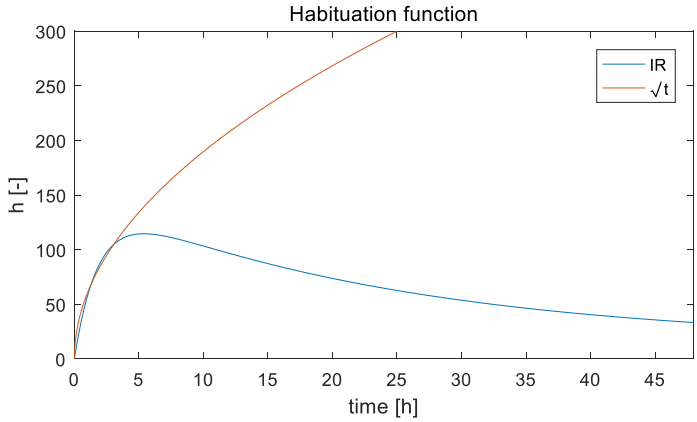

Susceptibility function

The susceptibility function (*S*) depends on age, gender and earlier experience with seasickness. This function has been described more detail in Bos et al, 2007[32]. Its shape is given by:

$$S = A\left(exp\left(-\frac{y-5}{40}\right) - exp\left(-\frac{y-5}{c}\right)\right)$$

Where *y* is the age in years and *A* and *c* given in the table below:

Gender	Sick before	A	c
Female	No	0.36	2
	Yes	0.72	2
Male	No	0.26	8
	Yes	0.72	8
Mixed	Mixed	0.5	5

The above susceptibility function is weighed with a factor 1/3 in order to match with ISO 2631-1:1997(E) Annex D in which a K_m value of 1/3 is suggested.

[32] Bos et al, *'Susceptibility to seasickness'*, Ergonomics Vol.50, No.6 page 890-901, June 2007

$$S' = \frac{S}{K_m}$$

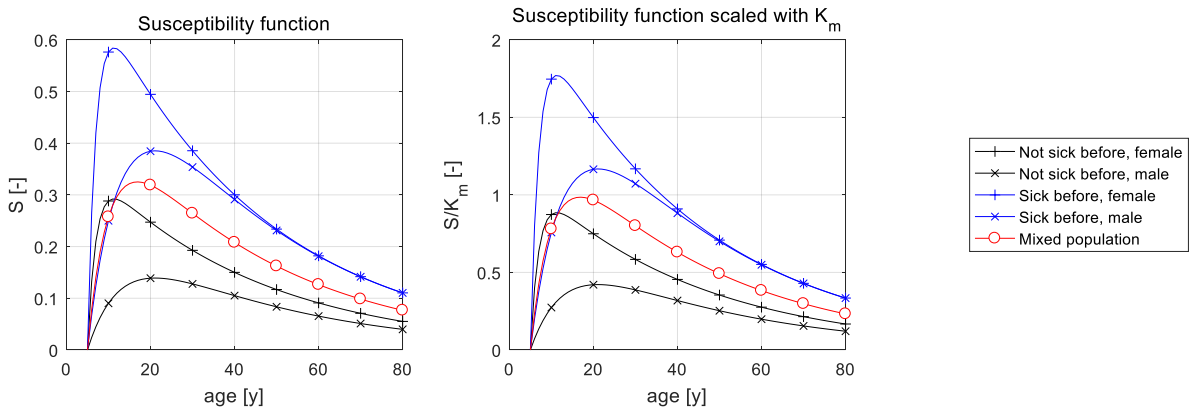

Motion Sickness Incidence (MSI)

The MSI (Motion Sickness Incidence) is a simple and concise statistically based measure for predicting the incidence of motion sickness by exposure to vertical accelerations. It expresses the percentage of people on board that will suffer from sea sickness after a certain exposure time. Several methods exist for the computation of MSI values. Here the method[33] that is specified by STANAG 4154[34] is outlined below.

MSI = $100\ \Phi(z_a)\ \Phi(z_t')$ in %

z_a = $2.128 \log(a/g) - 9.277 \log(f) - 5.809 (\log(f))^2 - 1.851$

z_t' = $1.134\ z_a + 1.989 \log(t) - 2.904$

$$\Phi(z) = \frac{1}{\sqrt{2\pi}} \int_{-\infty}^{z} e^{\frac{-\chi^2}{2}} d\chi$$

a	[m/s^2]	RMS value of generalised vertical acceleration estimator G_{av}
g	[m/s^2]	acceleration of gravity (g = 9.81)
f	[Hz]	peak frequency of the generalised vertical acceleration spectrum S_{GAv}
		$S_{GAv} = S_{av} + p^2 S_{aT} + q^2 S_g{*}\varphi$, where:
		S_{av} = spectrum of vertical acceleration
		S_{aT} = spectrum of transverse acceleration
		$S_g{*}\varphi$ = spectrum of roll (in radians) times g
		p,q = multiplication factors
t	[min]	duration of exposure

According to STANAG 4154, factors p and q should be set to 0, taking only the local vertical acceleration into account when computing MSI values.

---

33 J.L. Colwell, Human factors in the naval environment: a review of motion sickness and biodynamic problems, DREA Technical Memorandum 89/220, September 1989.

34 NATO STANAG 4154 Standardisation Agreement – Common Procedures for Seakeeping in the Ship Design Process.

APPENDIX III

MATHEMATICAL DESCRIPTION OF IRREGULAR PHENOMENA

General

A quantity x, varying irregularly in time or space, is called a stochastic variable. The stochastic variables that are most interesting in the field of seakeeping vary in time and can each be described by a distribution function of the probability that x fulfils a certain condition. Examples of such distribution functions are (see Figure A):

1. The probability distribution for the period of time that the value x lies between a and b.
2. The probability distribution of amplitudes of x lying between a and b.

Figure A

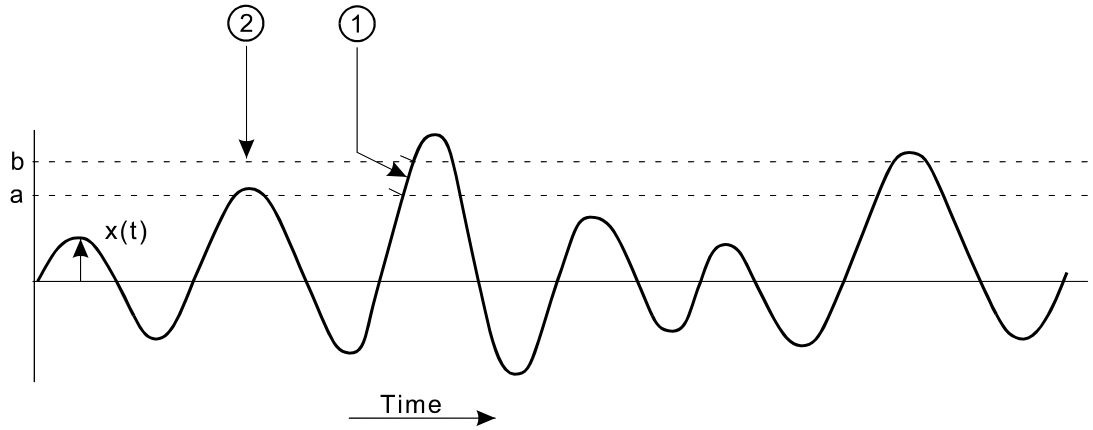

These various descriptions are discussed under the following subheadings. Before doing so, it is necessary to mention a few characteristics to classify random processes.

A process, described by a stochastic variable x, is completely defined if all statistical properties are known, or to be precise, when the expectation values E[x], E[x^2], E[x^3], ... are all known. In general this is not the case.

Processes can be classified by certain properties of their statistics. If for a process all statistical properties are invariant with respect to time shifts, the process is called ***stationary***. This means, for example, that:

$$E[x(t)] = E[x(t+\tau)] \qquad -\infty < \tau < \infty \tag{1}$$

E[x] is the ***mean value*** of x, also denoted by $\bar{x}$.

The statistical properties of a random process can be measured in several ways, depending on the character of the process. For instance, assume a sea with a large number of wave height measuring buoys of the same type, measuring simultaneously. The mean value of the wave elevations is established as the average of the registration of all buoys at time t = t_m. Now, the actual waves at sea are a weakly stationary process;

In the case of long periods of time the expectation values are not time invariant, but for practical purposes the wave elevation (and as a result: ship motions) can be considered as stationary processes.

A stationary process is called ergodic when it is allowed to replace the averaging over space by an averaging over time and to use the registration of one single buoy for the characterisation of the sea state, as described above, or to use one ship model to measure its motions.

Probability distribution of x(t)

The wave elevations are a continuous function of time (see Figure A) and the probability that $a \le x \le b$ is given by the probability density function $p_x(y)$ in such a way that:

$$P[a \le x \le b] = \int_a^b p_x(y)\, dy$$

where:

$$\int_{-\infty}^{\infty} p_x(y)\, dy = 1 \qquad (2)$$

If the process has a normal (Gaussian) distribution the probability density function is:

$$p(x) = \frac{1}{\sigma_x \sqrt{2\pi}} . \exp\left[- \frac{(x - \bar{x})^2}{2\sigma_x^2} \right] \qquad (3)$$

in which:

$\bar{x}$ = E[x], the mean value, and
σ_x = the standard deviation of the process.

The standard deviation is defined as the root of the variance and:

$$\sigma_x^2 = \text{VAR.} = E[x - E[x]]^2 = E[x^2] - (E[x])^2 \qquad (4)$$

Now it is possible to calculate for a normal distributed stochastic variable x the probability that, for instance, $(\bar{x} + \frac{n}{2}\sigma_x) \le x \le (\bar{x} + \frac{n+1}{2}\sigma_x)$ for several values of n. The result is shown in the histogram in Figure B on the next page. Note that the mean value does not necessarily coincide with the point of reference in the measuring system, so in the above definition of a Gaussian distribution x is given relative to $\bar{x}$.

Figure B: Normalised Gaussian distribution

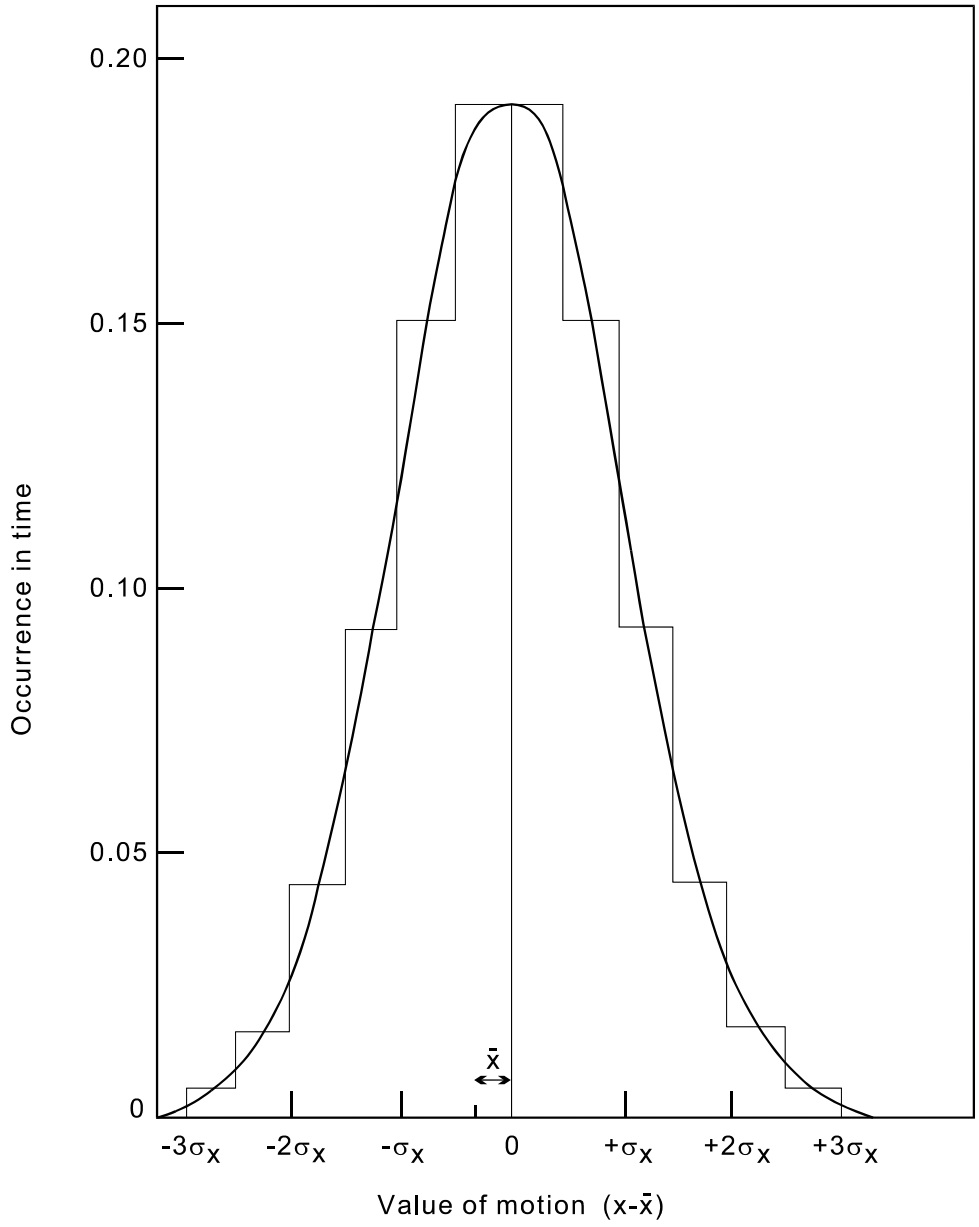

NOTE: width of the columns in the histogram = $\frac{1}{2}\sigma_x$
σ_x = standard deviation of the variable x

The probability that the value for $(x - \bar{x})$ exceeds a certain level xm can be expressed as:

$$P[x_m \leq (x - \bar{x}) < \infty] = \int_{x_m + \bar{x}}^{\infty} p_x(y)\, dy \tag{5}$$

Using (3), (4) and (5) the following table gives results for several values of xm.

x_m	Probability percentage $P[x_m \leq x < \infty]$	Probability percentage $P[-\infty < x \leq x_m]$
$\bar{x} - 3\sigma_x$	99.87	0.13
$\bar{x} - 2\sigma_x$	97.72	2.28
$\bar{x} - 1\sigma_x$	84.10	15.90
$\bar{x} + 1\sigma_x$	15.90	84.10
$\bar{x} + 2\sigma_x$	2.28	97.72
$\bar{x} + 3\sigma_x$	0.13	99.87

Probability distribution of amplitudes of x(t)

Additionally, the stochastic variable x can be described by the distribution of the amplitudes (= peak values) of x. When x has a normal distribution, the amplitudes follow a Rayleigh distribution. As regards these amplitudes, which are the most interesting quantities in the measurement of ship motions, several stochastic quantities can be defined:

when:

xa ≡ the amplitude of $[x - \bar{x}]$, then:

$x_{a1/3}$ ≡ the mean of the highest one-third of the amplitudes of xa, or as it is often called: the significant single amplitude of x;

$2x_{a1/3}$ ≡ mean of the highest one-third of the maximum to minimum values of xa, often called: the significant double amplitude of x.

The most probable maximum value 2xa max. (double amplitude) of the variable x depends on the number of oscillations No, as calculated by Longuet-Higgins35).

$$2x_{a\,max} = 2\sigma_x \sqrt{2\theta} \tag{6}$$

with:

$$\theta = \ln N_o - \ln\left[1 - \frac{1}{2\theta}(1 - e^{-\theta})\right] \tag{7}$$

For large values of No it can be shown that:

$$2x_{a\,max.} = 2\sigma_x \sqrt{2 \ln N_o} \tag{8}$$

35) Longuet-Higgins, M.S.; “On the Statistical Distribution of the Heights of Sea Waves”, Journal of Marine Research 1952, Number 3.

In actual measurements, the registration of x over a period of time is used. This period of time has to be long enough to give a reliable estimate of the statistical properties of the variable x as well as for the above introduced stochastic variables $xa_{1/3}$ and $2ax_{1/3}$. It is generally accepted to be sufficient when this period corresponds to half an hour real time or includes at least 180 oscillations. Then, the mean value is given by:

$$E[x] = \bar{x} = \frac{1}{T}\int_{t_1}^{t_2} x(t)\,dt \qquad \text{with} \qquad T = t_2 - t_1$$

and the standard deviation is:

$$\sigma_x = \sqrt{\frac{1}{T}\int_{t_1}^{t_2} [x(t) - \bar{x}]^2\,dt}$$

The observed processes are stationary - or at least weakly stationary - and ergodic. So the above described simplifications for the establishment of $\bar{x}$ and σ_x are allowed. When the duration of the measurement is sufficiently long, the difference between the standard deviation of the sample and the standard deviation of the actual density function can be neglected. The probability functions actually found from sampling an experiment generally conform very well with the theoretical distributions for x-values in the vicinity of $\bar{x}$. Due to the limited sample size the agreement at x-values far from $\bar{x}$ is hard to prove.

Spectral density of x

When the stochastic quantity x, varying irregularly in time t ($0 \leq t < T$ with $T \rightarrow \infty$), is plotted as a function of time and its variations between t and $t + \Delta t$ are bounded for $\Delta t \rightarrow 0$, then x(t) can be represented by an infinite number of harmonic components with arbitrary phase angles:

$$x(t) = x_0 + \sum_{n=1}^{\infty} x_n \cos(\omega_n t + \varepsilon_n) \qquad \text{(Fourier series)} \tag{9}$$

in which:

x_n = the amplitude of harmonic component n
ε_n = phase angle of the n-th component
ω_n = $n\omega_1$ = angular frequency of the n-th harmonic component
ω_1 = $2\pi/T$ (T = measuring time)

and so: $x_0 = \bar{x}$ the mean value of x.

Now, suppose there is a stationary, ergodic process, described by the stochastic variable $x_T(t)$ of which the observation takes place over a time interval ($-T < t < T$, $T \rightarrow \infty$), as shown in Figure C.

Figure C

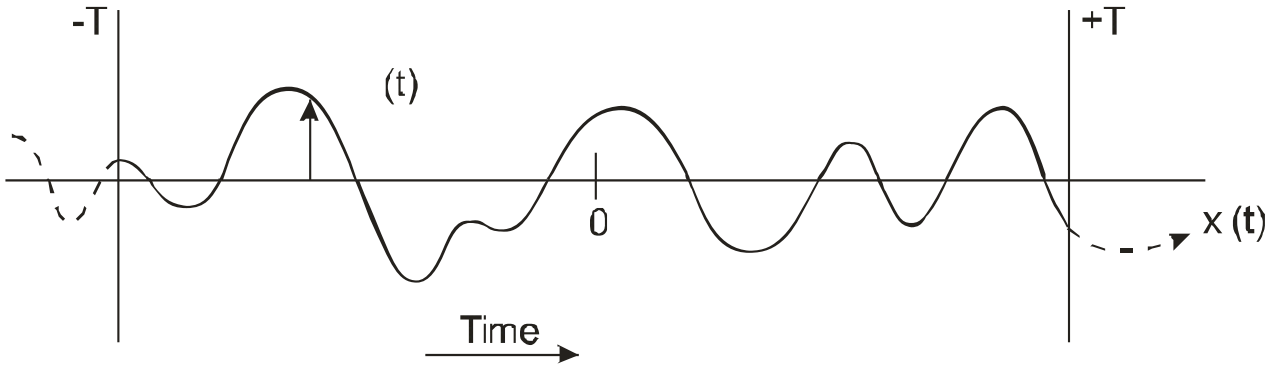

Then the Fourier series can be replaced by the Fourier transformation and the following relations result:

$$X_T(\omega) = \int_{-\infty}^{\infty} x_T(t)\, e^{-i\omega t}\, dt = \int_{-T}^{T} x(t)\, e^{-i\omega t}\, dt \tag{10}$$

$$x_T(t) = \frac{1}{2\pi} \int_{-\infty}^{\infty} X_T(\omega)\, e^{+i\omega t}\, d\omega \quad \text{(inverse Fourier transformation)}$$

The mean value and mean square value (= standard deviation when $\bar{x} = 0$) are defined as follows:

$$\bar{x} = \lim_{T\to\infty} \frac{1}{2T} \int_{-\infty}^{\infty} x_T(t)\, dt = \lim_{T\to\infty} \frac{1}{2T} \int_{-T}^{T} x(t)\, dt \tag{11}$$

$$\bar{M}_x = \lim_{T\to\infty} \frac{1}{2T} \int_{-\infty}^{\infty} \{x_T(t)\}^2\, dt = \lim_{T\to\infty} \frac{1}{2T} \int_{-T}^{T} \{x(t)\}^2\, dt \tag{12}$$

The spectral density function $S_{xx}(\omega)$ of the random process $x_T(t)$ can be proven to be[36]:

$$S_{xx}(\omega) = \lim_{T\to\infty} \frac{1}{2\pi T} |X_T(\omega)|^2 \tag{13}$$

---

[36] Therefore use is made of the auto-covariance function $R_{xx}(\tau)$, defined as:

$$R_{xx}(\tau) = E[\{x(t) - E[x(t)]\} . \{x(s) - E[x(s)]\}]$$

with $\tau = s - t$. In the representation of this section, with $\bar{x} = 0$, is:

$$R_{xx}(\tau) = \lim_{T\to\infty} \frac{1}{2T} \int_{-\infty}^{\infty} x_T(t)\, x_T(t+\tau)\, dt$$

Now, $S_{xx}(\omega)$ is defined as the Fourier transformation of the auto-covariance function:

$$S_{xx}(\omega) = \frac{1}{\pi} \int_{-\infty}^{\infty} R_{xx}(\tau)\, e^{-i\omega\tau}\, dt$$

Using Parceval's theorem on Fourier transformations[37], the mean square can be expressed in terms of frequency:

$$\bar{M}_x = \lim_{T\to\infty} \frac{1}{2T}\left\{\frac{1}{2\pi}\int_{-\infty}^{\infty} |X_T(\omega)|^2 \, d\omega\right\} = \frac{1}{2}\int_{-\infty}^{\infty} S_{xx}(\omega)\, d\omega \qquad (14)$$

The spectral density function can be related to the energy W which will be clarified in the following discussion. The Fourier transformation $X_T(\omega)$ is the continuous representation of the amplitudes x_n in the Fourier series of $x_T(t)$. Now, the potential energy E_n of the component with frequency ω_n is proportional to $(x_n)^2$ and analogously the potential energy in the frequency range of $\omega_i \le \omega \le \omega_j$ is:

$$W(\omega_i \le \omega \le \omega_j) \_ \int_{\omega_i}^{\omega_j} |X_T(\omega)|^2 \, d\omega$$

and the average potential energy over a period of time is, using (13):

$$W \sim \lim_{T\to\infty} \frac{1}{T}[W(\omega_i \le \omega \le \omega_j)] = \int_{\omega_i}^{\omega_j} S_{xx}(\omega)\, d\omega \qquad (15)$$

So, the average potential energy of $x_T(t)$, associated with the frequency band $\omega_i \le \omega \le \omega_j$, is given by the integral of $S_{xx}(\omega)$ over the frequency interval and hence $S_{xx}(\omega)$ may be called the ***energy spectral density function.***

The concept of response

Mechanical and physical systems may be interpreted as a transducer transmitting energy from the input x(t) towards the output or response y(t). Suppose the output is uniquely determined in terms of the input: y(t) = L[x(t)], then the system is completely defined if the nature of the operator L is known. The spectral density representation of a stochastic variable allows an output density function $S_{yy}(\omega)$ to the input density $S_{xx}(\omega)$ by means of a frequency response function, provided that the observed system is linear[38].

---

37) This theorem states that:

$$\int_{-\infty}^{\infty} \{x(t)\}^2 \, dt = \frac{1}{2\pi}\int_{-\infty}^{\infty} |X(\omega)|^2 \, d\omega$$

38) A system is linear if the response characteristics are additive and homogeneous:
$L[x_1(t) + x_2(t)] = L[x_1(t)] + L[x_2(t)] = y_1(t) + y_2(t)$
$L[ax(t)] = aL[x(t)] = ay(t)$ (a = constant).

Consider the situation where the unit impulse, described by the Dirac delta function[39] $\delta(t - t_0)$, is applied at time $t = t_0$ to a linear system and let $h(t - t_0)$ be the response of the system: $L[\delta(t - t_0)] = h(t - t_0)$. Because such an input-output system is causal, $h(t - t_0)$ does not exist for $t_0 > t$. Now, an arbitrary input $x(t)$ can be expressed as a sum of impulses, that is:

$$x(t) = \int_{-\infty}^{t} x(t_0)\,\delta(t - t_0)\,dt_0 \tag{16}$$

in which case, assuming that L is time-invariant:

$$y(t) = L[x(t)] = \int_{-\infty}^{t} x(t_0)\,L[\delta(t - t_0)]\,dt_0 = \int_{-\infty}^{t} x(t_0)\,h(t - t_0)\,dt_0 =$$

$$= \int_{0}^{\infty} x(t - \tau)\,h(\tau)\,d\tau$$

where: $t - t_0 = \tau$ was substituted.

For the truncated variables $x_T(t)$ and $y_T(t)$ as used before, with their Fourier transformations $X_T(\omega)$ and $Y_T(\omega)$, it is thus found that:

$$y_T(t) = \int_{0}^{\infty} x_T(t - \tau)\,h(\tau)\,d\tau \tag{17}$$

and:

$$\begin{aligned} Y_T(\omega) &= \int_{-\infty}^{\infty} e^{-i\omega t}\left[\int_{0}^{\infty} x_T(t - \tau)\,h(\tau)\,d\tau\right]dt \\ &= \int_{0}^{\infty} h(\tau)\left[\int_{-\infty}^{\infty} e^{-i\omega t}\,x_T(t - \tau)\,dt\right]d\tau \\ &= \int_{0}^{\infty} h(\tau)\left[\int_{-\infty}^{\infty} x_T(u)\,e^{-i\omega u}du\right]e^{-i\omega\tau}\,d\tau \end{aligned} \tag{18}$$

---

[39] The Dirac function or “unit impulse function” is an infinitely sharp peak function with the following character:

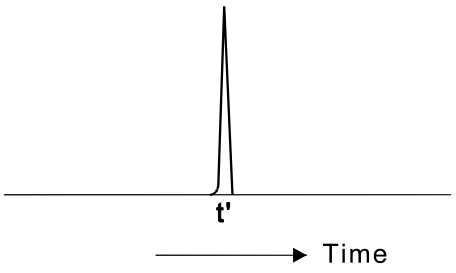

$\delta(t - t') = 0$ for $t \neq t'$

and:

$$\int_{t'-\varepsilon}^{t'+\varepsilon} \delta(t - t')\,dt = 1 \quad \text{for } \varepsilon \to +0$$

and:

$$\int_{-\infty}^{\infty} x(t)\,\delta(t - t')\,dt = x(t').$$

$$= X_T(\omega) \int_0^\infty h(\tau)\, e^{-i\omega\tau}\, d\tau$$
$$\equiv X_T(\omega)\, H(\omega)$$

in which $u = t - \tau$.

$H(\omega)$ is the Fourier transformation of $h(t)$ and is called the frequency response function. Using the definition for the spectral density function (13), it follows that for real processes $x_T(t)$ and $y_T(t)$:

$$S_{yy}(\omega) = \lim_{T\to\infty} \frac{1}{2\pi T} |Y_T(\omega)|^2 = \lim_{T\to\infty} \frac{1}{2\pi T} |X_T(\omega)|^2 |H(\omega)|^2$$

and thus:

$$S_{yy}(\omega) = S_{xx}(\omega) |H(\omega)|^2 \qquad (19)$$

So, the relation is derived that the output spectral density function is equal to the product of the input spectral density function and the square of the frequency response function.

In a graphic representation:

Figure D

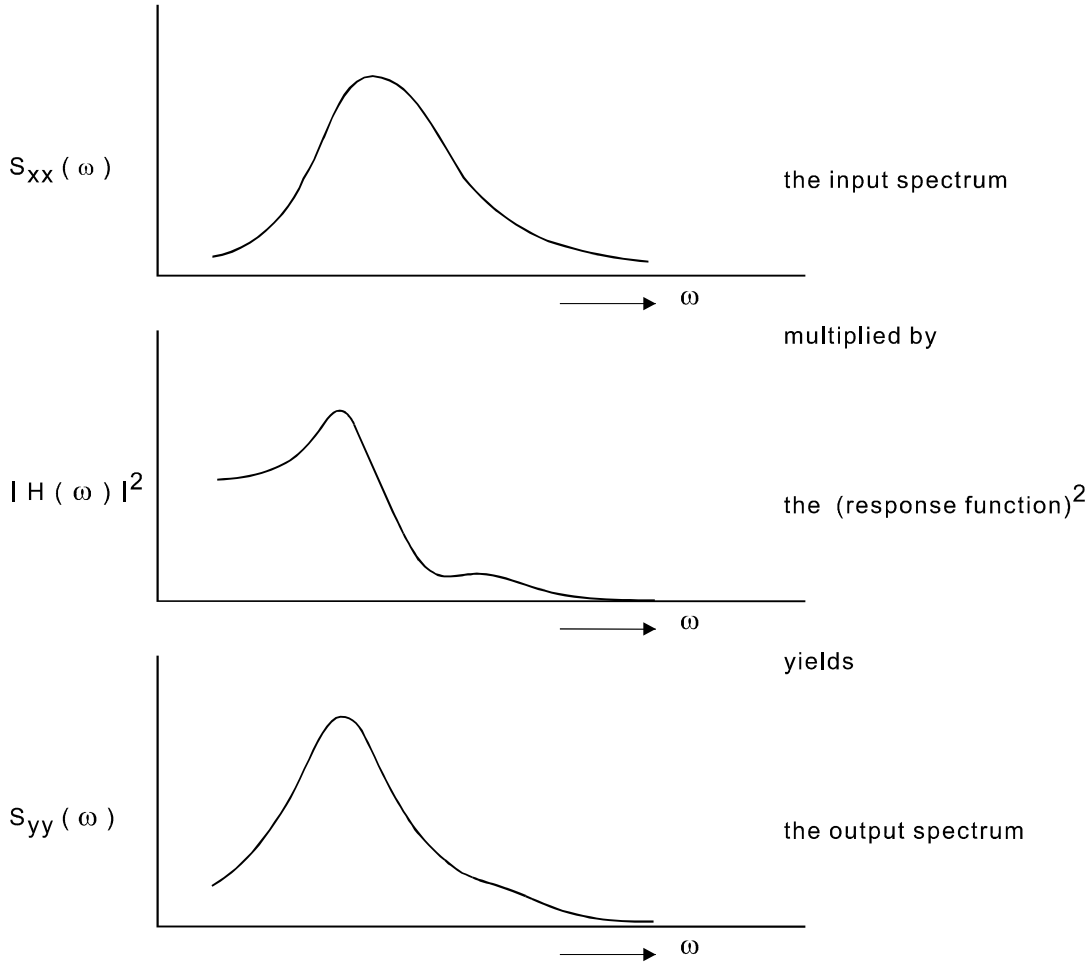

Some relations

The following quantities can now be calculated with use of the spectral density function:

$$m_{x0} = \int_0^\infty S_{xx}(\omega)\, d\omega \tag{20}$$

and

$$m_{x1} = \int_0^\infty S_{xx}(\omega)\, \omega\, d\omega \tag{21}$$

For a stochastic variable x, describing a stationary ergodic process, is:

$$\overline{M}_x = \frac{1}{2} \int_{-\infty}^{\infty} S_{xx}(\omega)\, d\omega \tag{14}$$

When $S_{xx}(\omega)$ is an even, real function and x has a narrow spectrum and zero mean value, it follows that:

$$\bar{M}_x = \int_0^\infty S_{xx}(\omega)\, d\omega = m_{x0}$$ (= area under the spectrum)

and:

$$\sigma_x = \sqrt{\bar{M}_x} = \sqrt{m_{x0}} \qquad (22)$$

$$T_1 = 2\pi \frac{m_{x0}}{m_{x1}} \qquad (23)$$

When x follows a normal distribution, then it can be calculated that:

$$4\sigma_x = 2x_{a1/3} \quad \text{(significant double amplitude)} \qquad (24)$$

Irregularity of waves

Since it is known that the distributions of the wave elevations at sea are approximately normal, all formulae mentioned earlier are valid to describe irregular sea conditions. To judge the behaviour of vessels at sea, irregular seas are assumed to have energy spectral density functions, or power spectra, that can be described by:

$$S_{\zeta\zeta}(\omega) = A \,.\, \omega^{-r} \,.\, e^{-B \,.\, \omega^{-s}} \qquad (25)$$

Formula (25) represents the hypothetical spectra, similar to the Pierson-Moskowitz[40] spectra for fully developed seas, when:

r = 5
s = 4
A = $172.8\ (\zeta_{w1/3})^2\ (T_1)^{-4}$
B = $691.0\ (T_1)^{-4}$

Assuming that the wave height is a random variable with a narrow band normal distribution and zero mean value one arrives at (see also (24) and (23)):

$$\zeta_{w1/3} \simeq 4\sqrt{m_{\zeta 0}}$$

$$T_1 \simeq 2\pi \frac{m_{\zeta 0}}{m_{\zeta 1}}$$

where $\zeta_{w1/3}$ is the significant wave height and T_1 the average wave period.

40) Pierson, W.J. and Moskowitz, L.; "A proposed Spectral Form for Fully Developed Wind Seas Based on Similarity Theory of S.A. Kitaigorodskii", Journal of Geophysical Research, Vol. 69, December 1964.

In relating the spectra (25) to observations, the average observed wave height ζ_w is assumed to coincide with the significant wave height $\zeta_{w1/3}$. The average observed period T is assumed to coincide with the average calculated period T_1. So, observed sea conditions can be represented by means of a spectrum, as shown in Figure E, where the observations of H.U. Roll on the North Atlantic Ocean are represented in Pierson-Moskowitz spectra.

Figure E

PIERSON-MOSKOWITZ SPECTRA
(s = 4) and (r = 5)
Significant wave height $\zeta_{w1/3}$ and average period T_1
according to Roll for the North Atlantic Ocean
$T_1 = 2\pi (m_{\zeta 0}/m_{\zeta 1})$

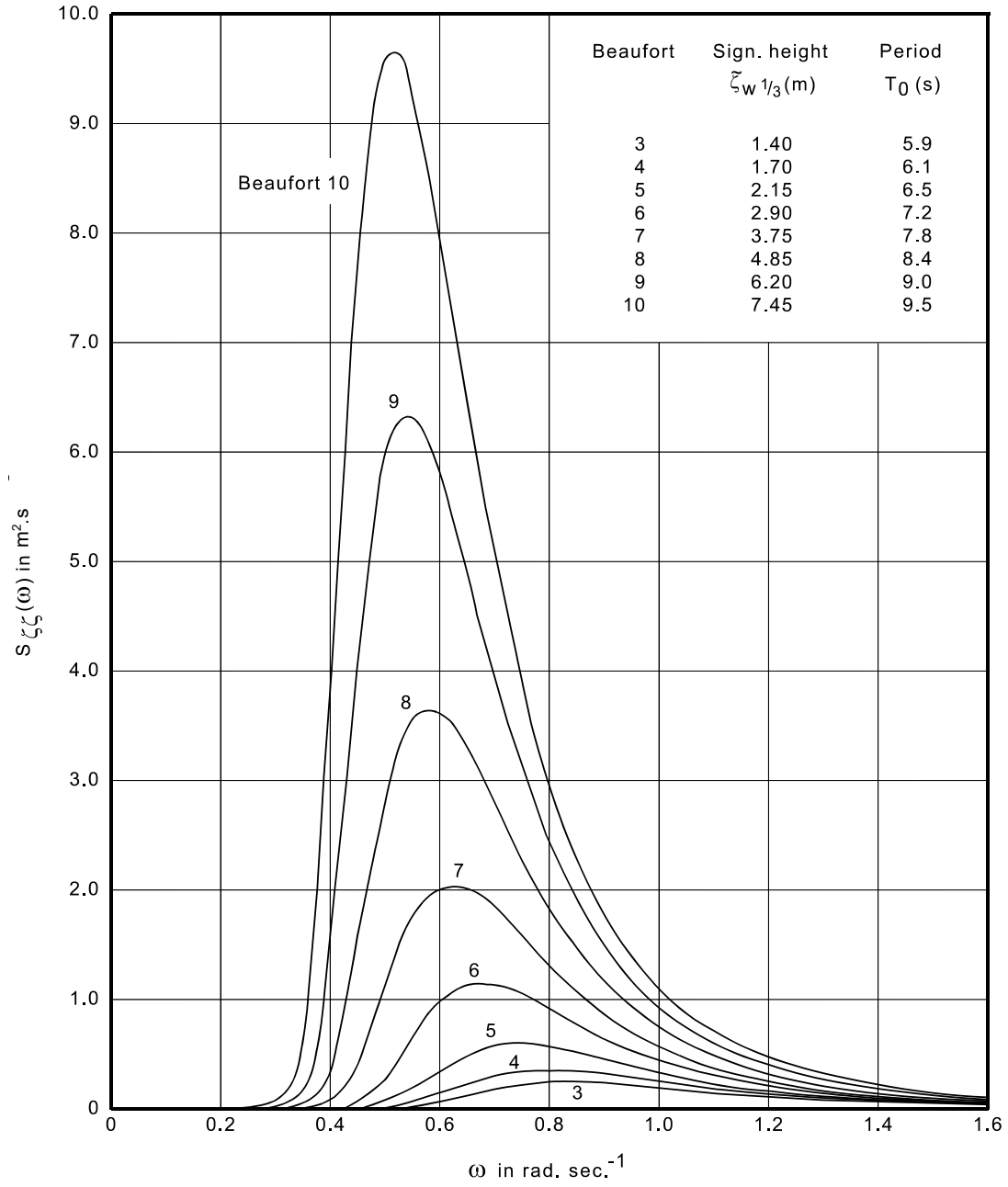

Irregularity of waves

Since it is known that the distributions of the wave elevations at sea are approximately normal, all formulae mentioned earlier are valid to describe irregular sea conditions. To judge the behaviour of vessels at sea, irregular seas are assumed to have energy spectral density functions, or power spectra, that can be described by the JONSWAP[41] formula:

$$S_{\zeta\zeta}(\omega) = \alpha \cdot g^2 \cdot \omega^{-5} \cdot \exp\left[-1.25\,(\omega/\omega_0)^{-4}\right] \cdot \gamma^{\exp\left[-(\omega-\omega_0)^2/(2\sigma^2\cdot\omega_0^2)\right]} \qquad (26)$$

$$\sigma = \begin{cases} \sigma_a \text{ for } \omega \le \omega_0 \\ \sigma_b \text{ for } \omega > \omega_0 \end{cases}$$

in which:

ω = circular frequency
ω_0 = spectral peak frequency
g = acceleration due to gravity

The dimensionless shape parameters α, γ, σ_a and σ_b are generally taken as:

$\alpha = 0.0989$; $\gamma = 3.3$; $\sigma_a = 0.07$; $\sigma_b = 0.09$

Assuming that the wave height is a random variable with a narrow band normal distribution and zero mean value one arrives at (see also (24) and (23)):

$$\zeta_{w1/3} \simeq 4\sqrt{m_{\zeta 0}}$$

$$T_1 \simeq 2\pi \frac{m_{\zeta 0}}{m_{\zeta 1}}$$

where $\zeta_{w1/3}$ is the significant wave height and T_1 the average wave period.

In relating the spectra (26) to observations, the average observed wave height ζ_w is assumed to coincide with the significant wave height $\zeta_{w1/3}$. The average observed period T is assumed to coincide with the average calculated period T_1. So, observed sea conditions can be represented by means of a spectrum, as shown in Figure F, for a range of Beaufort numbers.

[41] Hasselman, K. et al.; “Measurement of Wind-Wave Growth and Swell Decay During the Joint North Sea Wave Project (JONSWAP)”, Deutsches Hydrographisches Institut Hamburg, 1973.

NOTE: The relation between the average period T_1 and the peak period T_0 for the JONSWAP type spectra is $T_0/T_1 = 1.20$.

Figure F

JONSWAP SPECTRA

Significant wave height $\zeta_{w1/3}$ and peak period T_0
according to Roll for the North Atlantic Ocean

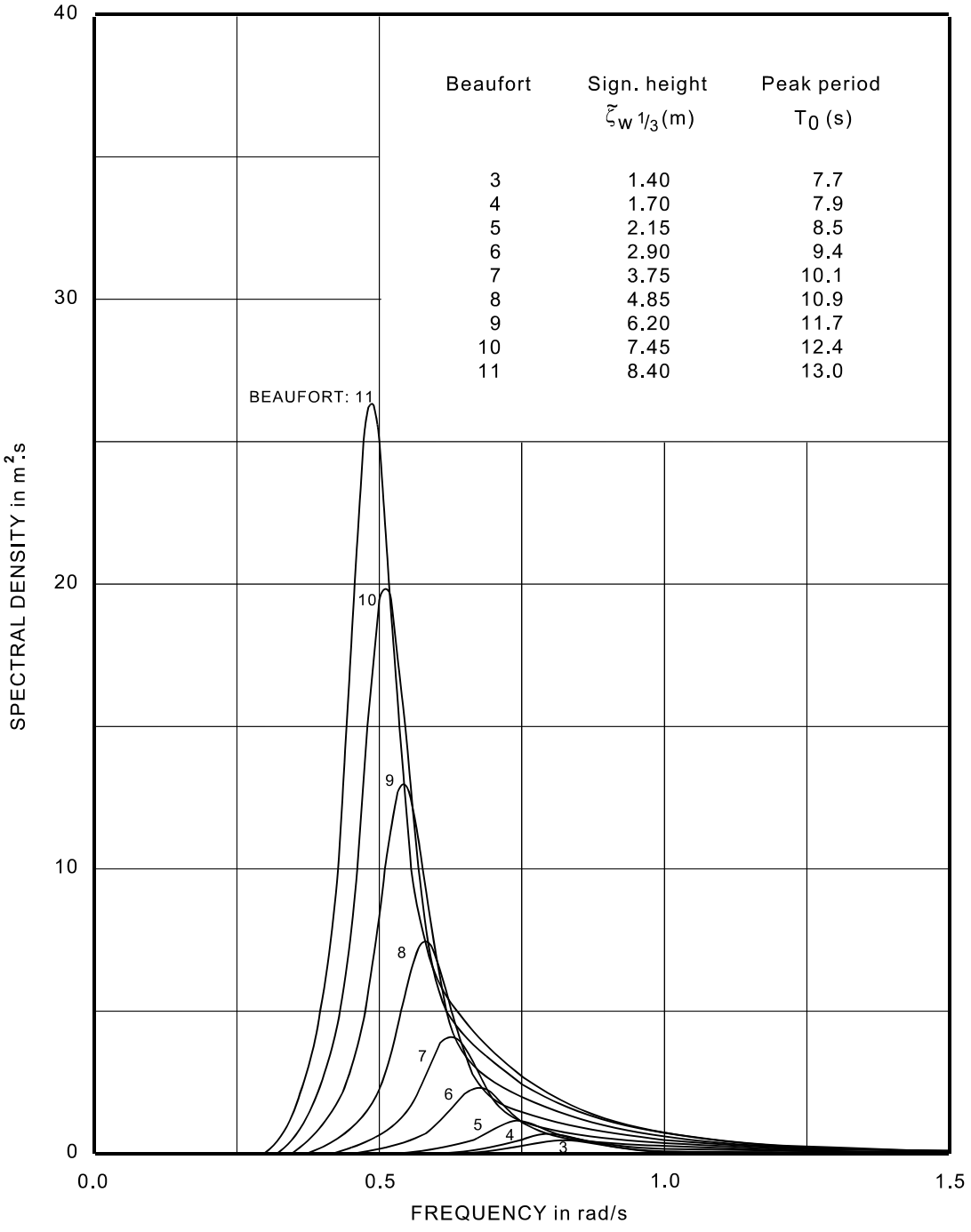

APPENDIX IV

DECAY TESTS, DETERMINING DAMPING AND PERIODICITY

Decay/free extinction tests are performed to determine the damping coefficients, damped period and natural period of a vessel or system. Decaying signals are characterised by a decaying oscillation around a mean value, with an approximately constant period. An example of a decaying signal is shown below:

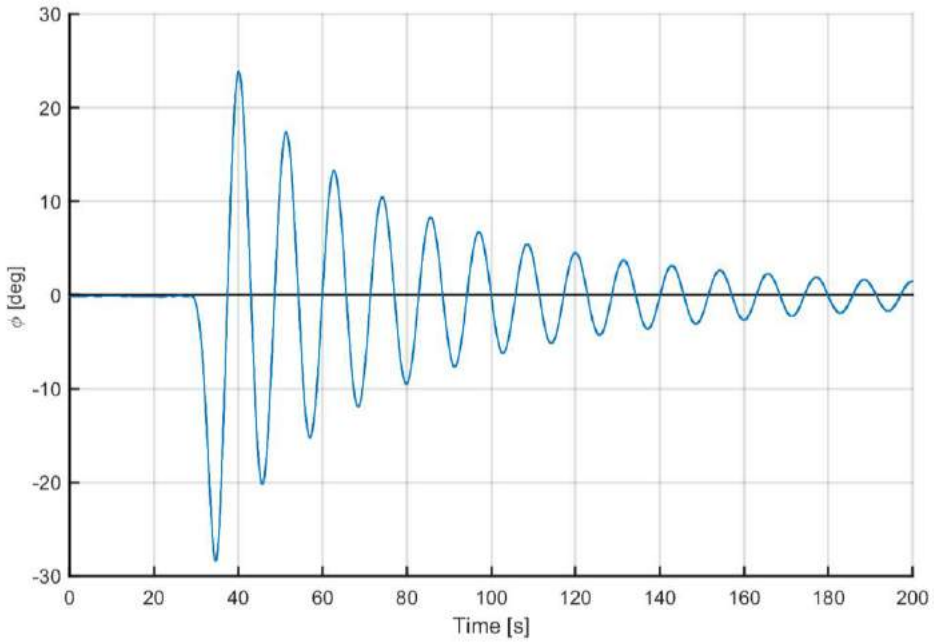

Time series of decaying roll signal

It is assumed that the decaying system can be accurately described by the following equation:

$$a\ddot{x} + b(\dot{x}) + cx = 0 \quad (1)$$

Where:

- x is a motion signal (e.g. roll, pitch or heave)
- $\dot{x}$ is the first derivative of the motion signal (e.g. roll velocity)
- $\ddot{x}$ is the second derivative (e.g. roll acceleration)
- a is the mass or inertia of the vessel (including added mass or added inertia)
- c is the restoring term of the vessel
- $b()$ is the damping function

The damping function can have various terms. The following terms are implemented for analysis at MARIN:

$$b(\dot{x}) = B_1\dot{x} + B_2\dot{x}|\dot{x}| + B_3\dot{x}^3 \quad (2)$$

Where:

- B_1 is the linear damping coefficient
- B_2 is the quadratic damping coefficient
- B_3 is the cubic damping coefficient

Solving only for B_1 is called the “first order solution”, solving for B_1 and B_2 is called the “second order solution” and solving for B_1, B_2 and B_3 is called the “third order solution”. In very rare cases B_1 and B_3 can be determined while leaving B_2 zero. This is called the “13 order solution”. Usually the second order solution is used. Only when a damping test clearly shows cubic behaviour is the third term determined as well.

Analysis of a motion signal alone does not provide absolute damping coefficients; it only provides relative damping coefficients in the form B/c. An absolute value of c has to be provided before an absolute value of B can be found. As an example, c can be defined as $g\Delta GM$ for a roll decay.

The relative damping can be analysed by three methods. First, Equation 1 can be solved by inserting the measured motion, velocity and acceleration and solving in a least squared sense. This is called the “least squares fit”. Secondly, classic “PQ analysis” can be performed. PQ analysis sets out all individual crests and troughs as a function of amplitude and fits a polynomial through. The polynomial coefficients are denoted by P and Q (and R in the cubic damping case). Lastly, the motion signal itself can be fit in an optimal sense by varying the relative damping and natural period of the system until an optimum is found. This is called “motion optimised”.

All three methods determine the same relative damping values, but with different approaches to what is optimal. The classic PQ analysis works very well for lightly damped systems, but has difficulties to provide accurate values for highly damped systems (e.g. ships sailing at speed). The least squares fit and motion optimised methods are closely related. The motion optimised method actually removes the need for fitting velocity and acceleration in the system of equations, which sometimes caused irregularities in the fitting.

The decay analysis results can be verified using a PQ-diagram, a recalculation of the time series and via a plot of the damped period per oscillation.

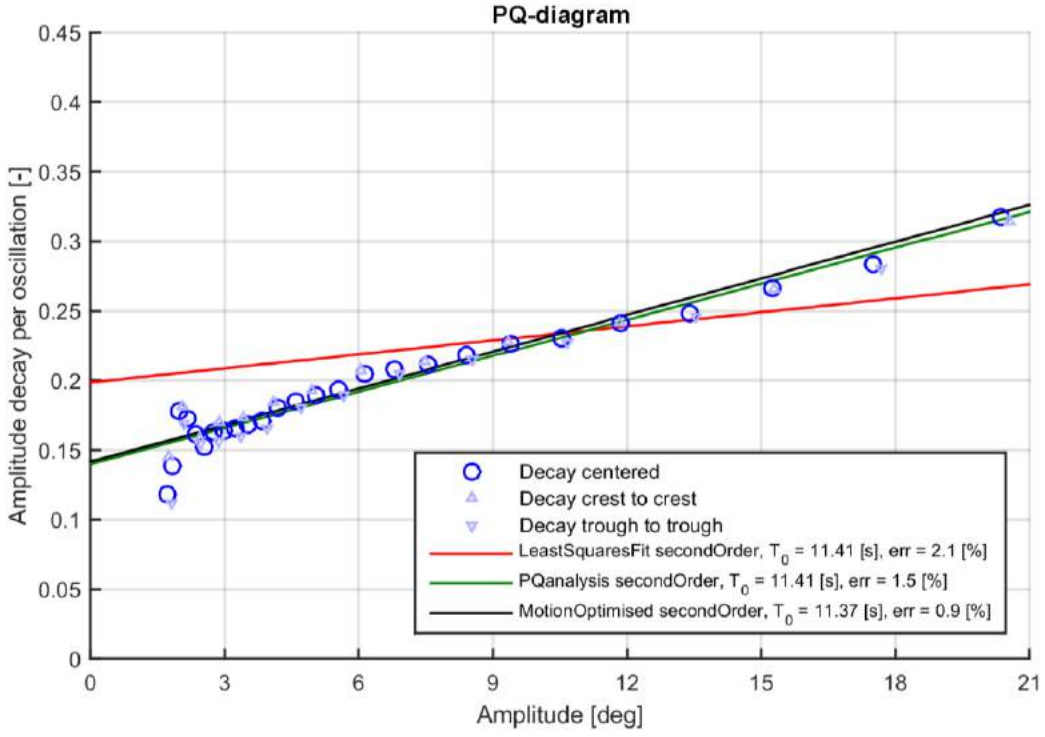

Example of a PQ-diagram showing all three methods

The PQ-diagram shows the decay of the crests and troughs in three ways. “Decay centred” shows the amplitude decay calculated as the difference between two consecutive crest-trough differences or trough-crest differences. This method is not sensitive to offsets in the signal. These values are also used in the PQ analysis method. The “crest to crest” and “trough to trough” decays are provided to indicate offsets and other irregularities in the signal. Ideally all three should coincide. In this case the second order results of all three fitting methods are indicated. Normally the best fitting method is used and the others are not shown.

The damping coefficients B_1, B_2, B_3 and P, Q, R values translate into one another as follows; see also “Slingergedrag van Schepen” door Ir J.J.W. van der Vegt, “KIVI-zeegangsdag”, March 1 1984:

$$\begin{aligned}\frac{B_1}{c} &= \frac{PT_0}{2\pi^2}\\ \frac{B_2}{c} &= \frac{3QT_0^2}{32\pi^2}\\ \frac{B_3}{c} &= \frac{RT_0^3}{6\pi^4}\end{aligned} \tag{3}$$

Where:

- P, Q and R are the zeroth, first and second order polynomial components of the fit of crest and trough decay
- T_0 is the natural or undamped period of the system

Ideally the natural period can be expressed as:

$$T_0 = 2\pi\sqrt{\frac{a}{c}} \tag{4}$$

The damped period T_d is the observed period and can change slightly with oscillation amplitude. In the case of an ideal linear damped system the damped and natural periods are related via:

$$\begin{aligned}T_0 &= T_d\sqrt{1-\zeta^2}\\ \zeta &= \frac{B_1}{2\sqrt{ac}}\end{aligned} \tag{5}$$

Where:

- ζ is the damping ratio

T_d and hence T_0 is (initially) determined from the mean crossings of the signal; however, it is further optimised when the motion optimised method is used.

The error mentioned in the legend of the PQ-diagram is actually the error function used in the motion optimised method, which is the L2-norm of the difference between the measured motion and the recalculated motion after fitting. An example of the recalculation is shown in the next figure:

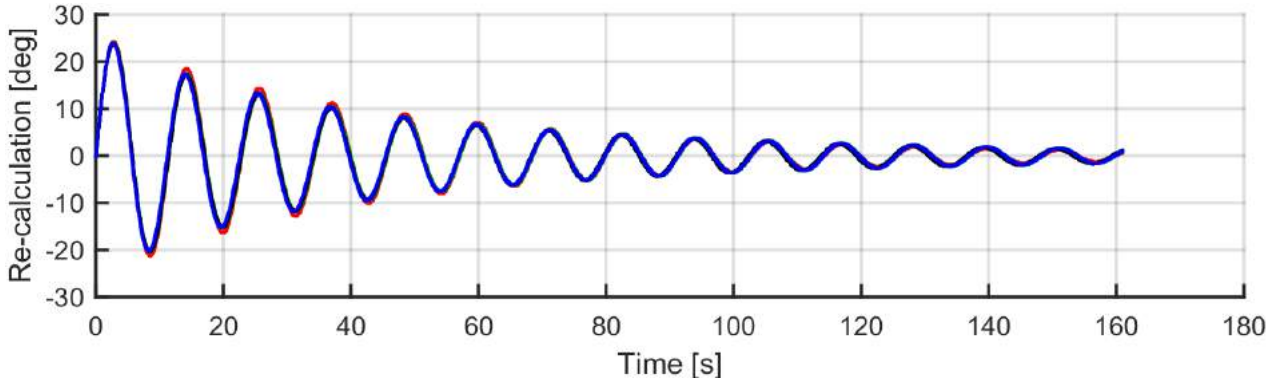

Example of a recalculation showing all three methods; the original signal is shown in blue

The recalculation diagram can be used to check whether the periods found and damping actually match with the measured signal. In this case the red line of the least square fit method shows too little damping at the beginning of the time series at large oscillation amplitudes and somewhat too much damping at the end of the time series. This was also indicated in the PQ-diagram. The other methods fit relatively accurate to the measured data.

The behaviour of the damped period is shown as a function of the number of oscillations as shown below:

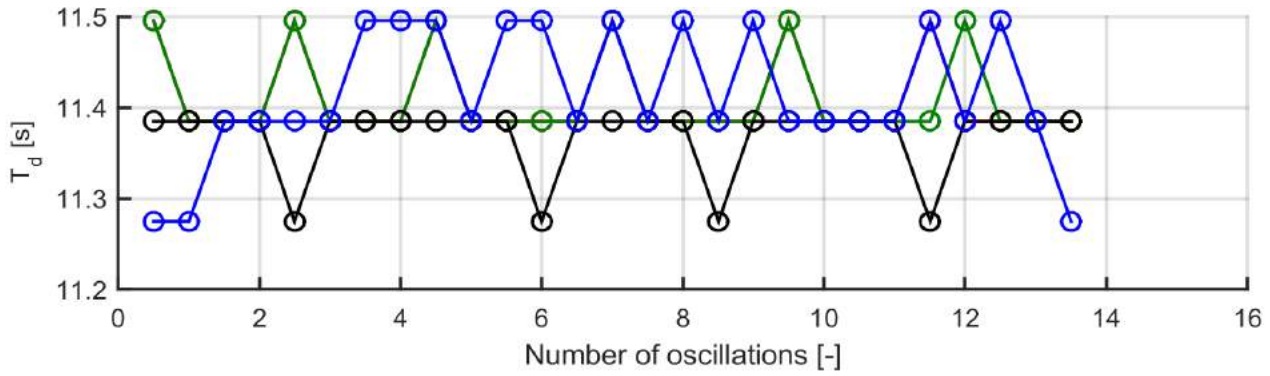

Example of a period overview; the original signal is shown in blue

This plot can be used to check for errors in the mean crossings (e.g. when a poorly conditioned signal has erratic mean crossings the average period estimate will be too small). In this case both the original signal and the three methods are in agreement and show a very constant damped period.

APPENDIX V

COMFLOW CFD and EXTRA analysis method

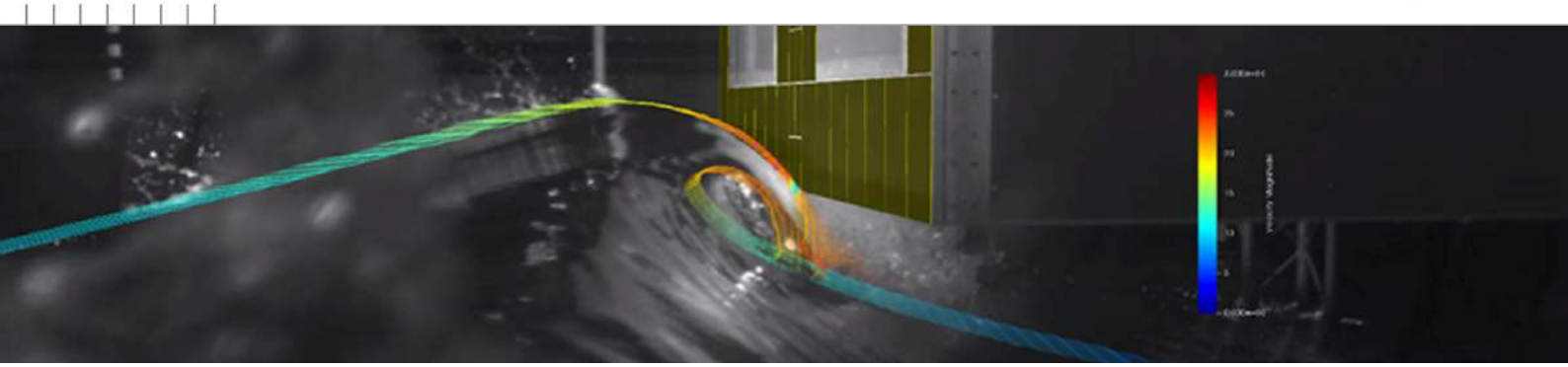

EXTReme event matching Analysis ('EXTRA')

Detailed flow analysis and visualisations by numerical reconstruction of extreme events, to answer questions on integrity, safety and design optimization

Extreme event matching has been developed at MARIN as an analysis methodology to complement and maximise your model test outcomes. Using CFD, an extreme event as encountered in our wave basin or from a specified design condition can be accurately reconstructed to obtain detailed information on local pressures, flow velocities and other quantities of interest.

Detailed information on flow quantities such as pressures, velocities and impulses during extreme events, by numerical (re)construction of the occurring phenomena.

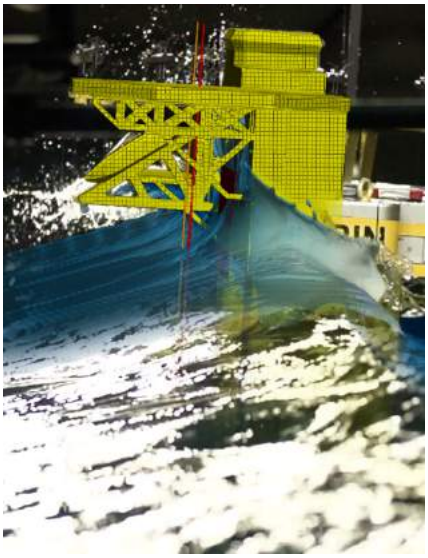

Top: Extreme event matching applied to breaking wave-in-deck (courtesy of BreaKin JIP). Bottom left: Impact assessment following DNV-GL's OTG 13 / 14 guidelines.

Motivation and background

When performing model tests in extreme environments, it is not uncommon that unforeseen hydrodynamic phenomena occur. A breaking wave could for instance impact an on-deck substructure unexpectedly, or larger amounts of green water than anticipated for could occur. For such events, detailed information about local flow phenomena, pressures and/or impulses can provide answers to important questions on integrity and safety of the structure, or help optimize design. Such information however is not always available in sufficient detail directly from the model test results. Therefore, extreme event matching has been developed at MARIN as a complementary analysis methodology to maximise the outcomes of your model tests.

Methodology

Using an iterative procedure together with our CFD tool ComFLOW (for details, see for instance [1] and the many references therein), the extreme event matching methodology is capable of accurately reconstructing the exact conditions encountered during an extreme event in our wave basin, or from a specific design condition. After the reconstruction is completed, the selected event can be replicated numerically while monitoring all areas and quantities of interest. Based on experience, MARIN can hereby assist in selecting the most representative event(s) for reconstruction. Using the outcomes of the extreme event matching analysis, questions concerning safety and/or integrity can be addressed at a higher level of confidence, and (re)design of existing and to-be-build ships and offshore structures can be optimized.

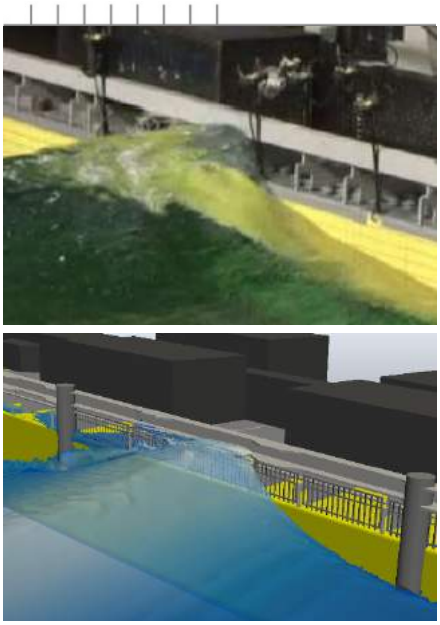

Extreme event matching applied to optimize deflector design against green water loading alongside a FPSO (courtesy of Bluewater Energy Services).

Applicability

The methodology has been successfully applied and validated using existing model test data, for a wide range of wave impact and green water related applications (also see [2], [3]):

- Impacts loads and dynamic response of offshore wind turbines subjected to extreme breaking waves;
- Local and global impacts loads on semi-submersibles (OTG 13 / 14);
- Wave loads on on-deck structures and optimization of mitigation design (e.g. deflectors for life boats on drill ships);
- Quantification of green water flow (e.g. on deck of FPSOs);
- Design optimization of bulwarks, green water protection and riser balconies;
- Green water loading on ships at forward speed (e.g. container vessels);
- Bow and stern slamming (e.g. cruise ships).

For more information on the extreme event matching methodology, contact MARIN:

Joop Helder
T + 31 317 49 35 11
E j.helder@marin.nl

Henry Bandringa
T + 31 317 49 33 19
E h.bandringa@marin.nl

[1] Veldman, A.E.P. et al. *"Computational Methods for Moving and Deforming Objects in Extreme Waves"*. Proc. of ASME 2019 38th Int. Conf. Ocean, Offshore, Arctic Eng. OMAE2019-96321.

[2] Helder, J.A. and Bunnik, T. *"Deterministic Breaking Wave Simulation for Offshore Applications"*. Proc. of 21th Offshore Symposium SNAME 2016.

[3] Bandringa, H. and Helder, J.A. *"On the Validity and Sensitivity of CFD Simulations for a Deterministic Breaking Wave Impact on a Semi Submersible"*. Proc. of ASME 37th Int. Conf. Ocean, Offshore, Arctic Eng. OMAE2018-78089.

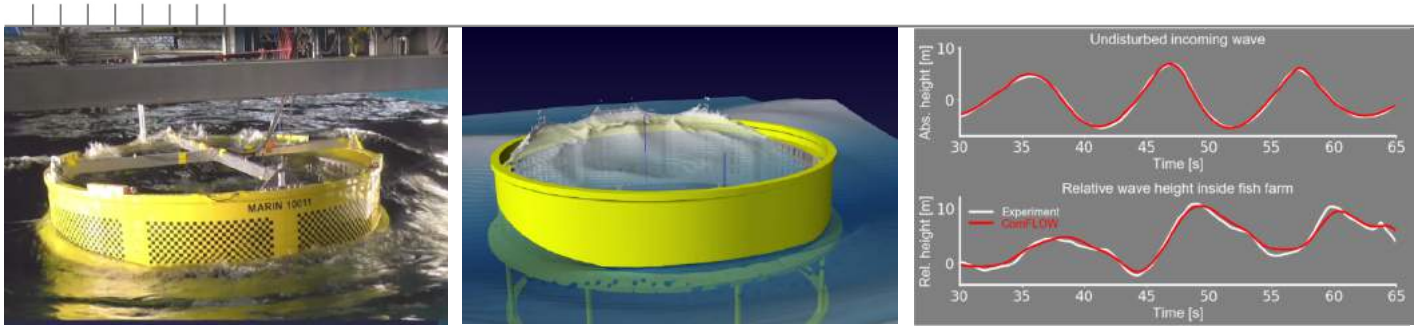

Extreme event matching applied to obtain local pressure distributions during internal sloshing inside a floating fish farm (courtesy of Viewpoint Seafarm AS - Spider Cage concept).

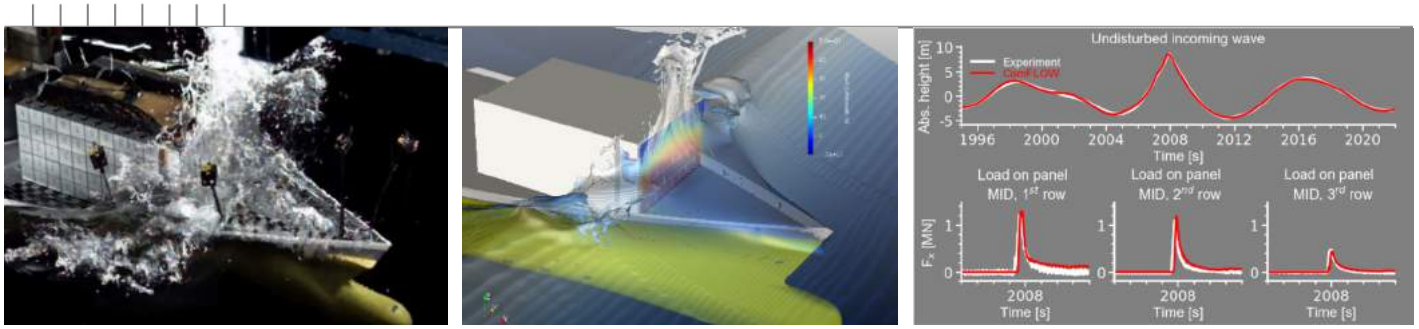

Extreme event matching applied to determine local and global wave impact loading on the breakwater of a container vessel (courtesy of the CRS working group green water).

DOCUMENTATION SHEET

Seakeeping and Manoeuvring Basin

To simulate and test the behaviour of ships at sea as closely as possible, we use free sailing models for most seakeeping and manoeuvring test campaigns. To ensure accurate test results by using adequately large models, a sufficiently wide and long basin is required. The Seakeeping and Manoeuvring Basin (SMB) with its 170 m x 40 m x 5 m is perfectly fit. The basin is fitted with flap-type wave makers on two adjacent sides and adjustable beaches on the opposite sides. This allows for free sailing ship models to sail in regular and irregular waves from any direction and for free sailing manoeuvring tests such as zig-zag and turning circles at the design speed of the ship.

Tests in the SMB:

- Seakeeping tests in regular and irregular waves.
- Free sailing manoeuvring tests in calm water and waves
- Captive (CPMC) manoeuvring tests
- Tests on (floating) offshore structures to determine the motions and load due to waves.
- Tests for wind assisted ships
- Wireless controlled models at high speeds.
- Underwater manoeuvring.
- Side by side operations.

Basin capabilities

Model size

Although ship models can vary between 0.3 and 11 metre of length, the typical length of free sailing models is between 4 and 6 metre. Scale depends on required speed, wave conditions, model outfitting and measurement requirements. For floating (offshore) structures the model size is also determined by water depth and required wave conditions.

Model instrumentation

Ship models are fitted with all relevant appendages, including propulsion line, steering gear, stabilising fins, ESD's and anti-roll tanks. All appendages are fully functional, adapted to work at model scale and with a realistic control based on the ship motions. Model tests for side by side operations and launch and recovery tests with multiple models can be performed as well. DP systems and control is available using an in-house developed control system.

Carriage

The carriage runs over the total length of the basin with a maximum speed of 6 m/s and consists of a main frame and sub frame. The main frame spans the full width of the basin, the sub frame can move along this main frame over the entire width of the basin at a maximum speed of 4 m/s. The carriage can follow all movements of a model that is sailing freely by itself under auto pilot control or it can follow a prescribed track with a ship model mounted to the carriage. The latter case is used for Computerized Planar Motion Carriage (CPMC) tests.

For each specific need MARIN has test facilities available:

- Offshore Basin
- Concept Basin
- Shallow Water Basin
- Deep Water Basin
- Depressurised Wave Basin
- Cavitation Tunnel
- Multi Phase Wave Lab

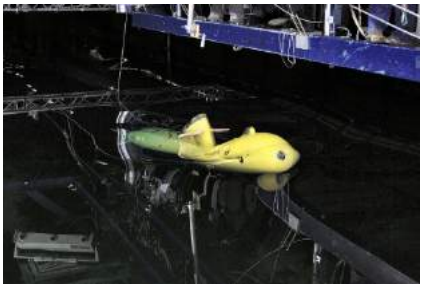

For more information contact MARIN;
department Ships
T + 31 317 49 34 72
E ships@marin.nl

Waves

Waves can be generated with peak periods ranging from 0.8 to 4.2 seconds and, depending on the peak period, up to a significant wave height of 0.45 m. At two adjacent sides of the basin, segmented wave generators are installed, consisting of 320 hinged flaps of 60 cm wide. Each flap is controlled separately by a servo motor. The wave generator can be used to produce regular and irregular, long and short crested waves from arbitrary directions. Opposite the wave generator passive sinkable wave absorbers are installed. To further dampen the waves, the wave generators are equipped with an active reflection compensation.

Wind

Wind forces can be modelled using portable wind fans or by attaching lines with controlled tension winches.

Measurement and observations

Models are tracked by a 6 degree of freedom position measurement system. Instrumentation of propellers rudders and accelerations, pressured, loads are well possible. Typical registration is with 200 Hz, but for high frequent phenomena, higher measurements rates are being used. Default close-up video recordings are made for allowing registration of important phenomena. To measure captive forces and moments on the complete model, a turn table and force measurement frame can be fitted between the model and carriage to also force yaw motions and to determine the current or manoeuvring forces.

Expertise and experience

Over the years MARIN has gained a vast experience in performing a wide range of tests for all kind of ships and offshore structures, varying from small fast craft, 400 m container vessels to autonomous submarines.
Besides ship motions, seakeeping tests can focus on any behaviour in waves. This includes added resistance in waves, optimisation of anti-roll devices and non-linear behaviour such as parametric roll, broaching and slamming. In addition, we perform IMO tests on a regular basis, for weather criterion, safe return to port and ships with an open top notations. Manoeuvring tests are often carried out to verify and improve the performance as required by IMO manoeuvring regulations (zig-zag and turning circles tests). Many custom manoeuvres are performed to verify market-specific performance criteria, such as for naval ships, towed FPSO's, tugs and submarines. CPMC tests are performed to compose mathematical models to perform fast time or real time simulations.

Publications

- Dallinga, R.P.: 'The New Seakeeping and Manoeuvring Basin of MARIN, Japanese workshop on waves', 1999.
- Quadvlieg, H.H.A.: 'A New Combined Seakeeping and Manoeuvring Basin for the Third Millennium Maritime Research', MARSIM 2000.
- ITTC leaflet: https://ittc.info/media/7879/seakeeping-and-manoeuvring-basin.pdf.

MARIN
P.O. Box 28

6700 AA Wageningen
The Netherlands

T +31 317 49 39 11
E info@marin.nl

I www.marin.nl